



Periodic Mesoporous Organosilicas for Application as low-k Dielectric Materials

Dissertation submitted in fulfillment of the requirements for
the degree of Doctor of Science: Chemistry

By

Frederik Goethals

Department of Inorganic and Physical Chemistry
Faculty of Sciences

Promoter: Prof. Dr. I. Van Driessche
Promoter: Prof. Dr. P. Van Der Voort

10/12/2012

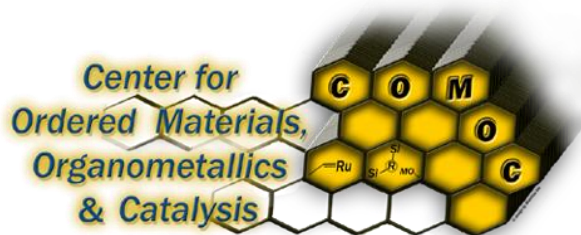
Composition of the reading and examination commission

Prof. Dr. A. Adriaens	Ghent University (chairwoman)
Prof. Dr. I. Van Driessche	Ghent University (promoter)
Prof. Dr. P. Van Der Voort	Ghent University (promoter)
Prof. Dr. C. Detavernier	Ghent University (reading committee)
Dr. M. R. Baklanov	IMEC, Leuven (reading committee)
Prof. Dr. J. Martens	Leuven University (reading committee)
Prof. Dr. P. Cool	Antwerp University (reading committee)

@ 2012 Ghent University, Department of Inorganic and Physical Chemistry, SCRIPTS – Sol-gel Centre for Research on Inorganic Powders and Thin films Synthesis & COMOC - Centre for Ordered Materials, Organometallics & Catalysis, Krijgslaan 281-S3, 9000 Ghent, Belgium

Alle rechten voorbehouden. Niets uit deze uitgave mag worden vermenigvuldigd en/of openbaar gemaakt worden door middel van druk, fotokopie, microfilm, elektronisch of op welke andere wijze ook zonder voorafgaandelijke schriftelijke toestemming van de uitgever.

All rights reserved. No part of the publication may be reproduced in any form by print, photoprint, microfilm, electronic or any other means without written permission from the publisher.



Preface

Before the start of this PhD research, I was aware about the world of nano-electronics, but I did not know the importance of every small component to provide a good and fast working of macroscopic machines such as personal computers. Even the dielectric layer that insulates the conductive wires of integrated circuits is very important and needs to be improved to obtain better performances. Several researchers are working on that and also this thesis deals with the development of dielectric layers or the so called low-k materials.

Besides the fact that nano-electronics is a very interesting field for research, one of the main reasons to start with these PhD research was the possibility to combine the experience and knowledge of the SCRiPTS and COMOC research groups of the department of Inorganic and Physical Chemistry (Ghent University) in one topic. SCRiPTS has experience in thin film synthesis, while COMOC focuses on the synthesis of nanoporous materials. Obviously, the low-k material must be very thin to be used in very small devices and porosity is needed to lower the dielectric constant of the insulator. A lower dielectric constant means a better insulation of the conductive wires and this improves the performance of the device.

As potential new low-k materials, we have chosen to investigate periodic mesoporous organosilicas because they are similar in chemical composition compared to the *state-of-the-art* organosilicate low-k materials with the advantage that low polarisable organic groups are integrated in the silica matrix.

To evaluate the synthesized materials, in depth characterization is very important. Fortunately, we could collaborate with the Solid State Sciences department and IMEC for the characterization of our materials. Furthermore, the collaboration with IMEC led and still leads to more insights in this research field and what the targets are for industrial application.

I hope that the experiments and results are presented in a comprehensive and attractive way, and that this contribution is enjoyable to read.

*Frederik Goethals,
Ghent, September 2012*

Dankwoord

Doctoreren is een bewijs van zelfstandig, origineel wetenschappelijk onderzoek. Gelukkig betekent zelfstandig niet dat je alles alleen moet uitvoeren. Daarom zou ik nu graag de personen bedanken die bijgedragen hebben tot het behalen van mijn doctoraat.

Als eerste wil ik mijn promotoren professor Isabel Van Driessche en professor Pascal Van Der Voort bedanken om mij de kans te geven aan dit doctoraat te beginnen. Ik heb het geluk gehad twee promotoren te hebben waarbij ik steeds terecht kon voor raad, goede ideeën en kritische kanttekeningen. Daarnaast kreeg ik ook voldoende vrijheid om zelf mijn weg te vinden en dingen uit te proberen binnen het onderzoekskader.

Daarnaast wil ik ook mijn leescommissie, prof. dr. C. Detavernier, prof. dr. J. Martens, prof. dr. P. Cool en dr. M. R. Baklanov bedanken voor hun positieve evaluatie van mijn manuscript en goede opmerkingen en suggesties om het nog te verbeteren.

Al snel bleek dat de wetenschappelijke waarde van mijn onderzoek vergroot kon worden door samen te werken met IMEC en ik zou hiervoor enkele mensen van IMEC speciaal willen bedanken. Firstly, I would like to thank Mikhail Baklanov again for helping with and believing in my research, and to give me the opportunity to attend several interesting and confidential meetings at IMEC. Further, the possibility to characterize my materials at IMEC gave a real boost to my research. Also thanks to Ivan Ciofi, Kris Vanstreels and Patrick Verdonck for performing several measurements, the interesting discussions and the nice talks.

Liesje, Davy en Jolien van de vakgroep Vaste Stof Wetenschappen bedank ik voor de hulp bij staalvoorbereidingen en porositeitsmetingen.

Natuurlijk mogen in dit deel van mijn thesis de collega-onderzoekers van de COMOC- en SCRiPTS-onderzoeksgroepen niet vergeten worden. Aangezien ik mijn bureau deelde met de andere COMOC-leden komen deze eerst aan de beurt. Els, Matthias, Karen, Thomas, Isabelle, Jeroen, Ying-Ya, Dolores en Shiam hartelijk dank voor de fijne samenwerking en toffe bureausfeer. Hierbij mag ik ook de personen die COMOC reeds verlaten hebben niet vergeten te bedanken: Bart, Nele, Hans, Carl, Elien en Ilke. Matthias wil ik ook nog eens extra bedanken voor de hulp bij het maken van de cover.

Van de SCRiPTS-leden bedank ik speciaal Jonas, Pieter, Nigel, Glenn, Kenny, Petra en Klaartje voor de leuke samenwerking en de hulp bij de metingen. Verder wens ik de vele bijgekomen doctoraatsstudenten alle succes toe bij hun onderzoek.

Ik wil ook een woordje van dank richten aan de personeelsleden die mij geholpen hebben met de praktische aspecten van mijn onderzoek. Pierre, Claudine, Tom, Danny,

Bart, Pat en Els zonder jullie bijdrage zou mijn onderzoek een heel stuk zwaarder en minder efficiënt geweest zijn.

Mijn thesisstudenten, Benjamin en Jordy, worden bedankt voor hun experimentele hulp bij het onderzoek.

De praktijkassistenten en -bedienden verdienen hier ook hun plaats. Het was telkens zeer aangenaam om samen met jullie de studenten de nodige labvaardigheden aan te leren.

In het algemeen bedank ik alle collega's van de vakgroep Anorganische en Fysische Chemie, of korter S3, voor de fijne tijd die ik hier kon doorbrengen.

Tijdens mijn doctoraatsonderzoek was er ook voldoende tijd voor de nodige ontspanning. Hierbij bedank ik Kasper, Pieter, Glenn, Mieke, Tjorven, David, Koen, Tim, Tom en Bjorn voor de vele toffe en plezierige momenten die we samen gehad hebben en nog zullen hebben en omdat ik weet dat ik op jullie kan rekenen.

Mijn familie was een grote steun tijdens mijn onderzoek en daarom wil ik ze ook uitgebreid bedanken. Mijn ouders op de eerste plaats omdat ze mij de kans gaven om te studeren en omdat ze altijd voor mij klaarstaan. Verder wens ik mijn grootouders, zus en mijn schoonfamilie te bedanken voor hun aanmoediging en interesse in hetgeen ik doe.

Tot slot besteed ik de laatste paragraaf van dit dankwoord aan mijn vrouw Lore. Bedankt dat je er steeds bent voor mij en dat je mij steeds kon blijven motiveren om dit werk tot een goed einde te brengen.

Samenvatting in het Nederlands

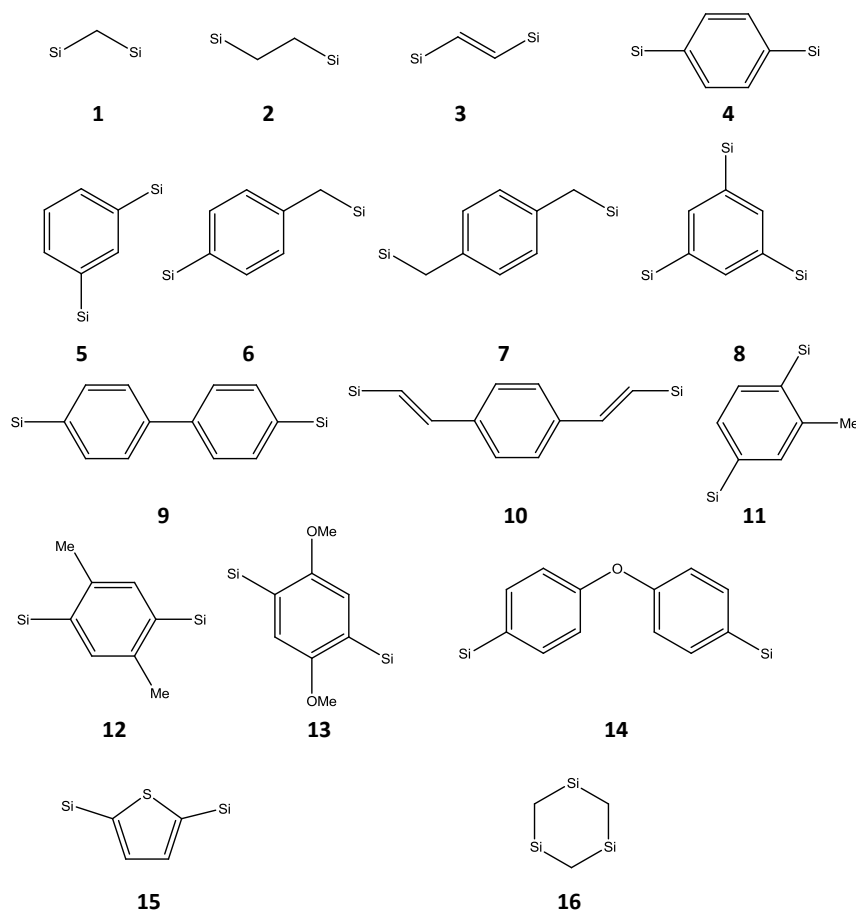
I Inleiding en doelstelling

De micro-elektronische industrie is verantwoordelijk voor de productie van geavanceerde microchips die steeds kleiner worden en sneller werken. Dit werd oorspronkelijk bereikt door de afmetingen van de componenten van de chip te verkleinen en meer transistors op eenzelfde oppervlakte te plaatsen. Door deze doorgedreven miniaturisatie komen de geleiders die de transistors verbinden zodanig dicht bij elkaar dat de toegenomen weerstand (R) en capaciteit (C) een verhoogd probleem van signaalvertraging, bekend als RC-vertraging, veroorzaken. Dit betekent dat geen verdere vooruitgang meer mogelijk is of zelfs kan leiden tot een vertraagde werking van de chip.

Om deze RC-vertraging zo veel mogelijk te reduceren zijn er twee paden mogelijk. Het eerst pad is het verlagen van de weerstand van de elektrische geleiders die de componenten van de elektrische stroomkringen met elkaar verbinden. Hiervoor werden de oorspronkelijke aluminiumgeleiders vervangen door koper aangezien koper een veel lagere weerstand heeft. Het tweede pad is het verlagen van de permittiviteit van de isolerende lagen tussen de geleiders waardoor het condensatoreffect verder gereduceerd wordt. Dit betekent dat nieuwe materialen met een zeer lage diëlektrische constante (k -waarde) moeten ontwikkeld worden. In essentie is k de maat van hoe gemakkelijk een materiaal wordt gepolariseerd in een extern elektrisch veld. Dus hoe lager de k -waarde van een materiaal hoe beter de isolerende eigenschappen van dat materiaal.

Naast een lage diëlektrische constante moeten deze materialen ook verschillende andere eigenschappen bezitten. Op elektrisch vlak is een lage lekstroom en hoge doorslagspanning vereist. Een hoge Young's modulus en hardheid zijn nodig voor een goede mechanische stabiliteit. Op structureel vlak verwacht men dat het materiaal kan afgezet worden als film met een uniforme dikte zonder te veel opbouw van interne spanningen. Ook dient het materiaal voldoende hechtingskracht te hebben zodat het niet los komt als het wordt gebruikt in een geïntegreerde schakeling. Verder mag het materiaal amper vocht opnemen, want water dat een k -waarde rond 80 heeft, zal een sterke stijging van de diëlektrische constante van het materiaal veroorzaken. Bovendien is er ook een goede chemische en thermische stabiliteit van het materiaal vereist zodat er geen ontbinding optreedt tijdens de productie van geïntegreerde schakelingen.

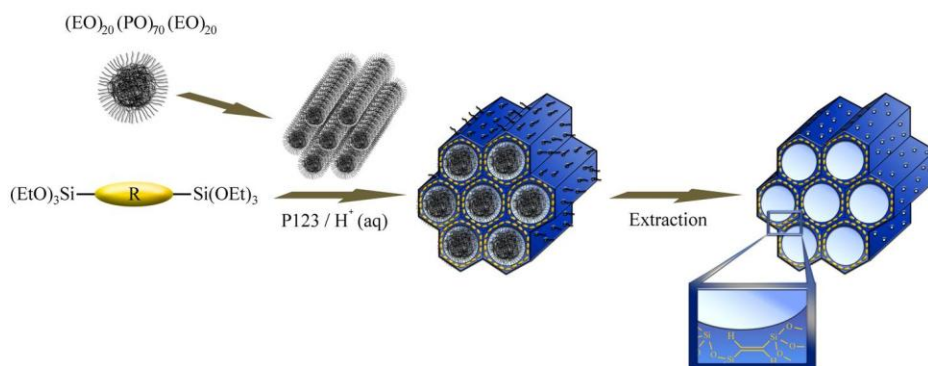
Periodieke mesoporeuze organosilicaten (PMO's) zijn een van de meest veelbelovende kandidaten om dienst te doen als geavanceerde diëlektrische lagen. PMO's zijn zeer poreus met relatief kleine poriën (mesoporeus = diameter tussen 2 en 50 nm) en dit is een belangrijke vereiste om lage k -waarden ($k < 2$) te bereiken aangezien de diëlektrische constante van lucht ongeveer 1 bedraagt. Verder zijn het synthetische, organisch-anorganische materialen die gebrugde organische groepen bevatten geïntegreerd in een goed geordend mesoporeus silicaneetwerk. PMO's hebben het voordeel dat ze uniforme poriën hebben en modificeerbaar zijn. Door de zuurstofatomen in het silicaneetwerk te vervangen door koolstofatomen wordt de geleidbaarheid van het materiaal sterk verlaagd en stijgt de hydrofobiciteit. PMO's worden gesynthetiseerd via hydrolyse en condensatie van organische gebrugde organosilaanprecursoren (zie figuur 1) met een zuur of base als katalysator (sol-gel reactie).



Figuur 1: Overzicht van PMO precursoren. De $\text{Si}(\text{OR})_3$ -groepen zijn voorgesteld door Si ter verduidelijking van de figuur. Voor nummer 16 zijn er maar 2 alkoxygroepen voor elk Si atoom.

Samenvatting in het Nederlands

Porositeit wordt geïnduceerd door tijdens de synthese templaatmoleculen (*i. e.* surfactanten) toe te voegen waarrond de condensatie plaatsvindt. De templaatmoleculen kunnen nadien verwijderd worden door een thermische behandeling of extractie waarna een porous materiaal overblijft (*i. e.* PMO). Een algemene syntheseroute voor PMO's wordt weergegeven in figuur II.



Figuur II: Algemene PMO syntheseroute.

De enorme keuze van polygesileerde precursoren met verscheidene types van overbruggende organische functionele groepen, waarvan de meest gebruikte voorgesteld zijn in figuur I, en een uitgebreide keuze aan surfactanten, maken van PMO's één van de *state-of-the-art* mesoporeuze materialen.

Het doel van dit doctoraat is om PMO's te ontwikkelen die potentieel toepasbaar zijn als diëlektrische laag in geavanceerde microchips. We hebben PMO's gekozen wegens hun interessante kenmerken en reeds gerapporteerde, veelbelovende diëlektrische eigenschappen. Als startprecursoren werden de silanen met een ethaanbrug (**2**), etheenbrug (**3**) en ringstructuur (**16**) geselecteerd. De reden hiervoor is dat de resulterende ethaan- en ring-PMO's goede elektrisch isolerende functionele groepen bevatten en om in het geval van de etheen-PMO's na te gaan of de dubbele koolstofbinding in de matrix bijdraagt tot een verhoogde stabiliteit.

Als eerste worden zeer poreuze PMO's in poedervorm gemaakt en wordt de stabiliteit van de PMO's met elkaar vergeleken. De reden waarom de PMO's eerst in poedervorm worden gemaakt, is omdat hun bulkeigenschappen kunnen worden onderzocht en karakterisatie mogelijk is met courante analysetechnieken.

Vervolgens worden de PMO's met goede eigenschappen gemaakt als dunne laag met de bedoeling lagen te maken met zeer lage diëlektrische constantes ($k < 2$).

Een nadeel van PMO's is echter dat de poriën met elkaar verbonden zijn en de poriën mesoporeus zijn. Dit betekent dat metaalionen of andere chemicaliën de poriën kunnen binnendringen en dit kan leiden tot een mindere isolerende werking. Om dit te vermijden is het noodzakelijk dat de porie-openingen voldoende klein of zelfs volledig gesloten zijn.

Daarom is het tweede doel van dit doctoraat een methode te vinden die ervoor zorgt dat de openingen van de poriën voldoende worden verkleind of gesloten worden. Om dit te bereiken zullen twee verschillende mogelijkheden worden onderzocht. De eerste is het opvullen van de poriemond via chemische reacties met grote sterische moleculen zonder dat de porie zelf wordt opgevuld. De tweede manier is via depositie van een niet-poreuze laag bovenop de poreuze laag zodat de porie-openingen worden afgesloten.

II Vergelijkende studie tussen ethaan en etheen PMO's

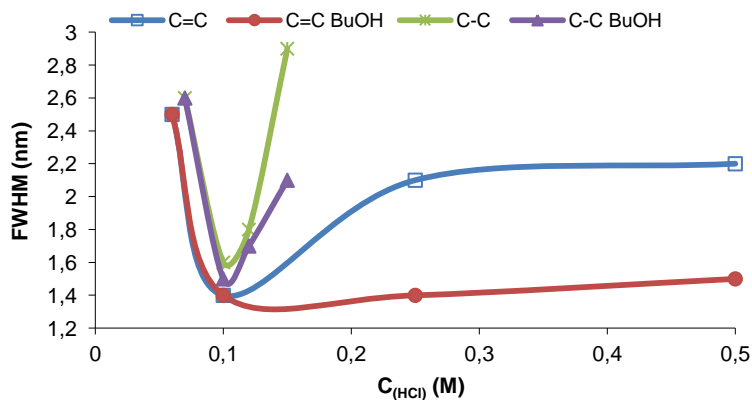
Het eerste experimenteel deel van het doctoraat gaat over de synthese van ethaan- en etheen-PMO's waarbij vooral onderzocht werd hoe een nauwe poriegroottedistributie kon bekomen worden. Een nauwe poriegroottedistributie en dus een uniform materiaal is belangrijk omdat dit ervoor zorgt dat de diëlektrische eigenschappen dezelfde zijn in heel het materiaal.

Typische syntheses van PMO's zijn dat eerst het surfactant in water (met daarbij de zuur- of base-katalysator) wordt opgelost en dat nadien de precursor wordt toegevoegd. Dit mengsel wordt gedurende een bepaalde periode geroerd waarbij de sol-gel reactie plaatsvindt en nadien wordt het mengsel verouderd op verhoogde temperatuur. Het templaet wordt nadien verwijderd door solventextractie. Voor deze synthese werd P123 als surfactant gebruikt en HCl als katalysator.

Om een nauwe poriegroottedistributie te verkrijgen bleek uit eerdere studies dat een juiste pH hiervoor belangrijk is en dat butanol een positieve invloed heeft op de poriegroottedistributie van etheen-PMO's. Daarom werd onderzocht of de toevoeging van butanol ervoor kan zorgen dat een nauwe poriegroottedistributie kan verkregen worden bij verschillende HCl concentraties.

Dit wordt weergegeven in figuur III. De figuur toont de invloed van de HCl-concentratie op de poriegroottedistributie van ethaan- en etheen-PMO's waarbij al dan niet butanol aan de synthese werd toegevoegd. De Y-as geeft de breedte van de distributie op halve hoogte weer (FWHM) en dit is een indicatie hoe uniform de grootte van de poriën is. Toevoegen van butanol heeft een positieve invloed op zowel ethaan- (C-CPMO BuOH)

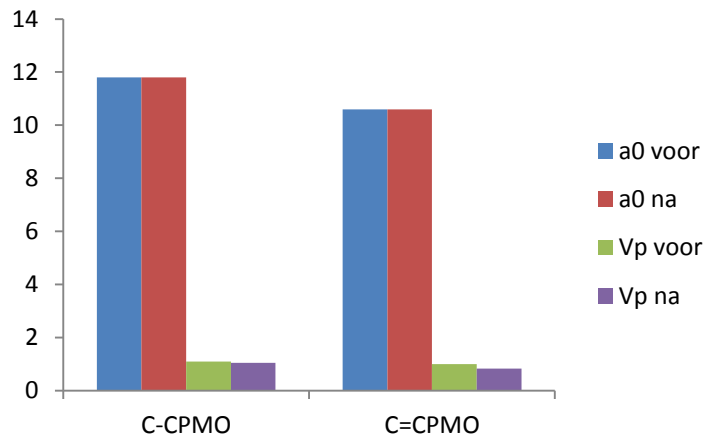
als etheen-PMO's (C=CPMO's BuOH) vooral indien de HCl-concentratie groter wordt. Er is wel een verschil tussen de twee PMO's. Het effect is namelijk minder uitgesproken voor de ethaan-PMO's in vergelijking met de etheen-PMO's. Dit kan mogelijk verklaard worden door de dubbele koolstof binding die een betere interactie toelaat met de templaاتمoleculen en HCl.



Figuur III: De invloed van de HCl-concentratie op de poriegroottedistributie van ethaan- (C-CPMO's) en etheen-PMO's (C=CPMO's) waarbij al dan niet butanol aan de synthese werd toegevoegd.

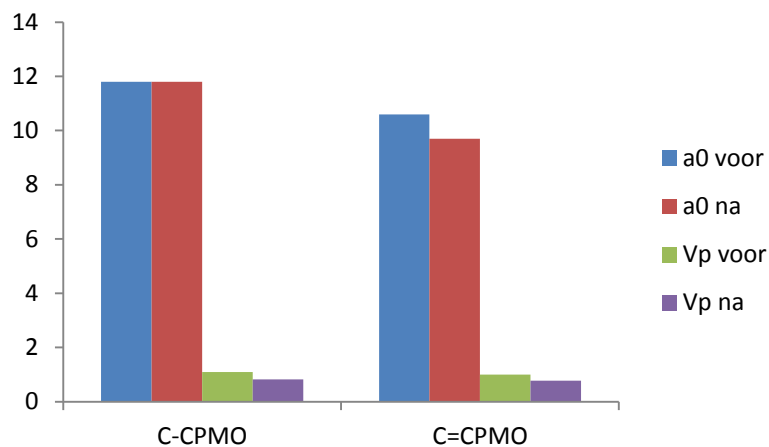
Het tweede deel van dit hoofdstuk vergelijkt de hydrothermale, mechanische en chemische stabiliteit van de ethaan- en etheen-PMO's. Hiervoor werd telkens de ordening (met XRD) en porievolume (met N_2 -adsorptie) voor en na elke stabiliteitstest bepaald. Om de hydrothermale stabiliteit te vergelijken werden de PMO's gestoomd in een autoclaaf voor 3 dagen op een temperatuur van 105°C . Om de mechanische stabiliteit te testen werden zowel hydrofiele als hydrofobe PMO's gedurende 1 minuut samengeperst bij een druk van 136 MPa. Hydrofobe PMO's werden bekomen door een behandeling met hexamethyldisilazaan (HMDS). De chemische stabiliteit werd vergeleken door de HMDS-behandelde en niet-behandelde PMO's onder de dompelen in een 1 M natriumhydroxideoplossing gedurende 2 uur en 30 minuten.

De eenheidscelparameters (a_0) en porievolumes (V_p) van de ethaan- en etheen-PMO's voor en na de hydrothermale behandeling worden weergegeven in figuur IV. Hier is duidelijk te zien dat de waarde van de eenheidscel (en dus ook de structuur) onveranderd blijft voor beide PMO's, maar dat het porievolume lichtjes gedaald is voor de etheen-PMO, terwijl dit gelijk blijft voor de ethaan-PMO. Dit betekent dat ethaan-PMO's een betere hydrothermale stabiliteit bezitten en dit kan verklaard worden door de hydrofobere ethaanbruggen.



Figuur IV: Eenheidscelwaarden (a_0) en porievolumes in ml/g (V_p) van ethaan-PMO's (C-CPMO's) en etheen-PMO's (C=CPMO's) voor en na hydrothermale behandeling.

De resultaten van de mechanische stabiliteit worden weergegeven in figuur V. Het porievolume is voor beide PMO's lichtjes gedaald na de mechanische compressie. De a_0 -waarde van de ethaan-PMO blijft gelijk, terwijl die wel verandert voor de etheen-PMO. Dit betekent dat in tegenstelling tot de etheen-PMO de structuur van de ethaan-PMO behouden blijft en dat de ethaan-PMO's een betere mechanische stabiliteit hebben.



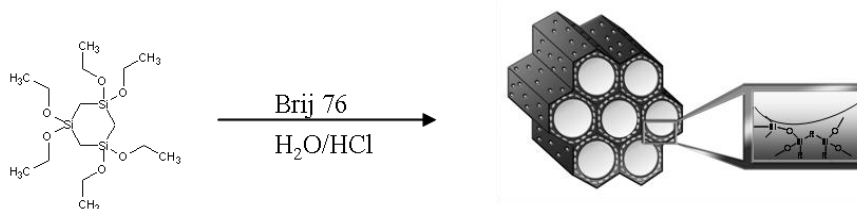
Figuur V: Eenheidscelwaarden (a_0) en porievolumes in ml/g (V_p) van ethaan-PMO's (C-CPMO's) en etheen-PMO's (C=CPMO's) voor en na mechanische compressie.

Na de hydrofobisering met HMDS is er geen significant verschil in stabiliteit voor en na de mechanische compressie bij de beide PMO's. Dit betekent dat de mechanische stabiliteit aanzienlijk verhoogd wordt door hydrofobisering. De reden hiervoor is de afwezigheid van geadsorbeerde watermoleculen. Die zorgen namelijk door de aangewende druk voor hydrolyse van de Si-O bindingen. Dit verklaart ook waarom de hydrofielere etheen-PMO's (zonder HMDS-behandeling) een mindere mechanische stabiliteit hebben dan de ethaan-PMO's.

Bij de test voor de chemische stabiliteit bleek dat alleen de HMDS-behandelde ethaan-PMO's niet opgelost werden in de basische oplossing en dus de beste chemische stabiliteit bezitten. Er werd wel een verschil in porievolume en ordening vastgesteld wat betekent dat deze materialen niet volledig bestand zijn tegen de basische moleculen.

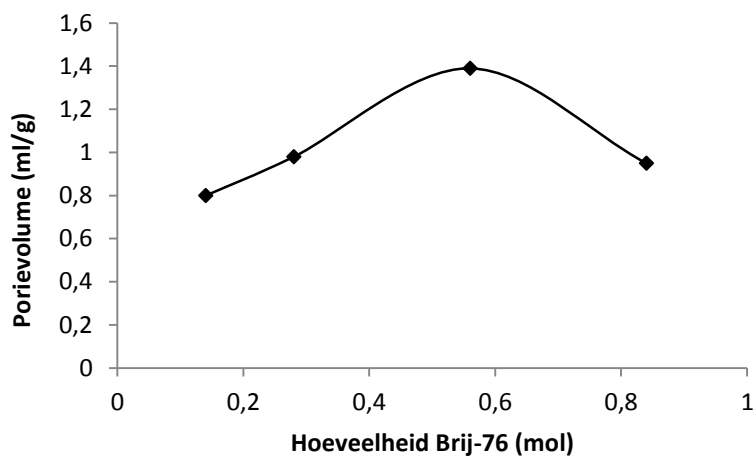
III Hydrofobe ring-PMO's met een zeer hoge stabiliteit

Voor de synthese van de ring-PMO's werd gebruik gemaakt van surfactant Brij-76 als templatmoleculen. De syntheseprocedure is schematisch voorgesteld in figuur VI.



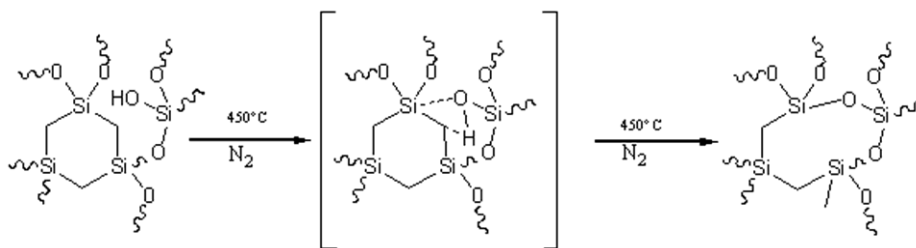
Figuur VI: Reactieschema voor de synthese van ring-PMO's met Brij-76 als templat.

Om een goede ordening van het materiaal te krijgen werd de HCl-concentratie geoptimaliseerd. Het porievolume kan gecontroleerd worden door de hoeveelheid surfactant in de startoplossing te veranderen met een optimum rond 0.56 mol voor 1 mol silaanprecursor (zie figuur VII).



Figuur VII: De invloed van de hoeveelheid surfactant op het porievolumen.

Hydrofobe ring-PMO's kunnen bekomen worden door een behandeling met HMDS of een thermische behandeling op 400°C onder stikstof. Bij dit proces worden enkele Si-C bindingen gebroken met vorming van hydrofobe, eindstandige methylgroepen en worden Si-O-Si bindingen gevormd waardoor ook het aantal hydrofiele silanolgroepen drastisch daalt. Dit proces is voorgesteld in figuur VIII.



Figuur VIII: Thermisch geïnduceerd silanol-eliminatieproces.

Gewone, thermisch en HMDS-behandelde ring-PMO's werden net zoals de de ethaan- en etheen-PMO's onderworpen aan hydrothermale, mechanische en chemische stabiliteitstesten. Alledrie de ring-PMO-materialen beschikken over een hoge stabiliteit, maar de HMDS-behandelde ring-PMO bezit de beste stabiliteit. Dit materiaal kan een stoombehandeling op 130°C gedurende minstens vijf dagen weerstaan alsook een mechanische compressie bij een druk van 272 MPa en een behandeling in een 1 M NaOH oplossing gedurende 2.5 uur zonder enige degradatie van de PMO-matrix.

IV Synthese van ethaan-PMO dunne lagen

Aangezien ethaan-PMO's over een goede mechanische en hydrothermale stabiliteit beschikken en de precursor relatief goedkoop is, werden eerst deze materialen als dunne lagen gemaakt via de 'evaporation induced self-assembly' methode waarbij surfactant Brij-76 als templaats en hoofdzakelijk siliciumwafers als substraat werden gebruikt.

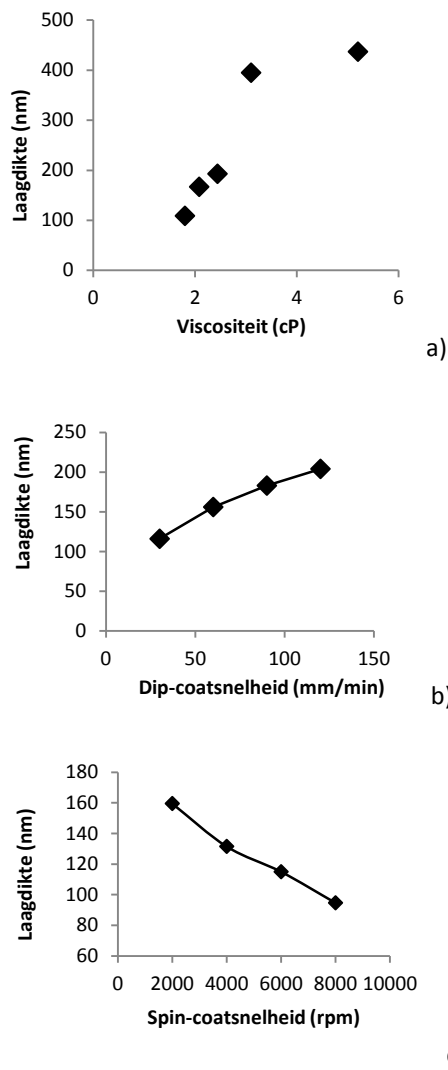
De films werden gesynthesiseerd via spin- en dip-coating van een oplossing bestaande uit de silaanprecursor, Brij-76, HCl, H₂O en ethanol als solvent. Hierbij werd zowel de invloed van de viscositeit als de dip- of spin-coatsnelheid op de laagdikte onderzocht.

De resultaten worden weergegeven in figuur IX. Hier is te zien dat hoe hoger de viscositeit hoe dikker de laag is. Hierbij moet wel opgemerkt worden dat het viscositeitsgebied om mooie uniforme lagen te krijgen beperkt is en de resultaten niet perfect reproduceerbaar zijn. Verder stijgt de laagdikte met toenemende dip-coatsnelheid en afnemende spin-coatsnelheid.

Alhoewel zowel dip- als spin-coating mogelijk is om uniforme PMO-lagen te synthetiseren werd voor verder onderzoek alleen spin-coating gebruikt aangezien afzetting slechts nodig is op 1 kant van het substraat.

Zoals bij de PMO-synthese in poedervorm kan de porositeit gecontroleerd worden door de hoeveelheid surfactant in het startmengsel te variëren. Hoe meer surfactant toegevoegd wordt, hoe hoger de porositeit en dus hoe lager ook de diëlektrische constante zal zijn. Een hogere porositeit resulteert echter ook in een lagere mechanische stabiliteit. Doordat ethaan-PMO's relatief hydrofiel zijn, konden geen lage diëlektrische constanten bereikt worden.

Na hydrofobisatie met HMDS bezitten de ethaan-PMO's een k -waarde van 2.15 bij een porositeit van 39% en een Young's modulus van 5 GPa. Deze waarden zijn echter niet beter (wel gelijkwaardig) dan de gerapporteerde waarden in de literatuur.

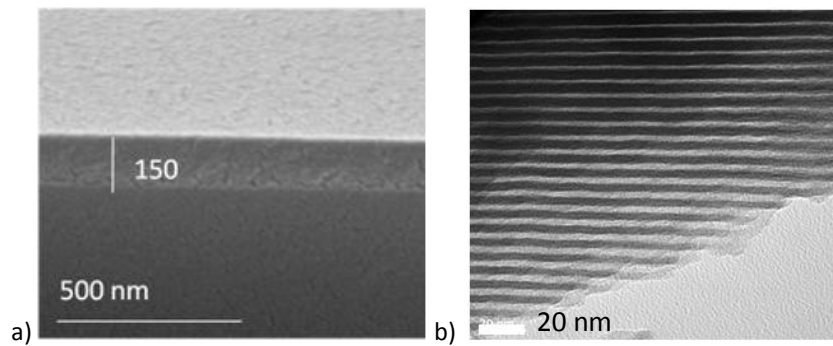


Figuur IX: De invloed van de a) viscositeit, b) dip- en c) spin-coatsnelheid op de laagdikte.

V Ring-PMO dunne lagen met een ultra-lage diëlektrisch constante en hoge chemische stabiliteit

Aangezien geen ultra-lage k -waarden ($k < 2$) bereikt werden met ethaan-PMO's, werd overgeschakeld op ring-PMO's. De lagen werden gemaakt via spin-coating van een mengsel bestaande uit 1,1,3,3,5,5-hexaethoxy-1,3,5-trisilacyclohexaan, HCl, water,

ethanol en Brij-76. Na surfactantverwijdering werd een film van 150 nm met uniforme poriën verkregen en dit wordt weergegeven in figuur X.

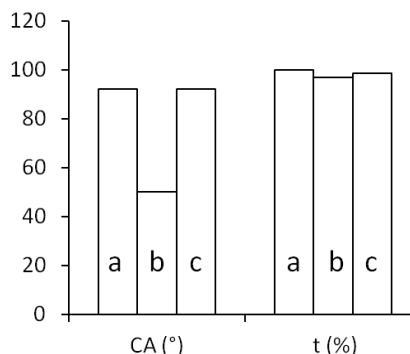


Figuur X: a) SEM en b) HRTEM afbeelding van een ring-PMO film.

Door de thermische behandeling na spin-coating is de laag hydrofoob (watercontacthoek = 92°). De totale porositeit van de laag is 55% en dit resulteert samen met het hydrofoob karakter in een ultra-lage k -waarde van 1.8. De Young's modulus van de laag is echter 2 GPa wat eigenlijk te laag is en dus is verdere optimalisatie hiervoor noodzakelijk. Na behandeling met HMDS werden geen verbeterde eigenschappen bekomen. De k -waarde steeg zelfs (1.93). Dit betekent dat een HMDS-behandeling overbodig is wanneer de diëlektrische film reeds hydrofoob is.

Om een idee te hebben over de chemische stabiliteit werden de lagen in een 1 M NaOH-oplossing gebracht gedurende 5 minuten en de dikte voor en na de behandeling werd bepaald. Het resultaat werd vergeleken met ring-PMO's gesynthetiseerd met CTAC (dit resulteert in kleinere poriën en dunnere poriewanden) en silica met gelijkaardige dikte en porositeit. In tegenstelling tot de laatste 2 materialen vertoont de ring-PMO gemaakt met Brij-76 geen verandering in dikte na de chemische behandeling.

Er werd wel een lagere contacthoek vastgesteld doordat enkele siloxaanbindingen gehydrolyseerd werden tijdens de behandeling. Deze contacthoek kan echter hersteld worden met een thermische behandeling waardoor er terug siloxaanverbindingen gevormd worden door hercondensatie van de ontstane silanolgroepen. Ook bij dit proces verandert de dikte niet (zie figuur XI).

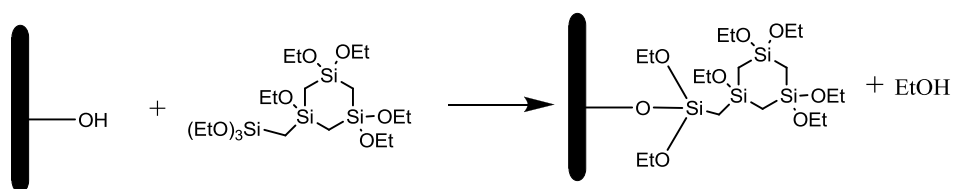


Figuur XI: Verandering in contacthoek (CA) en procentuele dikteverandering (t) van ring-PMO lagen (a) na een basische behandeling (b), gevolgd door een thermische behandeling (c).

VI Poriesluiting

Doordat de poriën van de meest poreuze diëlektrische lagen mesoporeus zijn, kunnen niet gewenste chemicaliën en/of metaalionen vrij gemakkelijk in de laag diffunderen en dit leidt tot verminderde diëlektrische eigenschappen of zelfs kortsluiting. Daarom moeten de porie-openingen voldoende vernauwd worden of, zelfs beter, volledig afgesloten worden.

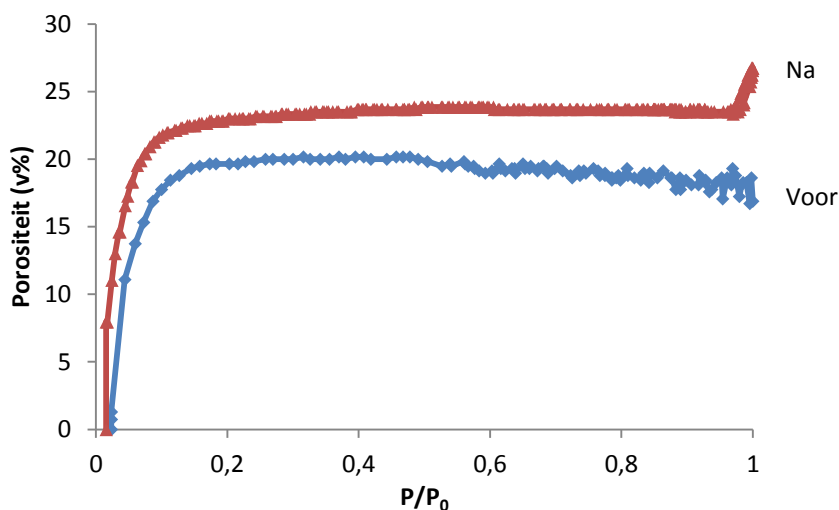
Een eerste methode die in deze thesis ontwikkeld en geëvalueerd werd, is grafting aan poreuze silica materialen met gesubstitueerde cyclische organosilaanprecursoren weergegeven in onderstaande reactie. Deze graftingsmoleculen hebben als voordeel dat ze vrij volumineus zijn en een lage diëlektrische constante bezitten.



Hierbij moet wel vermeden worden dat grafting ook gebeurt in de poriën zelf. Dit is mogelijk door het templaot nog niet te verwijderen tijdens de graftingsreactie. Nadien kan het templaot verwijderd worden en kunnen de inwendige OH-groepen vervangen worden door $\text{Si}(\text{CH}_3)_3$ -groepen door behandeling met HMDS. Dit proces leidt tot een vernauwing van de poriën waarbij de totale porositeit kan behouden blijven.

Deze methode kan ook succesvol toegepast worden op organosilica dunne lagen wat toekomstmogelijkheden biedt naar industriële toepassingen (zie de toluenadsorptie-

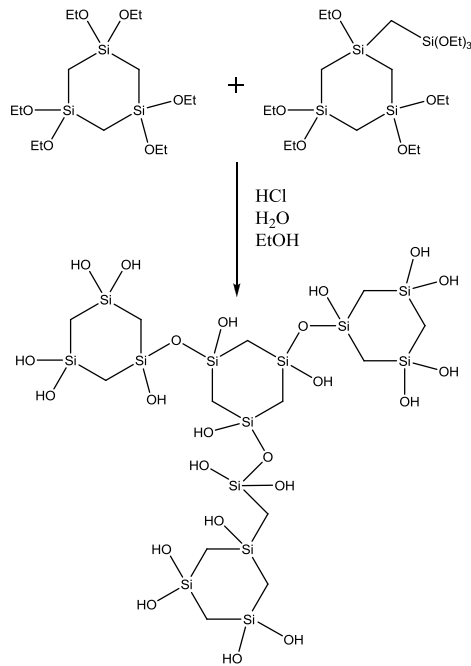
isothermen in figuur XII). De adsorptie van toluen gebeurt bij een iets lagere druk na de grafting wat wijst op vernauwing van de poriën. De totale porositeit is zelfs iets hoger na de grafting doordat het materiaal nu hydrofoob geworden is en er dus geen watermoleculen in de poriën aanwezig zijn.



Figuur XII: Tolueneadsorptie-isotherm van een organosilicafilm voor en na grafting gevolgd door HMDS-behandeling.

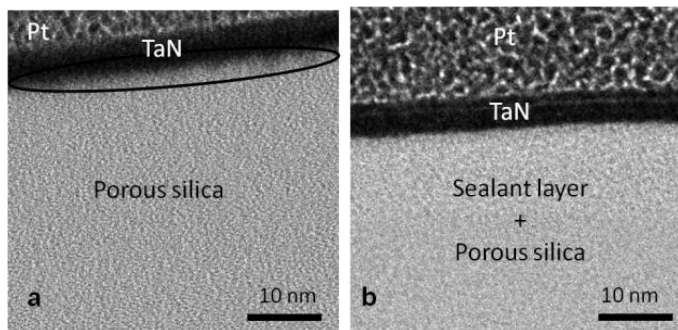
In principe zou het nu ook mogelijk zijn om de poriën volledig af te sluiten door verdere grafting aan de cyclische silaanmoleculen. Dit is echter nog niet op punt en verder onderzoek hieromtrent is noodzakelijk.

De tweede porieafsluitmethode die onderzocht werd, is de depositie van een organosilicalaag op een poreuze silicafilm via spin-coating vertrekkende van reeds geoligomeriseerde cyclische organosilaanprecursoren (zie figuur XIII). De oligomeren zijn groter dan de porie-openingen waardoor deze niet kunnen diffunderen in de poreuze laag. De afgezette toplaag heeft als voordeel een lage *k*-waarde te hebben door de aanwezigheid van weinig polariseerbare groepen in het netwerk.



Figuur XIII: Vorming van organosilaanligomeren.

Na de depositie van deze toplaag is het mogelijk om diffusie van metaalionen te verhinderen, terwijl dit niet mogelijk is wanneer er geen toplaag aanwezig is. Dit werd aangetoond door TaN af te zetten op een poreuze film met open en gesloten poriën (figuur XIV).

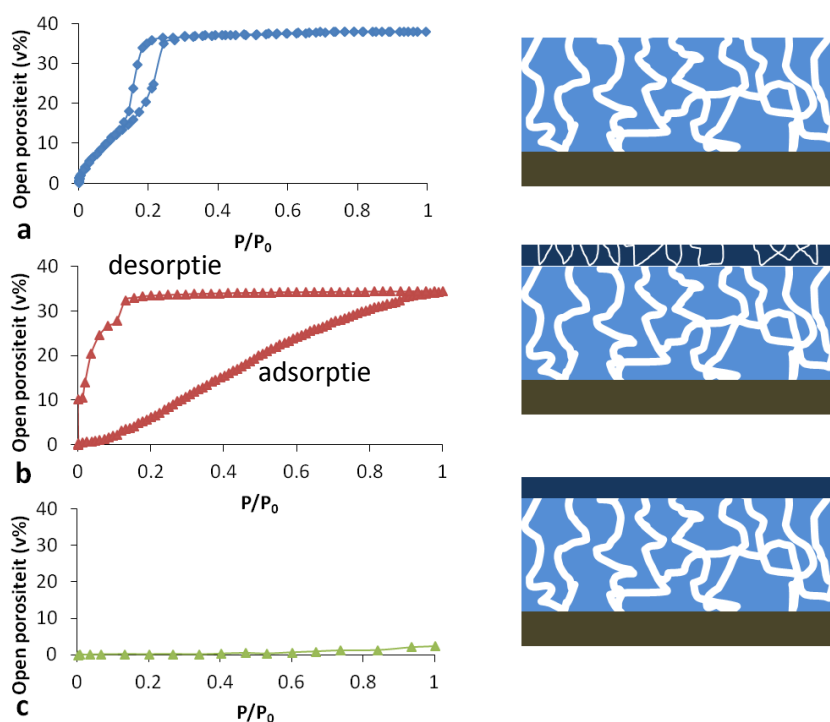


Figuur XIV: TaN-depositie op poreuze lagen (a) en op poreuze lagen waarop eerst nog een toplaag werd afgezet (b).

Solventen kunnen echter nog steeds doordringen in het materiaal hoewel het sterk verhinderd wordt. Dit is duidelijk te zien aan de vorm van de toluenisotherm in figuur XV b.

Samenvatting in het Nederlands

Om ook dit te verhinderen werd het materiaal na de depositie nog verder behandeld met HMDS en dit zorgde ervoor dat de poriën ook afgeschermd zijn voor toluëenmoleculen (figuur XV c).



Figuur XV: Toluëenfysisorptie-isothermen en schematische voorstelling van a) een mesoporeuze laag met open poriën, b) na depositie van de organosilica-toplaag en c) na HMDS-behandeling.

Aangezien diffusie van metaalionen reeds kan verhinderd worden door de depositie van de toplaag werd deze methode ook getest op ethaan-PMO dunne lagen. Hierbij werd het effect van deze depositie op de diëlektrische constante (k), lekstroom (I), watercontacthoek (CA), Young's modulus (E) en hardheid (H) onderzocht. De resultaten worden weergegeven in tabel I.

Tabel I: de porositeit (P), contacthoek (CA), k -waarde (k), Young's modulus (E), lekstroom (I) en hardheid (H) van ethaan-PMO (EPMO) en ethaan-PMO met een toplaag (EPMOD).

staal	P (%)	CA (°)	k -waarde	E (GPa)	I at 3 MV/cm (A/cm ²)	H (GPa)
EPMO	38	68	2.5	5.32	2.52E-05	0.58
EPMOD	41.5	71	2.07	5.86	5.07E-08	0.73

Uit deze tabel blijkt dat zowel de elektrische (k en l) als de mechanische eigenschappen (E en H) significant verbeteren na de depositie van de toplaag wat maakt dat deze methode interessant is om te proberen implementeren in het integratieproces van poreuze materialen in geïntegreerde circuits.

VII Algemeen besluit

Voor dit doctoraatsonderzoek werden ethaan-, etheen en ring-PMO's gesynthetiseerd door gebruik te maken van niet-ionische surfactanten als templaatmoleculen met als doel deze materialen te evalueren op hun toepasbaarheid als diëlektrische laag in geavanceerde microchips. Hiervoor werden belangrijke parameters zoals de porositeit, poriegrootte, hydrofobiciteit, hydrothermale, mechanische en chemische stabiliteit en diëlektrische constante bepaald.

In het eerste deel werden deze materialen in poedervorm gesynthetiseerd om een vlugge en eenvoudige karakterisatie toe te laten. Hierbij werd gevonden dat de etheen-PMO's een mindere stabiliteit bezitten vergeleken met de ethaan- en ring-PMO's en deze werd niet meer verder in het onderzoek betrokken.

In het tweede deel werden ethaan- en ring-PMO's succesvol gesynthetiseerd als dunne lagen met hoge porositeit via spin-coating. Wanneer we de ethaan-PMO's beschouwen, kan besloten worden dat hydrofobe lagen mogelijk zijn door behandeling met HMDS. Deze PMO's hebben een k -waarde van 2.15 en een Young's modulus van 5 GPa. Deze waarden zijn vergelijkbaar met de *state-of-the-art* lage- k materialen.

Anderzijds kunnen hydrofobe ring-PMO's verkregen worden zonder extra HMDS-behandeling en deze materialen hebben een zeer lage k -waarde van 1.8 en een hoge chemische stabiliteit. De mechanische stabiliteit is echter nog voor verbetering vatbaar. Indien deze materialen met HMDS behandeld werden, werden geen verbeterde eigenschappen verkregen.

In het laatste deel werden twee methodes om de poriën te vernauwen of af te sluiten ontwikkeld. De eerste methode moet nog verder uitgewerkt worden, maar toont reeds aan dat de poriegrootte kan verkleind worden door grafting aan het poreus materiaal met organosilicane-precursoren zonder dat de porositeit significant verandert.

De tweede methode is het afsluiten van de poriën door depositie van een organosilicalaag bovenop de poreuze laag. Diffusie in de poriën wordt vermeden door de organosilicane-precursoren eerst te laten oligomeriseren waardoor de fragmenten te groot worden om de poriën binnen te dringen.

Samenvatting in het Nederlands

Verder zorgt deze methode ervoor dat ook verbeterde elektrische en mechanische eigenschappen van de onderliggende poreuze laag verkregen worden. Deze resultaten maken dat deze methode veelbelovend is voor verder onderzoek naar de integratiemogelijkheid in geavanceerde microchips.

Scientific Activities

A1 publications

- 1 T. R. M. De Beer, M. Alleso, F. Goethals, A. Coppens, Y. V. Heyden, H. L. De Diego, J. Rantanen, F. Verpoort, C. Vervaet, J. P. Remon and W. R. G. Baeyens, *Anal Chem*, 2007, **79**, 7992-8003.
- 2 F. Goethals, C. Vercaemst, V. Cloet, S. Hoste, P. Van Der Voort and I. Van Driessche, *Micropor Mesopor Mat*, 2010, **131**, 68-74.
- 3 F. Goethals, B. Meeus, A. Verberckmoes, P. Van der Voort and I. Van Driessche, *J Mater Chem*, 2010, **20**, 1709-1716.
- 4 F. Goethals, M. R. Baklanov, I. Ciofi, C. Detavernier, P. Van Der Voort and I. Van Driessche, *Chem. Commun.*, 2012, **48**, 2797-2799.
- 5 F. Goethals, I. Ciofi, O. Madia, K. Vanstreels, M. R. Baklanov, C. Detavernier, P. Van Der Voort and I. Van Driessche, *J Mater Chem*, 2012, **22**, 8281-8286.
- 6 P. Van Der Voort, D. Esquivel, E. De Canck, F. Goethals, I. Van Driessche, and F. Romero-Salguero, *Chem. Soc. Rev.*, DOI:10.1039/C2CS35222B.
- 7 F. Goethals *et al.*, pore sealing by top layer deposition full paper in preparation.
- 8 F. Goethals *et al.*, pore sealing through grafting in preparation.

Patent

Title: METHOD FOR PORE SEALING OF A POROUS MATERIAL AND THE SEALED POROUS MATERIAL THEREOF

Inventors: F. Goethals, M. R. Baklanov, P. Van Der Voort, I. Van Driessche

UGent ref: P2011/056 - IMEC - CARBON-BRIDGED SILICAS

23/09/2011 (= priority date); US 61/538,431

US provisional

Oral presentations

1. 10^{de} Vlaams jongerencongres van de chemie VJC 1
Periodic Mesoporous Organosilicas as Potential Low-k Materials
Goethals, Frederik; Van Der Voort, Pascal; Van Driessche, Isabel
2010, Blankenberge, Belgium.

Scientific activities

2. Electroceramics XII
Hydrophobic Porous Organosilica Thin Films for Application as Low-k Material
Goethals, Frederik; Van Der Voort, Pascal; Van Driessche, Isabel
2010, Trondheim, Norway.
3. Nano VI
Ultra Low-k Mesoporous Organosilicas with an Improved Mechanical Stability
F. Goethals, P. Van Der Voort, I. Van Driessche
2011, Banff, Canada.
4. MRS Spring 2012
Pore sealing of high porosity mesoporous silica films by self-assembled carbon-bridged organosilicas
F. Goethals, M. R. Baklanov, P. Van Der Voort, I. Van Driessche
2012, San Francisco, USA.

Poster presentations

1. Dutch Zeolite Association (DZA).
Comparative study of ethylene- and ethenylene-bridged periodic mesoporous organosilicas
F. Goethals, P. Van Der Voort, I. Van Driessche
2008, Brussels, Belgium.
2. IMMS 2008
Comparative study of ethylene and ethenylene-bridged Periodic Mesoporous Organosilicas
Goethals, Frederik; Vercaemst, Carl; Van Der Voort, Pascal; Van Driessche, Isabel
2008, Namur, Belgium.
3. Doctoraatssymposium faculteit wetenschappen
Nanoporous organosilica thin films for application as low-k material
Goethals, Frederik; Van Der Voort, Pascal; Van Driessche, Isabel
2009, Ghent, Belgium.
4. International Symposium on Advanced Complex Inorganic Nanomaterials
Periodic Mesoporous organosilicas with ultra-low dielectric constants and an improved mechanical stability
F. Goethals, P. Van Der Voort, I. Van Driessche
2011, Namur, Belgium.

Table of Contents

<u>Preface</u>		i
<u>Dankwoord</u>		ii
<u>Samenvatting in het Nederlands</u>		iv
I	Inleiding en doelstelling	iv
II	Vergelijkende studie tussen ethaan en etheen PMO's	vii
III	Hydrofobe ring-PMO's met een zeer hoge stabiliteit	x
IV	Synthese van ethaan-PMO dunne lagen	xii
V	Ring-PMO dunne lagen met een ultra-lage diëlektrische constante en hoge chemische stabiliteit	xiii
VI	Poriesluiting	xv
VII	Algemeen besluit	xix
<u>Scientific Activities</u>		xxi
<u>Abbreviations</u>		xxvii
<u>Outline</u>		xxxii
<u>Chapter One: Introduction to Low-k Materials</u>		1
1.1	Integrated circuits	2
1.2	Low-k materials	4
1.3	Deposition methods	7
1.4	Evolution of low-k materials	10
1.4.1	<u>Fluorosilicate glasses (FSG)</u>	11
1.4.2	<u>Organic polymers</u>	12
1.4.3	<u>Organosilicate glasses (OSGs)</u>	16
1.4.4	<u>Porous materials</u>	19
1.5	References	27
<u>Chapter Two: The Search for Ultra Low-k Materials ($k < 2$)</u>		31
2.1	Introduction	32
2.2	Zeolites	34
2.3	Metal organic frameworks (MOFs)	36
2.4	Periodic Mesoporous Organosilicas (PMOs)	38
2.4.1	<u>General information</u>	38

Table of contents

2.4.2	<u>Multi organic-bridged PMOs</u>	41
2.4.3	<u>PMOs as low-k materials</u>	43
2.5	Aim of the PhD research	48
2.6	References	49
<u>Chapter Three: Comparative Study of Ethylene- and Ethenylene-Bridged Periodic Mesoporous Organosilicas</u>		52
3.1	Introduction	53
3.2	Experimental section	54
3.2.1	<u>Materials</u>	54
3.2.2	<u>Synthesis of C-CPMOs</u>	54
3.2.3	<u>Synthesis of the C=CPMOs</u>	54
3.2.4	<u>Hydrothermal, mechanical and chemical stability</u>	55
3.2.5	<u>Characterization</u>	56
3.3	Results and discussion	56
3.3.1	<u>The influence of butanol</u>	56
3.3.2	<u>Hydrothermal stability</u>	60
3.3.3	<u>Mechanical stability</u>	63
3.3.4	<u>Chemical stability</u>	67
3.4	Conclusions	68
3.5	References	70
<u>Chapter Four: Hydrophobic High Quality Ring PMOs with a very High Stability</u>		71
4.1	Introduction	72
4.2	Experimental section	73
4.2.1	<u>Chemicals</u>	73
4.2.2	<u>Synthesis</u>	73
4.2.3	<u>After treatment steps</u>	75
4.2.4	<u>Characterization</u>	75
4.3	Results and discussion	76
4.3.1	<u>Optimization of the synthesis method</u>	76
4.3.2	<u>Hydrophobicity study</u>	81
4.3.3	<u>Hydrothermal, mechanical and chemical stability</u>	83
4.4	Conclusions	89
4.5	References	91
<u>Chapter Five: Synthesis of Ethane PMO Films</u>		92
5.1	Introduction	93
5.2	Experimental section	93
5.2.1	<u>Chemicals</u>	93
5.2.2	<u>Synthesis</u>	94

5.2.3	<u>Characterization</u>	94
5.3	Results and discussion	96
5.3.1	<u>Dip- and spin-coating of ethane PMOs</u>	96
5.3.2	<u>Influence of the porosity and hydrophobicity on respectively the mechanical stability and dielectric constant</u>	100
5.4	Conclusions	102
5.5	References	103
<u>Chapter Six: Ultra low-k Cyclic Carbon-Bridged PMO Films with a High Chemical Resistance</u>		104
6.1	Introduction	105
6.2	Experimental section	106
6.2.1	<u>Chemicals</u>	106
6.2.2	<u>Synthesis</u>	106
6.2.3	<u>Characterization</u>	107
6.3	Results and discussion	108
6.4	Conclusions	116
6.5	References	118
<u>Chapter Seven: Pore Sealing</u>		119
7.1	Introduction	120
7.1.1	<u>Pore sealing by plasma treatment</u>	120
7.1.2	<u>Sealant deposition</u>	122
7.1.3	<u>New strategies</u>	125
7.2	Experimental section for sealing through grafting	127
7.2.1	<u>Chemicals</u>	127
7.2.2	<u>Synthesis</u>	127
7.2.3	<u>Characterization</u>	128
7.3	Results and discussion for sealing through grafting	129
7.3.1	<u>Grafting on MCM-41 without the presence of surfactant</u>	129
7.3.2	<u>Grafting on MCM-41 where the surfactant was initially left inside</u>	134
7.4	Conclusions for sealing through grafting	138
7.5	Supporting information: NMR study of the substituted cyclic organosilane precursor	139
7.6	Experimental section for sealing with top layer deposition	141
7.6.1	<u>Chemicals</u>	141
7.6.2	<u>Synthesis</u>	141

Table of contents

7.6.3	<u>Characterization</u>	142
7.7	Results and discussion for sealing with top layer deposition	143
7.7.1	<u>Investigation of effective sealing</u>	143
7.7.2	<u>Impact on the electrical and mechanical properties</u>	147
7.8	Conclusions for sealing with top layer deposition	149
7.9	References	151
<u>Chapter Eight: General Conclusions and Outlook</u>		153
8.1	General Conclusions	154
8.2	Outlook	156
8.2.1	<u>Concerning PMO as low-k materials</u>	156
8.2.2	<u>Concerning pore sealing</u>	157
8.3	References	160
<u>Appendix: Applied Characterization Methods for Thin Film Analysis</u>		161
A.1	Ellipsometry	162
A.2	Ellipsometric porosimetry	166
A.3	Nano-indentation	168
A.4	C-V measurements	171
A.5	References	175

Abbreviations

3M3VTSO	trimethyltrivinylcyclotrisiloxane
3MS	trimethylsilane
4MS	tetramethylsilane

A

AC	alternating current
ALD	atomic layer deposition

B

BET	Brunauer-Emmett-Teller
BJH	Barrett, Joyner & Halenda
Brij-30	polyoxyethylene (4) lauryl ether
Brij-56	polyoxyethylene (10) cetyl ether
Brij-76	polyoxyethylene (10) stearyl ether
BTESA	1,2-bis(triethoxysilyl) ethane
BTESE	1,2-bis(triethoxysilyl) ethene
BuOH	butanol

C

C=CPMOs	ethenylene-bridged periodic mesoporous organosilica
CA	contact angle
C-CPMOs	ethylene-bridged periodic mesoporous organosilica
cmc	critical micelle concentration
CMP	chemical mechanical polishing
C _n TMAB	alkyltrimethylammonium bromide
C _n TMACl	alkyltrimethylammonium chloride
COSY	correlation spectroscopy
CSM	continuous-stiffness measurement
CTAB	cetyltrimethylammonium bromide
CTAC	cetyltrimethylammonium chloride
CVD	chemical vapor deposition

D

DC	direct current
----	----------------

Abbreviations

DCM	dynamic contact module
DEMS	diethoxymethylsilane
DMDMOMS	dimethyldimethoxysilane
DMDOSH	dimehyldioxysilylcyclohexane
DMOMS	dimethoxymethylsilane
DMPCSO	decamethylcyclopentasiloxane
DMPS	dimethylphenylsilane
DPMS	diphenylmethylsilane
DRIFT	diffuse reflectance infrared fourier transform

E

EISA	evaporation induced self-assembly
EP	ellipsometric porosimetry
EPMO	ethane periodic mesoporous organosilica
EPMOD	ethane periodic mesoporous organosilica with organosilica top deposition
EtOH	ethanol

F

F127	poly(ethylene glycol)-poly(propylene glycol)-poly(ethylene glycol)
FIB	focused ion beam
FSG	fluorosilicate glass
FWHM	full width at half maximum

H

HDP-CVD	high density plasma chemical vapor deposition
HEPMO	HMDS treated ethane periodic mesoporous organosilica
HEPMOD	HMDS treated ethane periodic mesoporous organosilica with organosilica top layer
HMBC	heteronuclear multiple bond correlation
HMCTSO	hexamethylcyclotrisiloxane
HMDS	hexamethyldisilazane
HMDSO	hexamethyldisiloxane
HRTEM	high resolution transmission electron microscopy
HSQC	heteronuclear single quantum coherence

I

IC	integrated circuit
----	--------------------

ICP	inductive coupled plasma
ILD	interlayer dielectric
ITRS	international roadmap for semiconductors

M

MCM	Mobile composition of matter
MIS	metal insulator semiconductor
MOF	metal organic framework
MSE	Mean Squared Error
MTES	methyltriethoxysilane

N

NMR	nuclear magnetic resonance
-----	----------------------------

O

OMCTS	octamethylcyclotetrasiloxane
OSG	organosilicate glass
OTAB	octadecyltrimethylammonium bromide
OTAC	octadecyltrimethylammonium chloride

P

P123	poly(ethylene glycol)-poly(propylene glycol)-poly(ethylene glycol)
PC	personal computer
PECVD	plasma enhanced chemical vapor deposition
PMD	periodic mesoporous dendrisilicas
PMO	periodic mesoporous organosilica
p-plane	parallel to the plane of incidence
PSZ	pure silica zeolites
PVD	physical vapor deposition

R

rf	radio frequency
RI	refractive index
RPMO	ring periodic mesoporous organosilicas

S

SBA	Santa-Barbara amorphous materials
-----	-----------------------------------

Abbreviations

SDS	sodium dodecyl sulfate
SE	spectroscopic ellipsometry
SEM	scanning electron microscopy
SOG	spin-on organosilica
s-plane	perpendicular to the plane of incidence

T

TDSCH	1,3,5[tris(diethoxy)sila]cyclohexane
TEM	transmission electron microscopy
TEOS	tetraethyl orthosilicate
T _g	glass transition temperature
TGA	thermogravimetric analysis
THF	tetrahydrofuran
TMCS	trimethylchlorosilane
TMCTS	tetramethylcyclotetrasiloxane
TMOS	tetramethyl orthosilicate
TMSC	trimethylsilylchloride
TVMS	trivenylmethylsilane
TVTMCTS	tetravinyltetramethylcyclotetrasiloxane

U

UV	ultra-violet
----	--------------

W

WCA	water contact angle
-----	---------------------

X

XRD	X-ray diffraction
-----	-------------------

Z

ZLK	zeolite-like low-k
-----	--------------------

Outline

The first two chapters provide a background and literature overview related to the PhD research work. Chapters 3 to 7 contain the experimental work and their results. The conclusions and outlook are provided in chapter 8.

Chapter one briefly explains the building and evolution of integrated circuits as well as the important role of interlayer dielectrics (low-k materials) in the further progress and improvement of these integrated circuits. Also three possible deposition techniques to obtain low-k films are described and an overview of different low-k materials is given.

Chapter two evaluates three classes of materials with potential ultra low-k properties. The classes are zeolites, metal organic frameworks and periodic mesoporous organosilicas. From these three candidates, we have selected PMOs to investigate and tune their low-k properties. The aims of this research are also included at the end of this chapter.

Chapter three compares the synthesis conditions of ethane and ethene PMOs to obtain materials with a narrow pore size distribution. Furthermore, the hydrothermal, mechanical and chemical stability of both PMOs are compared.

Chapter four presents the synthesis of high quality hydrophobic ring PMOs with excellent hydrothermal, mechanical and chemical stability.

Chapter five describes how to synthesize ethane PMO films by dip- and spin-coating using the evaporation induced self-assembly method. Next the influence of the viscosity and dip- or spin-coat rate on the thickness of the films is investigated as well as the influence of the surfactant concentration on the porosity. In a second part, the influence of the porosity on the mechanical stability and the effect of the hydrophobicity on the dielectric constant are investigated.

Chapter six presents the synthesis of ring PMO films that combine an ultra-low dielectric constant with a high chemical stability.

Chapter seven focuses on the pore sealing of nanoporous materials. Firstly, the importance of pore sealing is explained and an overview of possible pore sealing methods with their advantages and disadvantages is presented. Secondly, two new pore sealing methods are developed and evaluated for their pore sealing efficiency.

Chapter eight summarises the main findings of this PhD work and provides suggestions for further research.

Chapter One: Introduction to Low-k Materials

In this chapter the building and evolution of integrated circuits (ICs) is briefly explained as well as the important role of interlayer dielectrics (low-k materials) in the further progress and improvement of these ICs. Also three possible deposition techniques to obtain low-k films are described and an overview of different low-k materials is given.

1.1 Integrated circuits

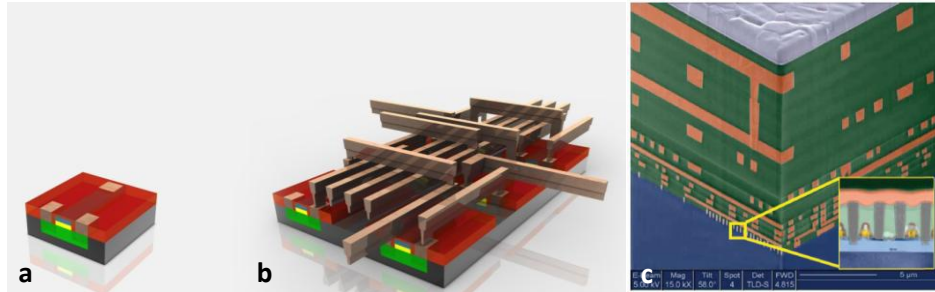


Figure 1.1: A schematic figure of a) a transistor and b) the connected transistors through electrically conductive wires,¹ and c) a cross section of an integrated circuit.²

The development of the microprocessor, which consists of an integrated circuit (IC), in 1971 made it possible to build the first personal computers (PCs). However, these PCs were slow and huge in size. Fortunately, due to the many still ongoing improvements made by the microelectronic industry, the PCs evolved from clunky commercial flops to slick, high-power machines that play a huge role in our daily lives, both for work and play. These better performances of PCs could mainly be attributed to the improvement of the ICs.³

An IC or microchip is an electronic circuit consisting of transistors and capacitors that are connected through electrically conductive wires. A schematic structure is shown in figure 1.1. A silicon wafer is used as base to build the electronic components which are forming the transistor or capacitor (figure 1.1a). The capacitors can be charged or discharged and are used to store data. The transistors function as digital data switches thereby controlling the digital data transfers through the system. These transistors are then connected by the electrically conductive wires to form an integrated circuit (figure 1.1b).¹ A detailed explanation about the principles of a chip will not be provided here, because this is beyond the scope of this thesis.

Better performances of ICs have been achieved by increasing the transistor speed, reducing the transistor size and packing more transistors onto a single chip. Gordon Moore, one of the founders of the Intel Company, already predicted in 1965 that the amount of transistors on the same chip doubles every two year. This is also known as Moore's law.⁴ Nowadays, it is possible to put more than two billion transistors on a chip.

The decrease in size of the transistor also implements a decrease in size of the interconnecting wires. However this shrinking increases the resistance (R) of the wires and this reduces the speed of the ICs. In real devices, these interconnects are insulated

by interlayer dielectrics (ILDs) as shown in figure 1.2. Since the beginning of the development of microelectronic devices, the insulator has been silicon dioxide (SiO_2) because SiO_2 has excellent properties for device manufacturing. It has a thermal stability above 500°C , a very high electrical breakdown ($> 6 \text{ MV cm}^{-1}$), a low leakage current and an exceptional mechanical stability (a Young's modulus between 55 and 73 GPa).²

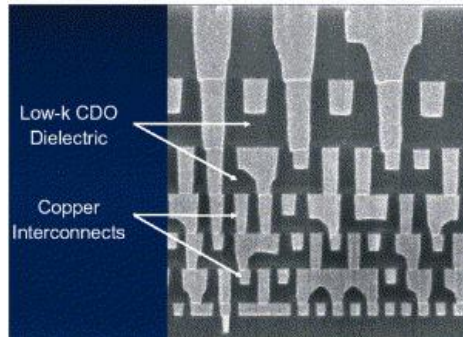


Figure 1.2: Cross-section of interconnections.⁵

However, the combination of the wires and the ILD acts as a capacitor and the created capacitance (C) also causes a signal delay. Bringing the interconnect wires closer together increases the capacitance between the wires. This phenomenon, the increased delay due to the resistance and capacitance, is known as RC -delay. So, this means that RC -delay increases when the device size decreases. This RC -delay will eventually exceed the transistor speed, limiting the performance improvement of the devices. The mathematic equation of the RC -delay is given by:⁶

$$RC = 2\rho k\epsilon_0 (4L^2/P^2 + L^2/T^2) \quad (1.1)$$

With:

- R = line resistance
- C = line capacitance
- L = line length
- P = metal pitch
- T = metal thickness
- ρ = resistivity
- ϵ = dielectric constant

To reduce the problem of RC -delay, two pathways can be followed. The first one is to lower the resistance of the wires by using metals with lower resistivity. Therefore, the

conventional Al wires were changed by Cu interconnects which have a 36% less resistivity.⁵

The second pathway is the replacement of the SiO₂ insulator by materials that have a lower relative dielectric constant (k) than 3.9 (*i. e.* dielectric constant of silicon dioxide) and these are called low-k materials. Although it is likely that all the properties, except the dielectric constant, of these low-k materials will be inferior compared to SiO₂, the replacement of the standard insulator is necessary to develop advanced ICs.⁷ Another issue is that miniaturization of the ICs also introduces cross talk.⁸ This means that signals from one conducting wire can interfere with the signals of another wire. Fortunately, this problem can also be solved by lowering the dielectric constant of the insulating material.

Another advantage of the incorporation of low-k materials is a lower power consumption of the devices because the power consumption is a function of the driving voltage V of the device, the operational frequencies f , and the capacitance C which is proportional to the k -value of the dielectric.⁶

$$Power = CV^2 f \quad (1.2)$$

1.2 Low-k materials

Low-k materials are materials that have a low relative dielectric constant compared to silicon dioxide. The dielectric constant or k -value is a measure of how easily a material is polarized in an external electric field. The k -value can be determined by measuring the capacitance of a parallel plate capacitor using the low-k material as dielectric.⁹ A capacitor consists of two electrical conducting plates separated by an electrical insulating material (dielectric). Also the distance between the plates is negligible compared to the plate area. A schematic illustration is shown in figure 1.3.

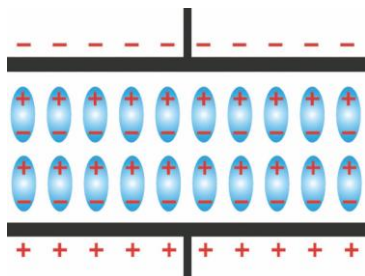


Figure 1.3: Schematic drawing of a parallel plate capacitor.⁵

A capacitor can be used to store energy and release it when the power supply is shut down. The capacitance (C) of the capacitor can be defined as the ratio of charge (Q) on each conductor to the voltage (V) between them.

$$C = Q / V \quad (1.3)$$

Considering a parallel plate capacitor, the capacitance can be determined by the dimensions of the plates and the dielectric. This leads to the following equation:

$$C = \epsilon A / d \quad (1.4)$$

With:

- ϵ = the permittivity or dielectric constant of the dielectric
- A = the plate area
- d = the distance between the plates

The permittivity of a material (ϵ) is often compared to the permittivity of vacuum (ϵ_0) which is equal to $8.85 * 10^{-12}$ F/m. The relative dielectric constant (k) can then be written as:

$$k = \epsilon / \epsilon_0 \quad (1.5)$$

The following equation, also known as the Clausius-Mossotti equation, shows that the k -value is dependant on the density (N) and polarizability (α) of the material.⁶

$$(k - 1) / (k + 2) = 4\pi/3 N\alpha \quad (1.6)$$

So from equation 1.6 follows that the dielectric constant can be lowered by decreasing the total polarizability and density of the material. The polarizability can be decreased by incorporating low polarisable chemical bonds such as Si-C, C-H, Si-H, Si-F, C-F and C-C.⁵ The decrease of the density of the low-k material can be achieved by two methods. The first method is increasing the free volume by a rearrangement of the material structure. This is known as constitutive porosity. However, the obtained porosity is mostly less than 15%. The second method is the addition of sacrificial substances during the manufacturing. These substances can be removed usually by thermal degradation, resulting in a porous material. The advantage of this approach is that very high porosities (more than 50%) can be obtained. This porosity is called subtractive porosity.⁵

Besides a low dielectric constant, these low-k materials should also have a lot of other good properties as well, preferably close to the superior properties of SiO₂.^{2, 5-12} A first important property is the mechanical stability. The low-k material should be stable

enough to withstand the manufacturing processes. This is mainly due to the replacement of Al conductors by Cu conductors. When Al was used, gaseous Al was deposited on the substrate and patterns were created by lithography processes and plasma etching. Then, the remaining gaps were filled with SiO_2 . Nowadays, Cu is the common metallization material. Therefore, the deposition scheme is reversed because Cu does not form volatiles during plasma etching (see figure 1.4).

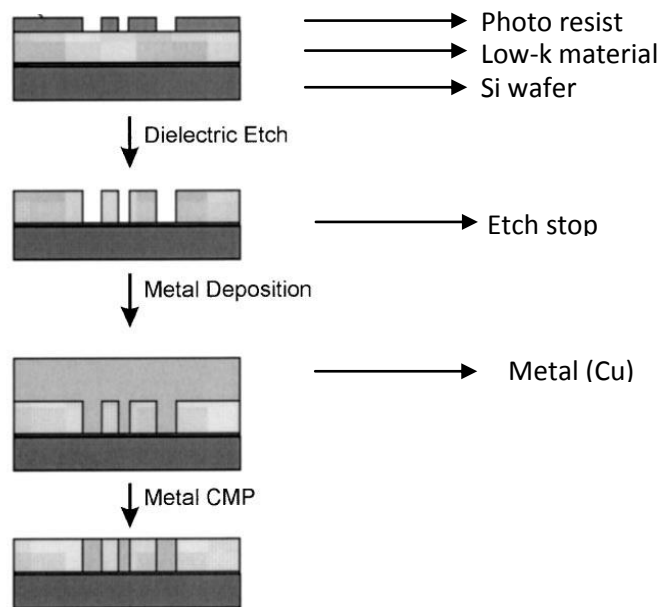


Figure 1.4: Interconnect fabrication scheme (single damascene).¹⁰

So, first the dielectric will be deposited and trenches are created by plasma etching. Electroplating is then applied to fill the trenches with Cu and the excess of Cu is polished away via a chemical and mechanical polishing process (CMP). During this process, an aqueous slurry, containing an abrasive (alumina particles) and an oxidant and/or a complexing agent ($\text{HNO}_3/\text{NH}_4\text{OH}$), polishes the metal surface. The abrasive removes particles from the surface and these particles are dissolved as Cu salts or as complexes, leading to planarization of the metal surface.¹⁰ So, the low-k material has to withstand this CMP. Also, a good mechanical stability of the ILD is needed during packing and transportation of the devices.

A second required property is hydrophobicity.⁶ The low-k material has to be hydrophobic to avoid water adsorption especially when it is porous. This is because water has a high dielectric constant ($k_{\text{H}_2\text{O}} = 80$) and this will increase the dielectric

constant and decrease the breakdown voltage of the material dramatically.¹³ When the ILD is porous and possesses a large surface area, even more water can adsorb and this will destroy the low-k property completely. By incorporating hydrophobic functional groups such as Si-CH₃ or Si-H, a hydrophobic ILD material can be obtained.¹¹ Another issue concerning porous materials is that the pores have to be closed to avoid diffusion of metals or other chemical compounds during processing. This will be fully explained in chapter seven.

Further, the low-k material must have high plasma etch resistance, a high thermal and chemical stability.⁶ The temperature is around 450°C during manufacturing processes. Also, the loss of hydrophobic groups during chemical and/or plasma etching will increase the dielectric constant significantly.

After the fabrication and packaging of the IC, the low-k material must have a high reliability to assure a long lifetime of the IC.⁵ This means that in depth investigation of the thermal conductivity, electrical breakdown and leakage current of new developed low-k materials is needed, because these are important reliability parameters.

1.3 Deposition methods

Thin low-k films can be obtained by liquid or gas phase deposition methods, such as chemical vapor deposition (CVD), spin-coating and dip-coating. Although CVD is the current deposition technique in the microelectronic industry, liquid phase deposition methods (dip- and spin-coating) were used during our research. This is mainly because our lab has a lot of experience with these techniques. Further, as will be mentioned in section 1.4, liquid phase deposition is very suitable to prepare advanced ultra low-k materials.

The dip-coating method means that a substrate is first immersed in a liquid that contains dissolved substances and afterwards the substrate is withdrawn with a fixed withdrawal speed.¹⁴ During the withdrawal, the excess of liquid drops off the substrate due to gravity and cohesive forces, while a small amount of the liquid stays attached to the substrate due to adhesion forces. After solvent evaporation, a thin film is formed on both sides of the substrate (see figure 1.5). To obtain uniform films, a good wettability of the substrate is crucial. Therefore, cleaning of the substrates is very important. Further, it is important to prevent cracking, which can occur when the films are too thick. In the case that thicker films are required, it is better to repeat the dip-coating several times to increase the thickness than trying to obtain the same thickness in a single dip-coat step.

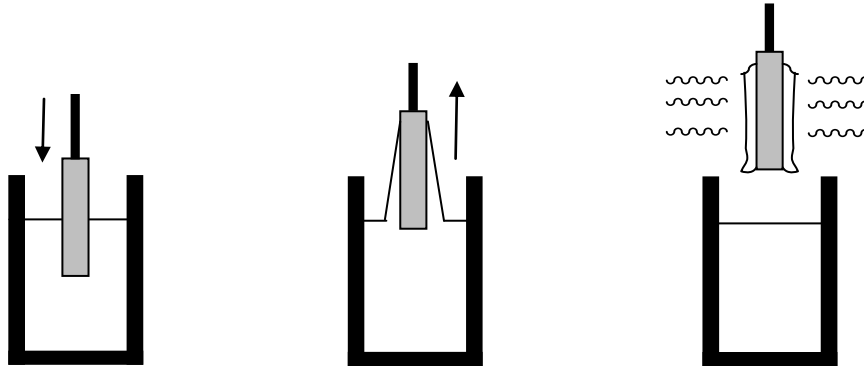


Figure 1.5: Schematic of the dip-coating process.

The thickness of the obtained films can be mainly controlled by the viscosity and density of the liquid, and the withdrawal speed. Higher values of these parameters will lead to thicker films. When the liquid is a Newtonian fluid and the viscosity and withdrawal speed are low, the thickness (t) of the coating can be calculated by the Landau-Levich equation:

$$t = 0.94 \frac{(\eta \cdot v)^{2/3}}{\gamma^{1/6} (\rho \cdot g)^{1/2}} \quad (1.7)$$

With: η = viscosity, v = withdrawal speed, γ = surface tension, ρ = density and g = gravity constant.¹⁵

Spin-coating is a method to obtain uniform films on one side of a substrate. An excess amount of liquid is put onto the substrate which then rotates at high speed (see figure 1.6). The liquid spreads out due to centrifugal forces, the excess amount of the liquid flies off the substrate and after drying a thin film will be obtained.¹⁴ The procedure can be divided in four stages.

The first stage is the dispersion of the fluid onto the substrate. In this stage, it is important to observe that the fluid covers the substrate completely otherwise some parts of the substrate will not be coated. So a good wetting of the substrate is also very important for obtaining good quality spin-coated films. The second stage is called the spin-up. During this stage the liquid spread out due to the centrifugal force. In the third stage or spin-off, the excess of liquid drops off the substrate and the film becomes thinner. In the fourth and last stage, evaporation of the solvent thins the film further out.

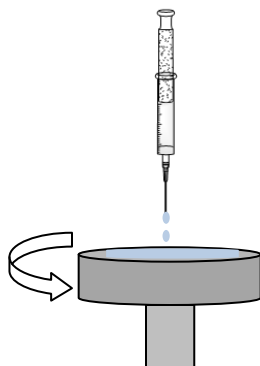


Figure 1.6: Scheme of the spin-coating process.

The thickness of the spin-coated film mainly depends on the viscosity of the initial liquid, the concentration of the different components of the liquid and the rotation rate. The higher the viscosity, the thicker the film will be. On the other hand, a higher amount of solvent will decrease the thickness and also a higher rotation rate will lead to thinner films.

Chemical vapor deposition (CVD) and more in particular plasma enhanced CVD (PECVD) is currently the method of choice in the microelectronic industry, because this technique can be fully integrated in the device manufacturing process. CVD is a process whereby precursors are brought in the gas phase and transferred to a vacuum reaction chamber (see figure 1.7).¹⁶ A heated substrate is also placed in this chamber. The heat delivers the thermal energy which is needed for reaction of the vaporized precursors to produce the desired layer on the substrate.

PECVD uses plasma to activate the monomer precursor. The vaporized precursors in the reaction chamber are subjected to bombardment of free electrons. This generates more free electrons, ions, radicals, atoms and molecules resulting in the activation and polymerization of the precursors resulting in a thin film. The main advantage of PECVD is that that the deposition can occur at relatively low temperatures on large areas.

In PECVD, there are several parameters important to obtain good quality dielectric films. The main parameters are the substrate temperature, pressure, the radio frequency (rf) power and the flow ratios of the reactant gases. For example, it was observed that the dielectric constant of SiC and SiOCH films from trimethylsilane increase when the temperature, total flow, rf power were increased and the trimethylsilane concentration was decreased.⁹ Also the ratio of the internal surface (S) and the reactor volume (V) is important. If the S/V ratio is too high, the reactive intermediates will be deactivated on the reactor and no solid products are formed. In

the case that the S/V ratio is too low, the concentration of the reactive species is too high and the polymerization will lead to powder formation instead of thin films.¹⁷

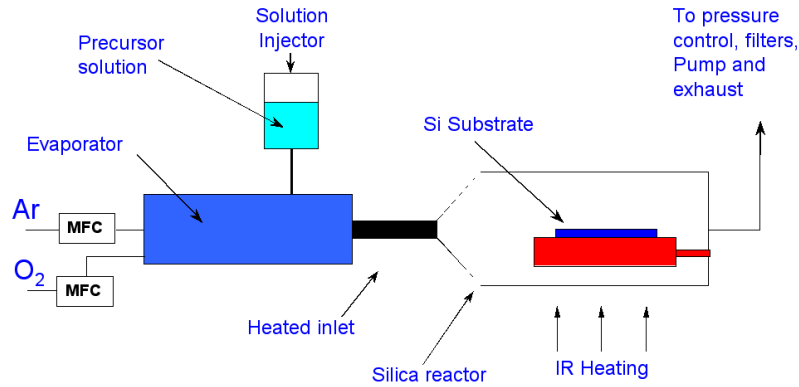


Figure 1.7: Schematic drawing of the CVD process.¹⁸

1.4 Evolution of low-k materials

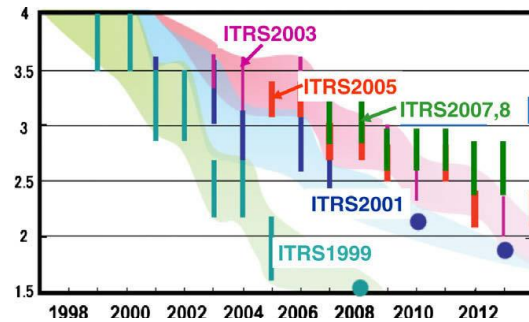


Figure 1.8: Predicted low-k trends for various version of ITRS.¹⁹

The international technology roadmap for semiconductors (ITRS), which is a guideline that proposes targets to be obtained at a certain time for the semiconductor industry, predicted that $k < 2$ materials would be applicable by 2003 in the 130 nm node (originally: lithography resolution, nowadays: the physical transistor gate length)¹⁹ and dielectric constants less than 1.5 would appear by 2009 in the 65 nm node. In 2006, the list of potentially viable low-k candidates has narrowed substantially and the integration of low-k materials has proven more difficult than ever imagined. As a result, the ITRS schedule for low-k dielectrics has slipped dramatically (see figure 1.8) and the

implementation of ultra low-k materials ($k < 2$) is now an issue for beyond the 22 nm node.²⁰ Below a brief overview of the evolution towards very low-k materials ($k < 2.5$) will be given. The aim of this overview is to inform the reader about the general achievements and progression on low-k materials from the last 2 decades, but it is far from complete. For more information, we refer to the review of Volksen et al.² which provides a more detailed overview about the different low-k materials.

1.4.1 Fluorosilicate glasses (FSG)

Because of the lower polarizability and density of the Si-F bond compared to the Si-O bond, fluorosilicate glasses (FSG) were one of the first investigated low-k materials. Also, the silicon fluorine bond is the second strongest single bond (129 kcal/mol), and is very resistant to homolytic scission and oxidation.⁸ With the incorporation of fluorine, k -values down to 3.6 can be obtained.² Thin films consisting of fluorosilicate glasses can be made by solution deposition and gas phase deposition methods. In the solution based synthesis, silica powder is dissolved in hydrofluosilicic acid. Afterwards water is added to enable supersaturation of the solution with silicic acid. Thin films were then obtained by immersing cleaned silicon wafers in the solution followed by spin-drying.²¹

Although the solution deposition method showed some promising results, chemical vapor deposition (CVD) methods were soon developed because of their compatibility with microelectronic manufacturing. A first possible CVD method is room temperature CVD.²² As the name already says, this process occurs at room temperature. A fluoro-trialkoxo-silane precursor provides the fluorine and silicon for the film, while water is the only other reagent. Both reagents are vaporized and the vapors are brought in a reaction chamber. The gases react and form oligomers which condense on the surface of the substrate forming a solid film.

A second CVD method is conventional plasma CVD. Within this technique, tetraethyl orthosilicate (TEOS) or silane (SiH_4) can be used as silicon source and these precursors can be combined with C_2F_6 or SiF_4 to form the FSG layer.^{23, 24} In the case that TEOS is used, gap filling can be obtained. The gaseous forms are brought in a dual frequency reactor (low and high frequency, resp. 0.35 MHz and 13.56 MHz). The high frequency dissociates the gases and free fluorine is produced. The low frequency causes ion bombardment at the surface of the substrate leading to thin layer formation. The free fluorine is incorporated in the film by bonding to Si. When SiF_4 is used as fluorine source, the deposition rate increases. This is because SiF_4 does not have to be broken to free fluorine to produce FSG films together with TEOS. The plasma produces SiF_x compounds which can incorporate into the film.

The third possible CVD method is high-density plasma CVD.^{25, 26} This method is a special form of plasma CVD that employs an inductively coupled plasma (ICP) source to generate a higher plasma density than that of a standard parallel plate plasma CVD system. Possible reactant combinations are $\text{SiF}_4/\text{SiH}_4/\text{O}_2/\text{Ar}$ or $\text{TEOS}/\text{CF}_4/\text{O}_2/\text{Ar}$. With HDP-CVD, stability from high power can be achieved along with fluorine incorporation, acceptable deposition rates and excellent gap fill. Therefore, HDP-CVD is the method of choice.

Disadvantages of FSG films relate to the fact that when the fluorine concentration is larger than 4.5% the films are not stable anymore.²⁷ They adsorb moisture leading to an increase in dielectric constant. Adsorbed water molecules will react with the Si-F bonds resulting in polar Si-OH bonds and HF. Besides the disintegration of the film, the released HF can react with metals during the processing resulting in corrosion of the metals. Although the FSGs have some disadvantages and the decrease in k -value is not spectacular, they are the first integrated low-k materials.

1.4.2 Organic polymers

In search to further decrease the k -value, organic thin films come into play. The huge advantage of polymers is the high amount of low polarisable groups such as C-C, C-F and C-H bonds. Further it is also possible to incorporate space-occupying groups such as methyl, ethyl and phenyl to increase the free volume which also decreases the dielectric constant. Thin organic polymer films can be obtained with CVD or spin-coating. However, CVD is limited to only a low number of polymers, while spin-coating can be applied to every soluble polymer. Several potential polymer groups are reported. However, a lot of polymers are not thermally and/ or mechanically stable for integration or are incompatible with device technological processes and so excluding themselves as low-k material. Therefore only a few of them are interesting as real low-k materials and will now be discussed briefly.

Polyimides

The fact that polyimides are compatible with semiconductor manufacturing processes makes them attractive to investigate their low-k properties. As the name says polyimide is the polymer of imides which are formed by reaction of diamines and dianhydrides (see figure 1.9).²⁸ Due to the fact that the polymer is not soluble, thin films are mostly obtained via spin-coating of a poly amic acid precursor which is soluble. The large variety of the monomers makes it possible to adjust the properties of the polymer. Common properties of polyimides are a high thermal stability, a high mechanical stability and a high transition temperature which are all required properties for ILD applications. The first reported polyimide films have k -values around 3 or higher but still significantly less than SiO_2 .²⁹ The main drawbacks of polyimides are that they

have a bad adhesion to copper and they easily absorb moisture which increases the dielectric constant.²

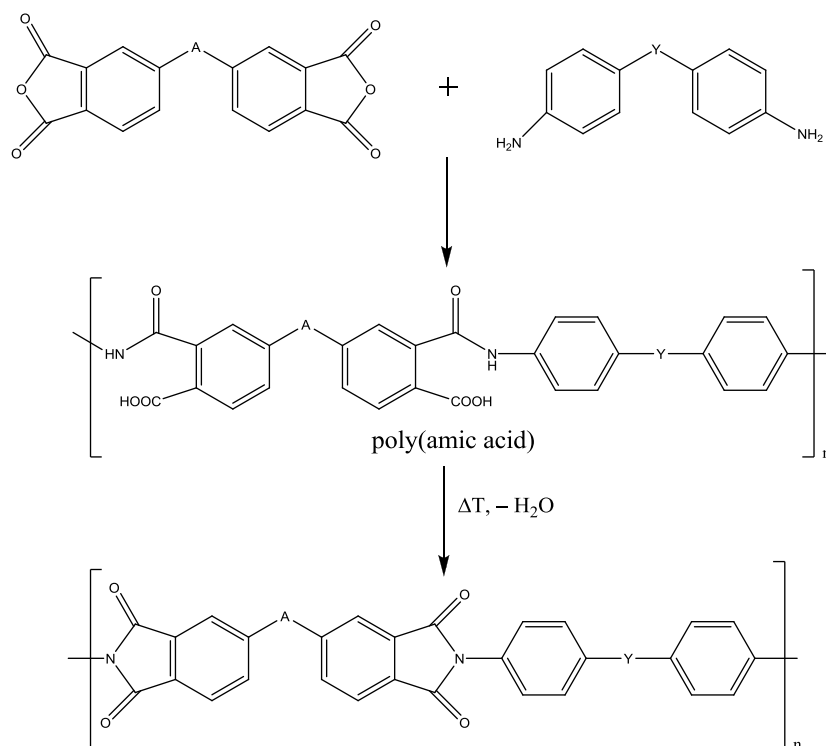


Figure 1.9: General synthesis of polyimides, with A for example C=O and Y for example S.

First attempts to further decrease the k -values of polyimides resulted in the incorporation of fluorine.³⁰ CF bonds are low polarisable and also increases the free volume.³¹ Another advantage is that water absorption is reduced due to the non-polar property of the CF bond. Whereas the k -value of polyimides situates around 3, the reported k -value of fluorinated polyimides is concentrated around 2.6.¹⁰ Although the k -value is decreased after fluorination, the adhesion is not improved and the use of fluorine is not encouraged by the microelectronic industry. Therefore, it is not likely that polyimides are suitable as low- k materials.

Polybenzoxazoles

Typically, the synthesis of polybenzoxazole thin films is a two-step process. First bis(*o*-aminophenols) and aromatic dicarboxylic acids condense to form a solvent soluble poly hydroxyamide precursor which can be spin-coated. During a thermal treatment the polymer undergoes a cyclization to form polybenzoxazoles (figure 1.10). The resulting

films are high temperature polymers with glass transition temperatures (T_g) around 300°C or higher. Higher T_g -values can be obtained when the polymer consists of highly fused-ring structures with intra-molecular H-bonding. Low k -values (around 2.15) can be achieved when fluorine is incorporated in the polymer.^{2, 10}

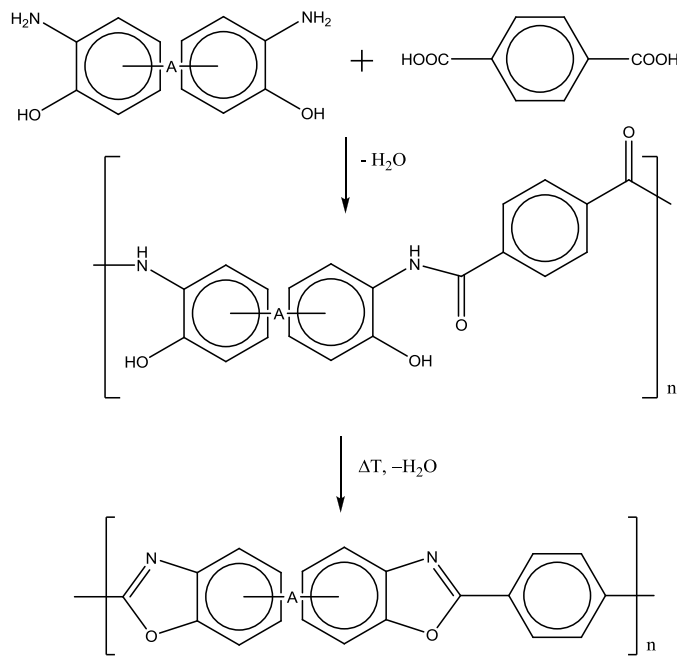


Figure 1.10: Synthesis of polybenzoxazoles with A for example $-C(CF_3)_2-$.

Polynaphthalenes

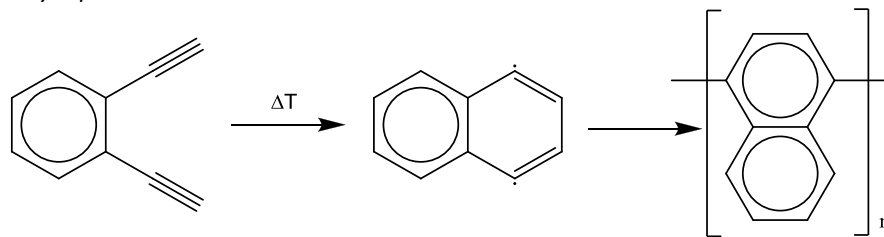


Figure 1.11: General synthesis of polynaphthalenes.

Polynaphthalene films can be deposited by CVD starting from 1,2-bisethynylbenzene (see figure 1.11).³² These films exhibit a k -value of 2.4 and a thermal stability to at least 530°C.

Polyarylethers

Polyarylethers are polymers with high T_g -values, good mechanical and adhesion properties and low moisture uptake. The polymers can be formed by condensation of diphenols and dihalides as shown in figure 1.12. Similar to the other polymers the dielectric constant can be lowered by fluorine substitution.³³ The most advanced polymers exhibit a T_g above 400°C, a k -value of 2.8 and excellent adhesion to inorganic substrates. In attempt to avoid the fluorine incorporation while maintaining the low-k property, polyarylethers without polar groups were developed. As starting monomers, aryl dibromides and bisphenols were chosen and polymerization is possible in the presence of a Cu (I) catalyst (Ullman condensation, see figure 1.12). The T_g of these polymers can be up to 289°C and the reported low k -value is 2.4.¹⁰

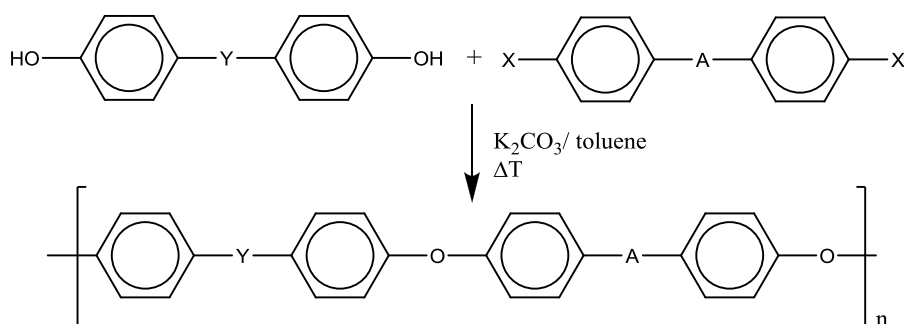


Figure 1.12: General synthesis of polyarylethers with Y: any linking group, A: electron-withdrawing group and X: Cl, F.

Polyarylenes

The most known example of a polyarylene low-k film is SiLK developed by DOW Chemicals. SiLK spin-on polymers can be obtained by cyclization of 1,2 diethynylarylenes or by condensation/aromatization of substituted cyclopentadienones (see figure 1.13).³⁴ The dielectric constant of SiLK is in the range 2.6-2.7 and the decomposition temperature is above 500°C. Furthermore the breakdown voltage of SiLK is above 4 MV/cm and the leakage current is below 10^{-9} A/cm² at 1 MV/cm. Also, the water uptake is very low and good mechanical properties were reported. Because of all these good low-k properties of the SiLK material, IBM tried to integrate this film. Unfortunately, it turned out that the integration failed due to the high coefficient of thermal expansion of the material.²

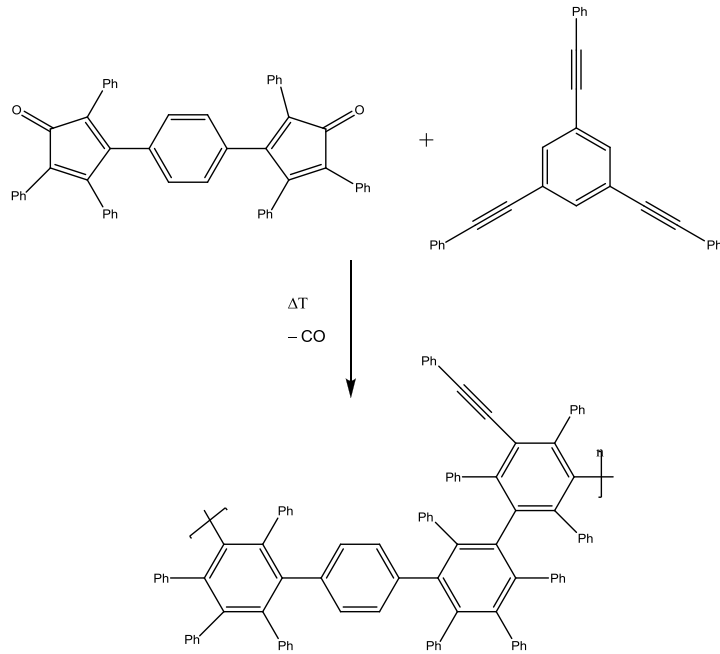


Figure 1.13: Diels Alder reaction to obtain polyarylenes.

1.4.3 Organosilicate glasses (OSGs)

Although organic films exhibit good low-k properties, the hard integration conditions made the industry decide to go for organosilicate glasses. Organosilicate glasses or OSGs have as chemical (non stoichiometric) composition SiOCH and they can be prepared by spin-coating or CVD. The incorporation of carbon and hydrogen lowers the polarisability and density of the silicate leading to k -values in the range 2.7-3. Because these materials also have a silicate backbone the properties will be more similar to SiO_2 than polymer films and thus the most deposition and integration methods can still be used.²

In the case of spin-on OSGs the synthesis occurs by means of a sol-gel reaction.¹⁴ As starting precursor, alkoxy organosilanes or halogenated organosilanes can be used. By adding a solvent, water and a catalyst (acid or base) the precursor starts to hydrolyze and will condensate with another hydrolyzed precursor molecule forming an inorganic polymer film (see figure 1.14). Films can be made by using just one starting precursor or by co-condensation of different precursors.

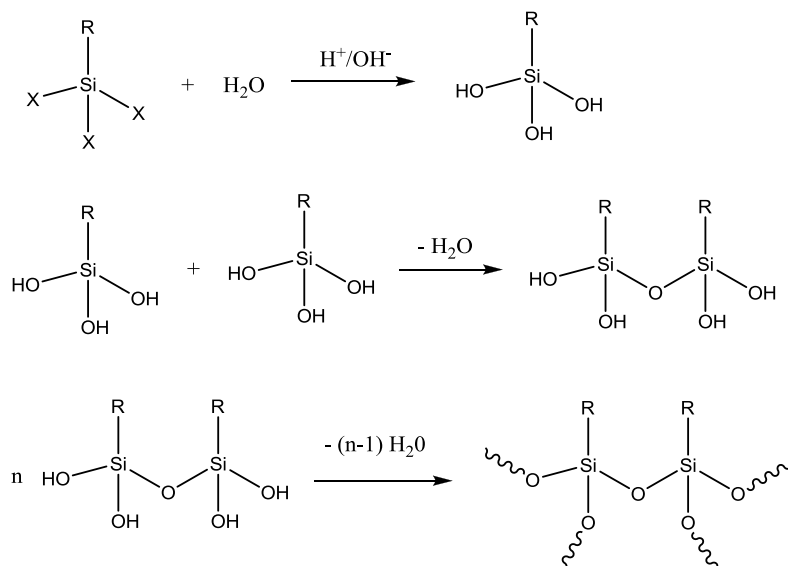


Figure 1.14: Sol-gel reaction scheme, with X = Cl or alkoxy groups, R = alkyl, aryl.

It should be expected that the polymerization occurs randomly, but this is rarely observed. The most OSG films have cage- or ladder-like structures.³⁵ By increasing the size of the organic substituent more polyhedral structures are obtained. However, this leads to a lower network connectivity and has an influence on the electrical and mechanical properties. The higher the network connectivity the higher the mechanical stability, but the lower the dielectric constant will be. Spin-on OSGs have high thermal stabilities, and at that time a low enough dielectric constant (2.7), but they mechanically failed during integration.²

On the other hand, PECVD produced OSG films did pass the requirements from the microelectronic industry and they were successfully integrated in microprocessors. Several organosilane precursors or precursor mixtures can be used to obtain high quality OSGs (figure 1.15).

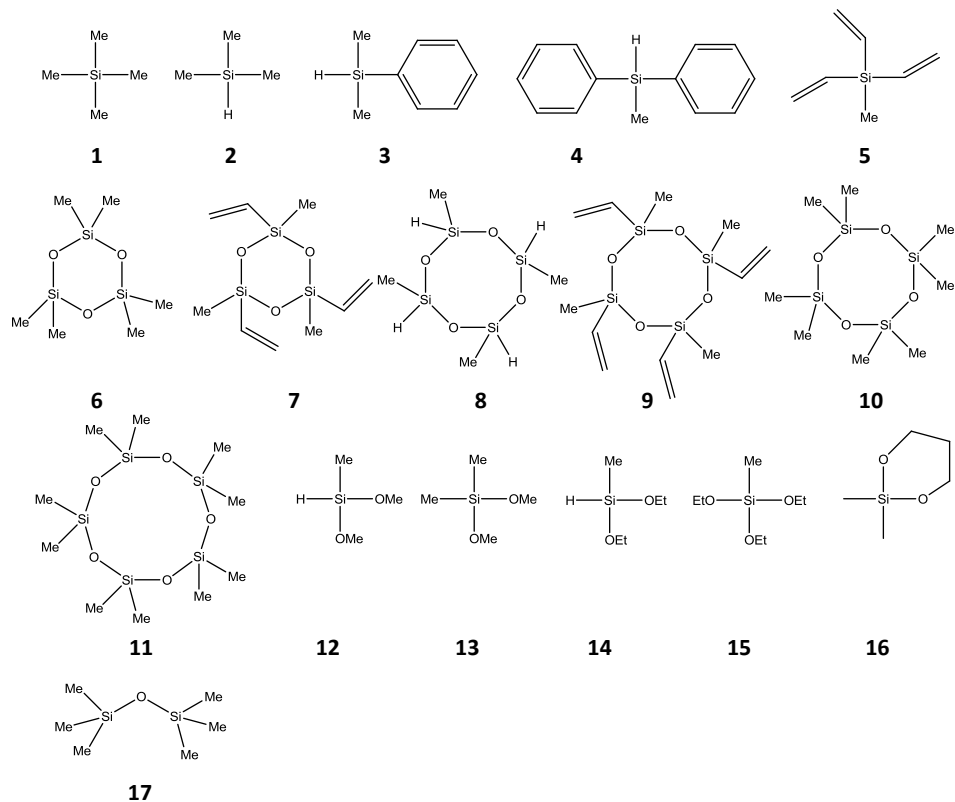


Figure 1.15: Precursors to synthesize CVD OSG films with **1** tetramethylsilane (4MS), **2** trimethylsilane (3MS), **3** dimethylphenylsilane (DMPS), **4** diphenylmethylsilane (DPMS), **5** trivinylmethylsilane (TVMS), **6** hexamethylcyclotrisiloxane (HMCTSO), **7** trimethyltrivinylcyclotrisiloxane (3M3VTSO), **8** tetramethylcyclotetrasiloxane (TMCTS), **9** tetravinyltetramethylcyclotetrasiloxane (TVTMCTS), **10** octamethylcyclotetrasiloxane (OMCTS), **11** decamethylcyclopentasiloxane (DMCPSO), **12** dimethoxymethylsilane (DMOMS), **13** dimethyldimethoxysilane (DMDMOMS), **14** diethoxymethylsilane (DEMS), **15** methyltriethoxysilane (MTES), **16** dimethyldioxysilylcyclohexane (DMDOSH), **17** hexamethyldisiloxane (HMDSO).

In the case that the starting precursor does not contain any oxygen (like tetramethylsilane, **1**; trimethylsilane, **2**; dimethylphenylsilane, **3**) an oxidant gas (N_2O or O_2) is needed to form the silica network. After annealing, good electrical properties are obtained.³⁶⁻³⁸

Oxidant free deposition is possible when there is already a high amount of oxygen in the starting precursor.³⁹ However, often O_2 is added in the plasma chamber.⁴⁰ The resulting films have good mechanical, thermal and electrical properties which can be optimized by changing the process conditions (plasma power, temperature, presence

of oxidant gases) within a certain range.⁴¹⁻⁴³ O'Neill *et al.*⁴⁴ found out that DEMS (**14**) has the best mechanical properties, while Grill *et al.*⁴⁵ reported that TMCTS (**8**) also possesses excellent mechanical properties.

1.4.4 Porous materials

When the transistor size further decreases to 45 nm node dimensions even the k -value of the organosilicate glasses is too high. Also, there are no other appropriate dense materials available that can meet all the requirements for the 45 nm node. Therefore, nanoporous materials were and are still thoroughly investigated as new low- k dielectric materials. As already mentioned, the introduction of porosity lowers the dielectric constant because air has a k -value of 1.01. However, porosity weakens the mechanical stability of the material. This means that there must be a trade-off between the dielectric constant and the mechanical properties. Furthermore, porosity reduces the plasma and chemical stability of the dielectric material and the chance to electrical failure (increase in leakage current, k -value and lower breakdown voltage) is much higher. This is because water or other unwanted components could diffuse into the pores, leading to destruction of the dielectric properties. Therefore, the pores size should be as small as possible and the formation of interconnected pores should be avoided. Therefore, the most reported porous low- k materials have micropores (diameter < 2 nm) or mesopores (diameter from 2 to 50 nm).

Porous CVD OSG films

Obviously, nanoporous CVD OSG films are one of the most suitable materials because there were already the materials of choice of the non-porous materials. Porosity can for instance be introduced by etching SiOCH films with a diluted HF solution.⁴⁶ However, the most common way to obtain porosity is the addition of a thermal or chemical labile component, which can be easily removed after deposition by a thermal treatment or UV- thermal curing, leaving behind a porous structure.^{47, 48} Some examples of these sacrificial porogens are: α -terpinene, epoxycyclohexane, 1-hexene, norbornene, etc. As precursors tetramethyl cyclotetrasiloxane, vinyltrimethylsilane, tertamethylsilane and divinyl dimethylsilane are typically used.

Grill⁴⁵ succeeded to prepare porous SiOCH dielectrics by PECVD using TMCTS with the addition of organic labile precursors. By adjusting the plasma conditions, it was possible to decrease the dielectric constant to 2.05. The porosity of these films is about 30% with an average pore size below 2.5 nm. The author also reported that it is possible to increase the porosity (= lower k -value) when more porogen is added. The Young's modulus and hardness of the 30% porosity film is 3.3 GPa and 0.21 GPa respectively. Grill *et al.*⁴⁹ also found out that the pore size increases when the k -value decreases which is of course unwanted. However, the pore size remained below 5 nm.

Park and Rhee⁵⁰ made porous OSG films with vinyltrimethylsilane as precursor. The films showed a low- k value of 2.1 and a leakage current density of 3×10^{-7} A/cm² at 1 MV/cm.

Flavennec *et al.*⁵¹ compared the shrinkage behavior during the porogen removal of two matrix precursors (decamethylcyclopentasiloxane and diethoxymethylsilane) in combination of oxygen. They observed that the higher the carbon content, the lower the ability to prevent significant shrinkage. This means that O₃-Si-Me configurations are favorable to prevent high film shrinkage, while on the other hand O₂-Si-Me₂ configurations lead to high film shrinkage. To obtain the right configuration, DEMS appears more appropriate than DMCPISO. The influence of the porogen loading was also investigated. The porogen loading can be controlled by changing the ratio of the porogen precursor in the plasma gas feed. The higher the loading, the higher the porosity will be. However, the amount of porosity that can be introduced is limited, because above this limit, collapsing during porogen removal takes place. Using the optimized conditions, the k -value of the SiOCH film is 2.3.

As already mentioned, chemical, plasma and mechanical stability becomes a more important issue when porosity is introduced. Grill and Patel⁵² investigated the effect of He/H₂, N₂/He and NH₃ plasmas on the properties of three porous SiOCH films. The plasma exposure led to modifications of the bonding structure, reduction in film thickness and increase in refractive index and dielectric constant of the films. The most damaging plasma was the He/H₂ plasma, while the NH₃ plasma caused the lowest damage. This plasma damage can be reduced by using a combined He and NH₃ plasma treatment which also results in pore sealing through densification of the top surface.⁵³

Another issue is the presence of porogen residue after porogen removal, which increases leakage current and decreases breakdown voltage of low- k materials.⁵⁴ Therefore, controlling the curing conditions and using the right porogens are necessary to minimize the amount of residue.⁵⁵ Particularly, the application of longer wavelengths for UV-curing leads to an improved porogen removal.⁵⁶ UV-curing also has an effect on the material properties and plasma damage resistance. A narrow band lamp ($\lambda = 172$ nm) modified the film by inducing more network Si-O bonds and Si-H bonds. Further, the film is also more dense leading to a slight increase in dielectric constant, but also to a significant increase in hardness and Young's modulus. If broad band UV-cure is used ($\lambda > 200$ nm) lower k -values and lower mechanical stability are obtained.⁵⁷

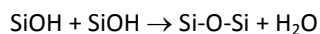
Although porosity causes extra problems for integration, porous 2.4 materials could be successfully integrated in devices. Integration of CVD based OSG films with lower k -values are still under research. However, it seems that there is a limit to values around 2.0 due to pore collapsing at higher porogen loadings.

Porous liquid phase deposited materials

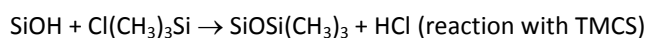
When porosity came into play, liquid phase deposition methods re-entered the scene again. Although non-porous organic polymers were not chosen as low-k materials, porous polymer films were also developed and screened for low-k applicability. The strategy behind this is that bulk polymers already have a low k -value which means that not much porosity has to be introduced to obtain very low k -values.² The general method to obtain porous polymers is adding porogen generators which can be removed thermally after the synthesis. However, the most reported porous polymers have pore sizes above 10 nm which make them unsuitable for effective integration (taking into account that the thickness of the dielectric also decreases with decreasing IC features).⁵⁸ Similar to the non-porous polymers, spin-coated porous SiLK, developed by DOW chemicals, has the best properties. Pores sizes lower than 2 nanometer could be achieved by using cross-linked polystyrene nanoparticles. The k -value of porous SiLK is in the range of 2.2-2.4.⁵⁹

Porous silicate and organosilicate films deposited by spin-coating or dip-coating are also thoroughly investigated for their low-k properties. Two methods can be applied to introduce porosity. The first one is the creation of pores by adjusting the synthesis parameters, thus without using templates. For instance, when using base catalyzed sol-gel reactions, the density of the films decreases. An example of this method is the commercially available LKD1509 with a Young's Modulus of 4.5 GPa and a dielectric constant of 2.2 which corresponds to a porosity of 39%.^{2,60}

The most known examples of template free porous silicate materials are aerogels and xerogels. Silica aerogels are prepared by sol-gel via spin-coating in a saturated solvent environment. Next, the films are immersed in a solvent. By adjusted the drying conditions (supercritical, freeze-drying), the solvent still present in the film can be removed without pore collapse leaving behind a very porous material (around 80% porosity).⁶¹ Obviously, very low dielectric constants are achieved ($k \leq 2$). Unfortunately, aerogels have some major drawbacks. The first one is that the material contains a lot of silanol groups which means that aerogels are very hydrophilic. To reduce the amount of silanol groups an extra thermal treatment step can be applied. This treatment leads to extra condensation of SiOH groups, releasing water molecules, when they are close enough to each other.²



Other possibilities are an after treatment with trimethylchlorosilane (TMCS) or hexamethyldisilazane (HMDS).²





The second drawback is that the material has extremely low mechanical properties making this material unsuitable for integration.

Xerogels are like aerogels synthesized by the hydrolysis and condensation of alkoxy silanes. Usually TEOS is used as starting precursor and a two step acid/base catalyst procedure is applied.⁶² The acid enhances the hydrolysis rate of the precursor while the base catalyst increases the condensation rate. Before the drying step, the silanols are already end-capped with HMDS or TMCS. This makes it possible to reverse the shrinkage during drying and thus preserving collapsing of the pores (springback effect of the end standing methyl groups). By adjusting the synthesis and drying conditions, xerogels with extremely low dielectric constant ($k < 2$) can be obtained.⁶³ However, the relatively large pore sizes of xerogels are a real concern for the microelectronic industry.

The second method to create porosity in liquid phase deposited silicates and organosilicates is the deposition of silane precursors in the presence of a porogen generator.⁶⁴⁻⁶⁶ Hedrick *et al.*⁶⁷ succeeded to prepare porous SOG films by adding well-defined branched macromolecules such as poly(ϵ -caprolactone)-based structures. Decomposition of the organic component takes place at elevated temperature, leaving behind a nanoporous structure with dielectric constant below 2.2.

Yim *et al.*⁶⁸ used functionalized cyclodextrins as porogens and cyclic silsesquioxanes precursors to prepare OSG films by spin-coating. They found out that the pore size and pore interconnection length can be controlled by varying the functional groups of the template while the same porosity could be maintained (about 35%). The obtained k -values were around 2.1 and the breakdown voltage was around 2.5 MV/cm. Their findings about the mechanical properties were that the longer the interconnection length, the worse the mechanical properties. Better mechanical properties can be achieved when also a linear chain is incorporated in the matrix.⁶⁹

Ree *et al.* investigated other porogen generators,⁷⁰⁻⁷² *e. g.* hyperbranched ketalized polyglycidol,⁷³ and wrote an excellent review about possible pore generators.⁷⁴

As a general remark of porogen templated films, it can be concluded that the porous fraction of the film is directly related to the porogen/precursor ratio and the pore size is related to the size of the used porogen.⁷⁵

Another possible method to obtain nanoporous silicate films is applying the evaporation induced self-assembly method (EISA), which was first reported by Brinker's group.⁷⁶ With this approach, they were able to synthesize mesoporous silica films by

sol-gel dip-coating. During this EISA process, an excess of volatile solvent (*e.g.* ethanol) is present in the starting solution, which further consists of the silane precursor, a porogen template (*i.e.* surfactants), water and a volatile catalyst (*e.g.* HCl). The excess of solvent ensures that the initial concentration of the surfactant remains below the critical micelle concentration (cmc). When the substrate is, after immersion, withdrawn out of the liquid, the solvent starts to evaporate. During the evaporation of the solvent, the surfactant concentration transcends the cmc and the silane precursor hydrolyzes and condensates around the micelles (self-assembly).⁷⁷ A thermal curing step is then performed to allow further condensation of the silica matrix. The surfactant can be afterwards removed by calcination, leaving behind a porous structure. Even more, mesostructured ordering, such as hexagonal or cubic, can be obtained with this procedure.⁷⁸ A schematic overview of the EISA process is shown in figure 1.16.

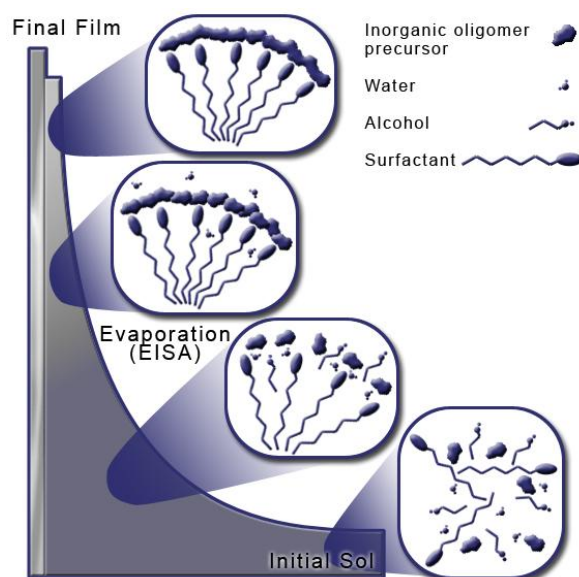


Figure 1.16: Graphical scheme of evaporation induced self-assembly.⁷⁹

The EISA method can also be applied to other liquid phase deposition techniques such as spin-coating or spraying. Grosso *et al.*⁸⁰ investigated the fundamentals of mesostructuring through EISA. They demonstrated that the organization depends mainly on the chemical composition of the film when it reaches the modulable steady state. At this state, the inorganic framework is still flexible and the composition is stable after reaching equilibrium in the diffusion of volatile species. Parameters that influence the film's composition are the chemical conditions in the solution, the relative vapor pressures in the environment and the evaporation conditions.

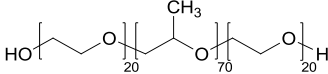
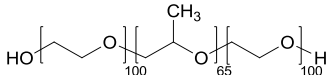
Chapter 1: Introduction to low-k materials

With the EISA method, the ordering, porosity and pore size of silica films can be fairly easily adjusted by selecting the right surfactant and thus the dielectric constant can be tuned.^{81, 82} As a rule of thumb, it can be stated that the longer the chain of the surfactant, the larger the pore size and the more surfactant the higher the porosity.⁸³ However, it is often observed that higher surfactant loadings also lead to an increase in pore size.^{84, 85}

In table 1.1 an overview of different surfactants which are frequently used for self-assembly is given.

Table 1.1: Frequently used surfactants.

abbreviation	full name	structural formula
CTAC/CTAB	cetyltrimethylammonium chloride/bromide	$\text{H}_3\text{C}-\overset{\text{CH}_3}{\underset{\text{CH}_3}{\overset{+}{\text{N}}}}(\text{CH}_2)_{15}\text{CH}_3 \quad \text{Cl}^- / \text{Br}^-$
OTAC/OTAB	octadecyltrimethylammonium chloride/bromide	$\text{H}_3\text{C}-\overset{\text{CH}_3}{\underset{\text{CH}_3}{\overset{+}{\text{N}}}}(\text{CH}_2)_{17}\text{CH}_3 \quad \text{Cl}^- / \text{Br}^-$
C _n TMACl/ C _n TMABr	alkyltrimethylammonium chloride/bromide	$\text{H}_3\text{C}-\overset{\text{CH}_3}{\underset{\text{CH}_3}{\overset{+}{\text{N}}}}(\text{CH}_2)_{n-1}\text{CH}_3 \quad \text{Cl}^- / \text{Br}^-$ <p style="text-align: right;">(n = 8, 10, 12, 14, 16, 18)</p>
Brij-30	polyoxyethylene (4) lauryl ether	$\text{HO} \left[\text{CH}_2\text{CH}_2\text{O} \right]_4 \text{CH}_2(\text{CH}_2)_{10}\text{CH}_3$
Brij-56	polyoxyethylene (10) cetyl ether	$\text{HO} \left[\text{CH}_2\text{CH}_2\text{O} \right]_{10} \text{CH}_2(\text{CH}_2)_{14}\text{CH}_3$
Brij-76	polyoxyethylene (10) stearyl ether	$\text{HO} \left[\text{CH}_2\text{CH}_2\text{O} \right]_{10} \text{CH}_2(\text{CH}_2)_{16}\text{CH}_3$

P123	<p>Pluronic P123</p> <p>poly(ethylene glycol)- poly(propylene glycol)- poly(ethylene glycol)</p>	
F127	<p>Pluronic F127</p> <p>poly(ethylene glycol)- poly(propylene glycol)- poly(ethylene glycol)</p>	

Several researchers used this EISA procedure to prepare mesoporous silica or organosilica films and investigated their potential as low-k dielectric.^{86, 87} Of course Brinker's group also explored the low-k properties.⁸⁸ They synthesized a series of highly porous silica thin films through co-assembly of silica and surfactant P123. They also added a swelling agent in different amounts to control the porosity ranging from 50% to 90%. The obtained dielectric constants were between 1.3 and 2.6 and better mechanical properties were achieved compared to aerogels.

de Theije *et al.*⁸⁵ prepared organosilicate films by mixing TEOS and MTMS in different ratios. They also varied the surfactant type (CTAB, Brij-76 and Pluronic F127) and concentration. They found out that a 50/50 precursor composition with 10 mol% CTAB leads to best low-k properties (k -value 2.0 and Young's Modulus (E) = 1.27 GPa).

Chen *et al.*⁸⁹ reported that end-capping the residual silanols with HMDS enhances the mechanical stability of the film, which is an interesting advantage because silanol removal has to be done anyway. Otherwise the film is too hydrophilic for low-k application. However, when HMDS is applied, the annealing temperature can not be too high (below 350°C). Otherwise the methyl groups will be replaced with silanol groups.^{90, 91}

Due to the fact that the mechanical stability drops significantly at high porosity, many other groups tried to find the best conditions between mechanical stability and dielectric constant. As already mentioned, trimethyl silylation of the silanol groups enhances the mechanical properties due to a springback effect of the end-standing trimethyl silyl groups.⁹² When 1,3,5,7-tetramethylcyclotetrasiloxane vapor is used, even better mechanical properties are achieved due the fact that TMCTS molecules can polymerize on pore wall surfaces.⁹³ Unfortunately, also the k -value increased from 2 to 2.2. Other parameters that influence the mechanical stability of the silica films are the

Chapter 1: Introduction to low-k materials

matrix composition,⁹⁴ the wall thickness⁹⁵ and the ordering of the film.⁸⁴ A higher cross-linking in the silica network, thicker walls and a good ordering all increase the mechanical stability. However, the porosity is still the most influential factor on the mechanical strength of the film.⁸⁴

Table 1.2 summarizes the progress of low-k materials and provides values of the most important properties of low-k materials. The last column shows the values that are desired for the next generation low-k materials.

Table 1.2: Overview of important properties of low-k materials and the desired value for the next generation low-k materials.^{2,7}

Property	Porous SiOC (45 -32 nm nodes)	SiOC (90-65 nm nodes)	SiO ₂ (reference)	desired value (22 nm node and below)
<i>k</i> -value	2.2-2.5	2.5-3	3.9	$k < 2$
Sensity to water	hydrophobic	hydrophobic	hydrophilic	hydrophobic
Young's modulus (GPa)	3-6	>10	72	>4
Hardness (GPA)	~0.8	1.7	10	>0.5
Leakage current (A/cm ²) at 1MV/cm	1×10^{-9}	1×10^{-9}	1×10^{-9}	$<1 \times 10^{-7}$
Breakdown voltage (MV/cm)	>4	>5	10	>4
Thermal stability (°C)	400-500	400-500	>500	>400

As a summary of the applicability of porous low-*k* materials, the dielectric constant can be decreased drastically when porosity is introduced. CVD porous organosilicate films with *k*-values around 2.4 could be successfully integrated and it is also likely that (probably CVD) 2.2 and maybe 2.0 materials will be successfully integrated in the near future. However, for *k*-values lower than 2 the porosity must be very high and it seems that none of the above mentioned materials have a sufficiently mechanical stability. Therefore, other materials have to be found that could fulfill the requirements and these will be discussed in chapter two.

1.5 References

1. www.intel.com.
2. W. Volksen, R. D. Miller and G. Dubois, *Chem Rev*, 2010, **110**, 56-110.
3. www.pcworld.com/article/165612/evolution_of_the_pc.html.
4. G. Moore, *Electronics*, 1965, **38**.
5. D. Shamiryan, T. Abell, F. Iacopi and K. Maex, *Materials Today*, 2004, **7**, 34-39.
6. M. R. Baklanov and K. Maex, *Philos T Roy Soc A*, 2006, **364**, 201-215.
7. M. Fayolle, G. Passemard, O. Louveau, F. Fusalba and J. Cluzel, *Microelectron Eng*, 2003, **70**, 255-266.
8. T. Homma, *Mat Sci Eng R*, 1998, **23**, 243-285.
9. K. Maex, M. R. Baklanov, D. Shamiryan, F. Iacopi, S. H. Brongersma and Z. S. Yanovitskaya, *J Appl Phys*, 2003, **93**, 8793-8841.
10. G. Maier, *Prog Polym Sci*, 2001, **26**, 3-65.
11. B. D. Hatton, K. Landskron, W. J. Hunks, M. R. Bennett, D. Shukaris, D. D. Perovic and G. A. Ozin, *Materials Today*, 2006, **9**, 22-31.
12. T. M. Long and T. M. Swager, *J Am Chem Soc*, 2003, **125**, 14113-14119.
13. Y. L. Li, I. Ciofi, L. Carbonell, N. Heylen, J. Van Aelst, M. R. Baklanov, G. Groeseneken, K. Maex and Z. Tokei, *J Appl Phys*, 2008, **104**.
14. C. J. Brinker and G. W. Scherer, *The Physics and Chemistry of Sol-Gel Processing*, Academic Press, Inc., San Diego, 1990.
15. C. J. Brinker, G. C. Frye, A. J. Hurd and C. S. Ashley, *Thin Solid Films*, 1991, **201**, 97-108.
16. K. L. Choy, *Prog Mater Sci*, 2003, **48**, 57-170.
17. F. N. Dultsev, L. A. Nenasheva and L. L. Vasilyeva, *J Electrochem Soc*, 1998, **145**, 2569-2572.
18. http://int.ch.liv.ac.uk/Lanthanide/Ln_oxides_folder/Ln_oxides.html.
19. H. Iwai, *Microelectron Eng*, 2009, **86**, 1520-1528.
20. International Technology Roadmap for Semiconductors_ITRS_, available at <http://www.itrs.net>.
21. C. F. Yeh, C. L. Chen and G. H. Lin, *J Electrochem Soc*, 1994, **141**, 3177-3181.
22. M. J. Shapiro, S. V. Nguyen, T. Matsuda and D. Dobuzinsky, *Thin Solid Films*, 1995, **270**, 503-507.
23. M. J. Shapiro, T. Matsuda, S. V. Nguyen, C. Parks and C. Dziobkowski, *J Electrochem Soc*, 1996, **143**, L156-L158.
24. S. Mizuno, A. Verma, H. Tran, P. Lee and B. Nguyen, *Thin Solid Films*, 1996, **283**, 30-36.
25. Y. L. Cheng, Y. L. Wang, C. P. Liu, Y. L. Wu, K. Y. Lo, C. W. Liu, J. K. Lan, C. Ay and M. S. Feng, *Mater Chem Phys*, 2004, **83**, 150-157.
26. Y. L. Cheng, Y. L. Wang, C. W. Liu, Y. L. Wu, K. Y. Lo, C. P. Liu and J. K. Lan, *Thin Solid Films*, 2001, **398**, 533-538.
27. G. Passemard, P. Fugier, P. Noel, F. Pires and O. Demolliens, *Microelectron Eng*, 1997, **33**, 335-342.
28. Y. J. Lee, J. M. Huang, S. W. Kuo, J. S. Lu and F. C. Chang, *Polymer*, 2005, **46**, 173-181.

29. W. Hung-Wei, W. Min-Hang, S. Yan-Kuin and Y. Ru-Yuan, *Microw. Opt. Technol. Lett.*, 2007, **49**, 79-8383.
30. Y. K. Lee and S. P. Murarka, *J. Mater. Sci.*, 1998, **33**, 5423-5426.
31. X. Y. Zhao and H. J. Liu, *Polym Int*, 2010, **59**, 597-606.
32. J. A. Moore, C. I. Lang, T. M. Lu and G. R. Yang, in *Microelectronics Technology: Polymers for Advanced Imaging and Packaging*, eds. E. Reichmanis, C. K. Ober, S. A. MacDonald, T. Iwayanagi and T. Nishikubo, Amer Chemical Soc, Washington, 1995, pp. 449-470.
33. N. H. Hendricks, *Solid State Technol*, 1995, **38**, 117-&.
34. Q. H. Lin, S. A. Cohen, L. Gignac, B. Herbst, D. Klaus, E. Simonyi, J. Hedrick, J. Warlaumont, H. J. Lee and W. L. Wu, *J. Polym. Sci. Pt. B-Polym. Phys.*, 2007, **45**, 1482-1493.
35. H. J. Kim, J. K. Lee, J. B. Kim, E. S. Park, S. J. Park, D. Y. Yoo and D. Y. Yoon, *J Am Chem Soc*, 2001, **123**, 12121-12122.
36. B. Narayanan, R. Kumar and P. D. Foo, *Microelectr J*, 2002, **33**, 971-974.
37. A. Grill, *In Dielectric Films for AdVanced Microelectronics*, Wiley, New York, 2007.
38. S. K. Kwak, K. H. Jeong and S. W. Rhee, *J Electrochem Soc*, 2004, **151**, F11-F16.
39. A. Grill and D. A. Neumayer, *J Appl Phys*, 2003, **94**, 6697-6707.
40. Y. H. Wang and R. Kumar, *J Electrochem Soc*, 2004, **151**, F73-F76.
41. Y. L. Cheng, Y. L. Wang, G. J. Hwang, M. L. O'Neill, E. J. Karwacki, P. T. Liu and C. F. Chen, *Surf Coat Tech*, 2006, **200**, 3134-3139.
42. R. Navamathavan, S. H. Kim, Y. J. Jang, A. S. Jung and C. K. Choi, *Appl Surf Sci*, 2007, **253**, 8788-8793.
43. C. Ye, Z. Y. Ning, T. T. Wang, X. Z. Yu, Y. X. Wei and X. M. Qian, *J Electrochem Soc*, 2007, **154**, G63-G68.
44. M. L. O'Neill, R. N. Vrtis, J. L. Vincent, A. S. Lukas, E. J. Karwacki, B. K. Peterson and M. D. Bitner, in *Materials, Technology and Reliability for Advanced Interconnects and Low-K Dielectrics-2003*, eds. A. J. McKerrow, J. Leu, O. Kraft and T. Kikkawa, Materials Research Society, Warrendale, 2003, pp. 321-326.
45. A. Grill, *J Appl Phys*, 2003, **93**, 1785-1790.
46. D. G. Shamiryan, M. R. Baklanov, S. Vanhaelemeersch and K. Maex, *Electrochem Solid St*, 2001, **4**, F3-F5.
47. H. J. Lee, C. L. Soles, D. W. Liu, B. J. Bauer, E. K. Lin, W. L. Wu and A. Grill, *J Appl Phys*, 2004, **95**, 2355-2359.
48. N. J. Trujillo, Q. G. Wu and K. K. Gleason, *Adv Funct Mater*, 2010, **20**, 607-616.
49. A. Grill, V. Patel, K. P. Rodbell, E. Huang, M. R. Baklanov, K. P. Mogilnikov, M. Toney and H. C. Kim, *J Appl Phys*, 2003, **94**, 3427-3435.
50. J. M. Park and S. W. Rhee, *J Electrochem Soc*, 2002, **149**, F92-F97.
51. L. Favennec, V. Jousseau, G. Gerbaud, A. Zenasni and G. Passemard, *J Appl Phys*, 2007, **102**.
52. A. Grill and V. Patel, *J Electrochem Soc*, 2006, **153**, F169-F175.
53. A. M. Urbanowicz, M. R. Baklanov, J. Heijlen, Y. Travalay and A. Cockburn, *Electrochem Solid St*, 2007, **10**, G76-G79.
54. M. R. Baklanov, L. Zhao, E. Van Besien and M. Pantouvaki, *Microelectron Eng*, 2011, **88**, 990-993.

55. P. Marsik, P. Verdonck, D. De Roest and M. R. Baklanov, *Thin Solid Films*, 2010, **518**, 4266-4272.
56. P. Marsik, A. M. Urbanowicz, P. Verdonck, D. De Roest, H. Sprey and M. R. Baklanov, *Thin Solid Films*, 2011, **519**, 3619-3626.
57. P. Verdonck, E. Van Besien, K. Vanstreels, C. Trompoukis, A. Urbanowicz, D. De Roest and M. R. Baklanov, *Jpn J Appl Phys*, 2011, **50**.
58. G. Maier, *Ieee Electr Insul M*, 2004, **20**, 6-17.
59. L. Shen and K. Y. Zeng, *Microelectron Eng*, 2004, **71**, 221-228.
60. R. Kumar, T. K. S. Wong, B. R. Murthy, Y. H. Wang and N. Balasubramanian, *J Electrochem Soc*, 2006, **153**, G420-G427.
61. G. S. Kim, S. H. Hyun and H. H. Park, *J Am Ceram Soc*, 2001, **84**, 453-455.
62. Y. Y. Huang and K. S. Chou, *Ceram Int*, 2003, **29**, 485-493.
63. S. V. Nitta, V. Pisupatti, A. Jain, P. C. Wayner, W. N. Gill and J. L. Plawsky, *J Vac Sci Technol B*, 1999, **17**, 205-212.
64. V. Meled, S. V. Babu and E. Matijevic, *J Electrochem Soc*, 2009, **156**, H460-H465.
65. Y. Chang, C. Y. Chen and W. C. Chen, *J. Polym. Sci. Pt. B-Polym. Phys.*, 2004, **42**, 4466-4477.
66. S. Z. Yu, T. K. S. Wong, X. Hu and K. Pita, *Thin Solid Films*, 2005, **473**, 191-195.
67. J. L. Hedrick, R. D. Miller, C. J. Hawker, K. R. Carter, W. Volksen, D. Y. Yoon and M. Trollsas, *Adv Mater*, 1998, **10**, 1049-+.
68. J. H. Yim, J. B. Seon, T. D. Jeong, L. Y. S. Pu, M. R. Baklanov and D. W. Gidley, *Adv Funct Mater*, 2004, **14**, 277-282.
69. Y. Y. Lyu, J. H. Yim, Y. Byun, S. Y. Lee, I. S. Jung and L. S. Pu, *Eur Polym J*, 2004, **40**, 2505-2512.
70. J. Yoon, K. Heo, W. Oh, K. S. Jin, S. Jin, J. Kim, K. W. Kim, T. H. Chang and M. Ree, *Nanotechnology*, 2006, **17**, 3490-3498.
71. B. Lee, J. Yoon, W. Oh, Y. Hwang, K. Heo, K. S. Jin, J. Kim, K. W. Kim and M. Ree, *Macromolecules*, 2005, **38**, 3395-3405.
72. B. Lee, W. Oh, Y. Hwang, Y. H. Park, J. Yoon, K. S. Jin, K. Heo, J. Kim, K. W. Kim and M. Ree, *Adv Mater*, 2005, **17**, 696-+.
73. J. S. Kim, H. C. Kim, B. Lee and M. Ree, *Polymer*, 2005, **46**, 7394-7402.
74. M. H. Ree, J. W. Yoon and K. Y. Heo, *J Mater Chem*, 2006, **16**, 685-697.
75. V. Jousseume, G. Rolland, D. Babonneau and J. P. Simon, *Thin Solid Films*, 2009, **517**, 4413-4418.
76. Y. F. Lu, R. Ganguli, C. A. Drewien, M. T. Anderson, C. J. Brinker, W. L. Gong, Y. X. Guo, H. Soyez, B. Dunn, M. H. Huang and J. I. Zink, *Nature*, 1997, **389**, 364-368.
77. C. J. Brinker, *Mrs Bull*, 2004, **29**, 631-640.
78. D. A. Doshi, A. Gibaud, V. Goletto, M. C. Lu, H. Gerung, B. Ocko, S. M. Han and C. J. Brinker, *J Am Chem Soc*, 2003, **125**, 11646-11655.
79. M. Ide, Ghent University, Gent, 2012.
80. D. Grosso, F. Cagnol, G. J. D. A. Soler-Illia, E. L. Crepaldi, H. Amenitsch, A. Brunet-Bruneau, A. Bourgeois and C. Sanchez, *Adv Funct Mater*, 2004, **14**, 309-322.

81. D. Zhao, P. Yang, N. Melosh, J. Feng, B. F. Chmelka and G. D. Stucky, *Adv Mater*, 1998, **10**, 1380-+.
82. C. H. Yang and W. L. Yang, *J Electrochem Soc*, 2006, **153**, G341-G346.
83. N. Hata, C. Negoro, K. Yamada and T. Kikkawa, *Jpn J Appl Phys 1*, 2004, **43**, 1323-1326.
84. C. Y. Ting, H. S. Sheu, W. F. Wu and B. Z. Wan, *J Electrochem Soc*, 2007, **154**, G1-G5.
85. F. K. de Theije, A. R. Balkenende, M. A. Verheijen, M. R. Baklanov, K. P. Mogilnikov and Y. Furukawa, *J Phys Chem B*, 2003, **107**, 4280-4289.
86. R. A. Farrell, K. Cherkaoui, N. Petkov, H. Amenitsch, J. D. Holmes, P. K. Hurley and M. A. Morris, *Microelectron Reliab*, 2007, **47**, 759-763.
87. J. Shen, A. Luo, L. F. Yao, X. J. Lin, B. Zhou, G. M. Wu and X. Y. Ni, *Mat Sci Eng C-Bio S*, 2007, **27**, 1145-1148.
88. H. Y. Fan, H. R. Bentley, K. R. Kathan, P. Clem, Y. F. Lu and C. J. Brinker, *J Non-Cryst Solids*, 2001, **285**, 79-83.
89. J. Y. Chen, F. M. Pan, A. T. Cho, K. J. Chao, T. G. Tsai, B. W. Wu, C. M. Yang and L. Chang, *J Electrochem Soc*, 2003, **150**, F123-F127.
90. J. T. Luo, W. F. Wu, H. C. Wen, B. Z. Wan, Y. M. Chang, C. P. Chou, J. M. Chen and W. N. Chen, *Thin Solid Films*, 2007, **515**, 7275-7280.
91. T. J. Ha, H. H. Park, S. B. Jung, H. Ryu and B. G. Yu, *J Colloid Interf Sci*, 2008, **326**, 186-190.
92. J. Y. Chen, F. M. Pan, D. X. Lin, A. T. Cho, K. J. Chao and L. Chang, *Electrochem Solid St*, 2006, **9**, G215-G218.
93. K. Kohmura, H. Tanaka, S. Oike, M. Murakami, N. Fujii, S. Takada, T. Ono, Y. Seino and T. Kikkawa, *Thin Solid Films*, 2007, **515**, 5019-5024.
94. S. Takada, N. Hata, Y. Seino, N. Fujii and T. Kikkawa, *J Appl Phys*, 2006, **100**.
95. S. B. Jung, T. J. Ha and H. H. Park, *Thin Solid Films*, 2007, **515**, 6521-6525.

Chapter Two: The Search for Ultra Low-k Materials ($k < 2$)

In this chapter, three classes of materials with potential ultra low-k properties will be evaluated. The classes are zeolites, metal organic frameworks (MOFs) and periodic mesoporous organosilicas (PMOs). From these three candidates, we have selected PMOs to investigate and tune their low-k properties. The aims of this research are also included at the end of this chapter.

A part of the PMO section is published in "*Chemical Society Reviews*": P. Van Der Voort, D. Esquivel, E. De Canck, F. Goethals, I. Van Driessche, and F. Romero-Salguero, *Chem. Soc. Rev.*, DOI:10.1039/C2CS35222B.

2.1 Introduction

At this moment the industry has not found the ideal low-k dielectric for the 22 nm node and beyond. The current integration processes are too hard for the known ultra low-k materials or *vice versa* the properties of the current ultra low-k materials are not sufficient. This is illustrated in figure 2.1. The first illustration shows the (predicted) progression of the low-k materials. However, solutions for low-k integration for 22 nm nodes (corresponding to *k*-values below 2) and beyond are not known.¹ The second illustration summarizes the already known solutions for the decreasing dimension sizes (nodes).

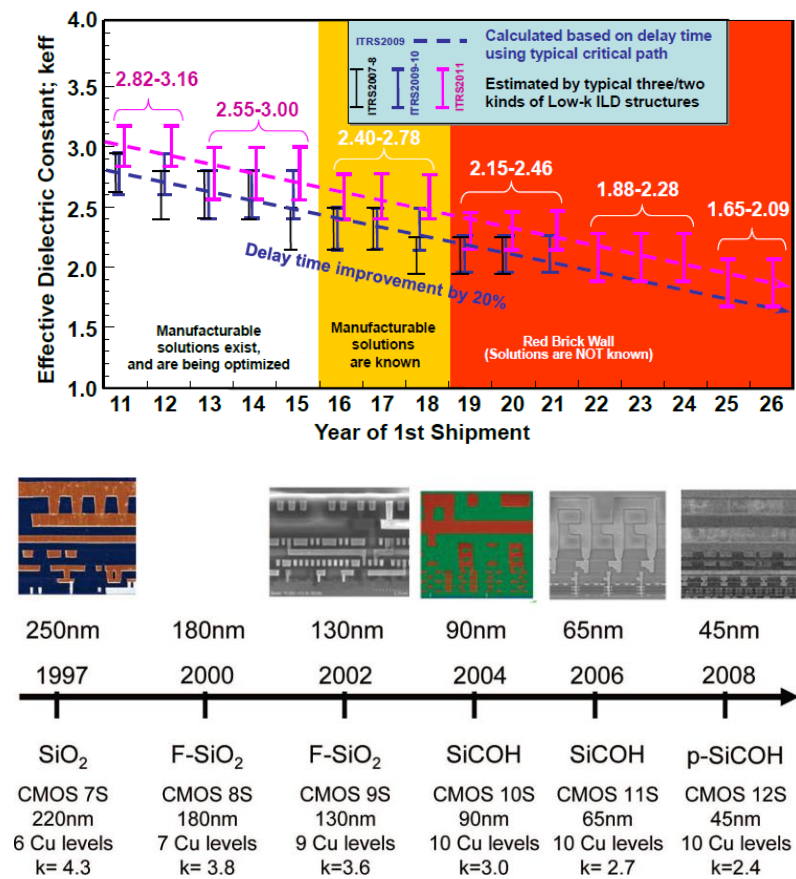


Figure 2.1: Low-k roadmap progression¹ and timeline for microprocessors from 1997 to 2008.²

To further increase the device speed, the industry has three possibilities. The first one is redesigning the size and shape of the device. The Intel Company recently succeeded this by the introduction of 3D-transistor technology.³ The developed 3D-transistor forms conducting channels on three sides instead of the planar design of conventional

transistors. The three-dimensional structure of these transistors allows chips to operate at lower voltage with lower leakage and better performances.³ However even within this approach, ideal ultra low-k materials can also contribute to even better performances.

A second option is that the microelectronic industry develops less hard integration processes which will not damage the low-k material. However, developing new and changing the current integration processes will be very time consuming and very expensive. Also the microelectronic industry is used to work with these setups and conditions.

As a chemist point of view the third possibility, which is the development and investigation of new materials, is the most attractive one. As already mentioned at the end of chapter one, the stability and in particular the mechanical stability of the ultra low-k materials has to improve. Improvements could be obtained when the material is ordered or has high matrix connectivity. Based on these findings, three new potential candidates are investigated, namely zeolites, metal organic frameworks (MOFs) and periodic mesoporous organosilicas (PMOs). These materials will be discussed in section 2.2, 2.3 and 2.4 respectively.

Another possibility is the introduction of air-gaps because this results in a k -value around one (the lowest possible value). Air-gaps can be created when layers of a sacrificial material are removed after Cu damascene integration. This can be done by decomposition of the sacrificial material through a cap layer or by etching of the material followed by sealing via a non-conformal CVD process (figure 2.2).⁴ However, the effective k -value is higher than one because the cap layer or sealant has k -values higher than those from SiO₂ (*i.e.* > 3.9). Also, electron migration is a real concern for air-gaps.⁵

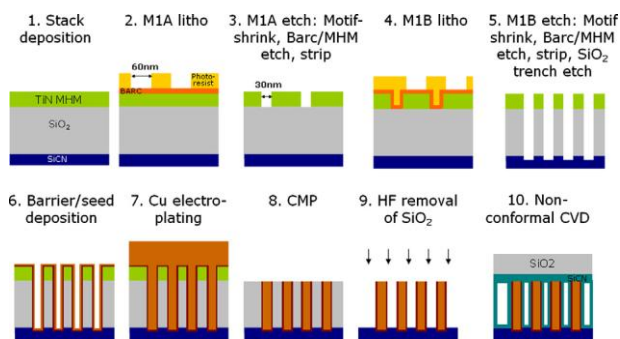


Figure 2.2: Procedure to introduce air-gaps.⁴

2.2 Zeolites

Zeolites (literally: boiling stones) are microporous materials that are already known for ages in the industry.⁶ They can be found in nature or can be synthesized. Zeolites are crystalline aluminosilicates with open frameworks and the matrix composition consists of SiO_4 and AlO_4 tetrahedra. A general zeolite structure is presented in figure 2.3. However, in many zeolites the Al/Si ratio is not equal to one. Because the network contains negative charges, counter ions (H^+ , Na^+ , ...) are necessary for the electron neutrality.⁷

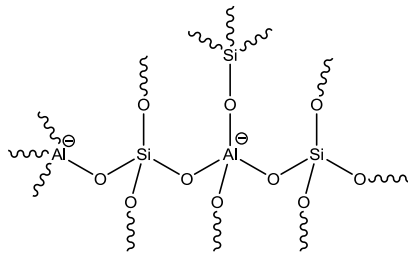


Figure 2.3: General zeolite composition.

Zeolites have a network of channels and cavities that can be tuned by changing the type of the zeolite structure by choosing its chemical composition and synthesis conditions. Zeolites are classified by the shape of their secondary building unit. Figure 2.4 shows some types of secondary building units (SBU). The SBUs can be linked together to form a complex three-dimensional structure.⁷

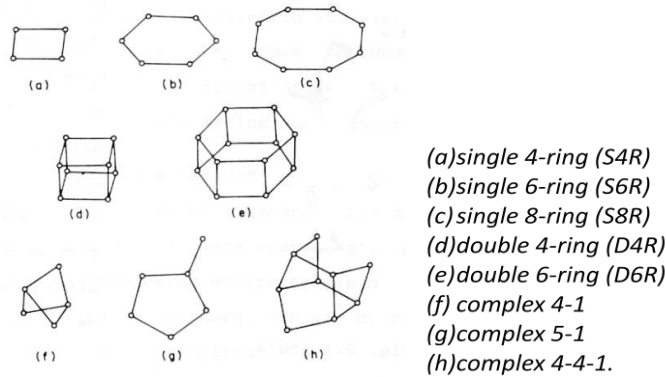


Figure 2.4: Types of secondary building units (taken from presentation of Prof P. Van Der Voort, Ugent).

The main applications of zeolites are as cationic exchangers, catalysts (especially in the petrochemical industry) and adsorbents. Because of their hydrophilic property, they are also used as drying agent for solvents.⁶

The question is now how can zeolites be utilized as ultra low-k materials? This would be remarkable, because they have a negatively charged network and are hydrophilic. Before giving a comment on these remarks, I will first focus on the good properties of zeolites. Firstly, they are highly porous which is needed to reduce the dielectric constant. Further, they have micropores which are preferable for integration. Finally, they are crystalline which should lead to better mechanical stability than their amorphous counterparts. However, the charged network and especially the cationic counter ions have a tremendous influence on the electrical properties. Luckily, it is also possible to synthesize pure silica zeolites (PSZ; silicalite) which also means that the zeolite is charge-free.

Yan *et al.*⁸ could synthesize silicalite films (MFI types) starting from TEOS as precursor with thicknesses in the range of 250-500 nm on silica wafers by in-situ crystallization. The films survived a polishing procedure, indicating a high mechanical stability and the dielectric constant is in the range 2.7-3.3. To obtain lower dielectric constants, a spin-on based synthesis was developed, resulting in *k*-values in the 1.8-2.1 range. With spin-coating higher porosities were obtained resulting in lower *k*-values, but this is due to the formation of interparticle pores with pore sizes of 17 nm which are too high for practical applications. Also the mechanical strength is poor.

By optimizing the synthesis conditions (a combination of a zeolite nanoparticle suspension with a amorphous silica component), the same group obtained spin-coated films with a dielectric constant of 2.1, a Young's modulus of 18 GPa and a bimodal pore size distribution (0.55 nm and 2.8 nm).⁹ When they compared the Young's modulus of the zeolites at a given dielectric constant with those from amorphous silicates, they found out that zeolites overclass amorphous silicates.¹⁰

The same group also wrote other publications on zeolite dielectric films. They could further decrease the dielectric constant to 1.8 by using cyclodextrin as porogen while still having an excellent mechanical stability ($E = 14$ GPa).¹¹

MEL type zeolite films seem also have good low-k properties. However, the particle size was first too large, but it could be lowered from 80 to 14 nm.^{12, 13} An increased hydrophobicity was obtained by a fluoro-organic functionalization.¹⁴

The group of Martens *et al.*¹⁵⁻¹⁸ also published several papers about zeolite thin films. They found out that MFI zeolite films also possess large voids in the range of tens of nanometers and that MEL zeolites still contain large particle sizes.^{15, 18} To overcome

these problems, they avoided the formation of large nanocrystals during the synthesis and added methyltrimethoxysilane to increase the hydrophobicity. In this case the films are not completely crystalline and are therefore called zeolite-like low-k materials (ZLK). The films have a pore radius around 0.8 nm, a particle size of 5 nm, dielectric constant around 2.2 and a Young's modulus of 6.8 GPa.¹⁶

Lu *et al.*¹⁹ added surfactant Tween 80 to the synthesis of MFI zeolites. The optimal values are a k -value of 1.83, a hardness of 1.39 GPa, a Young's modulus of 12.3 GPa and a leakage current of 1.35×10^{-7} A/cm².

To further improve the properties of MEL zeolites, Seino and coworkers performed different after treatments. By performing a calcination, TMCTS silylation, UV-curing and again a TMCTS silylation treatment step, better mechanical properties were obtained ($E = 10$ GPa for $k = 2.2$).²⁰ Also, the leakage current can be reduced to 1×10^{-8} A/cm² after a TMCTS treatment²¹ and the estimated lifetime is ten years when 3.4 MV/cm is applied at 125°C.²²

Besides the typical spin-coating or hydrothermal synthesis of zeolites, Cho *et al.*²³ could prepare pure silica zeolite films by a vapor phase transport method. With this technique it is possible to synthesize zeolite films from dry gel under a gas mixture of ethylenediamine, triethylamine and water. Unfortunately, the dielectric constant was relatively high ($k = 2.7$). Hunt *et al.* used a vapor phase transport method to synthesize new types of PSZ films: LTA, CHA, ITW,²⁴ and STT and SVR.²⁵ The lowest dielectric constant was obtained with the LTA film (1.69). However, the k -measurement occurred under dry conditions, thus it is likely that the film is hydrophilic.

As summary of the low-k applicability of zeolite materials, it is clear that zeolites have one of the best mechanical stability/dielectric constant ratio from all the reported materials. However, the ultra low k -value is mostly obtained by large voids between the particles or the zeolite film is not hydrophobic. To overcome these problems MTMS is added during the synthesis resulting in zeolite like low-k materials, but this leads to a significant decrease in mechanical stability.^{16, 26} However the obtained stability should be still sufficient making that ZLK materials are one of the most promising ultra low-k materials.

2.3 Metal organic frameworks (MOFs)

Metal organic frameworks are nanoporous, crystalline materials that consist of metal ions that are connected by organic linkers.²⁷ By varying the metal ion or linker, various sizes and shapes of channels or cavities can be obtained.²⁸ Further characteristics of MOFs are that a strong bonding robustness must be provided, the organic linkers are

available for modification by organic synthesis and the structure is geometrically well-defined.²⁹ Figure 2.5 shows a typical representation of a MOF.

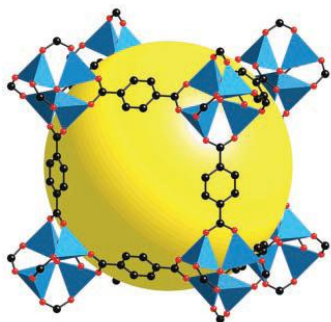


Figure 2.5: Single-crystal x-ray structure of a MOF type.³⁰

One of the first reported application of MOFs is as hydrogen storage materials.³⁰ At low temperature, good adsorption properties were reported, but the adsorption capacity at room temperature has to improve. Other potential applications are in the fields of adsorption,³¹ catalysis,^{32,33} separation³⁴ or sensing.³⁵

Because of their low density, among the lowest recorded for any crystalline material, MOFs are also being investigated as low-k materials. Therefore, thin MOF films have to be synthesized. Bétard and Fischer³⁶ wrote an extensive review on MOF thin films and how they could be synthesized. The most straightforward method is to prepare a mother solution similar as for powder synthesis and insert a substrate in the solution. MOF films will then grow at the surface of the substrate.

Recently Zagorodniy *et al.*³⁷ reported that MOFs are promising candidates for future ultra low-k dielectrics. They calculated the dielectric constant of a series of MOFs based on $Zn_4O(CO_2)_4$ units connected by different organic linkers. They found that all the investigated MOFs have k -values below 2 with good mechanical properties. However, to consider MOFs as really potential low-k materials, far more research is needed. First of all, it has to be experimentally confirmed that the k -values are indeed that low with good mechanical properties. Furthermore, the presence of metal ions in the low-k material raises questions about the electrical reliability (leakage and breakdown) of the film.

2.4 Periodic Mesoporous Organosilicas (PMOs)

2.4.1 General information

Periodic mesoporous organosilicas or PMOs are ordered mesoporous silica materials of which at least one siloxane bond in the matrix is replaced by an organic bridge. In contrast of zeolites and MOFs, PMOs are usually amorphous, but their pores and pore walls are arranged in a structural order. Therefore, they are similar to MCM and SBA (ordered mesoporous silicas) type materials except for the organic bridge. Typically PMO materials are synthesized by hydrolysis and condensation of bridged organosilanes $(R'O)_3Si-R-Si(OR')_3$ in the presence of a surfactant which acts as structure directing agent.³⁸ After an ageing period, the surfactant can be removed by an extraction procedure or by a thermal treatment under an inert atmosphere, leaving behind a porous PMO material. A typical synthesis scheme is given in figure 2.6.

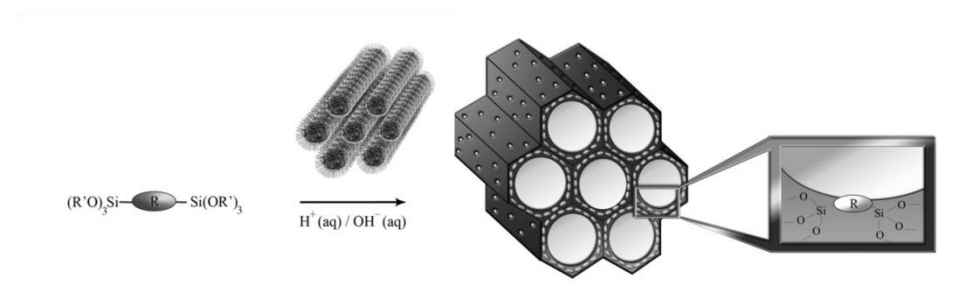


Figure 2.6: General synthesis procedure for PMOs, R represents aliphatic or aromatic functional groups.³⁹

The great advantage of PMOs over pure silica ordered mesoporous materials is the presence of uniformly distributed organic functional groups in the walls. This avoids leaching of the functional group or pore narrowing which is often observed in post-functionalized porous silicas.⁴⁰ Further, PMOs are hydrothermally and mechanically more stable than mesoporous silicas.⁴¹ These characteristics make them promising candidates for applications in catalysis, adsorption, drug-delivery and separation.⁴²⁻⁴⁵

By varying synthesis conditions, precursors and surfactants, it is possible to adjust the pore size, porosity, surface area, ordering, wall thickness and morphology of the PMOs.⁴⁴ Examples of frequently used surfactants are similar to those for mesoporous silicas and are already mentioned in chapter 1 (table 1.1). Possible precursors are methylene,⁴⁶ ethylene,⁴⁷ ethenylene,⁴⁸ phenylene,⁴⁹ thiophene,⁵⁰ etc. An overview of typical PMO precursors is given in figure 2.7.

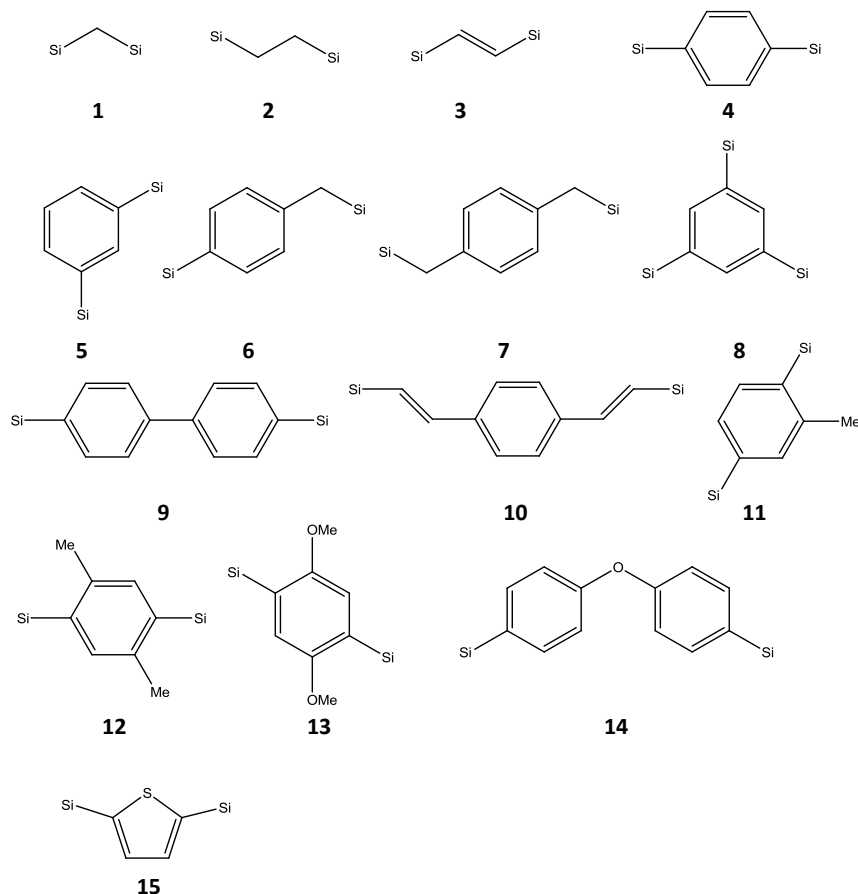
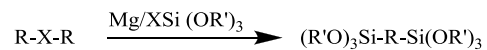
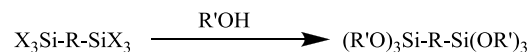


Figure 2.7: Overview of bridged organosilica precursors. The $\text{Si}(\text{OR})_3$ groups are only represented by Si for clarity reasons.

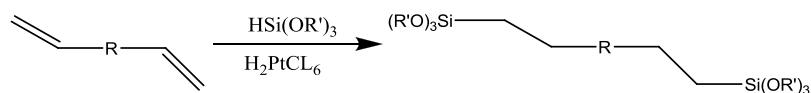
PMO precursors (bis-silanes) can be obtained by several synthetic routes.⁵¹ A first possible method is a Grignard reaction of dihalogenated hydrocarbons with halogenated trialkoxysilanes.



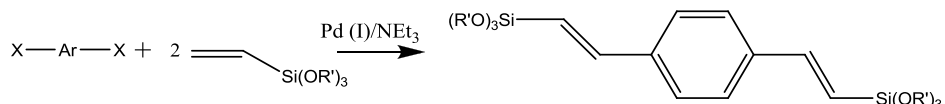
A second possible method is the alcoholysis of halogenated bis-silanes.



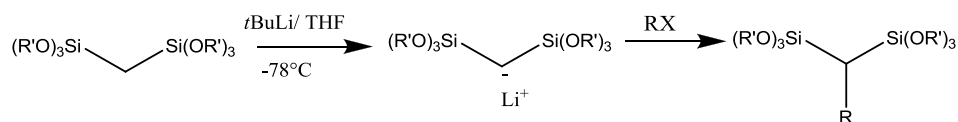
Hydrosilation is another reported method and this method uses a Pt catalyst to anchor alkoxy silanes on the rear ends of di-alkenes (see below).



For aromatic precursors, a Pd coupling Heck reaction can be applied



For further functionalization of methylene-bridged silane precursors, a lithiation process is a suitable method.



The first papers on PMO materials appeared in 1999. Three different research groups developed these types of materials almost at the same time. Inagaki *et al.*⁴⁷ reported on the synthesis of ethylene-bridged PMOs (= ethane PMOs). As starting precursor 1,2-bis(trimethoxysilyl)ethane was used and octadecyltrimethylammonium chloride (OTAC) was added as structure directing agent. The materials were highly ordered at the mesoscale, with 2D and 3D hexagonal symmetries and uniform pore sizes. The pore diameters were 3.1 and 2.7 nm, and the surface area was 750 and 1170 m²/g for respectively the 2D and 3D hexagonal ordered material.

Asefa *et al.*⁴⁸ obtained PMOs containing bridge-bonded ethene groups directly integrated into the silica framework (= ethene PMOs). They used a TEOS and 1,2-bis(trimethoxysilyl)ethene precursor mixture and surfactant cetyltrimethylammonium bromide (CTAB). They also obtained a hexagonal symmetry and a pore diameter of 4 nm. The surface area and pore volume were 637 m²/g and 0.6 ml/g respectively. Further, they also demonstrated the accessibility of the ethene groups by a bromination reaction.

The third group, Melde *et al.*,⁵² synthesized ethane and ethene PMOs following the MCM-41 synthesis method. The materials also had high surface areas and uniform pores, but only wormlike structures were obtained instead of highly ordered materials.

Since their development, many other researchers started to investigate single organic-bridged PMOs. Synthesis conditions and material properties are being optimized, new functional groups are being introduced and possible applications are being explored. Due to the fact that this thesis only focuses on one application (*i.e.*, low-k materials), these investigations will not be covered herein. Excellent reviews on this topic can be found elsewhere.^{38, 44, 53-61}

2.4.2 Multi organic-bridged PMOs

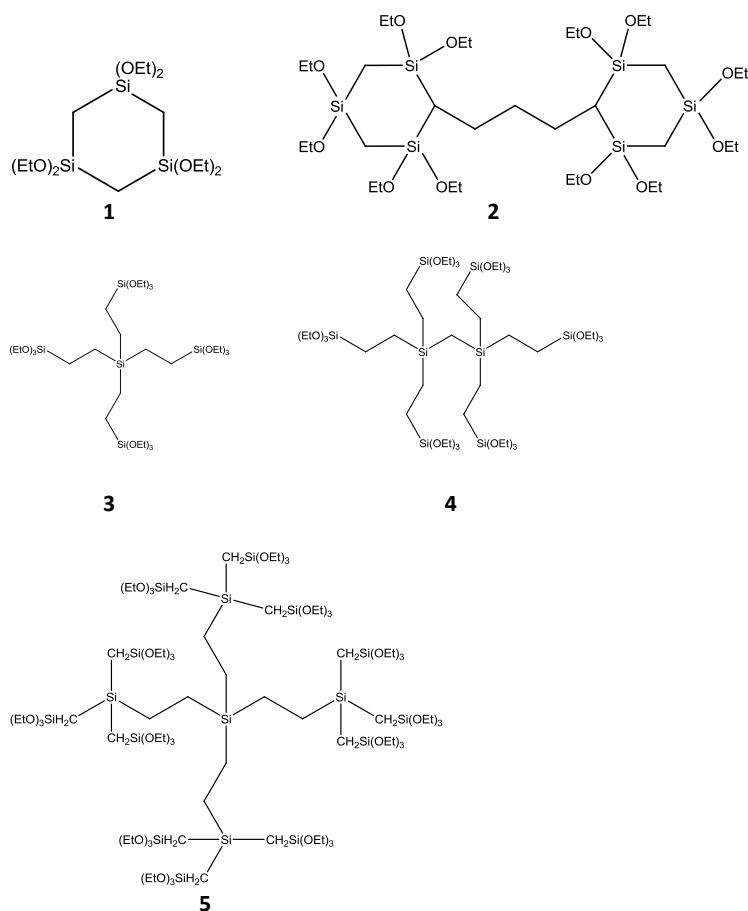


Figure 2.8: PMO precursors with multi organic bridges.

Besides the typical single bridged silanes, Ozin's group developed new classes of PMOs consisting of multi-bridged organic groups.^{62, 63} The main advantage of these high organic content PMOs is that more organic functional groups are directly incorporated in the silica network.

The first high organic content PMOs are periodic mesoporous organosilicas containing interconnected $[\text{Si}(\text{CH}_2)]_3$ rings reported in 2003.⁶² The synthesis of these ring PMOs is similar to the synthesis of single bridged PMOs but in this case 1,1,3,3,5,5-hexaethoxy-1,3,5-trisilacyclohexane is used as silane precursor (see precursor **1** in figure 2.8). For the synthesis, CTAB was used as structure directing agent. Meso-ordered powders with very high surface areas and a pore size of 2 nm were obtained. Furthermore, under inert atmosphere the mesoporous structure is stable up to 600°C with no pore shrinkage up to 400°C.

To prove that a new family of PMOs can be obtained, trisilacyclohexane precursors were functionalized via a lithiation process which was already known for single methylene-bridged precursors (figure 2.9).

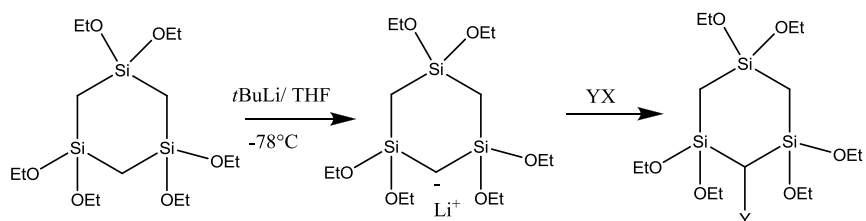


Figure 2.9: Functionalization of cyclic PMO precursors through lithiation with $Y = \text{I}, \text{Br}, \text{ethyl}$, $X = \text{I}, \text{Br}$.

After the lithiation, reactions with Br_2 , I_2 or iodoethane were induced to obtain substituted three rings. PMOs from these new precursors could be obtained with the use of a triblock copolymer in an acidic sodium chloride solution. The PMOs are well ordered and have pore sizes of 4.5 nm.

With this approach it is also possible to synthesize PMOs with two cyclic building blocks which are bridged by an organic group shown in figure 2.10. The resulting PMOs showed uniform periodic mesopores with pore sizes of 6 nm and a BET surface area of 967 m^2/g . Further the material displayed a high thermal stability with no mass loss up to 400°C in a nitrogen atmosphere.⁶⁴

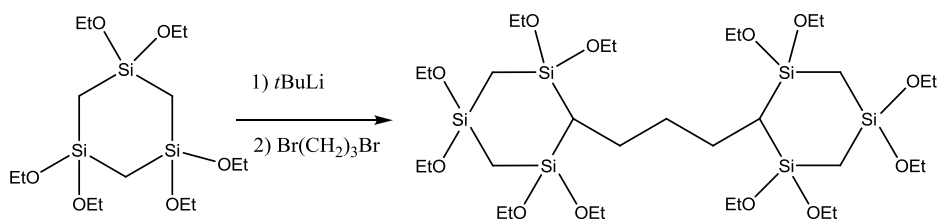


Figure 2.10: Synthesis of attached cyclic PMO precursors.

A second class of inert organic bridges PMOs are the periodic mesoporous dendrisilicas (PMDs).⁶³ They are prepared from dendrimers with trialkoxysilyl groups at the outmost shell (see precursors **3** to **5** in figure 2.8). The dendrisilica synthesis is based on acid- or base-catalyzed hydrolysis of the trialkoxysilyl groups and subsequent template-directed condensation of the dendrimers into an ordered template-dendrisilica nanocomposite. The obtained powders also have large surface areas, narrow pore size distributions and a high ordering. One of the main proposed applications of these materials could be as drug delivery systems.⁶³

2.4.3 PMOs as low-k materials

Already since the first publications on PMOs one of the proposed applications was as low-k material.⁴⁸ This is because PMOs have indeed interesting low-k characteristics. In fact, they are similar in chemical composition compared to the organosilicate low-k materials with the advantage that low polarisable organic groups are integrated in the silica matrix. Especially PMOs with the simplest organic bridges such as ethane and methane are extremely interesting for low-k applications because they have the lowest polarisable organic bridge. This means that more network connectivity can be obtained which should enhance the mechanical stability. Even more bridged organosilane precursors are also incorporated in OSG films resulting in a higher Young's modulus of the film.^{2, 65}

Other interesting characteristics are the possibility to obtain ordered structures which can also contribute to a better stability and the fact that the materials have tunable porosity.

Similar to mesoporous silicas, PMO thin films can be obtained with the EISA procedure. Lu *et al.*⁶⁶ reported the synthesis of ethane, benzene and butene PMOs thin films via the EISA approach. They have used different surfactants (CTAB, Brij-56, SDS and P123; SDS = sodium dodecyl sulfate) and investigated the influence of the surfactant on the ordering of the material.

For example, they found that ethane PMO films prepared with SDS leads to lamellar mesophases, while for CTAB and Brij-56 a hexagonal and cubic mesophase was respectively obtained. Secondly, they prepared a series of films from TEOS and BTESA with different molar ratios to investigate the influence of the organic bridge on the dielectric constant of the film. For a similar porosity, they observed a decrease in dielectric constant when more BTESA was used ($k = 2.15$ for a 75:25 TEOS:BTESA composition, $k = 1.98$ for a 25:75 TEOS:BTESA composition). Besides the decrease in dielectric constant, also an increase in mechanical stability is obtained.

At this moment Ozin's group reported the most papers related to PMOs and low-k. They prepared methane, ethane, ethene and ring PMO films using CTAC as template, and investigated their dielectric, mechanical and hydrophobic properties.^{62, 67} They also investigated the influence of the organic bridge on the dielectric constant by mixing the starting PMO precursor with TMOS and came to the same conclusion that the dielectric constant decreases and the mechanical stability increases with organic content.

The dielectric constant can be further decreased by annealing the samples above 400°C in a nitrogen atmosphere. The reason for this is an increase in hydrophobic character of the PMO. The more hydrophilic a material is, the more water that will adsorb and this leads to a dramatic increase in dielectric constant. For ethane PMOs, this beneficial effect can be attributed to extra condensation of hydrophilic silanol groups during annealing.

In case of methane and ring PMOs also a self-hydrophobization step takes place. During this latter process some of the Si-CH₂-Si bonds break and react with SiOH bonds to form end standing hydrophobic SiCH₃ groups and Si-O-Si bonds (see figure 2.11). This self-hydrophobizing thermal treatment makes an after treatment with vapor gases such as hexamethyldisilazane (HMDS) redundant.⁶⁸

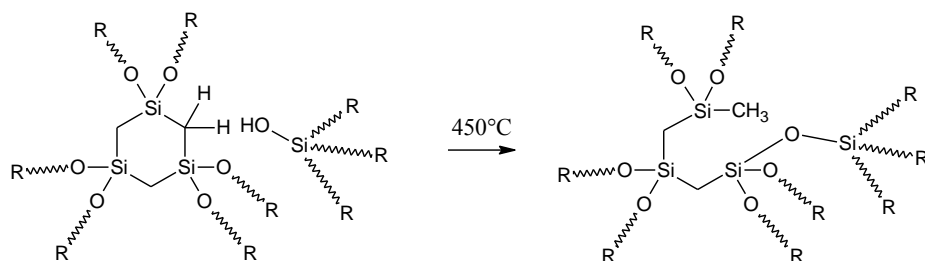


Figure 2.11: Thermally induced self-hydrophobization process.

A more detailed study on the hydrophobic properties of low-k PMO films was recently reported.⁶⁹ Water adsorption isotherms and water contact angles of methane, ethane, ethene and ring PMO films post-treated at different temperatures were obtained and discussed.

At lower temperatures ($T < 400^\circ\text{C}$) the sequence of hydrophobicity is: ring > ethane > methane > ethene. The authors explained this by the reduction of silanol groups per unit surface area. Ring PMOs can only have a maximum of two silanol groups per Si atom because of the two carbon bridges while the other three can have a maximum of three silanol groups. This also explains the difference in ethane and methane PMOs because ethane PMOs contain one more carbon in the bridge, reducing slightly the

silanol concentration. For ethene PMOs, the bridge is more attractive to water molecules because the π -electrons are more polarisable by the dipoles of the water molecules. At higher temperatures, the ring and methane PMOs are far more hydrophobic due to the already mentioned self-hydrophobization process.

The deposition techniques to prepare these PMO thin films via the EISA method are liquid phase deposition methods such as spin-coating and dip-coating. However, Wang *et al.*⁷⁰ succeeded to make PMO films via a vapor phase delivery system which is a more preferred method in industry than the liquid phase deposition methods. In this process, an aerosol is generated by atomizing a solution of PMO precursors, surfactant, and water in a chosen organic solvent. Evaporation of the solvent induces self-assembly inside the aerosol droplets. Then the aerosol is deposited through a converging nozzle on a spinning substrate forming a thin film. With this deposition technique they were also able to synthesize ethane PMO films with ultra low k -values and high mechanical stabilities.

The previously mentioned PMO films all have relative dense pore walls. Ozin's group⁷¹ developed a new class of PMOs with air pockets in the pore walls. This was achieved by a template-directed spin-coating of a polyhedral oligomeric silsesquioxane (POSS) precursor (see figure 2.12). The obtained POSS-PMO films exhibit a porosity of 39% and a k -value of 1.7.

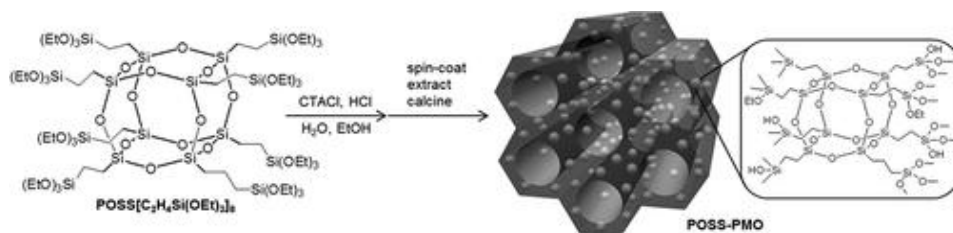


Figure 2.12: Preparation of POSS-PMO thin films.⁷¹

Table 2.1 summarizes the different types of PMO films with their reported porosity and dielectric constant. For each reference we report the lowest obtained k -value per PMO type. As observed, k -values experienced a great variation even for the same PMO type. A first explanation could reside in their different porosity. Normally, the dielectric constant decreases when the porosity increases. Other possible causes of these variations can be related to small amounts of adsorbed moisture or even to experimental variance, as the measurement of accurate k -values is rather difficult to perform.

Chapter 2: The search for ultra low-k materials

Table 2.1: Overview of different types of PMO films and their dielectric constants.

PMO	surfactant	Porosity (%)	k -value	Ref.
Methane PMO	CTAC	N.A.	1.8	67
	CTAC	53	1.6	69
Ethane PMO	Brij-56	56	1.98	66
	CTAC	N. A.	1.9	67
	CTAC	45	1.67	69
	CTAC	47	1.7	70
Ethene PMO	CTAC	44	1.7	69
Ring PMO	CTAC	N.A.	2.0	62
	CTAC	50	1.63	69
POSS-PMO	CTAC	39	1.7	71

Typically, the k -value is extracted from capacitance measurements of metal-insulator-semiconductor (MIS) capacitors using equation (1.4): $k = C d / \epsilon_0 A$

With C the capacitance, d the thickness of the low-k film, ϵ_0 the permittivity of vacuum and A the area of the top contact electrode.

The area of the top electrodes is typically in the range of μm^2 or mm^2 while the thickness of the film is in the nanometer range. Therefore, a precise determination of the area is very crucial to obtain accurate k -values. To minimize the error of the top electrode area, Ciofi *et al.*⁷² proposed to deposit top contacts with different areas and shapes. When recalculating the measured capacitance to F/cm^2 the values should be similar for all the different top electrode sizes.

The same authors stated that also a good ohmic back contact is needed to avoid inaccurate k -values even when highly doped wafers are used as bottom contact. For example, a good back contact can be obtained by removing the native oxide of the silicon wafer and the impedance analyzer can then be connected to the wafer with a gallium-indium alloy paste. Also, when MIS structures are used, the applied voltage should be in the accumulation range of the semiconductor to determine the capacitance. Otherwise the semiconductor will also act as a dielectric material. This means that a careful sample preparation and characterization setup is very important to obtain accurate dielectric constant values.

Although there is some variation in the reported k -values of PMO films, the microelectronic industry recognized that PMOs are one of the most promising ultra low-k materials to integrate in actual devices.² However, still a lot of research is required. This research should be focused on the development of new PMO materials

with improved low-k properties and more integration related characteristics of the current PMOs should be determined. For instance, it would be very interesting to see how stable PMO films are in different plasma environments which are common treatments in the semi-conductor industry. Further, good adhesion to other device components is very important to survive the whole manufacturing process. Finally, to date there is also not much information about the leakage current and electrical breakdown of highly porous PMO films. The leakage current should be as low as possible and the breakdown as high as possible to provide reliable materials with a long lifetime.

2.5 Aim of the PhD research

The aim of this PhD research is to develop materials with promising ultra low-k characteristics. Because of the already reported promising results, we have selected PMOs as research materials and in particular ethane, ethene and ring PMOs. Ethane and ring PMOs were chosen because of their low polarisable groups and ethene PMOs to investigate the effect of the double carbon bond in the matrix.

Firstly, we compare the best synthesis conditions and stabilities of these PMOs in powder form, because it is easier to investigate their bulk properties and also more straightforward characterization methods can be used.

Secondly, the PMOs with the best properties will be synthesized as thin films and the synthesis will be further optimized to obtain good quality porous films with ultra low dielectric constants.

A drawback of PMOs is the connectivity of the pores and the presence of mesopores instead of solely micropores. To solve this problem pore mouth narrowing or even better complete pore sealing is necessary.⁶⁸

Therefore the second aim of this research is to find a way to narrow or seal the pores of mesoporous low-k materials. To obtain this, two pathways will be followed. The first one is trying to fill only the pore mouth through grafting on the pore mouth walls of the low-k material. The second pathway is the deposition of a top layer which seals the pores without filling them.

2.6 References

1. International Technology Roadmap for Semiconductors_ITRS_2011.
2. W. Volksen, R. D. Miller and G. Dubois, *Chem Rev*, 2010, **110**, 56-110.
3. www.intel.com.
4. M. Pantouvaki, F. Sebaai, K. Kellens, D. Goossens, B. Vereecke, J. Versluijs, E. Van Besien, R. Caluwaerts, K. Marrant, H. Bender, A. Moussa, H. Struyf and G. P. Beyer, *Microelectron. Eng.*, 2011, **88**, 1618-1622.
5. I. Bauer, K. Weide-Zaage and L. Meinshausen, *Microelectron. Reliab.*, 2011, **51**, 1587-1591.
6. I. Fechete, Y. Wang and J. C. Vedrine, *Catal Today*, 2012, **189**, 2-27.
7. S. M. Auerbach, K. A. Carrado and P. K. Dutta, eds., *Handbook of Zeolite Science and Technology*, Marcel Dekker INC, New York, 2003.
8. Z. B. Wang, A. P. Mitra, H. T. Wang, L. M. Huang and Y. S. Yan, *Advanced Materials*, 2001, **13**, 1463-+.
9. Z. B. Wang, H. T. Wang, A. Mitra, L. M. Huang and Y. S. Yan, *Advanced Materials*, 2001, **13**, 746-749.
10. Z. J. Li, M. C. Johnson, M. W. Sun, E. T. Ryan, D. J. Earl, W. Maichen, J. I. Martin, S. Li, C. M. Lew, J. Wang, M. W. Deem, M. E. Davis and Y. S. Yan, *Angewandte Chemie-International Edition*, 2006, **45**, 6329-6332.
11. S. Li, Z. J. Li and Y. S. Yan, *Advanced Materials*, 2003, **15**, 1528-+.
12. L. Yan, S. Minwei, C. M. Lew, W. Junlan and Y. Yushan, *Adv. Funct. Mater.*, 2008, **18**, 1732-1738.
13. Y. Liu, C. M. Lew, M. Sun, R. Cai, J. Wang, G. Kloster, B. Boyanov and Y. Yan, *Angewandte Chemie-International Edition*, 2009, **48**, 4777-4780.
14. C. M. Lew, Z. Li, S. Li, S.-J. Hwang, Y. Liu, D. I. Medina, M. Sun, J. Wang, M. E. Davis and Y. Yan, *Adv. Funct. Mater.*, 2008, **18**, 3454-3460.
15. S. Eslava, M. R. Baklanov, A. V. Neimark, F. Iacopi, C. E. A. Kirschhock, K. Maex and J. A. Martens, *Advanced Materials*, 2008, **20**, 3110-3116.
16. S. Eslava, J. Urrutia, A. N. Busawon, M. R. Baklanov, F. Iacopi, S. Aldea, K. Maex, J. A. Martens and C. E. A. Kirschhock, *Journal of the American Chemical Society*, 2008, **130**, 17528-17536.
17. S. Eslava, C. E. A. Kirschhock, S. Aldea, M. R. Baklanov, F. Iacopi, K. Maex and J. A. Martens, *Microporous and Mesoporous Materials*, 2009, **118**, 458-466.
18. S. Eslava, J. W. Seo, C. E. A. Kirschhock, M. R. Baklanov, K. Maex and J. A. Martens, *Adv. Funct. Mater.*, 2010, **20**, 2377-2379.
19. H. Y. Lu, C. L. Teng, C. W. Yu, Y. C. Liu and B. Z. Wan, *Ind. Eng. Chem. Res.*, 2010, **49**, 6279-6286.
20. T. Yoshino, N. Ohnuki, N. Hata and Y. Seino, *Japanese Journal of Applied Physics*, 2009, **48**.
21. T. Seo, T. Yoshino, N. Ohnuki, Y. Seino, Y. Cho, N. Hata and T. Kikkawa, *J. Electrochem. Soc.*, 2009, **156**, H98-H105.
22. T. Seo, T. Yoshino, N. Ohnuki, Y. Seino, Y. Cho, N. Hata and T. Kikkawa, *J. Electrochem. Soc.*, 2011, **158**, H659-H665.
23. Y. Cho, T. Seo, K. Kohmura and T. Kikkawa, *Japanese Journal of Applied Physics*, 2008, **47**, 8360-8363.

24. H. K. Hunt, C. M. Lew, M. Sun, Y. Yan and M. E. Davis, *Microporous and Mesoporous Materials*, 2010, **128**, 12-18.
25. H. K. Hunt, C. M. Lew, M. Sun, Y. Yan and M. E. Davis, *Microporous and Mesoporous Materials*, 2010, **130**, 49-55.
26. M. L. Che, S. Chuang and J. Leu, *J. Electrochem. Soc.*, 2012, **159**, G23-G28.
27. H. Li, M. Eddaoudi, M. O'Keeffe and O. M. Yaghi, *Nature*, 1999, **402**, 276-279.
28. M. Eddaoudi, J. Kim, N. Rosi, D. Vodak, J. Wachter, M. O'Keeffe and O. M. Yaghi, *Science*, 2002, **295**, 469-472.
29. J. L. C. Rowsell and O. M. Yaghi, *Microporous and Mesoporous Materials*, 2004, **73**, 3-14.
30. N. L. Rosi, J. Eckert, M. Eddaoudi, D. T. Vodak, J. Kim, M. O'Keeffe and O. M. Yaghi, *Science*, 2003, **300**, 1127-1129.
31. M. Anbia, V. Hoseini and S. Sheykhi, *J Ind Eng Chem*, 2012, **18**, 1149-1152.
32. K. Leus, M. Vandichel, Y. Y. Liu, I. Muylaert, J. Musschoot, S. Pyl, H. Vrielinck, F. Callens, G. B. Marin, C. Detavernier, P. V. Wiper, Y. Z. Khimyak, M. Waroquier, V. Van Speybroeck and P. Van der Voort, *J Catal*, 2012, **285**, 196-207.
33. Y. Y. Liu, K. Leus, M. Grzywa, D. Weinberger, K. Strubbe, H. Vrielinck, R. Van Deun, D. Volkmer, V. Van Speybroeck and P. Van der Voort, *Eur J Inorg Chem*, 2012, 2819-2827.
34. R. Krishna, *Microporous and Mesoporous Materials*, 2012, **156**, 217-223.
35. P. Y. Wu, J. Wang, C. He, X. L. Zhang, Y. T. Wang, T. Liu and C. Y. Duan, *Adv. Funct. Mater.*, 2012, **22**, 1698-1703.
36. A. Betard and R. A. Fischer, *Chem Rev*, 2012, **112**, 1055-1083.
37. K. Zagorodniy, G. Seifert and H. Hermann, *Applied Physics Letters*, 2010, **97**.
38. F. Hoffmann, M. Cornelius, J. Morell and M. Froba, *Angewandte Chemie-International Edition*, 2006, **45**, 3216-3251.
39. P. Van der Voort, C. Vercaemst, D. Schaubroeck and F. Verpoort, *Physical Chemistry Chemical Physics*, 2008, **10**, 347-360.
40. N. Petkov, S. Mintova, B. Jean, T. Metzger and T. Bein, *Mat Sci Eng C-Bio S*, 2003, **23**, 827-831.
41. M. C. Burleigh, M. A. Markowitz, S. Jayasundera, M. S. Spector, C. W. Thomas and B. P. Gaber, *J Phys Chem B*, 2003, **107**, 12628-12634.
42. G. R. Zhu, D. M. Jiang, Q. H. Yang, J. Yang and C. Li, *J Chromatogr A*, 2007, **1149**, 219-227.
43. A. P. Wight and M. E. Davis, *Chem Rev*, 2002, **102**, 3589-3613.
44. W. J. Hunks and G. A. Ozin, *J Mater Chem*, 2005, **15**, 3716-3724.
45. T. Henning, J. J. Brandner, L. Eichhorn, K. Schubert, M. Schreiber, M. Gungerich, H. Gunther, P. J. Klar, V. Rebbin and M. Froba, *Microfluid Nanofluid*, 2007, **3**, 299-305.
46. T. Asefa, M. J. MacLachlan, H. Grondey, N. Coombs and G. A. Ozin, *Angewandte Chemie-International Edition*, 2000, **39**, 1808-+.
47. S. Inagaki, S. Guan, Y. Fukushima, T. Ohsuna and O. Terasaki, *Journal of the American Chemical Society*, 1999, **121**, 9611-9614.
48. T. Asefa, M. J. MacLachlan, N. Coombs and G. A. Ozin, *Nature*, 1999, **402**, 867-871.
49. S. Inagaki, S. Guan, T. Ohsuna and O. Terasaki, *Nature*, 2002, **416**, 304-307.

50. C. Yoshina-Ishii, T. Asefa, N. Coombs, M. J. MacLachlan and G. A. Ozin, *Chem Commun*, 1999, 2539-2540.
51. A. Sayari and i. M. Jaro, eds., *Nanoporous Materials III*, Elsevier Science, Amsterdam, 2002.
52. B. J. Melde, B. T. Holland, C. F. Blanford and A. Stein, *Chemistry of Materials*, 1999, **11**, 3302-3308.
53. D. M. Ford, E. E. Simanek and D. F. Shantz, *Nanotechnology*, 2005, **16**, S458-S475.
54. S. Fujita and S. Inagaki, *Chemistry of Materials*, 2008, **20**, 891-908.
55. B. Hatton, K. Landskron, W. Whitnall, D. Perovic and G. A. Ozin, *Accounts Chem Res*, 2005, **38**, 305-312.
56. F. Hoffmann, M. Cornelius, J. Morell and M. Froba, *Zeolites and Related Materials: Trends, Targets and Challenges, Proceedings of the 4th International Feza Conference*, 2008, **174**, 55-60.
57. F. Hoffmann and M. Froba, *Chemical Society Reviews*, 2011, **40**, 608-620.
58. M. Jaroniec, *Nature*, 2006, **442**, 638-640.
59. M. P. Kapoor and S. Inagaki, *Bulletin of the Chemical Society of Japan*, 2006, **79**, 1463-1475.
60. N. Mizoshita, T. Tani and S. Inagaki, *Chemical Society Reviews*, 2011, **40**, 789-800.
61. H. S. Xia, C. H. Zhou, D. S. Tong and C. X. Lin, *Journal of Porous Materials*, 2010, **17**, 225-252.
62. K. Landskron, B. D. Hatton, D. D. Perovic and G. A. Ozin, *Science*, 2003, **302**, 266-269.
63. K. Landskron and G. A. Ozin, *Science*, 2004, **306**, 1529-1532.
64. K. Landskron and G. A. Ozin, *Angewandte Chemie-International Edition*, 2005, **44**, 2107-2109.
65. S. M. Gates, G. Dubois, E. T. Ryan, A. Grill, M. Liu and D. Gidley, *J. Electrochem. Soc.*, 2009, **156**, G156-G162.
66. Y. F. Lu, H. Y. Fan, N. Doke, D. A. Loy, R. A. Assink, D. A. LaVan and C. J. Brinker, *Journal of the American Chemical Society*, 2000, **122**, 5258-5261.
67. B. D. Hatton, K. Landskron, W. Whitnall, D. D. Perovic and G. A. Ozin, *Adv. Funct. Mater.*, 2005, **15**, 823-829.
68. B. D. Hatton, K. Landskron, W. J. Hunks, M. R. Bennett, D. Shukaris, D. D. Perovic and G. A. Ozin, *Materials Today*, 2006, **9**, 22-31.
69. W. D. Wang, D. Grozea, S. Kohli, D. D. Perovic and G. A. Ozin, *Acs Nano*, 2011, **5**, 1267-1275.
70. W. D. Wang, D. Grozea, A. Kim, D. D. Perovic and G. A. Ozin, *Advanced Materials*, 2010, **22**, 99-+.
71. M. Seino, W. D. Wang, J. E. Lofgreen, D. P. Puzzo, T. Manabe and G. A. Ozin, *Journal of the American Chemical Society*, 2011, **133**, 18082-18085.
72. I. Ciofi, M. R. Baklanov, Z. Tokei and G. P. Beyer, *Microelectronic Engineering*, 2010, **87**, 2391-2406.

Chapter Three: Comparative Study **of Ethylene- and Ethenylene-** **Bridged Periodic Mesoporous** **Organosilicas**

In this chapter, a comparative study of hexagonal structured ethylene- and ethenylene-bridged powder PMOs is presented. For the PMO synthesis, 1,2-bis(triethoxysilyl)ethane and 1,2-bis(triethoxysilyl)ethene were used as precursors and pluronic P123 was used as structure directing agent. The effect of butanol on the pore size distribution and the morphology of ethylene-bridged and ethenylene-bridged PMOs were investigated. This was done by first varying the butanol concentration and next, it was investigated if the acidity range to get uniform pores can be broadened with the addition of butanol.

Further, the mechanical, hydrothermal and chemical stability of the PMOs were compared. The materials were characterized by N₂-physisorption, XRD, SEM and TEM. It was found that the addition of butanol has a positive influence to get more uniform pores for both PMOs. However, the effect is much higher for ethenylene-bridged PMOs. Further, it was observed that the mechanical, hydrothermal and chemical stability are better for the ethylene-bridged PMOs than for the ethenylene-bridged PMOs.

The results were published in "*Microporous and Mesoporous Materials*": F. Goethals, C. Vercaemst, V. Cloet, S. Hoste, P. Van Der Voort and I. Van Driessche, *Micropor Mesopor Mat*, 2010, **131**, 68-74.

3.1 Introduction

As already mentioned in chapter two, PMOs containing simple organic bridges are the most interesting PMOs for low-k applications. When comparing the composition of ethylene- and ethenylene-bridged PMOs, the only difference is the single carbon vs. double carbon bond of every organic bridge and therefore, it is interesting to investigate if this difference has an influence on the synthesis conditions and characteristics of these materials.

Ethylene-bridged PMOs are the most investigated PMOs. They can be synthesized in acidic and basic conditions, and different morphologies¹⁻⁶ and mesostructures^{5, 7-11} have been reported. The combination of low polarisable organic bridges and high porosity makes them promising candidates for application as low-k materials.⁴

Several researchers examined the influence of the synthesis conditions on the material properties of ethylene-bridged PMOs. Burleigh *et al.*¹² varied the surfactant template in acidic media. In different reports, the effect of the SiO₂/template ratio on the properties of the material is presented.^{13, 14} Bao *et al.*¹⁵ studied the effect of acid for the synthesis of large-pore PMOs. To get highly ordered PMOs, they found that these PMOs could only be synthesized under controlled low acid conditions. This small pH range can be broadened by adding inorganic salts to the solution.¹⁶ Burleigh *et al.*¹⁷ also studied the aging, mechanical and hydrothermal stabilities of ethylene-bridged PMOs with Brij-76 as template. This group concluded that the stabilities are far better for the PMOs compared to periodic mesoporous silicas. Guo *et al.*¹⁸ explained that the low hydrothermal stability of the mesoporous silicas is attributed to the easy hydrolysis of Si-O-Si bonds into Si-OH during the hydrothermal treatment.

Ethenylene-bridged PMOs are interesting because it is possible to modify them based on olefin chemistry. The accessibility of the C=C double bonds was tested by bromine addition.⁷ The PMOs can further be modified by substitution of the bromine. The first ethenylene-bridged organosilicas were synthesized in basic medium. However, only 10% of the sites could be brominated.⁷ Better bromination results were obtained by using nonionic surfactants in acidic medium.^{19, 20}

Unlike for the ethylene-bridged PMOs, the pH range to get ordered material is larger.²¹ Adding butanol or inorganic salts have a positive influence on the ordering of the material.^{20, 22} By optimizing the amount of butanol and HCl, PMOs with high surface areas (around 1000 m²/g) and narrow pore size distributions were obtained.²³ The influence of butanol has not been investigated yet for ethylene-bridged PMOs. For ethenylene-bridged PMOs, almost all the publications describe the accessibility and

reactivity of the C=C double bond, but there is little known on the hydrothermal, mechanical and chemical stability of this material.

Herein, we report a comparative study of hexagonal structured ethylene- and ethenylene-bridged PMOs. The effect of butanol on the pore size distributions and morphology of both PMOs was investigated. Butanol was chosen as co-solvent because butanol stimulates the growth along the fiber-axis, resulting in the formation of long and uniform micelle rods and consequently in uniform pores.²³ It was also investigated whether butanol can extend the pH region in which narrow pore size distributions are obtained, because this region is very narrow, especially for ethylene-bridged PMOs. Extending this region would contribute to a more reproducible synthesis method.

Further, the mechanical, hydrothermal and chemical stability of the PMOs were compared. The materials were characterized by N₂-physisorption, X-ray diffraction (XRD), scanning electron microscopy (SEM) and transmission electron microscopy (TEM).

3.2 Experimental section

3.2.1 Materials

1,2-bis(triethoxysilyl)ethane (BTESA, Gelest), triblock copolymer EO₂₀PO₇₀EO₂₀ (P123, Aldrich), hydrochloric acid (HCl, 37%, Aldrich), sodium hydroxide (NaOH, N.V. Fiers), acetone (N.V. Fiers), hexamethyldisilazane (HMDS, Aldrich) and butanol (BuOH, Across) were purchased and used without further purification. Pure trans 1,2-bis(triethoxysilyl)ethene (BTESE) was made in the lab following the method previously reported by our group.²³ Ethylene-bridged PMOs will be abbreviated to C-CPMOs and ethenylene-bridged PMOs to C=CPMOs.

3.2.2 Synthesis of the C-CPMOs

For the synthesis of the C-CPMOs was 0.5 g P123 mixed with 14 ml H₂O and different amounts of (1 M) HCl and BuOH were added to the mixture. Then 0.89 g BTESA was added and the mixture was stirred for 4 hours at 35°C and aged for 48 hours at 90°C. A Soxhlet extraction with acetone was used to remove the surfactant.

3.2.3 Synthesis of the C=CPMOs

An optimized method made by our group for the synthesis of C=CPMOs was used²² and modified by varying the amount of acid and BuOH. For a standard synthesis was 1 g

Chapter 3: Comparative study of ethylene- and ethenylene-bridged periodic mesoporous organosilicas

P123 mixed with 48 ml H₂O, 3.42 ml concentrated HCl and 2.45 ml butanol. This mixture was stirred at 35°C for 90 minutes. 1.78 g BTESE was added and this solution was stirred for 4 hours. After stirring, it was aged for 16 hours at 90°C. A Soxhlet extraction with acetone was used to remove the surfactant. An overview of the molar compositions is given in table 3.1.

Table 3.1: Molar reactant compositions for the synthesis of C-CPMOs and C=CPMOs.

sample	precursor	P123	HCl	H ₂ O	BuOH
C-CPMO1	1	0.034	0.58	318	0
C-CPMO2	1	0.034	0.58	318	0.23
C-CPMO3	1	0.034	0.58	318	0.37
C-CPMO4	1	0.034	0.58	318	0.42
C-CPMO5	1	0.034	0.38	318	0.37
C-CPMO6	1	0.034	0.78	318	0.37
C-CPMO7	1	0.034	0.97	318	0.37
C-CPMO8	1	0.034	0.38	318	0
C-CPMO9	1	0.034	0.78	318	0
C-CPMO10	1	0.034	0.97	318	0
C=CPMO1	1	0.034	8.09	557	0
C=CPMO2	1	0.034	8.09	557	3.91
C=CPMO3	1	0.034	8.09	557	5.27
C=CPMO4	1	0.034	8.09	557	5.95
C=CPMO5	1	0.034	0.64	557	5.27
C=CPMO6	1	0.034	1.08	557	5.27
C=CPMO7	1	0.034	2.7	557	5.27
C=CPMO8	1	0.034	5.4	557	5.27
C=CPMO9	1	0.034	0.64	557	0
C=CPMO10	1	0.034	1.08	557	0
C=PMO11	1	0.034	2.7	557	0
C=CPMO12	1	0.034	5.4	557	0

3.2.4 Hydrothermal, mechanical and chemical stability

Hydrothermal treatment

The PMOs were steamed in an autoclave for 3 days at 105°C.

Mechanical treatment

Before the mechanical treatment, a part of the PMO powder was treated with HMDS to make the material hydrophobic by creating Si(CH₃)₃ groups at the surface. This was done by mixing the powder with HMDS and keeping it at 130°C for 5 hours. The

extracted powders and the powders treated with HMDS were placed in a 13 mm die and compressed for 1 minute at different pressures. No primary drying occurred.

Chemical treatment

HMDS and non HMDS treated ethane and ethene PMOs were immersed in 1 M NaOH solution for 2.5 hours at room temperature and dried afterwards.

3.2.5 Characterization

N₂ sorption isotherms were measured on a Belsorp-Mini II apparatus at 77 K. Before the measurement, the samples were dried at 100°C for 16 hours under vacuum. The surface area was calculated using the BET method. The data of the adsorption branch were used to calculate the pore diameter using the BJH method.

X-ray powder diffraction (XRD) patterns were collected on a Siemens D5000 Diffractometer with Cu K α radiation of 0.15418 nm wavelength. The step size was 0.01 2 θ degree and the measurement time was 3.2 s for each step.

Scanning Electron Microscopy (SEM) images were obtained by a Quanta 200FEG from FEI with a resolution of 0.8 nm at 30 keV and under high vacuum. High-resolution Transmission Electron Microscopy (TEM) measurements were performed on a Jeol JEM 3010 apparatus. To obtain sufficient small particles, a very small amount of PMO powder were dispersed in acetone and put in an ultrasonic bath for 24 hours to obtain highly dispersed particles which were then afterwards put on Cu TEM grids.

Diffuse reflectance infrared Fourier transform spectroscopy (DRIFT) was performed on a Bruker Equinox 55S equipped with a Graseby Specac Selector Diffuse Reflectance Accessory. The samples were recorded in vacuum at 120°C.

The amount of trimethylsilyl groups on the surface was determined with CHN elemental analysis by calculation of the amount of carbon before and after the HMDS treatment, taking into account the weight changes.

3.3 Results and discussion

3.3.1 The influence of butanol

The effect of the butanol concentrations (C-CPMOs1-4 and C=CPMOs1-4) on the uniformity of the pores is shown in figure 3.1. The full width at half maximum (FWHM) was calculated from the pore size distributions and plotted in function of the butanol/HCl ratio. The BuOH/HCl ratio was used because it is known that addition of

alcohols slows down the hydrolysis rate of silica precursors while acid accelerates this hydrolysis rate. So, these parameters have an influence on the kinetic process of the reaction and their ratio makes it possible to compare both PMOs within the same region of hydrolysis rate.

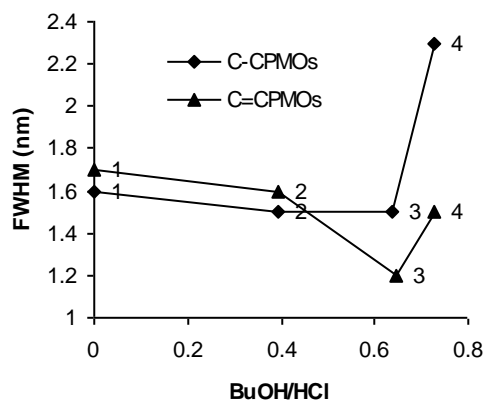


Figure 3.1: The influence of BuOH/HCl ratio on the pore size distribution of C-CPMOs and C=CPMOs. The numbers 1 to 4 refer to the C-CPMOs and C=CPMOs 1 to 4 from table 3.1 respectively.

For the C-CPMOs, there is a small decrease in FWHM value when the butanol amount is not too high (C-CPMOs2-3). At a higher butanol amount (C-CPMO4), the FWHM value increases strongly which means that the pores are less uniform. Looking at the graph of the C=CPMOs, it can be seen that a significant decrease in FWHM value can be obtained when butanol is added to the reaction mixture (C=CPMO3). However, at higher butanol amounts, the FWHM is increasing which means that the optimum BuOH/HCl ratio can be found around 0.64.

So, adding butanol results in a more uniform pore size distribution. This can probably be attributed to the fact that the butanol molecules keep the size of the surfactant micelles more uniform, because of their presence at the water/micelle interface.

However, higher butanol concentrations result also in more butanol molecules between the silica precursor and the micelles preventing good interaction between the precursor and micelles and resulting in less ordered materials. When comparing the results for both PMOs, it can be noticed that the optimum BuOH/HCl ratio is the same, but a strong decrease in FWHM value can only be obtained for the C=CPMOs. The reason for this is that the synthesis of the C=CPMOs occurs in high acidic media which results in partially blocked pores, (and so a broader distribution) due to excessive polycondensation of the precursor when no co-solvent is used. This is shown by the 2-

step desorption branch of the nitrogen sorption isotherm (figure 3.2). This phenomenon was observed and in depth investigated by Vercaemst et al.²³

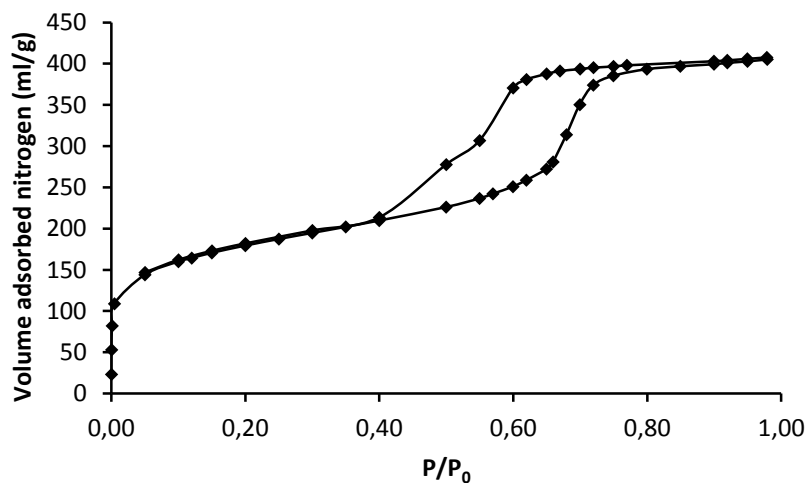


Figure 3.2: Nitrogen sorption isotherm of C=CPMO1.

The C-CPMOs and C=CPMOs with the most narrow pore size distribution are also highly ordered (see TEM images in figure 3.3).

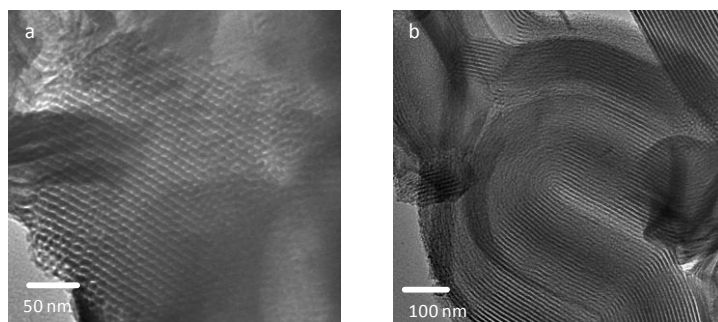


Figure 3.3: TEM images of a) C-CPMO3 and b) C=CPMO3.

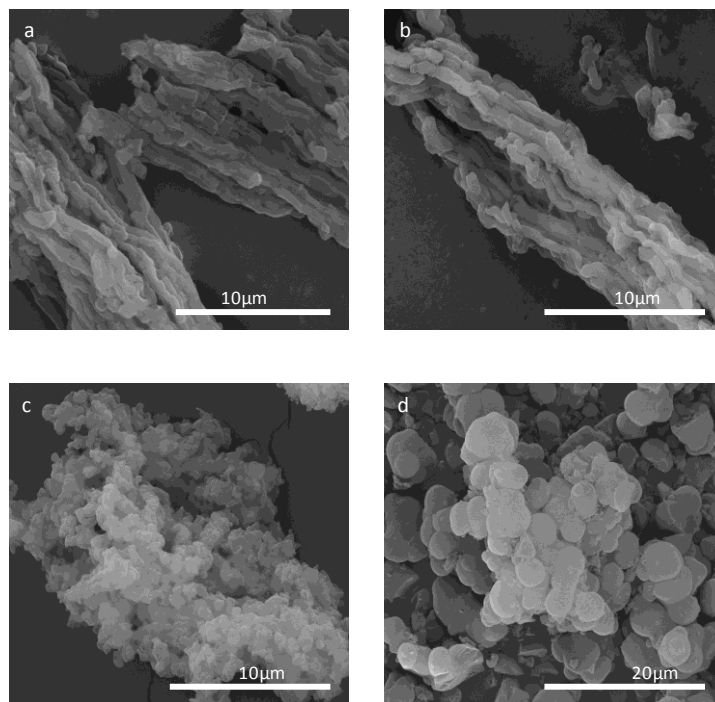


Figure 3.4: SEM images of a) C-CPMO2, b) C=CPMO2 (BuOH/HCl ratio = 0.39), c) C-CPMO4 and d) C=CPMO4 (BuOH/HCl ratio = 0.73).

The effect of butanol on the morphology of the PMOs is shown in figure 3.4. At low butanol concentrations (C-CPMO2 and C=CPMO2), ropelike particles are visible for both PMOs. When the butanol/HCl ratio is increased to 0.74 (C-CPMO4 and C=CPMO4), spherical and irregular particles can be seen for the C=CPMOs, while for the C-CPMOs, only irregular particles are visible.

In the next experiment, the FWHM values of the pore size distributions of C-CPMOs and C=CPMOs at different acid concentrations were calculated. The results are presented in figure 3.5. It can be seen that adding butanol has a positive influence on the uniformity of the pores of the C-CPMOs and C=CPMOs. Further, BuOH has a larger impact at higher acid concentrations. At a concentration of 0.1M and below, the FWHM values without butanol are more or less the same as those with butanol while at higher concentrations the decrease in FWHM values is significant when butanol is added. However, narrow pore size distributions at higher acid concentrations can only be obtained for the C=CPMOs. This can be explained by the fact that the C=CPMOs interacts better with the surfactant micelles which is probably related to the positive effect of the CH=CH bond in promoting the assembly of the organosilica with the micelles.²¹

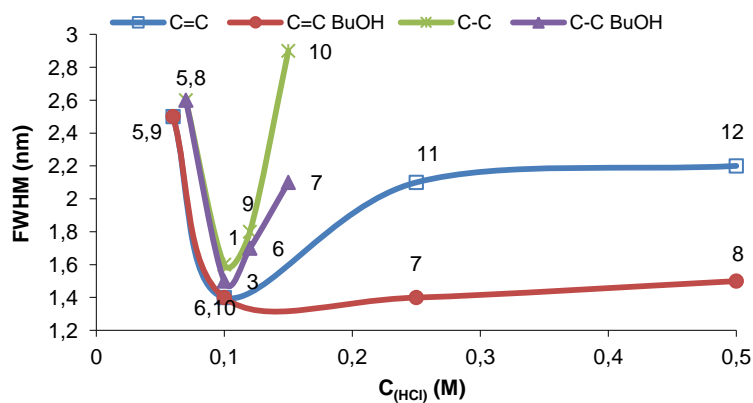


Figure 3.5: The influence of the acid concentration on the pore size distributions of C-C and C=CPMOs with or without the presence of BuOH. The numbers refer to the corresponding C-C and C=C PMOs from table 3.1.

To compare the hydrothermal and mechanical stability, the C-CPMO and C=CPMO with a high ordering, a high surface area and a narrow pore size distribution were used (C-CPMO3 and C=CPMO3 respectively).

3.3.2 Hydrothermal stability

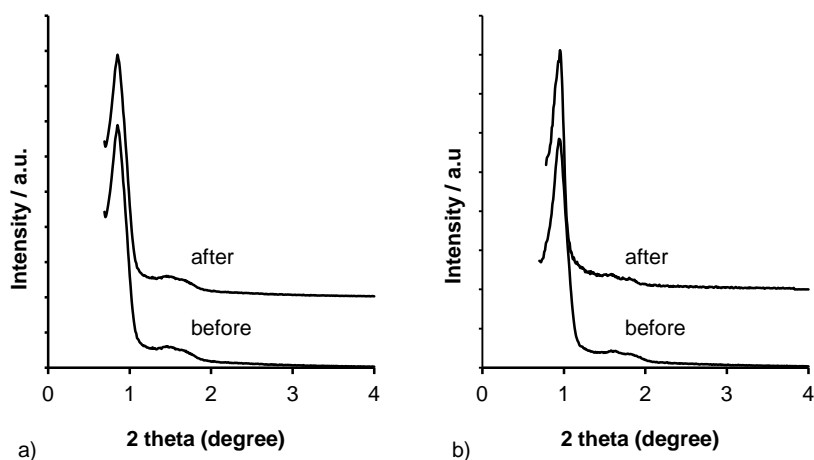


Figure 3.6: powder XRD patterns of hexagonal ordered a) C-CPMO3 and b) C=CPMO3 before and after hydrothermal treatment.

Figure 3.6 shows the X-ray diffraction results before and after hydrothermal treatment. The (100), (110) and (200) reflections are still present after the hydrothermal treatment

which proves that the PMOs keep their hexagonal structure. However, the (110) and (200) reflection of the C=CPMO are slightly broadened, indicating a slight decrease in ordering.

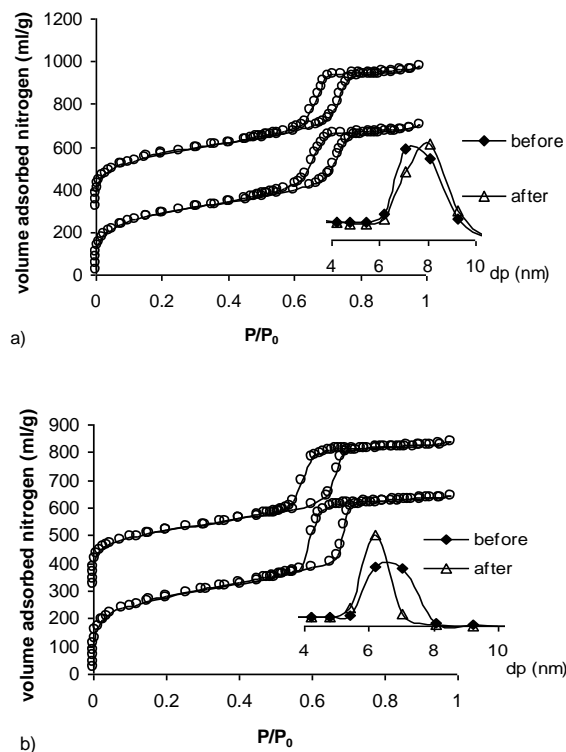


Figure 3.7: nitrogen physisorption isotherms and pore size distributions of a) C-CPMO3 and b) C=CPMO3 before and after hydrothermal treatment. The isotherms are offset vertically by 300 ml/g for the hydrothermal treated samples.

Figure 3.7 shows the nitrogen isotherms and the pore size distributions of the C-CPMOs and C=CPMOs before and after the hydrothermal treatment. The nitrogen sorption isotherms and pore size distributions are not significantly different after the hydrothermal treatment for the C-CPMO, while the pore size distribution of the C=CPMO is narrower probably due to collapsing of some pores.

The surface areas, the pore volumes and wall thicknesses are presented in table 3.2. It can be seen that the hydrothermal treatment has a slight influence on the properties of the C-CPMO. The decrease in surface area and pore volume are only 6% and 4% respectively. In contrast, the effect of the hydrothermal treatment on the properties of

Chapter 3: Comparative study of ethylene- and ethenylene-bridged periodic mesoporous organosilicas

the C=CPMO is significant. The surface area decreases with 20% and the pore volume decreases with 17%.

Further it is observed that the micropore volume is decreased with almost 50%, while for the C-CPMOs this decrease is only 12%. These results indicate that the C=CPMO has a lower hydrothermal stability than the C-CPMO. The explanation for the lower hydrothermal stability of the C=CPMO can be found in the composition of the walls. Besides the hydrophilic siloxanes bridges, the organic bridges present in the walls, -CH=CH- for C=CPMOs and -CH₂-CH₂- for C-CPMOs, have an influence on the stability. The Si-CH=CH-Si bond is less hydrophobic due to the π -bond than the Si-CH₂-CH₂-Si bond. Therefore, the water molecules can interact easier with the wall surface.

Table 3.2: Structural characteristics of C-CPMOs and C=CPMOs before and after hydrothermal treatment.

sample	d_{100} (nm)	a_0 (nm)	S_{BET} (m ² /g)	V_{total} (ml/g)	V_{micro} (ml/g)	D_{BJH} (nm)	wall thickness (nm) ^a
C-CPMO3	10.3	11.8	1027	1.09	0.18	7.5	4.4
C-CPMO3 (H ₂ O)	10.3	11.8	966	1.05	0.16	7.6	4.3
C=CPMO3	9.2	10.6	965	1.00	0.16	6.4	4.2
C=CPMO3 (H ₂ O)	9.2	10.6	774	0.83	0.09	6.2	4.4

^aPore wall thickness was determined by a_0 -pore size, where $a_0 = 2d_{100}/3^{1/2}$

To confirm this, an equal amount of both PMOs was dried and their water uptake was gravimetrically determined as a function of time at a constant relative humidity of 67%. The results are plotted in figure 3.8. Both materials adsorb a significant amount of water, but the rate of adsorption is higher for the C=CPMOs. This is evidenced by the slope of the water adsorption kinetic between 1 and 20 minutes, indicating that the C=CPMO is more hydrophilic.

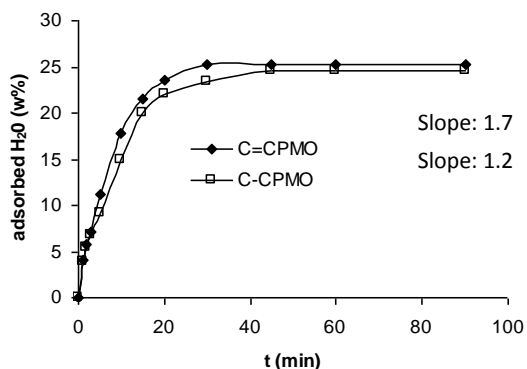


Figure 3.8: H₂O adsorption in function of the time on C-CPMOs and C=CPMOs.

3.3.3 Mechanical stability

Figure 3.9 shows the XRD data of the C-CPMOs and C=CPMOs before and after mechanical compression. At a compression of 68 MPa, there is no structural degradation of the C-CPMO while the 2θ value of the (100) reflection of the C=CPMO moved from 0.95 to 0.99. At a compression of 136 MPa, the peak of the (100) reflection of the C-CPMO is broadened, indicating a lower ordering of the material. The peak of the (100) reflection of the C=CPMO is strongly decreased and broadened.

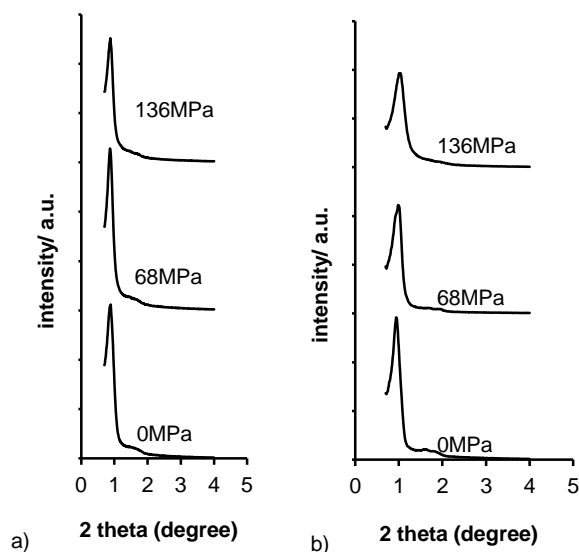


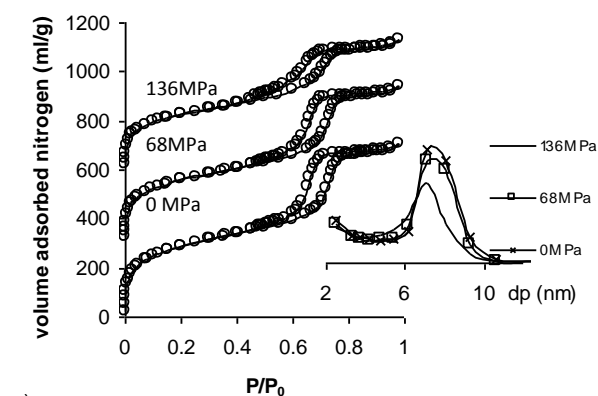
Figure 3.9: XRD patterns of a) C-CPMO3 and b) C=CPMO3 before and after mechanical compression.

Further, the 2θ value of the (100) peak moved to 1.05. The unit cell parameters are listed in table 3.4. The unit cell parameters remain the same for the C-CPMO, while for the C=CPMO compressed at 68 MPa, the unit cell parameter contracted 0.3 nm (about 3%), and at 136 MPa, the unit cell parameter contracted 0.9 nm (about 9%). The XRD results indicate that the C-CPMO has a higher mechanical stability than the C=CPMO.

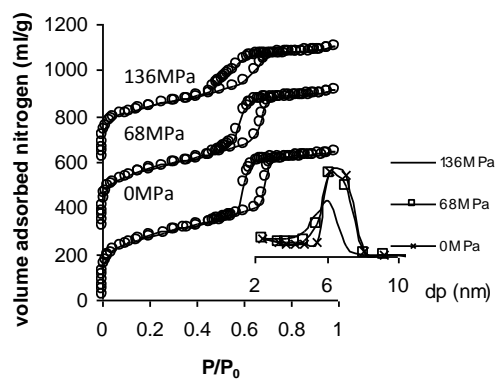
Chapter 3: Comparative study of ethylene- and ethenylene-bridged periodic mesoporous organosilicas

Table 3.3: Structural characteristics of C-CPMOs and C=CPMOs before and after mechanical compression.

sample	d_{100} (nm)	a_0 (nm)	S_{BET} (m^2/g)	V_{total} (ml/g)	V_{micro} (ml/g)
C-CPMO3 0MPa	10.3	11.8	1027	1.09	0.18
C-CPMO3 68MPa	10.3	11.8	935	0.99	0.14
C-CPMO3 136MPa	10.3	11.8	825	0.82	0.10
C=CPMO3 0MPa	9.2	10.6	965	1.00	0.16
C=CPMO3 68MPa	8.9	10.3	936	0.95	0.13
C=CPMO3 136MPa	8.4	9.7	830	0.78	0.12



a)



b)

Figure 3.10: Nitrogen physisorption isotherms and pore size distributions of a) C-CPMO3 and b) C=CPMO3 before and after mechanical compression. The isotherms are offset vertically by 300 ml/g and 600 ml/g for the 68 MPa and 136 MPa compressed samples respectively.

The nitrogen adsorption isotherms are given in figure 3.10. All samples give type IV isotherms, but the capillary condensation step of the PMOs compressed at 136 MPa spans a broad pressure range, indicating a lower uniformity of the mesopores. This is consistent with the XRD results.

Looking at the pore size distribution of the samples, it can be seen that at 68 MPa, nothing has significantly changed for the C-CPMO and C=CPMO. At 136 MPa, the pore size distribution of the C=CPMO is broader than the distribution of the C-CPMO which results in a less uniform material. The textural properties are listed in table 3.3. After compression of 68 MPa there is a small decrease in pore volume and surface area and this decrease continues at higher compression.

It is also known that adsorbed water plays a very important role in the mechanical stability of mesoporous silicas.¹⁸ Therefore, the PMOs were treated with HMDS to make them hydrophobic. The DRIFT spectra in figure 3.11 show that the peaks at 3749 cm^{-1} have disappeared after the HMDS treatment for both PMOs. This indicates that the free single OH groups are replaced by a trimethylsilyl group.²⁴ However, a small amount of inaccessible (geminal and interglobular) silanol groups remains. This can be seen by the presence of the band between 3742 cm^{-1} and 3200 cm^{-1} .

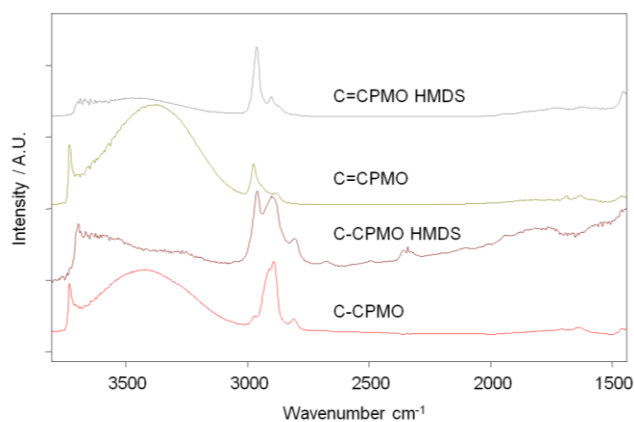


Figure 3.11: DRIFT spectra of C-CPMOs and C=CPMOs before and after hydrophobization with HMDS.

Carbon/hydrogen elemental analysis was performed before and after HMDS treatment to determine the amount of trimethylsilyl groups/ nm^2 after modification. It was found that the amount is 0.99 groups/ nm^2 for the C-CPMOs and 0.98 groups/ nm^2 for the C=CPMOs which are very similar results.

Chapter 3: Comparative study of ethylene- and ethenylene-bridged periodic mesoporous organosilicas

To confirm the hydrophobicity, the dried and evacuated materials were kept for one day at a relative humidity of 75%, but no water uptake was found from gravimetric analysis for both PMOs, proving that the surface is completely hydrophobic.

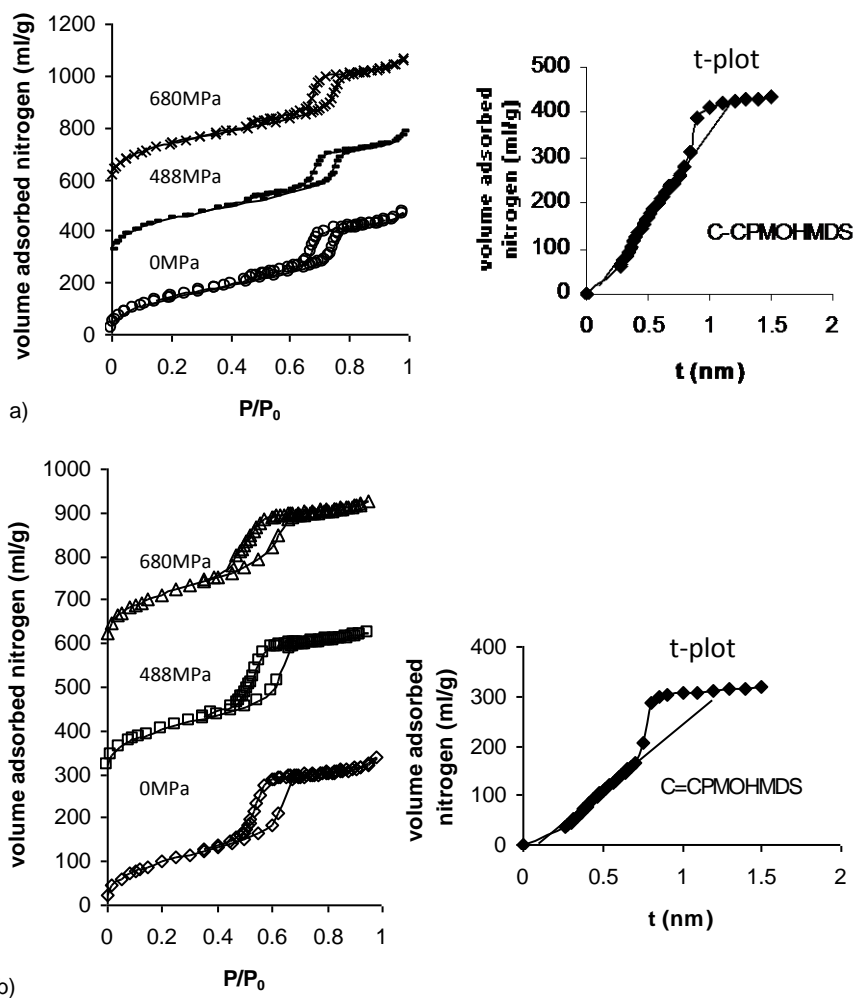


Figure 3.12: Nitrogen physisorption isotherms and t-plots of a) HMDs treated C-CPMO3 and b) HMDs treated C=CPMO3 before and after mechanical treatment. The isotherms are offset vertically by 300 ml/g and 600 ml/g for the 488 MPa and 680 MPa compressed samples respectively.

These HMDs treated PMOs were compressed at 488 MPa and 680 MPa and their nitrogen sorption isotherms and t-plots are given in figure 3.12. After the HMDs treatment, a long tail in the desorption step of the C-CPMO can be seen, indicating that the pores are partially blocked. Further, the isotherms of all the compressed HMDs

treated C-CPMOs are identical to the parent HMDS treated C-CPMOs which indicates a highly improved mechanical stability of this material after HMDS treatment. For the HMDS treated C=CPMOs, the isotherm is identical at 488 MPa, while at 680 MPa the capillary condensation is slightly less steep, which indicates a broader pore size distribution.

It is clear that the grafted PMOs have lower surface areas and pore volumes than the non-grafted ones. Also, the micropore volume is zero which is shown by the t-plot in figure 3.12. The intercept of the straight line is below zero indicating that the micropores are blocked by the $\text{Si}(\text{CH}_3)_3$ groups.

These results confirm that the removal of water has a drastic improvement on the mechanical stability and there is no great difference in mechanical stability between the ethylene- and ethenylene-bridged PMOs when they are hydrophobized. These results show that the contribution of the organic bridges to the mechanical stability is how strong they can prevent the interaction between the silanols groups and water under pressure.

3.3.4 Chemical stability

To investigate the resistance against alkaline solutions, the HMDS and non-HMDS treated C-CPMOs and C=CPMOs were immersed in a 1 M NaOH solution for 2.5 hours. After the immersion, we observed that the non-treated PMOs are completely dissolved after the immersion. However, the C=C PMOs dissolved/hydrolyzed much faster than the C-CPMOs. A likely explanation for this is again the more hydrophilic character of the C=CPMOs.

Surprisingly, also the hydrophobic HMDS treated C=CPMO dissolved completely after the immersion, while the HMDS treated C-CPMO was still present, indicating that the C-CPMOs have also a better chemical stability than the C=CPMOs even after hydrophobization of both materials.

The XRD pattern and nitrogen sorption isotherm of the HMDS treated C-CPMO before and after immersion is given in figure 3.13. When looking at the XRD pattern, it can be seen that the intensity of the (100) peak decreased and the (110) and (200) are not present anymore after the alkaline treatment, showing a structural degradation of the material.

On the other hand the nitrogen isotherm showed an increased amount in adsorbed nitrogen which means that the pore volume is higher after alkaline treatment. This can be explained by the fact that the base etches the PMO material, without completely destroying the silica network. This means that alkaline solutions can be used to further

optimize the pore volume of the C-CPMOs and likely PMOs in general by adjusting the etching conditions such like etching time and concentration.

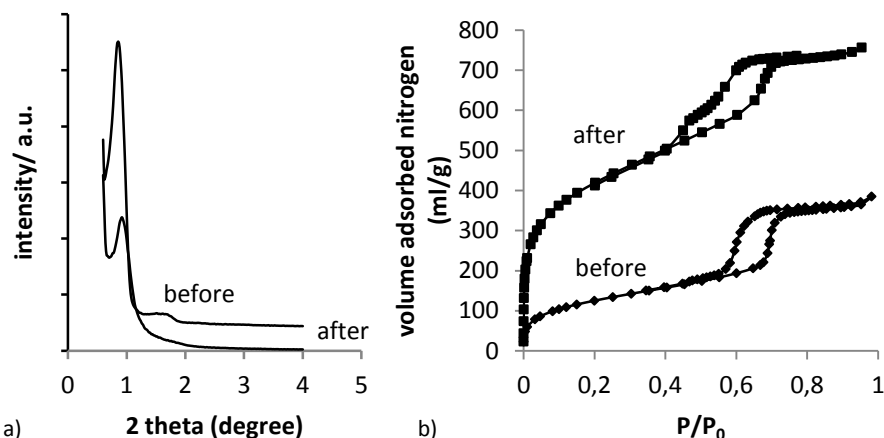


Figure 3.13: a) XRD pattern and b) N₂ sorption isotherms of HMDS treated C-CPMOs before and after alkaline immersion.

Also the capillary condensation step of the adsorption is less steep after immersion, indicating a broader pore size distribution. Further, the desorption branch shows a large tail after immersion which is due to the presence of bottle necks.

All these results show that a HMDS treatment of C-CPMOs can slow down the degradation of the material, but it can not fully prevent it. Further, the resistance of C-CPMOs against alkaline solutions is significantly better compared to the C=CPMOs.

3.4 Conclusions

In this chapter, the influence of butanol on the uniformity of the pores, the hydrothermal stability and the mechanical stability of hexagonal structured ethylene- and ethenylene-bridged PMOs were compared. Adding butanol to the reaction mixture has a positive influence on the uniformity of the pores for both PMOs, but the effect is much higher for C=CPMOs. Further, the acidity range where narrow pore sizes distributions are obtained, can only be broadened for the C=CPMOs when butanol is added.

The comparison of the hydrothermal, mechanical and chemical stability revealed better results for the ethylene-bridged PMOs, because the C-CPMOs are more hydrophobic than the C=CPMOs. When treated with HMDS, there is no large difference in the

Chapter 3: Comparative study of ethylene- and ethenylene-bridged periodic mesoporous organosilicas

mechanical stability of the PMOs, but the chemical stability of the C-CPMOs is far more better than the chemical stability of the C=CPMOs.

3.5 References

1. V. Rebbin, M. Jakubowski, S. Potz and M. Froba, *Micropor Mesopor Mat*, 2004, **72**, 99-104.
2. Y. F. Lu, H. Y. Fan, N. Doke, D. A. Loy, R. A. Assink, D. A. LaVan and C. J. Brinker, *J Am Chem Soc*, 2000, **122**, 5258-5261.
3. M. P. Kapoor and S. Inagaki, *Chem Mater*, 2002, **14**, 3509-3514.
4. B. D. Hatton, K. Landskron, W. Whitnall, D. D. Perovic and G. A. Ozin, *Adv Funct Mater*, 2005, **15**, 823-829.
5. S. Guan, S. Inagaki, T. Ohsuna and O. Terasaki, *J Am Chem Soc*, 2000, **122**, 5660-5661.
6. Y. Goto and S. Inagaki, *Chem Commun*, 2002, 2410-2411.
7. T. Asefa, M. J. MacLachlan, N. Coombs and G. A. Ozin, *Nature*, 1999, **402**, 867-871.
8. S. Inagaki, S. Guan, Y. Fukushima, T. Ohsuna and O. Terasaki, *J Am Chem Soc*, 1999, **121**, 9611-9614.
9. C. Yoshina-Ishii, T. Asefa, N. Coombs, M. J. MacLachlan and G. A. Ozin, *Chem Commun*, 1999, 2539-2540.
10. W. P. Guo, I. Kim and C. S. Ha, *Chem Commun*, 2003, 2692-2693.
11. Y. C. Liang, M. Hanzlik and R. Anwender, *Chem Commun*, 2005, 525-527.
12. M. C. Burleigh, M. A. Markowitz, M. S. Spector and B. P. Gaber, *J Phys Chem B*, 2002, **106**, 9712-9716.
13. X. Y. Bao, X. S. Zhao, X. Li and J. Li, *Appl Surf Sci*, 2004, **237**, 380-386.
14. R. M. Grudzien, B. E. Grabicka and M. Jaroniec, *Colloid Surface A*, 2007, **300**, 235-244.
15. X. Y. Bao, X. S. Zhao, S. Z. Qiao and S. K. Bhatia, *J Phys Chem B*, 2004, **108**, 16441-16450.
16. S. Z. Qiao, C. Z. Yu, Q. H. Hu, Y. G. Jin, X. F. Zhou, X. S. Zhao and G. Q. Lu, *Micropor Mesopor Mat*, 2006, **91**, 59-69.
17. M. C. Burleigh, M. A. Markowitz, S. Jayasundera, M. S. Spector, C. W. Thomas and B. P. Gaber, *J Phys Chem B*, 2003, **107**, 12628-12634.
18. W. P. Guo, X. Li and X. S. Zhao, *Micropor Mesopor Mat*, 2006, **93**, 285-293.
19. K. Nakai, Y. Oumi, H. Horie, T. Sano and H. Yoshitake, *Micropor Mesopor Mat*, 2007, **100**, 328-339.
20. W. H. Wang, S. H. Xie, W. Z. Zhou and A. Sayari, *Chem Mater*, 2004, **16**, 1756-1762.
21. X. Y. Bao, X. Li and X. S. Zhao, *J Phys Chem B*, 2006, **110**, 2656-2661.
22. C. Vercaemst, M. Ide, B. Allaert, N. Ledoux, F. Verpoort and P. Van der Voort, *Chem Commun*, 2007, 2261-2263.
23. C. Vercaemst, M. Ide, H. Friedrich, K. P. de Jong, F. Verpoort and P. Van der Voort, *J Mater Chem*, 2009, **19**, 8839-8845.
24. E. F. Vansant, P. V. D. Voort and K. C. Vrancken, *Characterization and Chemical Modification of the Silica Surface.*, Elsevier, Amsterdam, 1995.
25. M. Ide, Ghent University, Gent, 2012.

Chapter Four: Hydrophobic High Quality Ring PMOs with a very High Stability

In this chapter, we first present an optimized synthesis method of periodic mesoporous organosilicas containing interconnected $[\text{Si}(\text{CH}_2)]_3$ rings in the presence of surfactant Brij-76. Therefore, two important synthesis parameters, which are the acid and surfactant concentration, were systematically varied. This optimization method results in highly ordered mesoporous materials with very high surface areas, high pore volumes, uniform cylindrical pores and thick walls. Further, it was found that the porosity can be controlled by the surfactant concentration without changing the pore diameter.

In the second part, it is demonstrated that a post modification with HMDS or an auto-hydrophobization step leads to PMOs which are totally hydrophobic without losing their mesoporosity. In the last part, the impact of the hydrophobization on the (a) hydrothermal, (b) mechanical and (c) chemical stability is investigated. The results reveal that post modification with HMDS creates ordered materials that can withstand (a) steaming at 130°C, (b) a mechanical compression of 272 MPa and (c) a treatment with 1 M NaOH for 2.5 hours without any degradation of the silica network.

The results were published in "*Journal of Materials Chemistry*": F. Goethals, B. Meeus, A. Verberckmoes, P. Van der Voort and I. Van Driessche, *J Mater Chem*, 2010, **20**, 1709-1716.

4.1 Introduction

As mentioned in chapter one, a hydrophobic character of the nanoporous material is required for applications in the field of nano-electronics.¹ Besides the hydrophobic property, a good chemical and mechanical stability are crucial to apply these materials. Mesoporous silicas of the M41S type are limited in use due to their lack in stability which can be attributed to their thin amorphous pore walls that disintegrate in the presence of water molecules.²⁻⁴

SBA type mesoporous silicas have larger pore diameters and thicker pore walls which lead to an improved mechanical and hydrothermal stability.⁵⁻⁷ However, SBA materials are hydrophilic due to their siloxane bridges and most importantly, their silanol groups on the surface. An effective method to increase the hydrophobicity is a trimethylsilylation of the surface with hexamethyldisilazane (HMDS) or trimethylsilylchloride (TMSC).^{8, 9} Hydrophobization of the silicas also improves their mechanical and hydrothermal stability, because they are less vulnerable to silicate hydrolysis.¹⁰

Another method to increase the hydrophobic character of mesoporous ordered materials is to directly incorporate organic functional groups in the silica network by using poly(trialkoxysilyl)organic precursors ((R'O)₃Si-R-Si(OR')₃), resulting in PMO materials.

Because the organic group is responsible for the hydrophobic character of the PMO, it is interesting to further replace the oxygen atoms in the network by organic groups. Consequently, improved physical properties could be achieved. As already mentioned in chapter 2, Landskron *et al.*¹¹ accomplished the synthesis of PMOs with more organic groups by the self assembly of the 1,3,5-tris[diethoxysila]cyclohexane [(EtO)₂SiCH₂]₃ cyclic silsequioxane precursor. These ring PMOs were synthesized in alkaline medium and cetyltrimethylammonium bromide (CTAB) was used as structure directing agent. The introduction of more low polarisable organic groups makes these PMOs very appropriate for application as low-k materials.

Although, the ring PMOs are more hydrophobic compared to silicas, they also contain silanol groups on the surface, making that they still have a hydrophilic character. Thus, a post treatment step is necessary to make them completely hydrophobic. It was found that between 400°C and 500°C under inert atmosphere a silanol-eliminating transformation takes place which leads to more hydrophobic materials.¹¹ This self-hydrophobization process can be a good alternative compared to the post-grafting method with hexamethyldisilazane (HMDS). However, a detailed study about the

hydrophobicity of the ring PMOs and its impact on the stability of the material has not been available yet.

Herein, we first present an optimized synthesis method for ring PMOs in acid media. Surfactant Brij-76 or polyoxyethylene (10) stearyl ether was used as structure directing agent, because it leads to materials with thicker pore walls compared to CTAB.¹² It also generates smaller pore sizes compared to P123 which is more beneficial for low-k applications. Potassium chloride was also added to assist in the formation of ordered materials.¹³

Two important synthesis parameters, which are the concentration of acid and Brij-76, were varied and their influence on the structural properties were investigated. In the second part, the ring PMOs were hydrophobized with HMDS and with the self-hydrophobization method. The effect of these two methods on the structural properties of the ring PMOs was investigated.

Further, the difference in water uptake between the extracted ring PMOs and the hydrophobized ring PMOs was determined. Finally, the impact of the hydrophobicity on the chemical, hydrothermal and chemical stability was systematically studied and compared with the results of SBA-15 hydrophobized with HMDS.

4.2 Experimental section

4.2.1 Chemicals

Chloromethyltriethoxysilane and tetraethyl orthosilicate (TEOS) were purchased from ABRC, hydrochloric acid (HCl, 37%), sodium hydroxide (NaOH), dry tetrahydrofuran (THF) and pentane were obtained from Fiers and Mg turnings, Brij-76, P123 and potassium chloride (KCl) were purchased from Aldrich. All materials were used as received.

4.2.2 Synthesis

1,3,5[tris(diethoxy)sila]cyclohexane (TDSCH) was made in our lab, based on a modified synthesis method of Brondani *et al.*¹⁴ A solution of 70 ml 0.5 w% FeCl₃ in dry THF was added to 7 g Mg turnings and stirred till a grey colored mixture was visible. This mixture was kept under inert atmosphere.

Then, a solution of 100 ml 14.2 v% chloromethyltriethoxysilane in dry THF was added to the mixture and stirred for 32 h at 50°C. The mixture was filtered off and the solvent

was removed from the filtrate. Pentane was added to the residue and this mixture was also filtered. After the evaporation of pentane, the residue oil was vacuum distilled to give the desired product with a yield of 55%.

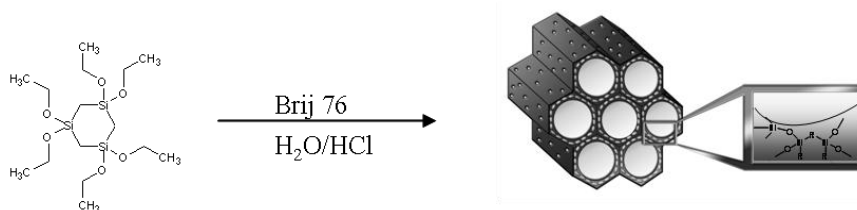


Figure 4.1: Reaction scheme for the synthesis of ring PMOs.

For a typical synthesis of the ring PMO (RPMO, figure 4.1), Brij-76 and KCl were dissolved in a 0.16 M HCl aqueous solution at 45°C. Then TDSCH was added and this mixture was stirred for 24 hours at 45°C. The molar composition was 1 TDSCH: 0.28 Brij-76: 5.36 KCl: 0.6 HCl: 293 H₂O. After stirring, the mixture was transferred to an autoclave and kept at 90°C for 24 hours. The white powder was filtered off and the surfactant was removed by Soxhlet extraction using acetone as extracting solvent. To investigate the effect of the acid and surfactant concentration, a series of different concentrations were used. An overview is given in table 4.1.

Table 4.1: Molar compositions for the synthesis of RPMOs.

Sample	TDSCH (mol)	Brij-76 (mol)	KCl (mol)	H ₂ O (mol)	HCl (mol)
RPMO1	1	0.28	5.4	293	0.4
RPMO2	1	0.28	5.4	293	0.6
RPMO3	1	0.28	5.4	293	1.2
RPMO4	1	0.28	5.4	293	1.4
RPMO5	1	0.28	5.4	293	2.4
RPMO6	1	0.28	5.4	293	5.3
RPMO7	1	0.14	5.4	293	1.2
RPMO8	1	0.28	5.4	293	1.2
RPMO9	1	0.56	5.4	293	1.2
RPMO10	1	0.84	5.4	293	1.2

For the synthesis of SBA-15, 4 g P123, 7 ml (37%) HCl and 200 ml H₂O were stirred for 1 h at room temperature. Then 9.1 ml TEOS was added and this mixture was stirred for 5 hours at 45°C, followed by an ageing period of 18 h at 80°C. The white powder was filtered off and the surfactant was removed by heating the powder at 500°C for 6 hours.

4.2.3 After treatment steps

Hydrophobization with HMDS was performed by mixing dry SBA-15 and ring PMO powder with HMDS and stirring for 5 hours at 135°C. After reaction, the powders were filtered off, extracted with pentane and dried at 150°C for 3 hours. Self-hydrophobized ring PMOs were obtained by heating the samples to 450°C and holding them at this temperature for 5 hours under inert atmosphere.

To investigate the hydrophobicity, the amount of adsorbed water was determined after 3 days at a constant relative humidity of 55%. This test was performed on extracted ring PMOs, thermal treated ring PMOs at 350°C under nitrogen (condition to remove the surfactant thermally), the hydrophobized ring PMOs, SBA-15 and SBA-15 treated with HMDS.

For the investigation of the mechanical stability, the samples were placed in a 13 mm die and compressed for 1 minute at a pressure of 272 MPa and for the hydrothermal stability, the samples were steamed in an autoclave for 5 days at an extreme steaming temperature of 130°C. The chemical stability was investigated by stirring SBA-15, ring PMOs and the hydrophobized powders in a very alkaline solution (1 M NaOH) for 2.5 hours at room temperature.

4.2.4 Characterization

The proton NMR spectrum of the cyclic organosilane precursors was measured on a ^1H NMR 300 MHz Varian Unity-300 Spectrometer. NMR samples were prepared by dissolving 100 μl of the precursor in 600 μl deuterioform.

N_2 sorption isotherms were measured on a Belsorp-Mini II apparatus at 77K. Before the measurement, the samples were dried at 100°C for 16 hours under vacuum. The surface area was calculated using the BET method. The data of the adsorption branch were used to calculate the pore diameter using the BJH method.

Scanning Electron Microscopy (SEM) images were obtained by a Quanta 200FEG from FEI with a resolution of 0.8 nm at 30 keV and under high vacuum.

X-ray powder diffraction (XRD) patterns were collected on a Siemens D5000 Diffractometer with $\text{Cu K}\alpha$ radiation of 0.15418 nm wavelength. The step size was 0.01 2θ degree and the measurement time was 3.2 s for each step.

High-resolution Transmission Electron Microscopy (TEM) measurements were performed on a Jeol JEM 3010 apparatus. To obtain sufficient small particles, a very small amount of PMO powder were dispersed in acetone and put in an ultrasonic bath

for 24 hours to obtain highly dispersed particles which were then afterwards put on Cu TEM grids.

For the determination of the amount of water, thermogravimetric analysis (TGA) was performed using a SDT 2960 Simultaneous DSC-TGA of TA instruments. The samples were heated to 200°C at a heating rate of 10°C/min. under ambient atmosphere. The weight loss between 20 and 120°C was attributed to the loss of adsorbed water.

Diffuse reflectance infrared Fourier transform spectroscopy (DRIFT) was performed on a Bruker Equinox 55S equipped with a Graseby Specac Selector Diffuse Reflectance Accessory. The samples were recorded in vacuum at 120°C.

4.3 Results and discussion

4.3.1 Optimization of the synthesis method

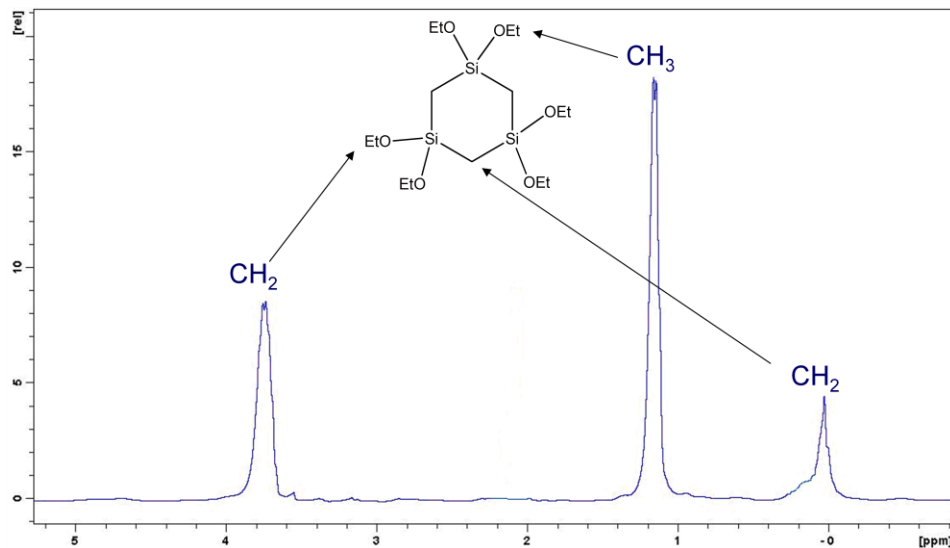


Figure 4.2: NMR spectrum of 1,3,5[tris(diethoxy)sila]cyclohexane.

Figure 4.2 shows the NMR spectrum of 1,3,5[tris(diethoxy)sila]cyclohexane. For this precursor, peaks at 0 ppm, 1.2 ppm and 3.9 ppm are observed and are in good correlation with those reported in the literature. The peaks can respectively be attributed to the Si-CH₂-Si, CH₃ and OCH₂ functional groups.

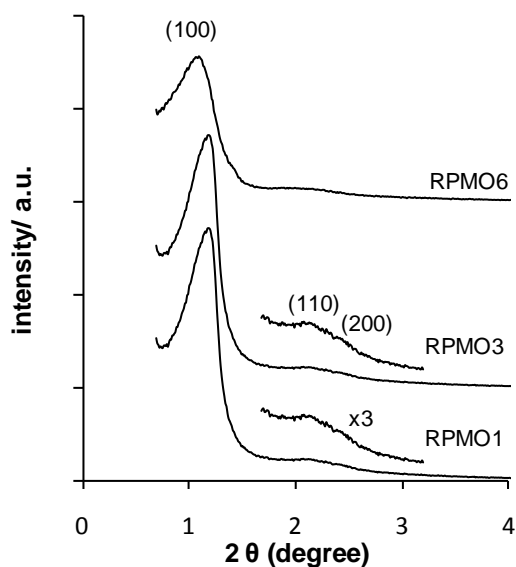


Figure 4.3: XRD patterns of ring PMOs synthesized at low (RPMO1 from table 4.1), medium (RPMO3 from table 4.1) and high (RPMO6 from table 4.1) acid concentrations.

Figure 4.3 shows the XRD results of the ring PMOs synthesized in relatively low (RPMO1), medium (RPMO3) and high (RPMO6) acid media. A highly intensive (100) reflection together with less resolved (110) and (200) reflections can be seen for the ring PMOs synthesized in medium conditions, indicating mesoporous materials with a hexagonal ordering.

High acid concentrations result in broader and less intense reflections, showing a decrease in ordering. These results can be explained by looking at the role of the acid during the synthesis. Acid accelerates the rates of hydrolysis and condensation of organosilica/silica precursors. However, if the amount of the acid is too high, disordered materials are obtained. This is due to the fast condensation, preventing the organosilica precursor to interact well with the surfactant micelles.¹⁵ The optimum pH range to get ordered materials is dependent on the organosilica precursor, due to the inductive effect of the organic bridges.¹⁶

The nitrogen isotherms shown in figure 4.4 are consistent with the XRD results. A H1 hysteresis and a steep capillary condensation step are observed for the ring PMOs synthesized in medium and low acid media, RPMO1 and RPMO3, proving the existence of uniform cylindrical pores. At high acid concentrations, RPMO6, the capillary condensation steps are less steep indicating that the pores are less uniform. For the clarity of the figure, the isotherms of the ring PMOs synthesized at other acid

concentrations are not presented herein, but are in between the steepest and least steep isotherms.

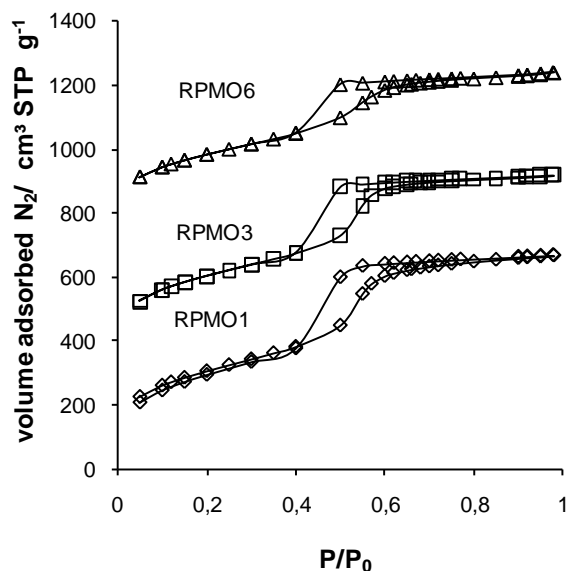


Figure 4.4: Nitrogen sorption isotherms synthesized at relatively low (RPMO1 from table 4.1), medium (RPMO3 from table 4.1) and high (RPMO6 from table 4.1) acid concentrations. RPMO3 and RPMO6 are vertically offset by $300 \text{ cm}^3 \text{ STP/g}$ and $700 \text{ cm}^3 \text{ STP/g}$ respectively.

Table 4.2: Structural characteristics of ring PMOs synthesized at different acid concentrations.

Sample	HCl (mol)	S_{BET} (m^2/g)	V_{tot} (cm^3/g)	V_{micro} (cm^3/g)	D_{BJH} (nm)
RPMO1	0.4	1050	1.02	0.01	4.2
RPMO2	0.6	1000	0.97	0.05	4.2
RPMO3	1.2	1085	0.98	0.03	4.2
RPMO4	1.4	1120	0.97	0.02	4.2
RPMO5	2.4	1096	1.01	0.05	4.8
RPMO6	5.3	1012	0.83	0.03	4.4

The structural characteristics are listed in table 4.2. It can be seen that highly porous materials with high surface areas can be obtained up to a molar acid composition of 1.4 (RPMO5). The pore diameter is equal for the RPMOs synthesized at low and medium acid concentrations (RPMO1 to 4), while at high acid concentrations, there is a slight increase in pore diameter (RPMO5 to 6). Probably, higher HCl concentrations slightly expand the size of the surfactant micelles, resulting in bigger pores. The ring PMOs

have very low micropore volumes and the variation of the acid concentration has no significant influence on this pore volume.

The influence of the acid concentration is shown by the SEM images in figure 4.5. At lower acid concentrations, the particles have a sharp and angular shape. On the other hand, higher acid concentrations lead to more aggregated spherical particles.

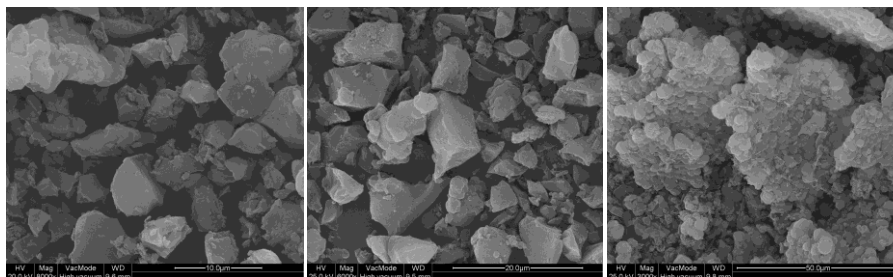


Figure 4.5: SEM images of ring PMOs synthesized at a) low (RPMO2 from table 4.1), b) medium (RPMO4 from table 4.1) and c) high (RPMO5 from table 4.1) acid concentrations.

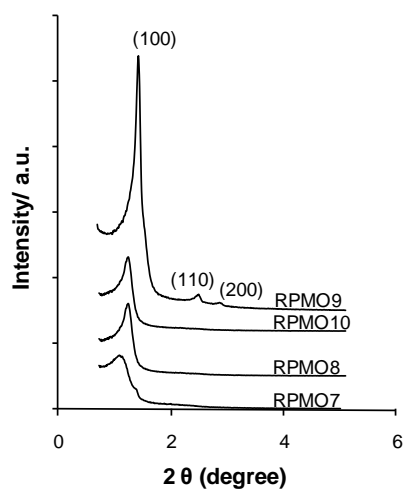


Figure 4.6: XRD patterns of ring PMOs synthesized at low (RPMO7 from table 4.1), medium (RPMO8 from table 4.1), high (RPMO9 from table 4.1) and very high (RPMO10 from table 4.1) Brij-76 concentrations.

For the investigation of the Brij-76/TDSCH ratio, the molar acid composition was fixed at 1.2, which is in the optimum range to obtain highly porous and ordered ring PMOs, while the amount of Brij-76 was varied (RPMO7 to 10). The XRD patterns are given in figure 4.6. It can be seen that a Brij-76/TDSCH ratio of 0.56 (RPMO9) gives (100), (110)

and (200) reflections indicating a highly ordered hexagonal structure. This is also confirmed by the TEM image in figure 4.7.

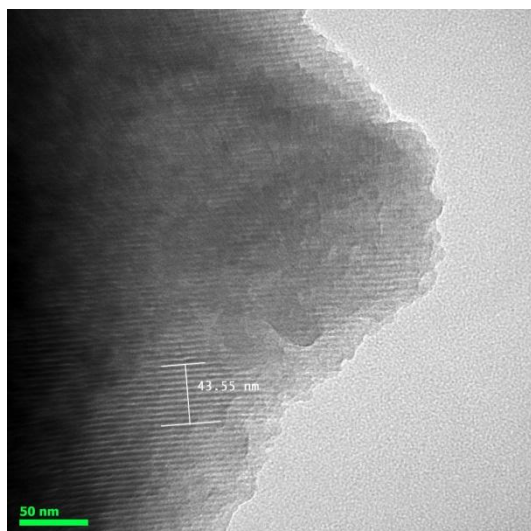


Figure 4.7: TEM image of RPMO9.

Increasing or decreasing the Brij-76 concentration leads to a broader (100) peak, indicating less ordered materials. For the ring PMOs synthesized at a low Brij-76 concentration (RPMO7), the (100) peak is very broad what means that a sufficient amount of Brij-76 is necessary to obtain ordered materials. Further, it is observed that the peak positions and consequently the unit cell parameters change when a different amount of surfactant is used.

Table 4.3: Structural characteristics of ring PMOs synthesized at different surfactant concentrations.

Sample	Brij-76 (mol)	S_{BET} (m^2/g)	V_{tot} (cm^3/g)	D_{BJH} (nm)	a_0^{a} (nm)	Wall thickness ^b (nm)
RPMO7	0.14	1006	0.80	4.2	9.3	5.1
RPMO8	0.28	1085	0.98	4.2	8.6	4.4
RPMO9	0.56	1199	1.39	4.2	7.1	2.9
RPMO10	0.84	1082	0.95	4.2	8.6	4.4

^a a_0 was calculated from the $d(100)$ spacing ($a_0 = (2\sqrt{3}/3)/d_{(100)}$)

^b wall thickness was estimated from a_0 – pore size

The structural parameters are listed in table 4.3. It can be seen that changing the Brij-76/TDSCH ratio has no influence on the pore diameter which is constant at 4.2 nm. Further, by optimizing the Brij-76/TDSCH ratio, it is possible to obtain highly ordered

ring PMOs with very high surface areas and pore volumes (RPMO9). It is also observed that an increase in pore volume results in a decrease in wall thickness. Looking at these results, it is possible to tune the pore volume and wall thickness of the PMOs in a certain range.

At low surfactant concentrations, there is a lot of space left between the micelles for the ring precursor to condensate, resulting in thicker walls and also a less ordered mesostructure. This is because the precursor/micelles rods have more freedom to aggregate/condensate in different directions. Higher surfactant concentrations decrease this aggregation/condensation freedom and also limit the space between the surfactant micelles resulting in ordered materials with thinner pore walls. Further increasing the surfactant concentration leads to oversaturation which disturbs the interaction between the micelles and the organosilica precursor.

4.3.2 Hydrophobicity study

Table 4.4 presents the impact of the HMDS treatment (RPMO-HMDS) and the self-hydrophobization (RPMO-450°CN₂) on the structural characteristics of the ring PMOs. Both methods result in a similar decrease in surface area, pore volume and pore diameter, and a slight increase in wall thickness, respectively due to a contraction of the ring PMO during the heating and the addition of trimethyl groups on the surface.

Table 4.4: Structural characteristics of ring PMOs before and after hydrophobization.

Sample	S_{BET} (m ² /g)	V_{tot} (cm ³ /g)	D_{BJH} (nm)	a_0^{a} (nm)	Wall thickness ^b (nm)
RPMO	1020	0.89	4.2	8.1	3.9
RPMO-HMDS	704	0.66	4.0	8.0	4.0
RPMO-450°CN ₂	730	0.64	3.7	7.9	4.2

^a a_0 was calculated from the $d(100)$ spacing ($a_0 = (2\sqrt{3}/3)/d_{(100)}$)

^b wall thickness was estimated from a_0 – pore size

Table 4.5: Amount of adsorbed H₂O.

Sample	Amount H ₂ O (w%)
SBA-15	18
SBA-15-HMDS	0
RPMO	14
RPMO-350°CN ₂	3
RPMO-450°CN ₂	0
RPMO-HMDS	0

The TGA results of the hydrophobicity test of the different porous materials are presented in table 4.5. It can be seen that the extracted ring PMOs (RPMO) still adsorb water, although the amount is significantly lower than the amount adsorbed on SBA-15. No water uptake is observed for the ring PMOs heated at 450°C (RPMO-450°CN₂), the ring PMOs and SBA-15 treated with HMDS (RPMO-HMDS and SBA-15-HMDS) what can be explained by the hydrophobic CH₃ groups on the surface. So, these materials are totally hydrophobic. When the ring PMO is treated at 350°C (RPMO-350°CN₂) the amount of adsorbed water is only 3%. This suggests that silanol-eliminating transformations also take place at this temperature.

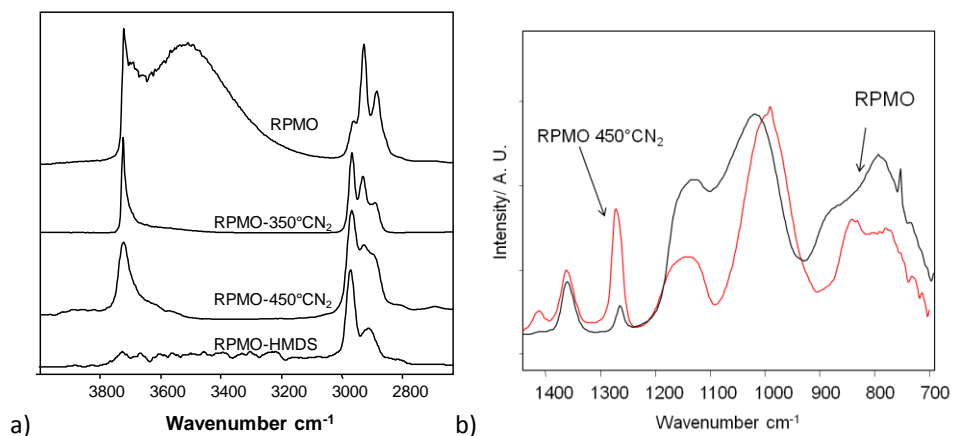


Figure 4.8: a) DRIFT spectra in the region 4000 cm⁻¹ - 2600 cm⁻¹ of extracted ring PMOs (RPMO), HMDS treated ring PMOs (RPMO-HMDS) and thermal treated ring PMOs (RPMO-350°CN₂ and RPMO-450°CN₂) under inert atmosphere; b) DRIFT spectra of RPMO and RPMO-450°CN₂ in the region 700 cm⁻¹ - 1500 cm⁻¹.

To confirm these results, DRIFT spectra of the extracted, HMDS and thermal treated ring PMOs in the region between 2700 cm⁻¹ and 4000 cm⁻¹ were obtained and are shown in figure 4.8 a. The large band between 3600 cm⁻¹ and 3200 cm⁻¹ is characteristic for the interaction of adsorbed water molecules with the surface. This band is only visible for the extracted ring PMOs what is consistent with the TGA results.

The peak at 3750 cm⁻¹ can be assigned to the O-H stretch vibrations of the silanol groups. This peak is visible for all the ring PMOs except the HMDS treated ones, indicating that after the self-hydrophobization process, there are still hydrophilic silanol groups present. The peaks in the region between 3000 cm⁻¹ and 2800 cm⁻¹ are characteristic for symmetric and anti-symmetric stretch vibrations of C-H bonds. The anti-symmetric (2929 cm⁻¹) and symmetric (2862 cm⁻¹) stretch vibrations of the CH₂ groups of the ring PMOs are observed for the extracted ring

PMOs. The small peak at 2969 cm^{-1} can be assigned to the anti-symmetric CH_3 stretch vibrations what means that some Si-C bonds have been cleaved during the synthesis.

When looking at the ring PMOs treated at 350°C , there is a relative decrease of the intensities of the CH_2 stretch vibrations and a relative increase of the CH_3 stretch vibrations. This means that more end-standing CH_3 groups are formed during the thermal treatment which results in a more hydrophobic material.

At 450°C , this trend continues and also a relative higher organic/silanol ratio is observed, indicating a lower amount of silanol groups present in the material which proves the silanol-eliminating transformations.

Based on these results, it is possible to control the organic/silanol ratio and thus the hydrophobic character of the ring PMOs by just varying the temperature.

The DRIFT spectra of RPMO and RPMO- $450^\circ\text{C}/\text{N}_2$ in the region $700\text{ cm}^{-1} - 1500\text{ cm}^{-1}$ further confirm the silanol-elimination process (fig. 4.8 b). The peak at 1271 cm^{-1} (SiCH_3) increases while the peak at 1139 cm^{-1} decreases (SiCH_2Si) relatively to the Si-O-Si peak (around 1000 cm^{-1}) after the thermal treatment.

A proposed reaction scheme for this self-hydrophobization process is given in figure 4.9 and is based on the reaction schemes of other thermally treated PMOs.^{17, 18}

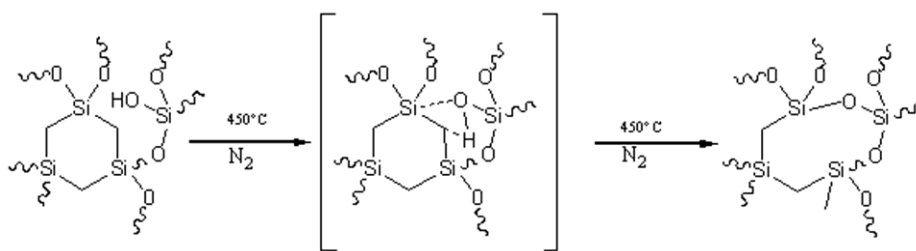


Figure 4.9: Thermally induced silanol-eliminating process.

4.3.3 Hydrothermal, mechanical and chemical stability

To investigate the hydrothermal stability, the extracted ring PMOs (RPMO), the hydrophobized ring PMOs (RPMO- $450^\circ\text{C}/\text{N}_2$ and RPMO-HMDS) and HMDS treated SBA-15 (SBA-15-HMDS) were steamed in extremely severe conditions (130°C , autogenous pressure) for 5 days.

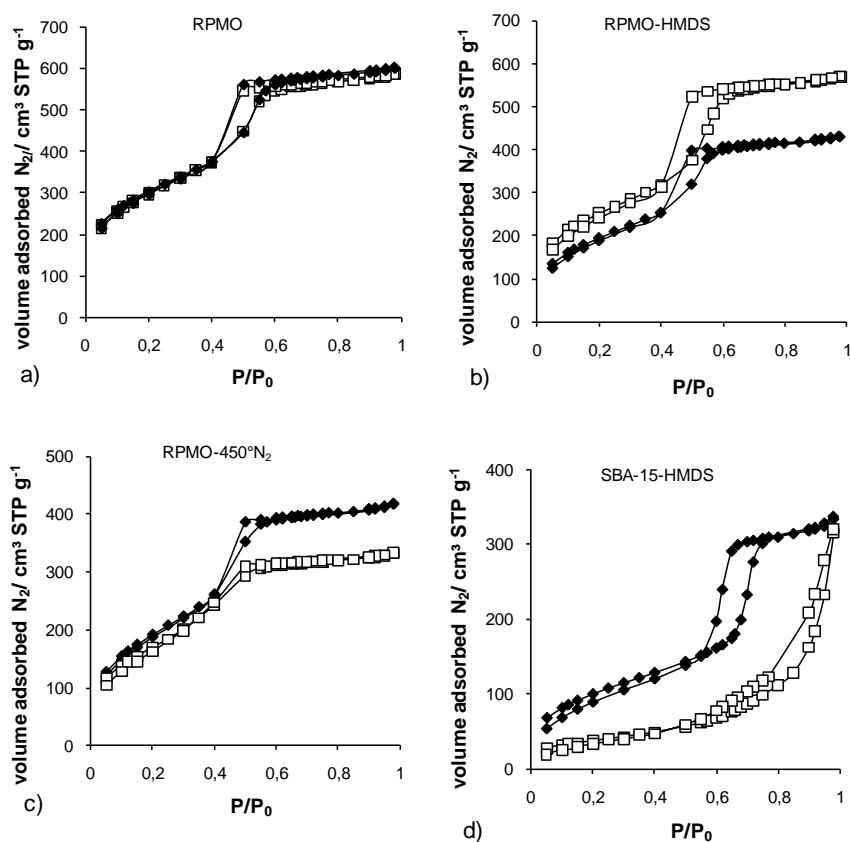


Figure 4.10: Nitrogen physisorption isotherms of a) RPMO, b) RPMO-HMDS, c) RPMO-450°CN₂ and d) SBA-15-HMDS before (♦) and after (□) the hydrothermal treatment.

The nitrogen physisorption isotherms in figure 4.10 show no difference before and after the steaming period for the extracted ring PMOs, indicating an exceptionally high hydrothermal stability. For the self-hydrophobized ring PMOs, there is a decrease in pore volume and also the capillary condensation step is less steep, indicating a broader pore size distribution. This means that the self-hydrophobized ring PMOs have a lower stability compared to the extracted ring PMOs. The reason for this is the fact that the creation of end-standing methyl groups on the surface also results in an extra siloxane bridge in the network, which can hydrolyze in the presence of water molecules.

The isotherms of the HMDS treated ring PMOs are remarkable because the total amount of adsorbed nitrogen is higher after the steaming period and is about the same value of the extracted ring PMOs. This suggests that the $\equiv\text{Si-O-Si}(\text{CH}_3)_3$ bonds on the surface are hydrolyzed during the hydrothermal treatment.

To confirm this, DRIFT spectra were obtained and are shown in figure 4.11. It can be seen that after the steaming period the peak of the anti-symmetric C-H stretch vibrations (2969 cm^{-1}) typical for end-standing methyl groups decreases and O-H stretch vibrations (3750 cm^{-1}) are appearing.

Compared to SBA-15-HMDS, the ring PMOs exhibit an excellent hydrothermal stability. For SBA-15-HMDS, the isotherm does not even show a type IV for isotherm after the steaming period, indicating that the mesoporous structure is lost. The hydrophobic methyl groups can not prevent the interaction of the water molecules with the silica network in these extreme conditions, making the material vulnerable to silicate hydrolysis.

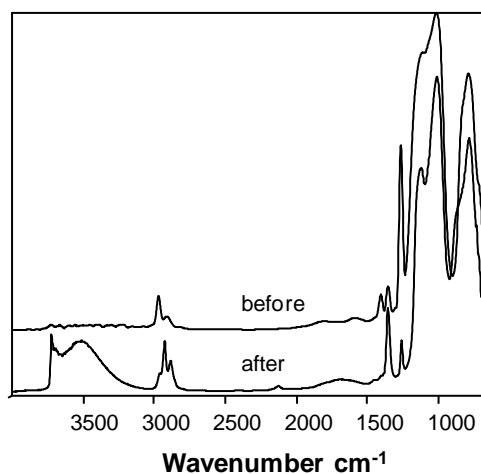


Figure 4.11: DRIFT spectra of RPMO-HMDS before and after the hydrothermal treatment.

The XRD patterns in figure 4.12 are consistent with the nitrogen physisorption isotherms. No difference is observed for the extracted ring PMOs, proving that they maintain their structure. A little increase and a little decrease of the intensity of the (100) reflections are observed for the RPMO-HMDS and RPMO-450°CN₂ respectively, indicating a slight increase and decrease in ordering of the material after the hydrothermal treatment. A strong decrease and a shift to a higher 2 theta value of the (100) reflection and the disappearance of the (110) and (200) reflections show a strong decrease in ordering of SBA-15-HMDS. According to these results, building hydrophobic organic groups in the silica network is far more important than a hydrophobic surface to obtain very hydrothermally stable materials.

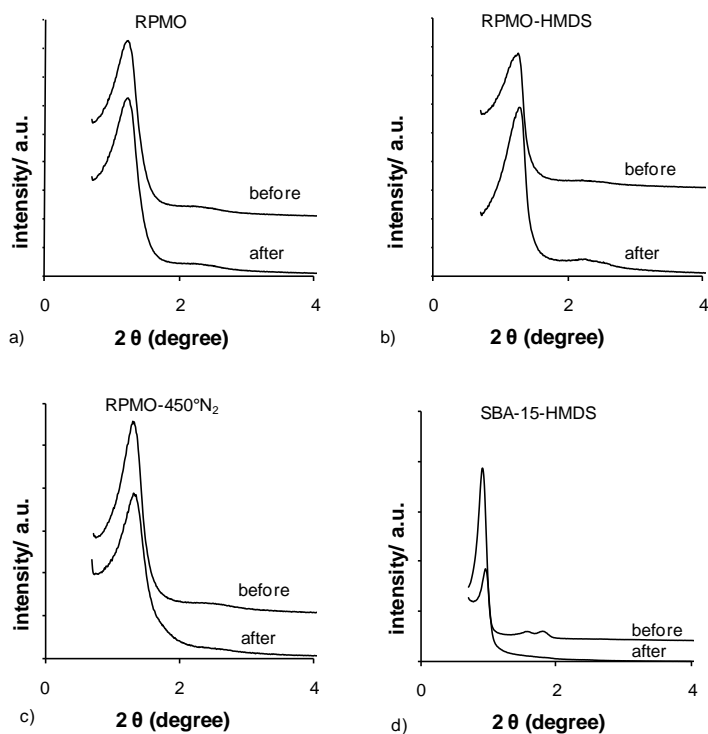


Figure 4.12: XRD patterns of a) RPMO, b) RPMO-HMDS, c) RPMO-450°C/N₂ and d) SBA-15-HMDS before and after the hydrothermal treatment.

Figure 4.13 shows the nitrogen physisorption isotherms before and after the mechanical compression of the porous materials. According to these isotherms, the ring PMOs have the lowest mechanical stability, because they have the strongest decrease in the total amount adsorbed nitrogen and the least steep capillary condensation step after the mechanical compression. Further, there is a little decrease in nitrogen adsorption for RPMO-450°C/N₂ and SBA-15-HMDS materials after the mechanical compression, while there is no difference in nitrogen adsorption for the RPMO-HMDS materials, indicating a high mechanically stable material. These findings are also confirmed by the XRD patterns in figure 4.14. The intensity of the (100) reflection is strongly decreased and broadened, indicating a poorly ordered material.

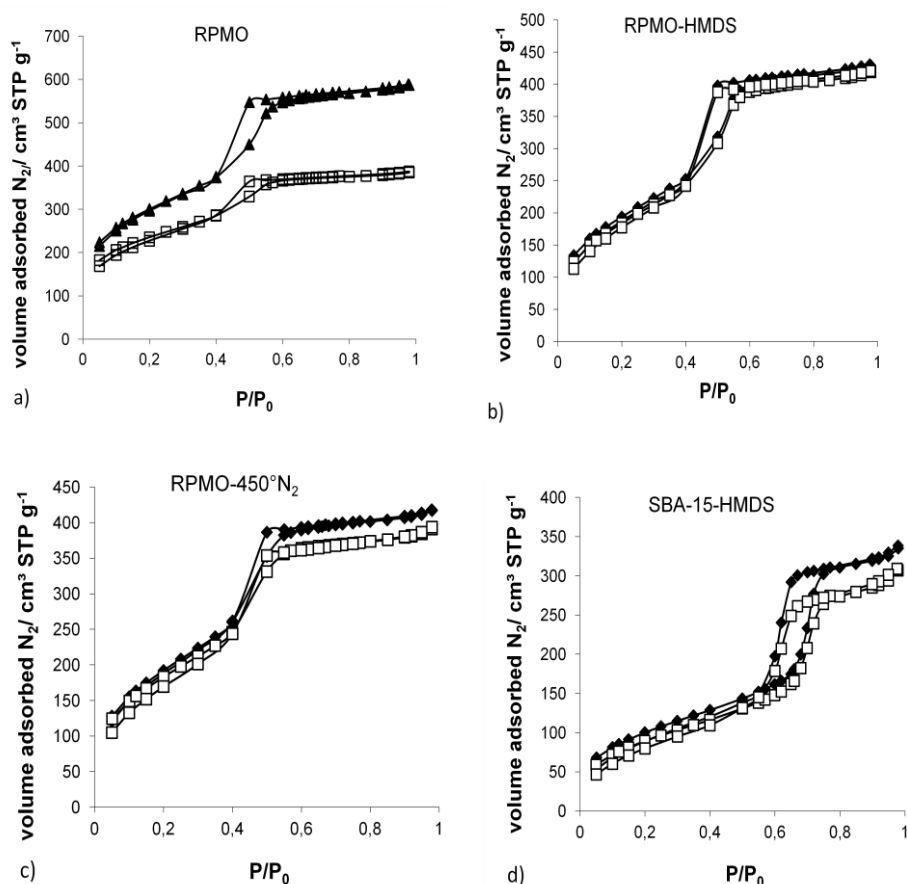


Figure 4.13: Nitrogen physisorption isotherms of a) RPMO, b) RPMO-HMDS, c) RPMO-450°CN₂ and d) SBA-15-HMDS before (♦) and after (□) a mechanical compression of 272 MPa.

The intensity of the (100) reflection of SBA-15-HMDS is also strongly decreased and shifted to a higher 2 theta value, indicating a change in unit cell parameter, while the decrease in intensity for RPMO-450°CN₂ is less strong after the compression. No significant differences are observed for RPMO-HMDS, proving a high mechanical stability. These results show a better mechanical stability for the hydrophobized samples, what can be explained by the fact that there are no water molecules present in the pores. Water molecules in the pores react under high pressure with the siloxane bridges of the ring PMOs, resulting in a disintegration of the pore walls. Without water molecules in the pores, a similar trend as for the hydrothermal stability can be noticed, which is that more organic groups in the silica network improve the mechanical stability.

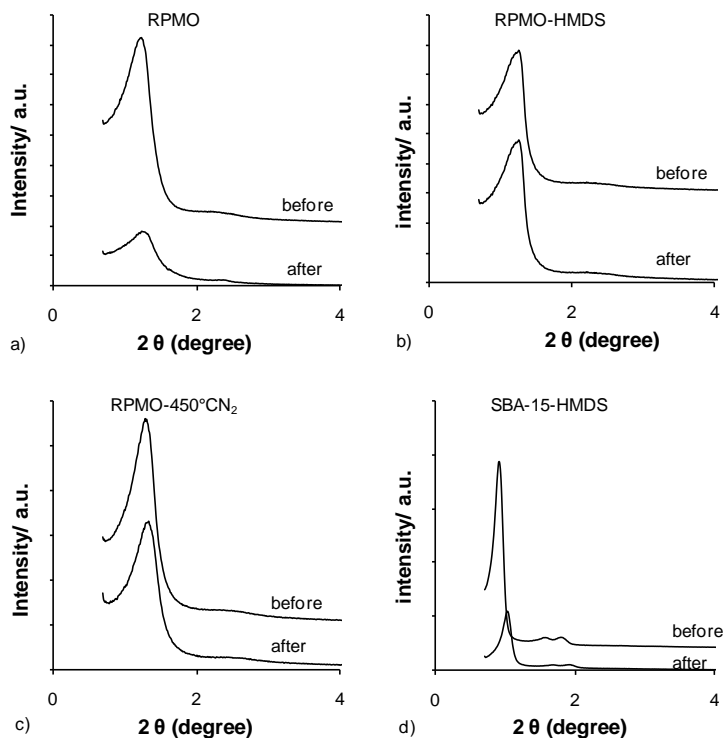


Figure 4.14: XRD patterns of a) RPMO, b) RPMO-HMDS, c) RPMO-450°C/N₂ and d) SBA-15-HMDS before and after a mechanical compression of 272 MPa.

Because the XRD patterns are consistent with the nitrogen physisorption isotherms for the hydrothermal and mechanical stability, only the results of the nitrogen adsorption measurements are presented for the chemical stability. Figure 4.15 shows the surface areas and total pore volumes before and after the stirring period in 1 M NaOH for 2.5 hours.

It can be seen that none of the porous materials are resistant against a very alkaline solution, but increasing the hydrophobicity improves the chemical stability. Looking at the non hydrophobized materials, which are SBA-15 and the ring PMOs, it can be seen that the ring PMOs have a far better chemical stability, because SBA-15 was completely dissolved after a stirring period of 2.5 hours. The less disintegration of the hydrophobized materials is because they are floating on the water surface, reducing the contact with the alkaline solution. Like it was observed for the hydrothermal stability, the surface area and pore volume of the HMDS-treated ring PMO increase after the stirring period.

This can again be explained by the fact that the $\equiv\text{Si-O-Si}(\text{CH}_3)_3$ bond will first hydrolyze before the siloxane bonds in the network. In that way, the trimethylsilyl groups protect the silica network of the ring PMOs, making the ring PMOs resistant against very alkaline solutions for a period.

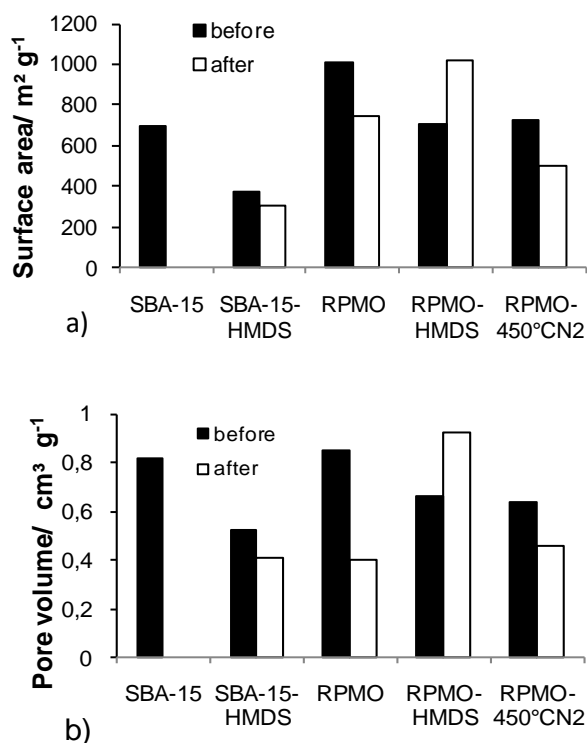


Figure 4.15: a) surface areas and b) pore volumes of mesoporous materials before and after stirring in alkaline conditions (1 M NaOH).

4.4 Conclusions

Highly porous and hexagonal ordered ring PMOs with narrow pore size distributions can be obtained in the presence of Brij-76 as a structure directing agent and in low to medium acid media. Increasing the concentration of Brij-76 up to a molar Brij-76/silane precursor ratio of 0.56, increases the porosity of the ring PMOs, but results in a decrease in wall thickness. It is possible to tune the porosity and wall thickness of the ring PMOs in a certain range.

Hydrophobic ring PMOs can be obtained by a treatment with HMDS or a thermal treatment under inert atmosphere. By varying the temperature, it is even possible to control the hydrophobic character of the ring PMOs. The two methods have a similar impact on the structural properties of the ring PMOs. They both decrease the surface area and pore volume and increase the wall thickness.

To get very high mechanically and chemically stable materials, a hydrophobization with HMDS is more preferable because the organosilica network is maintained. However, the advantage of the self-hydrophobization method is the remaining presence of silanol groups that can be functionalized. For a good hydrothermal stability, it is more important to have a high carbon/oxygen ratio in the silica network than a hydrophobic surface, resulting in a collapse of the HMDS treated SBA-15 materials by steaming at 130°C, while the ring PMOs maintain their structure under the same conditions. This steaming temperature can also be used to remove the trimethylsilyl groups of the HMDS treated ring PMOs without destroying the bulk of the ring PMOs.

4.5 References

1. B. D. Hatton, K. Landskron, W. J. Hunks, M. R. Bennett, D. Shukaris, D. D. Perovic and G. A. Ozin, *Materials Today*, 2006, **9**, 22-31.
2. M. Broyer, S. Valange, J. P. Bellat, O. Bertrand, G. Weber and Z. Gabelica, *Langmuir*, 2002, **18**, 5083-5091.
3. J. M. Kim and R. Ryoo, *B Kor Chem Soc*, 1996, **17**, 66-68.
4. P. Van Der Voort, M. Baltes and E. F. Vansant, *Catal Today*, 2001, **68**, 119-128.
5. K. Cassiers, T. Linssen, M. Mathieu, M. Benjelloun, K. Schrijnemakers, P. Van Der Voort, P. Cool and E. F. Vansant, *Chem Mater*, 2002, **14**, 2317-2324.
6. D. Y. Zhao, J. L. Feng, Q. S. Huo, N. Melosh, G. H. Fredrickson, B. F. Chmelka and G. D. Stucky, *Science*, 1998, **279**, 548-552.
7. D. Y. Zhao, Q. S. Huo, J. L. Feng, B. F. Chmelka and G. D. Stucky, *J Am Chem Soc*, 1998, **120**, 6024-6036.
8. M. L. Hair and C. P. Tripp, *Colloid Surface A*, 1995, **105**, 95-103.
9. C. P. Jaroniec, M. Kruk, M. Jaroniec and A. Sayari, *J Phys Chem B*, 1998, **102**, 5503-5510.
10. K. A. Koyano, T. Tatsumi, Y. Tanaka and S. Nakata, *J Phys Chem B*, 1997, **101**, 9436-9440.
11. K. Landskron, B. D. Hatton, D. D. Perovic and G. A. Ozin, *Science*, 2003, **302**, 266-269.
12. M. C. Burleigh, M. A. Markowitz, M. S. Spector and B. P. Gaber, *J Phys Chem B*, 2002, **106**, 9712-9716.
13. S. Z. Qiao, C. Z. Yu, Q. H. Hu, Y. G. Jin, X. F. Zhou, X. S. Zhao and G. Q. Lu, *Micropor Mesopor Mat*, 2006, **91**, 59-69.
14. D. J. Brondani, R. J. P. Corriu, S. Elayoubi, J. J. E. Moreau and M. W. C. Man, *Tetrahedron Lett*, 1993, **34**, 2111-2114.
15. X. Y. Bao, X. S. Zhao, X. Li, P. A. Chia and J. Li, *J Phys Chem B*, 2004, **108**, 4684-4689.
16. X. Y. Bao, X. Li and X. S. Zhao, *J Phys Chem B*, 2006, **110**, 2656-2661.
17. C. Vercaemst, J. T. A. Jones, Y. Z. Khimyak, J. C. Martins, F. Verpoort and P. Van der Voort, *Phys Chem Chem Phys*, 2008, **10**, 5349-5352.
18. B. D. Hatton, K. Landskron, W. Whitnall, D. D. Perovic and G. A. Ozin, *Adv Funct Mater*, 2005, **15**, 823-829.

Chapter Five: Synthesis of Ethane PMO Films

In this chapter, it will be presented how to synthesize ethane PMO films by dip- and spin-coating using the evaporation induced self-assembly method. The utilized structure directing agent is Brij-76. Next the influence of the viscosity and dip- or spin-coat rate on the thickness of the films is investigated as well as the influence of the surfactant concentration on the porosity.

It was found that also for these films the thickness increases when the viscosity or dip-coat rate increases and it decreases when the spin-coat rate increases. By increasing the surfactant concentration, higher porosities are obtained.

In the second part, the influence of the porosity on the mechanical stability and the effect of the hydrophobicity on the dielectric constant are investigated. Good mechanical properties can be obtained up to a porosity of 40%. However, an extra trimethylsilylation step is needed to obtain a low-dielectric constant.

5.1 Introduction

From chapters 3 and 4, it can be concluded that ethane PMOs and especially ring PMOs synthesized in the presence of non-ionic surfactants have good stabilities. Therefore, also good low-k properties can be expected. However, the characterization of their properties was performed on powder particles instead of on a thin film which is of course the morphology needed for low-k application. As already mentioned in chapter 2, PMO films can be easily prepared by the EISA method via liquid phase deposition methods.

Ozin's group already prepared these materials as thin films, but they used CTAC as structure directing agent.^{1, 2} However, the use of ionic surfactants should be avoided, because residual ions after template removal can lead to a bad reliability.

Although the low-k properties of ring PMOs seem to be better than those of ethane PMOs, they are also more expensive due to the more complex starting precursor.

Therefore in this chapter, we will synthesize ethane PMO films via the EISA method using surfactant Brij-76 as structure directing agent. Brij-76 was chosen above P123 because smaller pores are obtained for this surfactant^{3, 4} which is beneficial for the low-k applicability. Dip- and spin-coating are used as deposition methods and the synthesis conditions to obtain crack-free films are examined. Further, the influence of several synthesis parameters on the thickness, hydrophobicity and porosity of the PMO films are investigated. Finally, the impact of the porosity and the hydrophobicity on the mechanical stability and dielectric constant is presented.

Scanning electron microscopy (SEM), spectroscopic ellipsometry, water contact angle measurements, nano-indentation and capacitance voltage (C-V) measurements were performed for characterization of the films.

5.2 Experimental section

5.2.1 Chemicals

1,2-bis(triethoxysilyl)ethane (BTESA) and hexamethyldisilazane (HMDS) were purchased from ABCR, hydrochloric acid (HCl, 37 %), and absolute ethanol (EtOH) were obtained from Fiers, and polyoxyethylene (10) stearyl ether (Brij-76) was purchased from Aldrich. All materials were used as received.

5.2.2 Synthesis

The ethane PMO films were prepared using a sol-gel method based on the evaporation induced self assembly (EISA) mechanism.⁵ For a general synthesis of ethane PMO films, a mixture of Brij-76, HCl and ethanol was stirred at 50°C until a clear solution was obtained. Then a specific amount of BTESA and water was added to the solution and this was stirred for 15 minutes at 50°C. Next, the solution was aged for 90 minutes at room temperature. The aged solution was then dip- or spin-coated at a certain withdrawal or spin-coat rate on glass or silicon substrates. After a drying step of 24 hours, the film was heated to 400°C and kept at this temperature for 5 hours under nitrogen to remove the porogen template.

To investigate the effect of hydrophobicity, some films were grafted with HMDS. Therefore, dry films were immersed in a pentane/HMDS solution and kept there for 3 hours at room temperature. Afterwards the film were rinsed with pentane and treated at 300°C under nitrogen to remove the unreacted HMDS molecules.

5.2.3 Characterization

Scanning Electron Microscopy (SEM) images were obtained by a Quanta 200FEG from FEI with a resolution of 0.8 nm at 30 kV and under high vacuum.

Water contact angles images were obtained by using a Krüss-DSA 30 Drop Shape Analysis System and the “tangent 1” model was used to calculate the contact angle.

The refractive index and thickness of the layer is analyzed on a J. A. Woollam ellipsometer alpha-SE. This non destructive method measures the change in polarization of the reflected light off a sample. By using a mathematical model (Cauchy), the thickness and refractive index are calculated. Having knowledge of the refractive index, it is now possible to calculate the theoretical porosity by using the Lorentz-Lorenz equation.

$$\frac{n^2 - 1}{n^2 + 2} = V_p \frac{n_p^2 - 1}{n_p^2 + 2} + (1 - V_p) \frac{n_s^2 - 1}{n_s^2 + 2}$$

In this formula, n_p stands for the refractive index of the material inside the pores (in our case air with $n_p = 1$). The refractive index of the material containing the pores n_s (in our case the organosilica matrix with $n_s \cong 1.48$). By measuring n by ellipsometry, we can now easily calculate the porosity V_p .

The Young's modulus and hardness of the low-k dielectric films was measured by nano-indentation using a Nano Indenter XP system from MTS Corporation, with a dynamic

contact module (DCM) and a continuous-stiffness measurement (CSM) option under constant strain rate condition (0.05 s^{-1}). A standard three-sided pyramid diamond indenter type (Berkovich) was used for the indentation experiments. The Young's modulus was calculated based on its relationship with the contact area (A) and the measured contact stiffness (S),

$$S = \beta \frac{2}{\sqrt{\pi}} E_r \sqrt{A}$$

Where A is the projected contact area of the indenter with the sample surface, β is a correction coefficient ($\beta = 1.034$ for a Berkovich tip) and E_r is the effective Young's modulus defined by,

$$E_r = \left[\frac{1-\nu^2}{E} + \frac{1-\nu_i^2}{E_i} \right]^{-1}$$

With ν the Poisson ratio of the sample (assumed to be 0.17), ν_i the Poisson ratio of the Berkovich tip, E the Young's modulus of the sample and E_i the Young's modulus of the Berkovich tip.

The effective Young's modulus takes into account the fact that elastic displacements occurred in both sample (Young's modulus E and Poisson's ratio ν) and indenter tip (Young's modulus E_i and Poisson's ratio ν_i).

The hardness was calculated from the load (P) and contact area,

$$H = P/A$$

For k -value evaluations, Al dots were deposited on blanket wafer pieces in order to form MIS capacitors. The dots were e-beam evaporated through high precision bi level nickel shadow masks. Special magnetic carriers were used to hold the masks on the samples and reduce the evaporation shadows. As a result, the area of the fabricated top contacts was very well controlled within an error of only 1%.

The samples were provided with an ohmic back contact by applying Ga-In alloy paste on the scratched backside (n-type Si), following one of the practical methods described by Ciofi *et al.*⁶ The capacitance-voltage ($C-V$) measurements were performed by means of an impedance analyzer (HP4284A precision LCR meter) in the frequency range from 100 Hz to 100 kHz. The series model was used to obtain the capacitance from the measured impedance. Besides, the dissipation factor (D) was always monitored, as impedance analyzers generally lose accuracy for capacitance measurements when the dissipation factor is greater than 0.1. As the diameter of the fabricated dots is much larger than the deposited film thickness, the parallel plate capacitance approximation

could be used to extract the k -value from the film capacitance, which is given by the measured capacitance with the Si substrate in accumulation.

5.3 Results and discussion

5.3.1 Dip- and spin-coating of ethane PMOs

Dip-coating on glass substrates

After several attempts to obtain crack-free PMO films, a good quality film deposited on a glass substrate was achieved by using a starting mixture with following molar composition: BTESA 1; Brij-76 0.073; HCl 0.005; H₂O 5.8; EtOH 32. This solution was first aged for 90 minutes before dip-coating. The applied withdrawal speed was 60 mm/min and the obtained thickness is around 280 nm. The Young's modulus of the film was measured to be 6 GPa which should be sufficient for low- k application. A SEM picture is shown in figure 5.1.

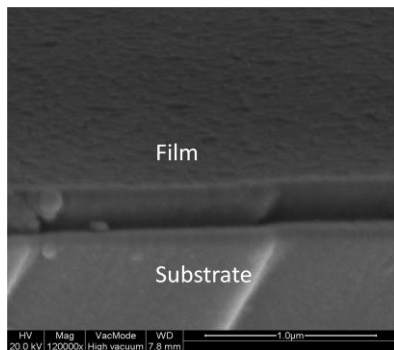


Figure 5.1: Cross section of ethane PMO film.

Starting from this composition, synthesis parameters were varied to control the properties of the films. Figure 5.2 presents the influence of the withdrawal speed on the thickness of the film. As expected the thickness of the film increases with increasing withdrawal speed, making it possible to control the thickness of the film.

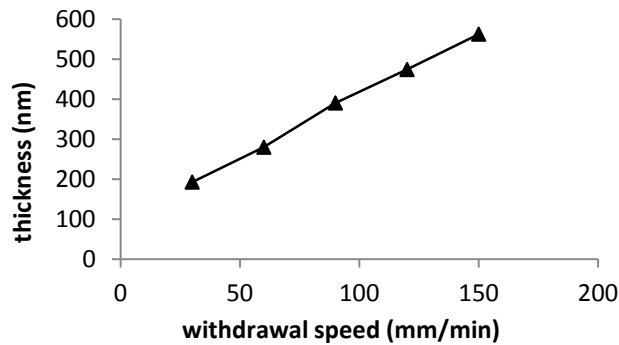


Figure 5.2: The influence of the withdrawal speed on the thickness.

Another important parameter to control the thickness of the film is the viscosity of the starting mixture. The viscosity of the sol can be easily adjusted by changing the solvent concentration or by aging the solution. During the aging, the precursor molecules will form more viscous oligomers via sol-gel reaction. The influence of the viscosity on the thickness is given in figure 5.3.

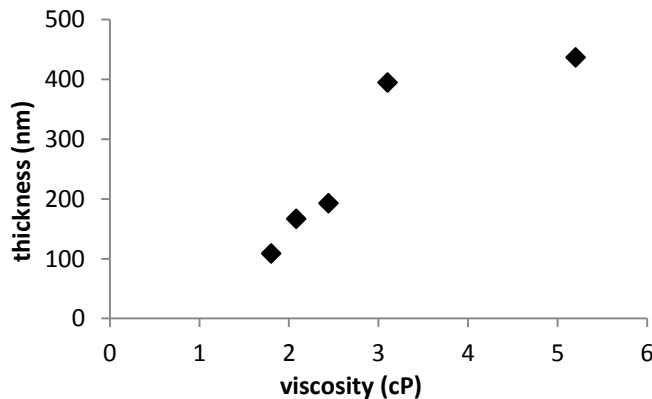


Figure 5.3: Influence of the viscosity on the thickness.

Similar to the withdrawal speed, the thickness increases when the viscosity increases. However, the increase is not gradually, making it more difficult to control the thickness. Further, it was also observed that the quality of the films at high viscosity (above 3 cP) was bad (cracks were visible), which means that the viscosity is a very important synthesis parameter.

The deposition on glass substrates allows characterization of the (microscopic) visible properties of the films, but an easy determination of the dielectric constant and porosity of the film is not possible. Therefore, we switched to silicon substrates.

Dip-coating on silicon substrates

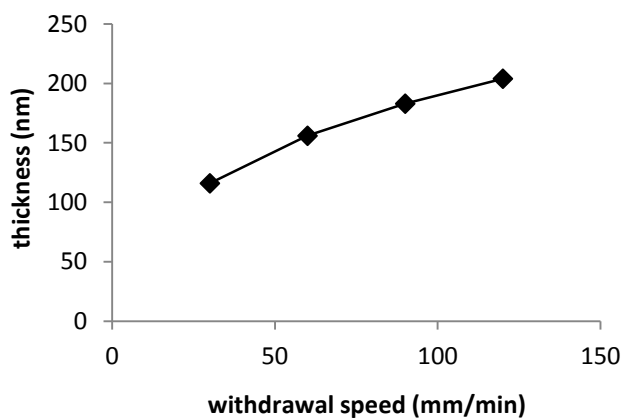


Figure 5.4: The influence of the withdrawal speed on the thickness.

By dip-coating the same starting mixture on Si substrates, it was found that the thickness of the resulting film was much lower compared to films on glass substrates. This is probably due to the fact that Si substrates are polished and this will make that more fluid will drop off from the substrate. As shown in figure 5.4 the film thickness also varies with the withdrawal speed, but the differences are less pronounced.

To vary the porosity of the film, the amount of surfactant was changed and the results are shown in figure 5.5. It can be seen that increasing the surfactant/precursor ratio results in higher porosities which is in good agreement with earlier reported papers.⁷⁻⁹

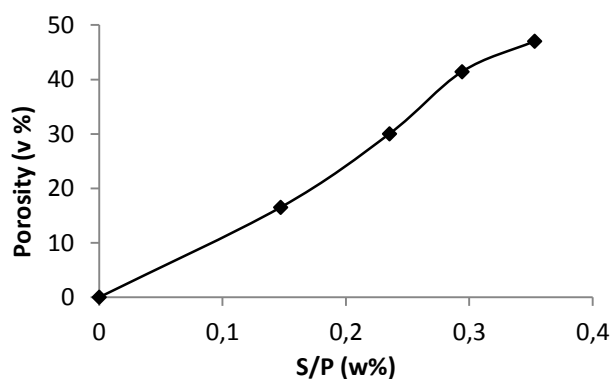


Figure 5.5: Influence of the surfactant (S)/precursor (P) ratio on the porosity.

Although, it is possible to prepare ethane PMOs via dip-coating, there are some drawbacks. The first one is that the backside is also coated with the PMO layer and this is not needed for low-k applications. It is possible to solve this by protecting the backside of the substrate or by carefully washing off the layer immediately after dip-coating.

However, this means extra processing steps which are also dangerous to damage the low-k material. Secondly, the side effects caused by dip-coating make that only the center of the substrate is very uniform in thickness. Therefore in the next section we investigated if more uniform films can be obtained with spin-coating.

Spin-coating on silicon substrates

Because the viscosity should be low enough to obtain good films, a starting mixture with a viscosity around 1.8 cP was prepared and this was spin-coated at different spin-coat rates. The effect on the thickness is presented in figure 5.6

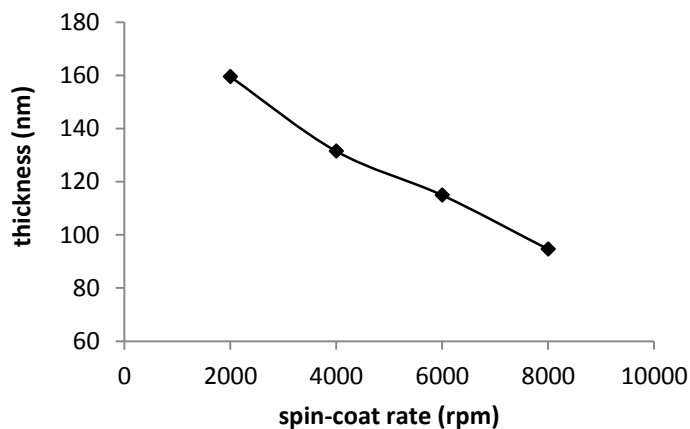


Figure 5.6: The influence of the spin-coat rate on the thickness.

As can be seen from the figure the thickness of the film decreases when the spin-coat rate increases. However, it was observed that it is very difficult to reproduce the values. The reason for this is probably that not all the deposition conditions could be precisely controlled or reproduced in our lab.

When investigating the effect of the surfactant/precursor ratio on the porosity it is also found that the porosity increases when more surfactant is added (see figure 5.7).

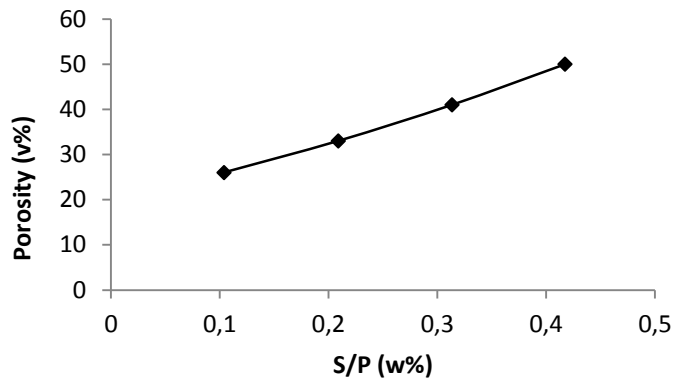


Figure 5.7: Influence of the surfactant (S)/precursor (P) ratio on the porosity.

In the next section the results of the effect of the porosity and hydrophobicity on the mechanical stability and dielectric constant will be presented and discussed.

5.3.2 Influence of the porosity and hydrophobicity on respectively the mechanical stability and dielectric constant

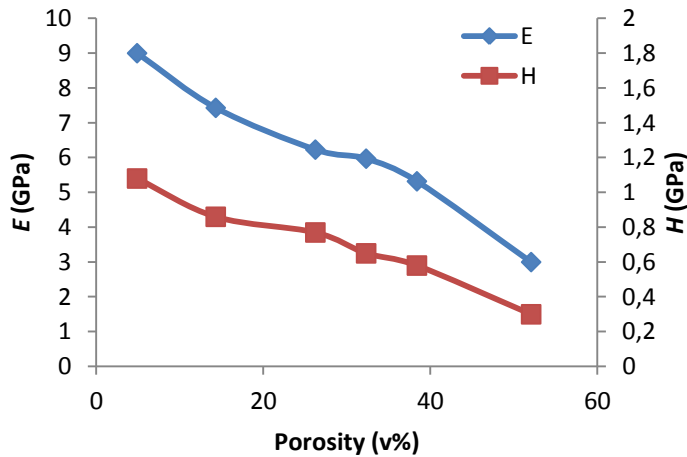


Figure 5.8: The influence of the porosity on the Young's modulus (E) and hardness (H) of ethane PMO films.

Figure 5.8 shows the effect of the porosity on the Young's modulus (E) and hardness (H) of the ethane PMO films. Similar to other porous materials the Young's modulus and hardness decreases when the porosity increases. For low-k applications the Young's

modulus should be preferable above 4 GPa. On the other hand a high porosity is needed to obtain a low dielectric constant.

By looking at the figure the ethane PMO with a porosity of around 40% would be the most suitable. However, the measured k -value of this sample was measured to be 2.5 which is far from the targeted value. Also compared to values from literature the obtained value is rather high. The reason for this high value is probably moisture that is adsorbed in the pores. To have an idea about the hydrophobic character of the PMO, the contact angle was measured and is shown in figure 5.9.

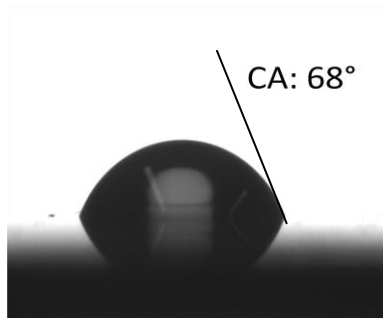


Figure 5.9: Water contact angle of ethane PMO film.

The value of 68° indicates that the material is not completely hydrophobic and water can adsorb in ambient atmosphere. To increase the hydrophobicity, ethane PMO films treated with HMDS were prepared. Again the water contact angle contact was measured and a very high water contact of 100° is obtained, meaning that the film is hydrophobic (see figure 5.10).

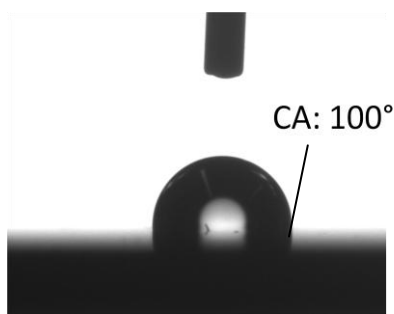


Figure 5.10: Water contact angle of HMDS treated ethane PMO film.

The obtained porosity of this film is also around 40% and therefore the influence of the HMDS treatment on the dielectric constant and mechanical stability can be investigated. As already mentioned, the dielectric constant of the non HMDS treated

ethane PMOs is 2.5 with a Young's modulus of 5.3 GPa. After the HMDS treatment, the dielectric constant is 2.15 which is significantly lower than the non-treated film, considering an error of $k \pm 0.1$. The Young's modulus of this film is 5 GPa which is on first sight lower than the non treated film. However, the error on the measurement is 0.5 GPa and therefore the difference is not significant.

Compared to literature values, the dielectric constant and Young's modulus of the HMDS-treated PMO is in the same range of organosilica films,¹⁰ but the k -values are significantly lower than those of the already reported ethane PMO films.^{1, 11, 12} A possible explanation for this is that the experiment conditions were not exactly the same and this can lead to different values. So, to solve this unambiguously, those films and our prepared films should be characterized at the same time with the same experimental conditions and setups.

5.4 Conclusions

In this work, it was first shown how good quality ethane PMO films can be obtained in the presence of surfactant Brij-76 by dip- and spin-coating. In the case that dip-coating is used, the thickness can be controlled by changing the viscosity and/or the withdrawal speed. For spin-coating, changing the spin-coat rate is the easiest way to change the thickness in a certain range.

Further, the porosity can be controlled by changing the surfactant concentration. By adding more surfactant, the porosity increases. On the other hand the mechanical stability decreases.

Finally, it is also shown that an extra hydrophobization of ethane PMOs is absolutely necessary to obtain low-dielectric constants. However, no significant improvements compared to literature were obtained.

5.5 References

1. B. D. Hatton, K. Landskron, W. Whitnall, D. D. Perovic and G. A. Ozin, *Adv Funct Mater*, 2005, **15**, 823-829.
2. K. Landskron, B. D. Hatton, D. D. Perovic and G. A. Ozin, *Science*, 2003, **302**, 266-269.
3. F. Goethals, B. Meeus, A. Verberckmoes, P. Van der Voort and I. Van Driessche, *J Mater Chem*, 2010, **20**, 1709-1716.
4. F. Goethals, C. Vercaemst, V. Cloet, S. Hoste, P. Van Der Voort and I. Van Driessche, *Micropor Mesopor Mat*, 2010, **131**, 68-74.
5. Y. F. Lu, R. Ganguli, C. A. Drewien, M. T. Anderson, C. J. Brinker, W. L. Gong, Y. X. Guo, H. Soyez, B. Dunn, M. H. Huang and J. I. Zink, *Nature*, 1997, **389**, 364-368.
6. I. Ciofi, M. R. Baklanov, Z. Tokei and G. P. Beyer, *Microelectron Eng*, 2010, **87**, 2391-2406.
7. N. Hata, C. Negoro, K. Yamada and T. Kikkawa, *Jpn J Appl Phys 1*, 2004, **43**, 1323-1326.
8. C. H. Yang and W. L. Yang, *J Electrochem Soc*, 2006, **153**, G341-G346.
9. F. K. de Theije, A. R. Balkenende, M. A. Verheijen, M. R. Baklanov, K. P. Mogilnikov and Y. Furukawa, *J Phys Chem B*, 2003, **107**, 4280-4289.
10. P. Verdonck, E. Van Besien, K. Vanstreels, C. Trompoukis, A. Urbanowicz, D. De Roest and M. R. Baklanov, *Jpn J Appl Phys*, 2011, **50**.
11. W. D. Wang, D. Grozea, A. Kim, D. D. Perovic and G. A. Ozin, *Adv Mater*, 2010, **22**, 99-+.
12. W. D. Wang, D. Grozea, S. Kohli, D. D. Perovic and G. A. Ozin, *Acs Nano*, 2011, **5**, 1267-1275.

Chapter Six: Ultra low-k Cyclic Carbon-Bridged PMO films with a High Chemical Resistance

In this paper, PMO thin films that combine an ultra low k -value, a hydrophobic property and a high resistance against aggressive chemical conditions are presented. The films are synthesized via spin-coating of a 1,1,3,3,5,5-hexaethoxy-1,3,5-trisilacyclohexane, hydrochloric acid, water and ethanol mixture using polyoxyethylene (10) stearyl ether as porogen template (Brij-76). The obtained highly porous films are hydrophobic, crack-free and an ultra low k -value of 1.8 is achieved with a Young's modulus of 2 GPa. Finally, the chemical resistance of these PMO films against alkaline solutions is investigated in detail and compared with the resistance of mesoporous silicas and PMOs synthesized with cetyl trimethylammonium chloride.

The results were published in "*Journal of Materials Chemistry*": F. Goethals, I. Ciofi, O. Madia, K. Vanstreels, M. R. Baklanov, C. Detavernier, P. Van Der Voort and I. Van Driessche, *J Mater Chem*, 2012, **22**, 8281-8286.

6.1 Introduction

Chapter 5 showed that by varying the concentration of the non-ionic surfactant Brij-76, the porosity and thus the mechanical and dielectric properties of ethane PMO films can be adjusted. This led to materials with k -values of 2.15 and a Young's modulus of 5 GPa. However, to get beyond the state of the art low-k materials, k -values below 2 combined with other good properties have to be developed.¹

Landkron *et al.*² showed already that ring PMO films have interesting properties (very low k -value, good mechanical stability). However, there is little known of the chemical stability of these ultra low-k PMO films. A high chemical stability is needed to withstand the chemical treatments of the low-k films during device manufacturing.

Therefore, this work addresses the development of PMO thin films that combine an ultra low k -value with a superior chemical etch resistance against aggressive alkaline solutions. Hydrophobic ultra low-k PMO thin films containing $[\text{Si}(\text{CH}_2)]_3$ rings (RPMOs) were synthesized via spin-coating and Brij-76 is used as porogen template instead of the usual ionic surfactant cetyl trimethylammonium bromide or chloride. This surfactant was again chosen because it creates thicker pore walls which should enhance the resistance against etching chemicals. Also, relatively small mesopores are obtained with this template and it interacts well with silane precursors³ which was also already shown in chapter 5.

The structural properties of these films were determined with SEM, TEM, ellipsometric porosimetry, water contact angle measurements and diffuse reflectance infra-red Fourier transform (DRIFT) spectroscopy. The dielectric constant was obtained through high-frequency capacitance-voltage (C - V) measurements on metal insulator semiconductor (MIS) planar capacitors, used as a test vehicle. The accurate determination of the dielectric constant is fundamental for the estimation of the actual gain in interconnect performance (RC delay) that can be achieved by the use of a new material.⁴ Therefore, as described later in this chapter, we paid special attention to the preparation of the samples, the choice of the measurement conditions and the analysis of the data. In addition, we also evaluated the error bar on the obtained k -value to provide a measure of the confidence in the characterization procedure we implemented.

Further, we investigated the etching resistance by immersing the thin films in alkaline solutions (pH 9 and pH 14) in function of time and compared the change in thickness with mesoporous silica thin films and RPMOs prepared with cetyl trimethylammonium chloride (CTAC). Finally, the hydrophobic character of the RPMO films after immersion was followed by infrared spectroscopy and water contact angle measurements.

6.2 Experimental section

6.2.1 Chemicals

1,1,3,3,5,5-hexaethoxy-1,3,5-trisilacyclohexane, HMDS and tetraethyl orthosilicate (TEOS) were purchased from ABCR, hydrochloric acid (HCl, 37 %) and absolute ethanol were obtained from Fiers, and polyoxyethylene (10) stearyl ether (Brij-76) and cetyl trimethylammonium chloride (25 w%, CTAC) were purchased from Aldrich. All materials were used as received.

6.2.2 Synthesis

The RPMO thin films were prepared using a sol-gel method also based on the evaporation induced self assembly (EISA) mechanism.⁵ 0.6 g Brij-76, 0.5 ml (0.1 M) HCl and 18 ml ethanol were mixed at 50°C until a clear solution was obtained. Then 1 ml of 1,1,3,3,5,5-hexaethoxy-1,3,5-trisilacyclohexane and 0.5 ml water were added to the solution and this was stirred for 15 minutes at 50°C. The temperature was set at 50°C to increase the solubility of the components. Next, the clear solution was left to cool down to room temperature and additionally aged for 90 minutes at room temperature. The aged solution was then spin-coated at a rate of 5000 rpm onto a silicon wafer. After a drying step of 24 hours, the film was heated to 400°C and kept at this temperature for 5 hours under nitrogen to remove the porogen template.

Also some RPMO films were treated with HMDS, because chapter 4 showed that they have the best stability in powder form. To obtain this, dry films were immersed in a pentane/HMDS solution and kept there for 3 hours at room temperature. Afterwards the film were rinsed with pentane and treated at 300°C under nitrogen to remove the unreacted HMDS molecules.

For comparing the resistance against alkaline solutions also mesoporous silica thin films were prepared using the same synthesis method. Only 1,1,3,3,5,5-hexaethoxy-1,3,5-trisilacyclohexane was changed by tetraethyl orthosilicate (TEOS).

The synthesis of the PMO films prepared with CTAC is based on a method of Wang *et al.*⁶ 1 ml of 1,1,3,3,5,5-hexaethoxy-1,3,5-trisilacyclohexane is mixed with 3.2 g 25 w% CTAC, 0.7 ml 1 M HCl and 5 ml ethanol. After an aging period of 60 minutes, the solution was spin-coated at a rate of 5000 rpm onto a silicon wafer. After a drying step of 24 hours, the film was also heated to 400°C and kept at this temperature for 5 hours under nitrogen to remove the porogen template.

6.2.3 Characterization

Scanning Electron Microscopy (SEM) images were obtained by a Quanta 200FEG from FEI with a resolution of 0.8 nm at 30 kV and under high vacuum. Diffuse reflectance infra-red Fourier transform (DRIFT) spectra were obtained on a Thermo 6700 FLEX FTIR/FT-Raman system, equipped with nitrogen cooled MCT-A detector. A spectrum of a pristine silicon wafer was first measured to use as background.

High resolution transmission electron microscopy (TEM) measurements were performed on a Jeol JEM 3010 apparatus. The samples were prepared by scratching the film off the substrate. Next, the pieces were dispersed in acetone and put in an ultrasonic bath for 24 hours to obtain highly dispersed particles which were then afterwards put on Cu TEM grids. Water contact angles images were obtained by using a Krüss-DSA 30 Drop Shape Analysis System and the “tangent 1” model was used to calculate the contact angle.

The thickness, porosity and pore size distribution were determined with ellipsometric porosimetry which is an excellent technique to determine the porosity of nanoporous thin films. This novel technique is a combination of conventional adsorption porosimetry which is frequently used for characterization of porous materials and ellipsometry which provides thin film properties such as the thickness and refractive index.^{7,8}

For the porosity measurement, a spectroscopic ellipsometer Sentech 801 is mounted in a vacuum chamber that can be filled with solvent vapor (toluene) in a controlled way. The pressure of the toluene vapor is raised in steps from the vacuum level up to the saturation pressure. The pressure dependent condensation occurs in the open pores and the refractive index of the sample is changed. The total pore volume is calculated from the change in refractive index at saturation pressure using the Lorentz-Lorenz equation.

$$P = \left(\frac{n_{rf}^2 - 1}{n_{rf}^2 + 2} - \frac{n_{re}^2 - 1}{n_{re}^2 + 2} \right) / \left(\frac{n_{ads}^2 - 1}{n_{ads}^2 + 2} \right)$$

With P the porosity, n_{re} the refractive index of the film with empty pores, n_{rf} the refractive index of the film with filled pores and n_{ads} the refractive index of the solvent. The pore radius is calculated from the adsorption branch with the Kelvin equation taking into account the physical properties of toluene.

$$\ln \frac{P}{P_0} = \frac{-2\gamma V}{rRT}$$

With P/P_0 the relative pressure, γ the surface tension of toluene, V the molar volume of toluene, r the pore radius, R the gas constant and T the temperature. The correction for the thickness of the film of adsorbate on the surface was made with the method described by Baklanov *et al.*⁸

The Young's modulus of the low-k dielectric films was measured by nano-indentation using a Nano Indenter XP system from MTS Corporation, with a dynamic contact module (DCM) and a continuous-stiffness measurement (CSM) option under constant strain rate condition (0.05 s^{-1}).

The dielectric constant of the films was calculated from the capacitance of a parallel plate capacitor at 100 kHz using a HP 4192A LF impedance analyzer. Aluminum dots with diameters of 1070, 1954, 2764 and 3385 μm were used as top contacts and a heavily doped silicon wafer was used as bottom contact. The bottom of the silicon wafer was scratched to remove the native silicon dioxide and an eutectic indium/gallium alloy was attached to make a good ohmic contact with the impedance analyzer.

6.3 Results and discussion

Figure 6.1 shows a SEM image of the cross section of the RPMO film after template removal. A crack-free and uniform surface is obtained, and a thickness of 150 nm can be roughly estimated. This is in good agreement with the more precise thickness of 157 nm determined with ellipsometry (see table 6.1).

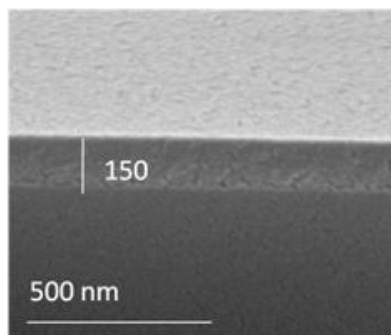


Figure 6.1: SEM image of the RPMO film.

Figure 6.2 shows the DRIFT spectrum of the RPMO thin film. The peak at 1037 cm^{-1} can be assigned to stretch vibrations of the Si-O-Si bonds and the sharp peak at 1272 cm^{-1} represents the stretch vibrations of the Si-CH₃ bonds.⁹ The presence of Si-CH₃ can be

explained by the self-hydrophobization process at elevated temperatures ($T > 350^{\circ}\text{C}$). The relative broad peak around 780 cm^{-1} represents vibrations of SiOSi and SiC bonds.⁹ The inset is a magnification of the spectrum to show the presence of C-H stretch vibrations in the region $2900\text{ cm}^{-1} - 3000\text{ cm}^{-1}$ because the representative peaks are not well resolved. The peak with the highest intensity (2970 cm^{-1}) can be assigned to the C-H stretch vibrations of the CH_3 bonds and the peak around 2930 cm^{-1} represents the C-H stretch vibrations of the methylene bridges.¹⁰

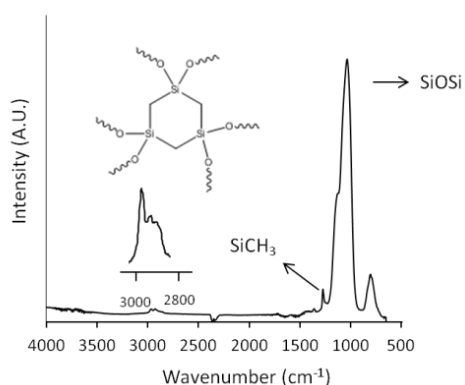


Figure 6.2: DRIFT spectrum of the RPMO film.

The region between 3600 cm^{-1} and 3200 cm^{-1} is flat which means that no water is adsorbed and thus a very hydrophobic film is obtained. This is also confirmed by the high contact angle shown in table 6.1. Thus the heating of the as synthesized film above 350°C combines the surfactant removal and the hydrophobization process.²

Table 6.1: Physical properties of the RPMO films.

Sample	Porosity (%) ^a	Pore diameter (nm) ^a	Contact angle (°) ^b	Thickness (nm) ^a	Young's modulus (GPa) ^c
RPMO	55	4	92	157	2
HRPMO	55	4	100	150	1.9

^a determined with ellipsometric porosimetry

^b calculated with the tangent 1 model

^c determined with nano-indentation

Figure 6.3 shows the toluene adsorption/desorption isotherm measured by ellipsometric porosimetry and the pore radius distribution of the RPMO thin film. The type IV isotherm with a steep capillary condensation step is typical for mesoporous materials with a narrow pore size distribution. The mean pore diameter is around 4 nm,

Chapter 6: Ultra low-k cyclic carbon-bridged PMO films with a high chemical resistance

which should be suitable for low-k applications. Although, smaller pores are more preferable, they collapse rather quickly at high porosities due to their thin pore walls.¹¹ The shape of the hysteresis (a delayed desorption step) indicates pore blocking effects probably created during surfactant removal. The total porosity of the RPMO film is equal to the porosity measured at $P/P_0 = 1$ and is 55% (see table 6.1).

The last column of table 6.1 lists the Young's modulus of the PMO film and a value of approximately 2 GPa is obtained. The Young's modulus of the PMO film is similar compared to methylsilsequioxanes and PMO films at a similar porosity.^{12, 13} However, further optimization of the mechanical stability is needed for low-k applications. The HMDS-treated RPMO films (HRPMO) have similar values and do not show a better mechanical stability as it was observed for the HMDS treated ring PMOs in powder form in chapter four.

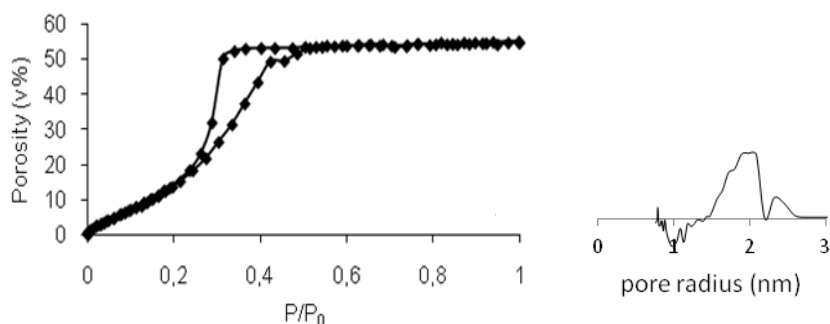


Figure 6.3: Toluene adsorption/desorption isotherm and pore radius distribution of the RPMO film.

The TEM image presented in figure 6.4 confirms the highly porous structure and a 'thick' pore wall of approximately 4 nm can be estimated.

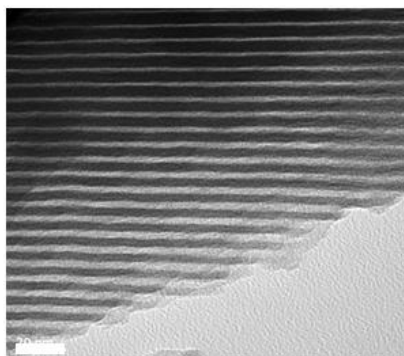


Figure 6.4: TEM image of the RPMO film. The length of the scale bar represents 20 nm.

Figure 6.5 shows accumulation capacitance (C) per unit area (F/cm^2) as a function of frequency (f) for the four dots of different diameter. The four C - f curves overlap within an error of less than 2% in the whole range of frequencies. As the error on the measured film thickness was lower than 1%, the accuracy on the extracted k -value is better than 3%. Besides, the C - f curves are flat. Therefore, the dielectric constant is stable with frequency as it is expected for hydrophobic low- k films in the explored frequency range.

Based on the measured capacitance and thickness, a k -value of 1.8 was extracted for the investigated RPMO film from 100 Hz to 100 kHz. This makes these PMO films very attractive for the next generation low- k materials. In literature, k -values are often estimated only at 1 MHz, using a single capacitor size. For the capacitor structures that are typically used for low- k characterization, the dissipation factor (D) rapidly increases above 100 kHz to become greater than 0.1 at 1 MHz. This typically results in a gradual decrease of the measured capacitance with frequency above 100 kHz, which only relates to the non optimal conditions ($D > 0.1$) in which the impedance analyzer has to operate for extracting the reactance ($1/2\pi fC$) from the measured impedance. The k -value of the HMDS-treated film was found to be 1.93 which is also higher than without the HMDS treatment. The means that an extra HMDS treatment is not beneficial when the film is already hydrophobic

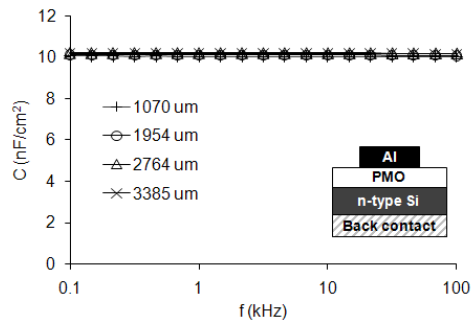


Figure 6.5: Measured accumulation capacitance per unit area as a function of frequency for the four dots of different diameters.

Besides an ultra low k -value a high chemical stability is also important because the microelectronic industry uses several chemicals during the manufacturing of microelectronic devices. It is also known that the siloxane bonds of silicates hydrolyze rather easily in alkaline solutions,¹⁴ although the stability increases when thicker pore walls are obtained.¹⁵⁻¹⁷

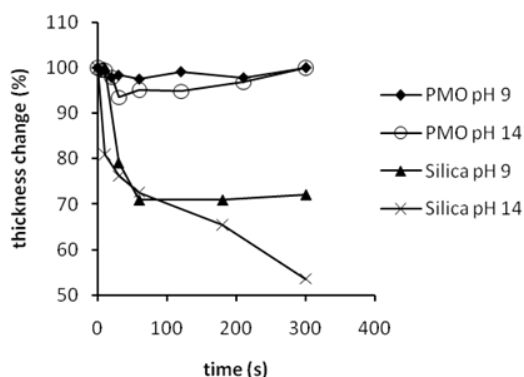


Figure 6.6: Thickness change of RPMO and mesoporous silica films after immersion in alkaline solutions with pH 9 and 14.

Further, we already showed that cyclic carbon-bridged PMOs have good chemical stabilities in powder form.¹⁰ Therefore, to investigate if the incorporation of Si-C bonds can protect the hydrolysis of the RPMO thin films, the films were immersed in two alkaline solutions with pH 9 and 14 respectively and the change in thickness was measured in function of time. This test was also performed on mesoporous silica films with similar thickness and porosity. The results are shown in figure 6.6. It can be seen that the decrease in thickness is not significant for the RPMO film even after immersion in a solution with pH 14, showing a very high resistance against alkaline solutions. On the other hand the mesoporous silica film degrades first fast and then it remains constant in mild alkaline conditions (pH 9).

In high alkaline medium (pH 14) this fast degradation is also observed during the first 30 s and this is followed by a slower and gradual degradation in function of time. So the RPMO films have a better resistance compared to the porous silica film. This can be explained by the hydrophobic methyl groups on the surface which reduces the contact of the siloxane bonds with the alkaline solution and/or by the incorporated organic bridges which are less sensitive for hydrolysis (Si-C versus Si-O).

To further investigate the impact of the organic groups and also the role of the surfactant on the chemical stability, we compared the stability of the hydrophobic Brij-templated PMO films (RPMO-Brij) with PMO films prepared with CTAC (RPMO-CTAC) and PMO films without the hydrophobization treatment (RPMO-Brij-H₂O). To obtain the latter film, the porogen was removed at 300°C which is below the self-hydrophobization temperature.² The RPMO films were immersed for 5 minutes in a 1 M NaOH solution and a 50 v% 1 M NaOH/ethanol mixture respectively. The ethanol in the mixture allows an easier diffusion of the base into the pores. After the immersion

Chapter 6: Ultra low-k cyclic carbon-bridged PMO films with a high chemical resistance

the samples were rinsed with H₂O and dried for 2 hours at 150°C and the change in thickness, porosity and water contact angle was determined.

Table 6.2: Physical properties of PMO films before and after alkaline solution treatment.

	RPMO-Brij	RPMO-CTAC	RPMO-Brij-H ₂ O
Thickness (nm)	157	174	181
Porosity (v%)	55	52	52
Water contact angle	92	92	70
Pore size (nm) ^a	4	2.1	4.2
<u>After NaOH immersion</u>			
Thickness (nm)	157	160	180
Porosity (%)	55	52	52
Contact angle (°)	50	50	37
<u>After NaOH/EtOH immersion</u>			
Thickness (nm)	149	122	176
Porosity (%)	55	52	52
Contact angle (°)	72	72	33

The results of the RPMOs before and after immersion are shown in table 6.2. As seen from the table, we tried to keep the difference in film thickness and porosity as small as possible. Further, it can be clearly seen that the pore size of RPMO-CTAC is smaller compared to the RPMO prepared with Brij and that the water contact angle of RPMO-Brij-H₂O is much lower and thus more hydrophilic compared to the high temperature treated PMO films. When first looking at RPMO-Brij treated with the NaOH solution no change in porosity and thickness is observed, showing a high chemical resistance. However, the water contact angle decreases to 50° meaning that the surface is more hydrophilic. For RPMO-CTAC similar results are obtained for the porosity and water contact angle. However, there is a significant decrease in thickness meaning that a part of the film is etched away. When looking at RPMO-Brij-H₂O, there is no change in porosity and film thickness, but a very high decrease in water contact angle is observed.

After the treatment with the NaOH/ethanol solution, again no change in porosity is observed for the three PMO films. On the other hand, a decrease in thickness of 30% is observed for RPMO-CTAB while for the RPMO-Brij and RPMO-Brij-H₂O the decrease in thickness is only 5 and 3% respectively. The water contact angles for the hydrophobic PMO films decreases to 72° after the treatment while again the water contact angle drops drastically for the RPMO-Brij-H₂O. These results show that the RPMOs prepared with Brij-76 have a better chemical etch resistance compared to RPMOs prepared with CTAC. This also confirms that highly porous films with small pores collapse more easily as mentioned before. Besides the larger pore size, several papers reported that mesoporous organosilicas have thicker pore walls when Brij surfactants are used

Chapter 6: Ultra low-k cyclic carbon-bridged PMO films with a high chemical resistance

instead of cetyl trimethyl ammonium chloride and this will probably also attribute to a better chemical resistance.^{6, 10, 18}

Surprisingly, the more hydrophilic RPMO film shows also a very high etching stability although the water contact angle becomes very low. This means that the incorporation of carbon bridges plays a very important role to withstand chemical solution etching.

Furthermore, the films are more etched when utilizing a NaOH/ethanol solution. This is due to the fact that the etching solution can enter the pores of the hydrophobic material more easily and thus more damage is observed. Although, RPMO-Brij films seem to have a very high chemical resistance, the decrease in water contact angle suggests that some siloxanes bonds are hydrolyzed during the alkaline treatment.

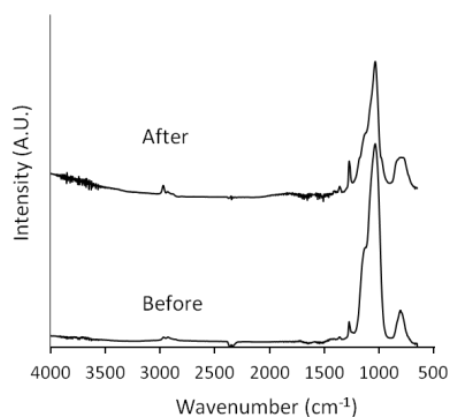


Figure 6.7: DRIFT spectrum of RPMO before and after immersion in 1 M NaOH solution.

To clarify this result, DRIFT measurements were performed on RPMO-Brij films before and after the treatment with the NaOH solution. When comparing the two spectra in figure 6.7, it can be clearly seen that the SiOSi peak at 1032 cm⁻¹ is less intense after the alkaline treatment proving the hydrolysis of some siloxane bonds. The DRIFT spectrum of the immersed film also shows a broad band in the region 3200-3600 cm⁻¹ which reveals that water molecules are adsorbed to the surface.

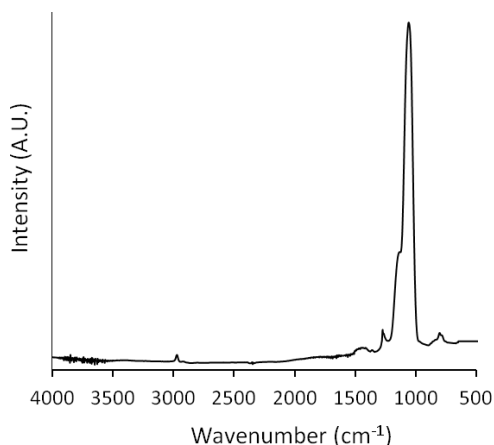


Figure 6.8: DRIFT spectrum of the NaOH treated RPMO-Brij film after annealing.

To have a more quantitative value and assuming that SiCH_3 bonds are almost no sensitive to hydrolysis, the SiOSi/SiCH_3 peak ratio is also calculated (respectively the intensity at 1032 and 1272 cm^{-1}). For the pristine RPMO a value of 8 is found while after the NaOH treatment the ratio has decreased to 3.67. As a conclusion the NaOH treatment with an exposure time of 5 minutes causes some hydrolysis of siloxane bonds making the film hydrophilic without affecting the porosity and thickness of the film.

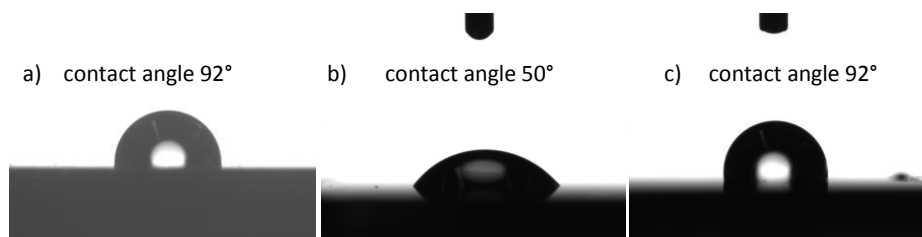


Figure 6.9: Water droplet images of a) the pristine PMO film, b) the dried PMO film after immersion in a pH 14 solution for 5 min. and c) the annealed PMO film after immersion.

However, a hydrophilic film is not suitable for low-k applications. Therefore, to attempt a full restoration of the hydrophobic property, the film was annealed at 400°C under N_2 atmosphere. The DRIFT spectrum of the annealed film (figure 6.8) does not show adsorbed moisture anymore. Furthermore, the SiOSi/SiCH_3 peak ratio (*i.e.* 7.78) has almost returned to its original value. This can be explained by a recondensation of the hydrolyzed siloxane bonds at elevated temperatures. Also the water contact angle after the annealing procedure has returned to its original high value (see figure 6.9)

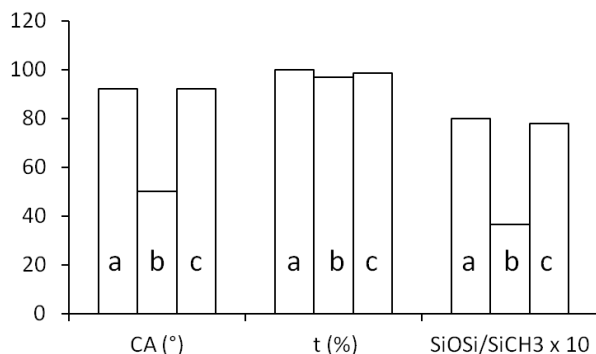


Figure 6.10: Water contact angles (CA), remaining thickness (t) and SiOSi/SiCH₃ ratio of a) the pristine PMO film, b) the dried PMO film after immersion in a pH 14 solution for 5 min. and c) the annealed PMO film after immersion.

Figure 6.10 summarizes the characteristics of the ring PMO films during the different treatment steps. The thickness of the films does not change after the alkaline and annealing treatment while the contact and condensation degree of the network can be restored after an annealing step.

These findings show that at short exposure times, the PMO film is very stable. Furthermore, it would also be interesting how the PMO film behaves at longer exposure time. Therefore, we also immersed the PMO film for 1 hour in the alkaline solution. After the immersion again no change in porosity was observed, but the measured thickness was only 75% of its original value. So this means that 25% is etched away. Since we observed that the other structural properties were not affected, this alkaline treatment can also be used to fine tune the thickness of PMO films when longer exposure times are used.

6.4 Conclusions

Hydrophobic cyclic carbon-bridged PMO thin films are successfully prepared by spin coating of 1,1,3,3,5,5-hexaethoxy-1,3,5-trisilacyclohexane mixed with surfactant Brij-76, water, hydrochloric acid and ethanol. This material shows very promising dielectric properties because an ultra low dielectric constant of 1.8 is obtained. However, further optimization of the Young's modulus is still necessary. In the case that the film is already hydrophobic, an extra HMDS treatment does not improve the low-k properties of the low-k film.

PMO films prepared with Brij-76 also have a very high resistance against alkaline solutions compared to mesoporous silica films and cyclic carbon-bridged PMO thin films prepared with CTAC, although some hydrolysis occurred. Finally, we showed that the hydrophobic property can be easily restored through recondensation of the silanol groups by an annealing step at 400°C under nitrogen atmosphere without affecting the thickness of the film.

6.5 References

1. W. Volksen, R. D. Miller and G. Dubois, *Chem Rev*, 2010, **110**, 56-110.
2. K. Landskron, B. D. Hatton, D. D. Perovic and G. A. Ozin, *Science*, 2003, **302**, 266-269.
3. S. B. Jung, C. K. Han and H. H. Park, *Appl Surf Sci*, 2005, **244**, 47-50.
4. I. Ciofi, M. R. Baklanov, Z. Tokei and G. P. Beyer, *Microelectron Eng*, 2010, **87**, 2391-2406.
5. Y. F. Lu, R. Ganguli, C. A. Drewien, M. T. Anderson, C. J. Brinker, W. L. Gong, Y. X. Guo, H. Soyez, B. Dunn, M. H. Huang and J. I. Zink, *Nature*, 1997, **389**, 364-368.
6. W. D. Wang, D. Grozea, S. Kohli, D. D. Perovic and G. A. Ozin, *Acs Nano*, 2011, **5**, 1267-1275.
7. M. R. Baklanov and K. P. Mogilnikov, *Opt Appl*, 2000, **30**, 491-496.
8. M. R. Baklanov, K. P. Mogilnikov, V. G. Polovinkin and F. N. Dultsev, *J Vac Sci Technol B*, 2000, **18**, 1385-1391.
9. K. Maex, M. R. Baklanov, D. Shamiryana, F. Iacopi, S. H. Brongersma and Z. S. Yanovitskaya, *J Appl Phys*, 2003, **93**, 8793-8841.
10. F. Goethals, B. Meeus, A. Verberckmoes, P. Van Der Voort and I. Van Driessche, *J Mater Chem*, 2010, **20**, 1709-1716.
11. A. R. Balkenende, F. K. de Theije and J. C. K. Kriege, *Adv Mater*, 2003, **15**, 139-+.
12. W. D. Wang, D. Grozea, A. Kim, D. D. Perovic and G. A. Ozin, *Adv Mater*, 2010, **22**, 99-+.
13. F. K. de Theije, A. R. Balkenende, M. A. Verheijen, M. R. Baklanov, K. P. Mogilnikov and Y. Furukawa, *J Phys Chem B*, 2003, **107**, 4280-4289.
14. S. A. Greenberg, *J Phys Chem-Us*, 1957, **61**, 960-965.
15. K. Cassiers, T. Linssen, M. Mathieu, M. Benjelloun, K. Schrijnemakers, P. Van Der Voort, P. Cool and E. F. Vansant, *Chem Mater*, 2002, **14**, 2317-2324.
16. W. P. Guo, X. Li and X. S. Zhao, *Micropor Mesopor Mater*, 2006, **93**, 285-293.
17. R. Mokaya, *J Phys Chem B*, 1999, **103**, 10204-10208.
18. M. C. Burleigh, M. A. Markowitz, S. Jayasundera, M. S. Spector, C. W. Thomas and B. P. Gaber, *J Phys Chem B*, 2003, **107**, 12628-12634.

Chapter Seven: Pore Sealing

In this chapter, the importance of pore sealing of porous low-k materials is explained and the state of the art pore sealing methods are discussed. As will be shown, all currently applied methods have some difficulties to seal mesoporous films. Therefore, two new pore sealing methods to close the pores or narrow the pore entrances of mesoporous materials are investigated in this work.

The first method we have explored is pore closing or pore narrowing of porous materials through grafting of a cyclic-bridged organosilane precursor. As porous material, MCM-41 powder was selected to allow an easy characterization of the grafting reactions. Firstly, it was shown that it is possible to graft on the MCM-41 with the organosilane precursor. Secondly, it is demonstrated that pore narrowing can be obtained without losing porosity by removing the porogen template after grafting. Further, the silanols left in the pores can then be end-capped with HMDS to prevent grafting inside the pores. Unfortunately a complete sealing by further grafting on the surface was not achieved. However, the narrowing of the pores can already be considered as a huge improvement.

The second method is a molecular self-assembling of cyclic organosilane precursors which allows the formation of intermediate fragments with molecular sizes exceeding pore sizes of 3 nm. Chemical solution deposition of these fragments on top of porous films therefore allows efficient sealing of mesoporous low-k materials. Moreover, a completely sealed and hydrophobic material is obtained by grafting the remaining hydroxyl groups of the organosilica top layer with trimethylsilyl groups through hexamethyldisilazane (HMDS) treatment. We also demonstrate that the partial sealing, realized after deposition of the organosilica layer without extra HMDS treatment, is already sufficient to prevent diffusion of metal ions of copper barrier layers which are deposited on top of low-k materials in actual device applications.

Further, the partial sealing method was applied on ethane PMO films and it was found that partial sealing leads to improved electrical and mechanical properties.

Part of the results of the “pore sealing through dense layer deposition” are published as a communication: F. Goethals, M. R. Baklanov, I. Ciofi, C. Detavernier, P. Van Der Voort and I. Van Driessche, *Chem. Commun.*, 2012, **48**, 2797-2799.

A patent of this method is filed with number: US 61/538,431

7.1 Introduction

In chapter one, it was mentioned that low- k materials must fulfill a lot of other requirements than a low dielectric constant. During integration processes, several problems can occur when using porous materials. Firstly, chemical products are used that can diffuse into the porous material. Further, metal ions from the wires can diffuse deeply in the pores and this can lead to short circuits.

In the case that the pores are very small or not interconnected this is not really a problem. However, as the dielectric constant approaches $k < 2.2$, pore sizes tend to increase and the pores are highly interconnected. Therefore, a pore sealing step is necessary. The procedure is graphically summarized in figure 7.1.

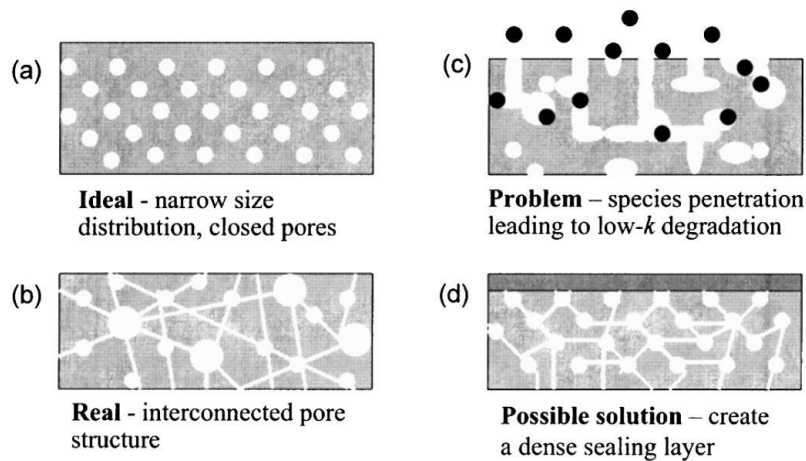


Figure 7.1: Schematic diagrams of porous low- k dielectric materials showing (a) ideal uniformly dispersed closed pores with a narrow size distribution, (b) interconnected pores with a random size distribution, (c) diffusion and penetration of species into a porous network, and (d) uniformly dispersed interconnected pores with a dense sealing layer.¹

To achieve this, two pathways are explored. These pathways are pore sealing by plasma treatment and pore sealing by deposition of a sealant. These methods will now be discussed in more detail.

7.1.1 Pore sealing by plasma treatment

The general principle of plasma sealing is that the low- k film is exposed to plasma which leads to densification of the film starting at the film/air interface. By optimizing the plasma power and exposure time, the thickness of the densified layer can be controlled. During this treatment, the cage structure of the silica matrix transforms to a more condensed network.² When only the surface is densified, the inside layer can

maintain its original k -value.³ However, the line between sealing and damaging the low- k film is very thin meaning that plasma treatments have to be performed very carefully.^{4,5}

Cui *et al.*⁶ investigated the impact of N_2/H_2 plasma on a PECVD porous SiCOH film with a pore size of 1.5 nm. After the treatment a dense layer is formed at the surface while the bulk of the film remained intact. However, the low- k film showed significant damage after the treatment, including thickness reduction, increase in k -value and leakage current. The reason for the bad electrical properties is that the film adsorbs moisture due to carbon depletion and silanol formation during the plasma exposure.

Aimadeddine *et al.*⁷ compared CO/O_2 and NH_3 plasma treatments. Pore sealing was only achieved with the NH_3 plasma. Furthermore, by applying the oxygen based plasma severe carbon depletion and a high increase in k -value were observed (from 2.4 to 3.5). On the other hand, there was a slight carbon depletion and only a 10% increase in k -value when NH_3 was used.

Puyrenier *et al.*⁸⁻¹⁰ also characterized the impact of several treatments (He , NH_3/N_2 , $C_4F_8/Ar/N_2$ followed by CO/O_2 and NH_3) on low- k films with a porosity of 25% and pore diameter of 2 nm. All the treatments lead to formation of a thin and dense layer at the surface. However, after He and NH_3/H_2 plasma treatments the film still exhibits an open porosity. On the other hand pore sealing was obtained for the other two plasma treatments. The dielectric constant increased not only due to the dense layer, but also due to a water-uptake effect especially for the applied NH_3/N_2 plasma.

After trying several plasma treatments Posseme *et al.*¹¹ came to the same conclusion that NH_3 plasma is the most efficient. They used spin-on OSG films with a porosity of 40% and a k -value of 2.2. Also here, the k -value increased after sealing. In contrast to the results of Puyrenier, the pores were also not completely sealed. Solvents could still diffuse into the pores. A possible explanation for this difference is that the porosity is higher in this case, which means that it is likely that the pore size will also be larger, making it more difficult to seal the pores.¹² Nevertheless, metallic diffusion could be prevented indicating that a complete pore sealing is not mandatory.

The relation between the pore size and sealing efficiency of porous OSG films by plasma treatment was investigated in more detail by Shoeb and Kushner.¹³ Figure 7.2 shows the influence of the pore radius on the sealing efficiency of the top surface and sidewalls of patterned low- k films.

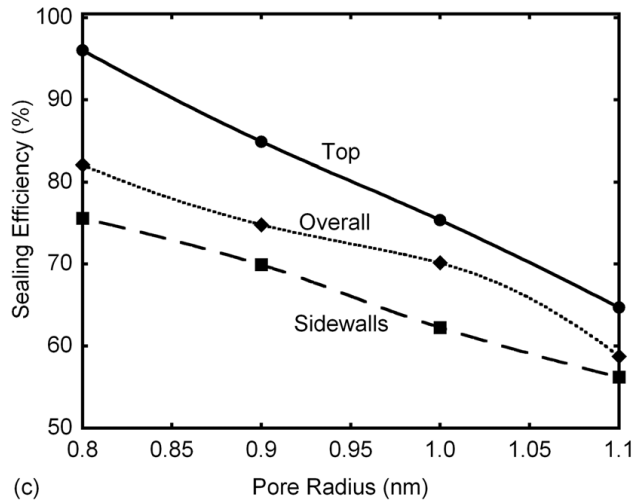


Figure 7.2: Sealing efficiency as a function from the pore radius.¹³

It can be seen that the pore sealing efficiency decreases with increasing pore sizes and that the side walls are not completely sealed. Therefore, plasma sealing is only useful for microporous films. Further, other drawbacks of plasma treatments are a reduced hydrophobic character of the film and possible film shrinkage.^{10, 14}

7.1.2 Sealant deposition

Another possible sealing method is the deposition of a non porous layer on the porous low-k film. As it was also observed with plasma sealing, pore sealing with this approach will be also more challenging when the pore size of the low-k material increases. This is due to the fact that larger pores can be filled with the sealing material. Possible sealing deposition methods are physical vapor deposition (PVD), chemical vapor deposition (CVD) or atomic layer deposition (ALD). When considering PVD, TaN is a common used Cu barrier.¹⁵⁻¹⁷ The barrier is needed to prevent copper diffusion into the porous low-k material. Iacopy *et al.*¹⁵ deposited TaN layers on porous films with different surface roughness, pore size, porosity and chemical composition to investigate which factors affect an efficient sealing. It was found that thicker TaN layers are required to seal mesoporous films, but also that a higher carbon concentration of the low-k film leads to faster sealing.

Besides TaN barriers also TiN barriers can be utilized.^{18, 19} However, the barrier layer has to scale down with the technology node to maintain or improve the electrical properties. This means that PVD is not applicable due to the poor step coverage when the line width shrinks. Furthermore, due to the shrinkage, the dielectric constant of the

barrier/sealant should be also as low as possible otherwise the effective k -value (*i.e.* low- k material + barrier) will be too high.²⁰

The most obvious alternative is sealing by CVD. Wang *et al.*²¹ compared SiC, SiCO and SiCN barriers. The starting precursors for the SiCO film were tetramethyl silane and CO₂ gas. SiC films were obtained from trimethylsilane (3MS) and for SiCN films, 3MS was combined with NH₃. The three films have k -values around 4.3, but the high leakage and low breakdown of the SiC film indicates a bad insulating property. The other two have shown good barrier properties. However, the sealing efficiency was not investigated.

Yang *et al.*²² compared TaN and SiCN as Cu barriers on porous polymers. The results revealed a strong intermixing at the two interfaces of the Cu/TaN/low- k structure but no metal diffusion is observed when SiCN is used. By further optimization of the composition of the SiCN film better mechanical and electrical properties can be achieved.²³

Bonitz *et al.*²⁴ deposited thin CVD TiN layers on porous low- k materials with pore sizes of 3 and 7 nm and investigated the TiN diffusion. On some samples also a pre-sealing with SiO₂ was performed. They found that smaller pore sizes facilitate the pre-sealing and TiN barrier growth. Also no TiN diffusion was observed when the porous materials were pre-sealed in contrast to the non pre-sealed samples where TiN diffusion was visible. However, the effect of the pre-sealing on the dielectric constant of the porous film was not mentioned.

Joussemau *et al.*²⁵ investigated SiC and SiO₂ pore sealing liners, deposited by CVD to prevent TiN diffusion in porous materials. Both liners have a k -value around 4.4 while the value of the low- k material was 2.2. After the deposition of a 5 nm thick SiO₂ layer the k -value increased to 2.3 for a low- k material with a thickness of 300 nm. On the other hand, after a 5 nm thick SiC liner the k -value only increased to 2.25. However, it was observed that a 5 nm thickness was not sufficient to completely prevent TiN diffusion and the minimum thickness to prevent TiN diffusion into the porous material was found to be 7.5 nm.

Besides inorganic sealing materials also organic polymers were investigated as sealant materials.^{26, 27} The advantage of organic films is that the dielectric constant is relatively low and thus little diffusion of the organic sealant will not dramatically influence the effective dielectric constant. It is reported that efficient sealing can be obtained however similar as for the organic low- k materials, the rather low thermal stability and adhesion properties make the use of organic barriers questionable.

Another CVD based sealing approach was reported by Liu *et al.*²⁸ They first tried to block the pores through grafting with organosilanes. However they observed that it

was not sufficient to prevent moisture penetration. Therefore, they used other alkylsilsesquioxanes which could bridge the pore openings by cross linking among themselves (see figure 7.3). Pore sealing has been achieved with a sealant thickness less than 10 nm. However, there was no evidence provided that these sealant molecules did not enter the pores.

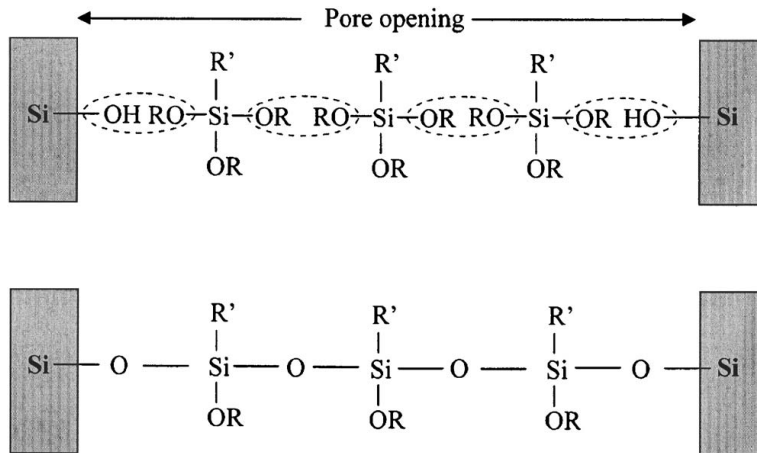


Figure 7.3: Pore sealing with organosilicate sealant.²⁸

The shrinking of the devices means that the sealant layers have to be uniform and conform almost at the atomic level. Therefore ALD could be a suitable sealing deposition method. The concept of ALD is that a precursor molecule can react with a surface forming only a non-reactive atomic monolayer on the surface. This monolayer can then be activated and react with the precursor molecules forming a second layer. By repeating this cycle, a uniform layer with a precise thickness can be made. To be successful as sealant deposition method, two requirements are important. The first one is that the low-k material has reactive groups on the surface and secondly, the precursor molecules should not penetrate into the porous material. It is obvious that the latter will be more difficult when the pore size of the low-k material increases.

Travaly *et al.*²⁹ investigated the diffusion of typical metal ALD precursors, TaN and WNC, inside porous dielectric films and how surface treatments can be used to prevent ALD coatings inside the pores. They came to the conclusion that ALD diffusion depends on the substrate as well as on the size and shape of the precursors. Further, most typical ALD precursors will enter circular pores with a diameter larger than 1.3 nm. This means that surface engineering of the low-k material is necessary. For microporous materials this is possible by plasma treatment already mentioned in section 7.1.1, while for mesoporous materials an additive sealing approach must be performed.

To overcome the diffusion problem, de Rouffignac *et al.*³⁰ first deposited an alumina catalyst on the pore opening of mesoporous low-k materials. This was also done by ALD, but the exposure time was very short to avoid diffusion of the catalyst. Secondly, 4 nm of ALD SiO₂, which grows on the alumina surface, was deposited to close the pores. Afterwards WN was deposited to test the sealing efficiency and no diffusion was observed. Although, this approach seems effective, the precise reaction conditions to limit the diffusion of the alumina catalyst makes it difficult to apply this method.

Another possible method is applying plasma assisted ALD.³¹ In this case ALD occurs in a plasma environment which activates the precursor molecules. Because the molecule mean free path in a typical plasma exceeds the pore dimensions of a low-k material, the plasma will not have access to the internal porosity. On the other hand, plasma can damage the low-k material especially when it is mesoporous and this approach also requires very controlled and precise synthesis conditions.

7.1.3 New strategies

The described sealing methods have proven to be efficient to seal pores with pore sizes smaller than 2 nanometer or using sealing materials with high dielectric constants ($k > 4$). However, advanced nanoelectronics are presently developing materials and processes for 22 nm technology nodes and beyond. In this case the dielectric constant of the interlayer dielectrics must be smaller than 2.0. Such ultra low-k materials generally have a porosity exceeding 50% and a pore size of 3 nm or more.³² Here, all existing sealing technologies are no longer efficient.

Therefore, new strategies to seal pores larger than 3 nm have to be developed. Kruk *et al.*³³ reported on another method the closing of spherical mesopores by a thermal treatment. However, this was only tested on powders and not on thin films. Also to accomplish this, high temperatures and oxygen were needed and this makes it not possible to transfer this to organosilicas without losing the organic function.

Therefore, two new pore sealing methods are developed and evaluated for their pore sealing efficiency. The first one is sequentially grafting with a substituted cyclic organosilane precursor, **2**, because it has a more flexible side chain which should be easier for chemical reactions. This is a kind of ALD process, where we tried to prevent deposition in the pores. Firstly, it is shown that the grafting on the porous film is successful and it is presented that it is possible to perform several grafting reactions. In a second step, it is investigated if grafting before surfactant removal can prevent diffusion of the precursor molecules. As a proof of concept, the experiments were performed on MCM-41 powders. MCM-41 powders consist of a pure silica matrix

making it easier to monitor the different graftings with organosilanes. Finally, the method was applied on thin organosilica films.

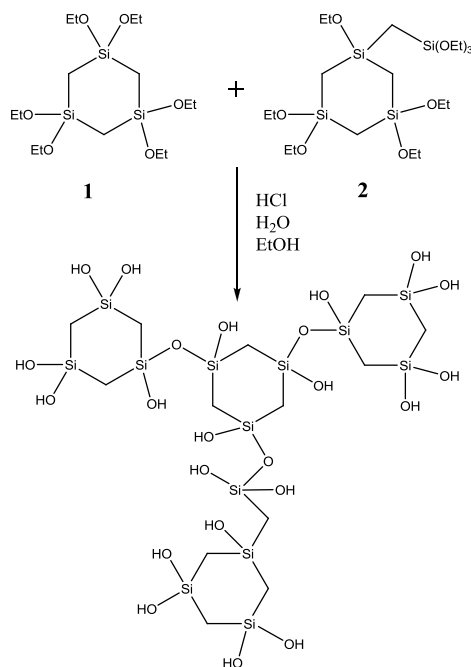


Figure 7.4: Scheme of oligomer formation of cyclic carbon-bridged organosilane precursors.

The second method is the deposition of a precondensed organosilica layer by spin-coating. This method involves the molecular self-assembling of cyclic carbon-bridged organosilane precursors which allows the formation of intermediate fragments with molecular sizes exceeding pore sizes of 3 nm (figure 7.4). Spin-coating of these fragments on top of porous films therefore allows efficient sealing of mesoporous low- k materials. Moreover, the sealing layers can be further hydrophobized by grafting the remaining hydroxyl groups with trimethylsilyl groups through hexamethyl disilazane (HMDS) treatment.

A huge advantage of the developed sealant layer is the intrinsic low k -value (≈ 3.5) owing to the high amount of low polarisable organic groups. As already known, these organosilicas are promising low- k materials by themselves when the film contains pores.³⁴ These materials are thus also more favorable for applications as interlayer insulation instead of the traditional SiCN with k equal to 4-4.5.²¹

To accomplish this, the time needed to form sufficiently large molecules to prevent diffusion is first determined. Secondly, the impact on the total porosity and hydrophobicity of mesoporous silica films is investigated. Finally, we applied our

method to etch PMO films to evaluate the change in electrical and mechanical properties.

7.2 Experimental section for sealing through grafting

7.2.1 Chemicals

Chloromethyltriethoxysilane, 1,2-bis(triethoxysilyl)ethane (BTESA), TEOS and HMDS were purchased from ABCR, hydrochloric acid (HCl, 37 %), tetrahydrofuran (THF), pentane and absolute ethanol were obtained from Fiers, and CTAC (25%) and CTAB were purchased from Aldrich. All materials were used as received.

7.2.2 Synthesis

Preparation of the substituted cyclic carbon-bridged organosilane precursor

A solution of 70 ml 0.5 w% FeCl_3 in dry THF was added to 7 g Mg turnings and stirred until a grey colored mixture was visible. This mixture was kept under an inert atmosphere. Then, a solution of 100 ml 14.2 v% chloromethyltriethoxysilane in dry THF was rapidly added to the mixture and stirred for 48 h at 50°C. The mixture was filtered off and the solvent was removed from the filtrate. Pentane was added to the residue and this mixture was also filtered. The remaining oil consists of cyclic carbon-bridged organosilanes as shown in figure 7.3. The substituted cyclic silane precursor was separated by distillation of the non-substituted cyclic precursor. The remaining oil consists then almost completely of the substituted cyclic precursor. This was confirmed by an in depth NMR study which is provided as supplementary information after the conclusion section. A schematic synthesis procedure for this precursor is given in figure 7.5

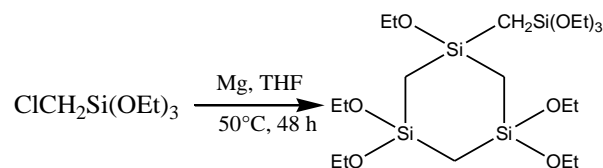


Figure 7.5: Synthesis of substituted tri-silacyclohexane.

Synthesis of MCM-41

The synthesis of MCM-41 was based on the method of Mortera *et al.*³⁵ CTAB, H_2O , EtOH and NH_4OH were mixed and stirred for 1 hour at room temperature. Next, TEOS was added and the mixture was 1 hour left for reaction. The total molar composition was: TEOS: 1; CTAB: 0.3; H_2O : 144; EtOH: 58; NH_4OH : 8. The precipitated powder was filtered and washed with water. The obtained powder was then separated in two parts.

From one part the surfactant was removed by calcinations at 550°C, while for the other part the surfactant was left inside.

Synthesis of organosilica films

3.2 g 25 w% CTAC was dissolved in 10 ml ethanol and 0.7 ml (1M) HCl. Then 1 ml of BTESA was added to the solution and this was aged for 1 day. The solution was then spin-coated on a Si wafer at a rate of 5000 rpm. The porogen was removed by treating the film at 400°C for 5 hours.

Grafting on MCM-41

To attach the cyclic organosilane precursor on MCM-41, 0.3 g of MCM material with or without surfactant was first dried under vacuum at 150°C. Then, 0.9 ml of the organosilane precursor was added and refluxed for 5 hours to allow reaction of the molecule with the MCM powder. The powder without surfactant was filtered and the excess amount of unreacted precursor was removed by Soxhlet extraction with pentane. For the powders with surfactant, only filtration and washing with acetone was performed to prevent removal of the surfactant.

After a first grafting the material was treated with a 0.01 M HCl solution to substitute the ethoxy groups by silanol groups to activate the surface again with the precursor molecules. By repeating this procedure several graftings can be performed.

Grafting on the organosilica films

The films were dried overnight at 90°C under vacuum. Next, an argon flow was applied and the precursor was added. The temperature was elevated to 130°C and the system was again put under vacuum to bring the precursor in the gas phase. The precursor was allowed to react for 3 hours. Afterwards, the films were rinsed with pentane and the surfactant was thermally removed at 400°C under nitrogen. Finally, the films were immersed for 3 hours in pentane containing HMDS to allow reaction with the HMDS molecules and afterwards dried at 150°C for 2 hours.

7.2.3 Characterization

N₂ sorption isotherms were measured on a Belsorp-Mini II apparatus at 77K. The data of the adsorption branch were used to calculate the pore diameter using the BJH method.

Diffuse reflectance infra-red Fourier transform (DRIFT) spectra were obtained on a Thermo 6700 FLEX FTIR/FT-Raman system, equipped with a nitrogen cooled MCT-A detector.

The open and total porosity of the films were determined with ellipsometric porosimetry using the same setup as described in chapter 6.

Water contact angles values were obtained by using a Krüss-DSA 30 Drop Shape Analysis System using the tangent 1 model.

1D and 2D ^1H and ^{13}C NMR spectra were recorded on a Bruker Avance 300 MHz spectrometer. Chemical shift values (δ) are given in parts per million (ppm) and are referenced to the residual CDCl_3 .

7.3 Results and discussion for sealing through grafting

7.3.2 Grafting on MCM-41 without presence of surfactant

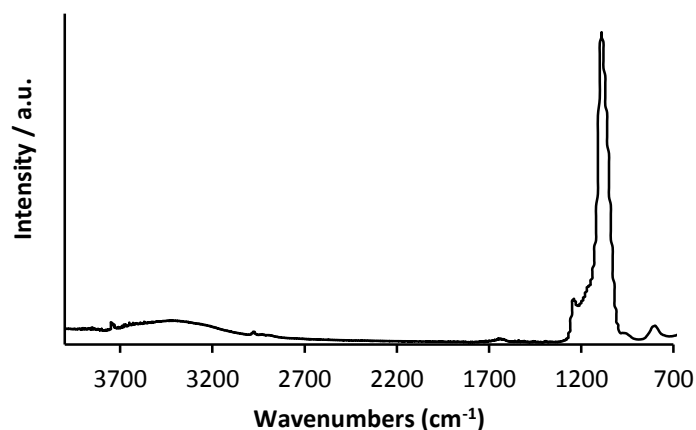


Figure 7.6: DRIFT spectrum of MCM-41.

Before a grafting was applied on the MCM-41 powder, the material was characterized with DRIFT spectroscopy and N_2 sorption. The DRIFT spectrum in figure 7.6 shows a typical spectrum for MCM materials. At 1150 cm^{-1} the Si-O-Si peak is clearly visible and the peak at 3750 cm^{-1} can be assigned to the free silanol groups.

The N_2 sorption isotherm is presented in figure 7.7 and shows a typical type IV isotherm. The pore volume is 0.83 ml/g and the average pore diameter is 2.2 nm .

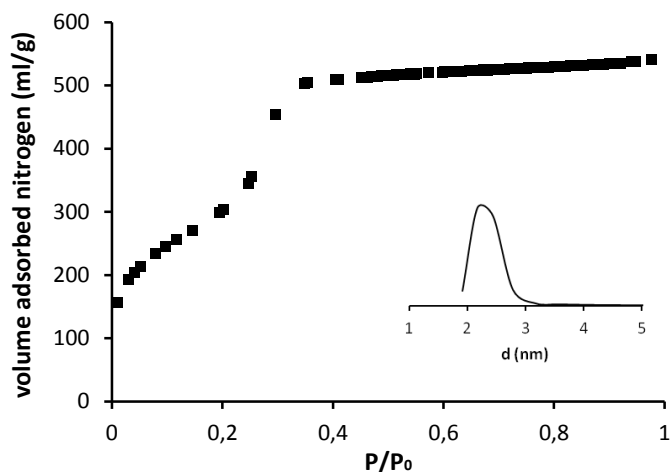
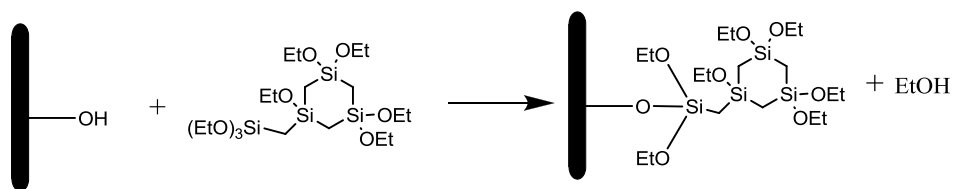


Figure 7.7: Nitrogen sorption isotherm and pore size distribution of MCM-41.

On this material, a first grafting is performed, according to the reaction given below:



The silanols of the MCM material react with the Si centers of the silane precursor and ethanol is released. After the grafting reaction, the material was rinsed several times with pentane and dried at 400°C under nitrogen to remove remaining precursor molecules.

Proof for this reaction is given by the DRIFT spectrum shown in figure 7.8. The peak of the free silanols disappeared and C-H stretch vibrations of the organosilanes are clearly visible around 2970 cm⁻¹ as well as C-H bend vibrations around 1400 cm⁻¹.

Due to the removal of a large amount of silanol groups by these silane molecules, the material is more hydrophobic. This was observed by pouring the grafted powder in water. The grafted powder floated on the water surface while on the other hand pure (hydrophilic) MCM powder immediately sinks to the bottom.

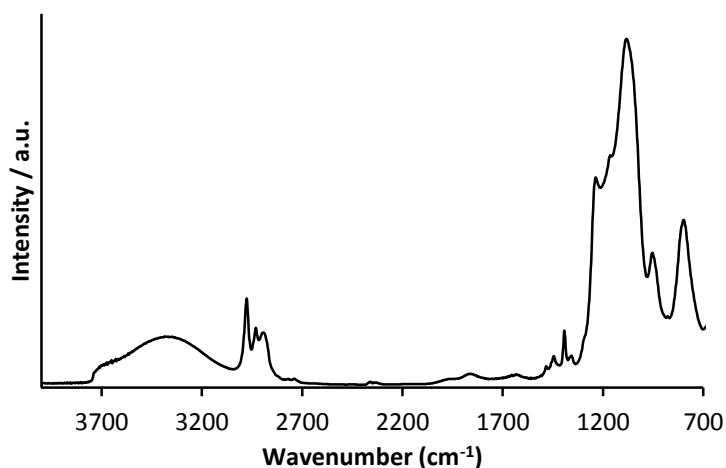


Figure 7.8: DRIFT spectrum of MCM-41 after grafting with the cyclic organosilane precursor.

The nitrogen adsorption isotherm of the grafted powder gives a type I isotherm revealing that the material is microporous instead of mesoporous (figure 7.9). The pore volume has decreased to 0.30 ml/g. These results also indicate that bulky molecules are grafted on the silica surface.

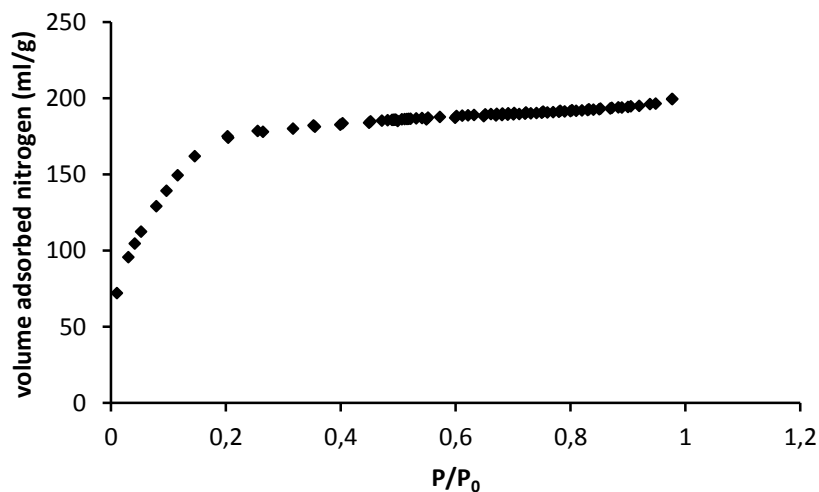
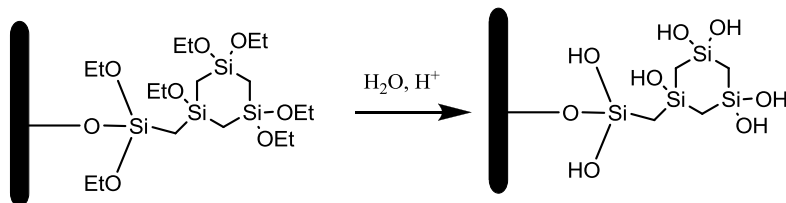


Figure 7.9: Nitrogen adsorption isotherm of grafted MCM-41.

To allow further reaction on the grafted material, the powder was stirred in an acidic solution (pH ~2.3). During this stirring, the powder slowly sinks to the bottom indicating hydrolysis of the material according to the reaction given below:



The infrared spectrum in figure 7.10 shows a very large silanol peak around 3700 cm^{-1} proving the hydrolysis reaction. Further the characteristic peaks representing CH vibrations are still present meaning that there is no leaching of the grafted precursor after stirring in the acidic solution. However the intensity of these peaks is much lower than before, which can be explained by the substitution of ethoxy groups by OH groups.

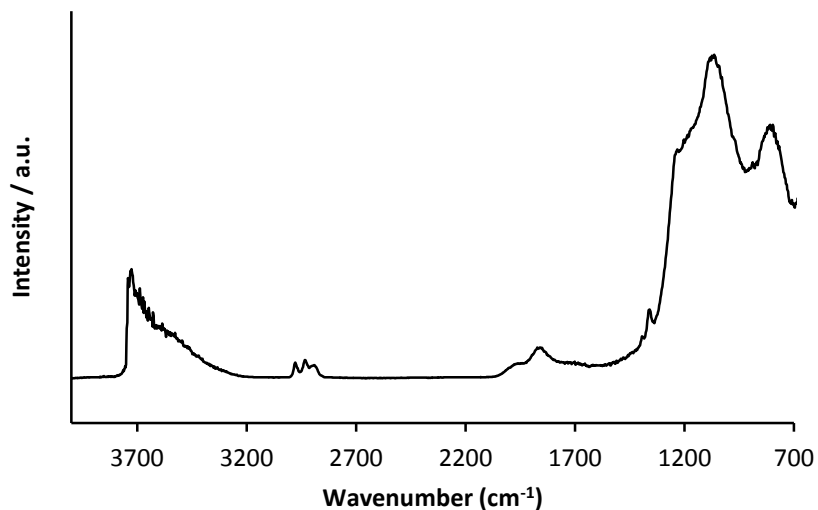


Figure 7.10: DRIFT of MCM after grafting and hydrolysis.

The resulting isotherm (figure 7.11) can be described between a type IV and type I indicating that the pore size is slightly larger after the hydrolysis which is logic because hydroxide groups are less voluminous compared to ethoxy groups. This is also reflected by the higher pore volume (0.52 ml/g).

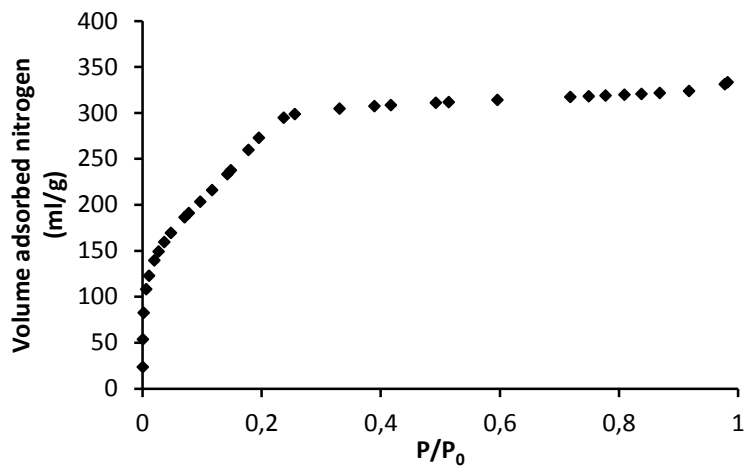


Figure 7.11: Nitrogen adsorption isotherm of grafted MCM-41 after hydrolysis.

By repeating this procedure, grafting and hydrolysis, several graftings cycles can be performed. Figure 7.12 summarizes the nitrogen adsorption isotherms from 0 to 3 grafting cycles.

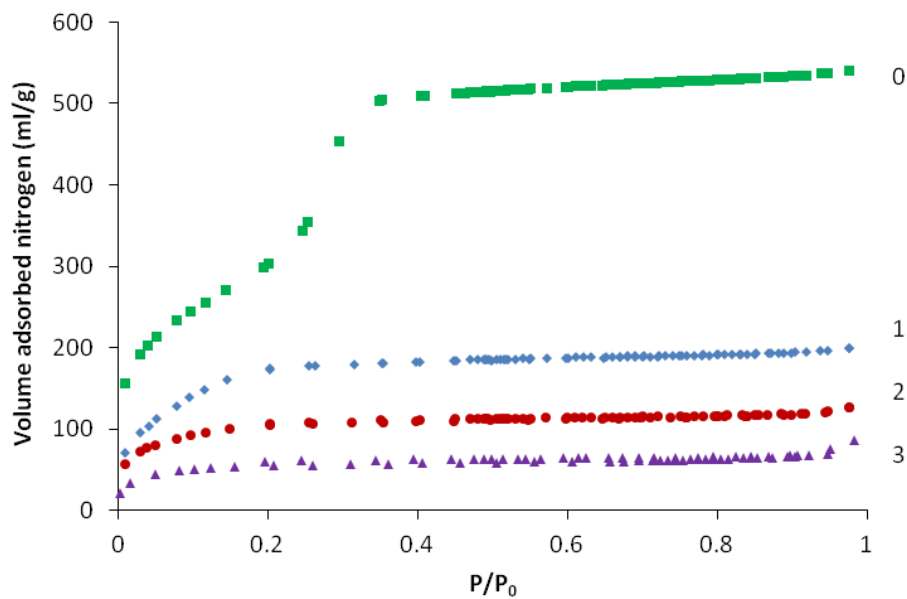


Figure 7.12: Nitrogen sorption isotherms of MCM-41 after 0, 1, 2 and 3 grafting cycles.

It can be seen that after the first grafting the highest decrease in pore volume is obtained. This is because the precursor molecules can easily diffuse into the porous

system and react with the inner silanol groups. After the second grafting there is again a decrease in pore volume but the difference is lower. Probably two phenomena are responsible for this. The first one is that the precursors are already sterically hindered to go deeply into the porous system. Secondly, grafting on a porous material means that the total weight increases and this also results in a lower pore volume per g material. After the third grafting, the decrease in pore volume is mainly attributed to the increase in weight by grafting on the surface. This indicates that the precursor molecules can not enter the pores anymore. However, nitrogen can still enter at least a part of the pores. On the other hand nitrogen molecules are really small in size and it is already shown that a complete sealing is not necessary to prevent barrier diffusion.¹¹

As a summary, these results show that it is possible to graft on mesoporous materials thereby reducing the pore size. However, the molecules can diffuse quite easily in the porous system, resulting in a high decrease in pore volume. Therefore, it should be prohibited that grafting takes place in the inner pore system.

7.3.3 Grafting on MCM-41 where the surfactant was initially left inside

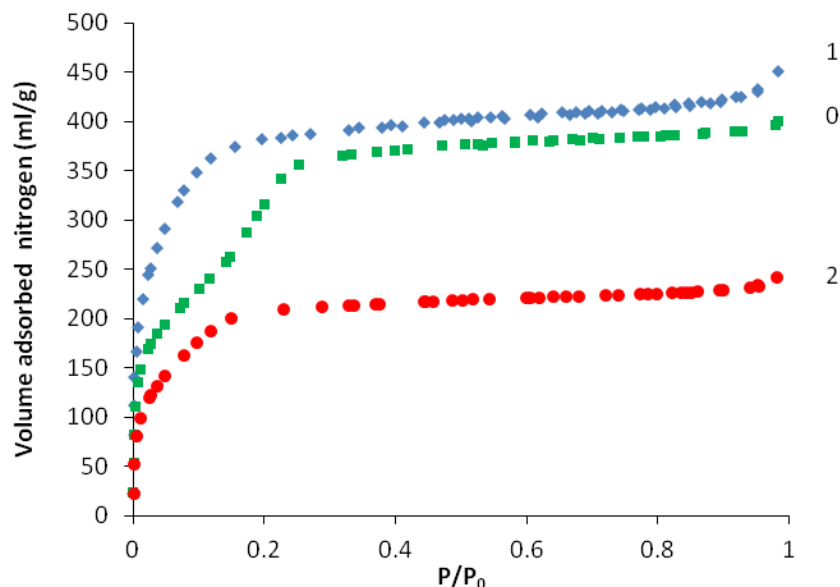


Figure 7.13: Nitrogen sorption isotherms after 0, 1 and 2 grafting cycles whereby grafting 1 was performed before surfactant removal.

To avoid precursor diffusion, the grafting reaction was performed on MCM-41 powders where the pores were still filled with the surfactant. After the grafting, the surfactant was thermally removed (at 400°C) and nitrogen adsorption measurements were

performed. Further, because the surfactant still has to be removed out of the pores, it will leave behind an open porous structure. Therefore, also a second grafting cycle was performed to investigate if pore sealing can be obtained. The results are presented in figure 7.13.

When comparing the isotherms after 1 grafting cycle and no grafting, it can be seen that the total pore volume is similar within the experimental error (0.66 ml/g and 0.62 ml/g respectively), showing that a high porosity is maintained. Furthermore, the type I isotherm reveals that after grafting micropores are obtained which is beneficial for low- k application and could already prevent barrier metal penetration. However, after the second grafting, the pore volume decreased to 0.4 ml/g. This means that the precursor can still diffuse and react with the inner silanol groups.

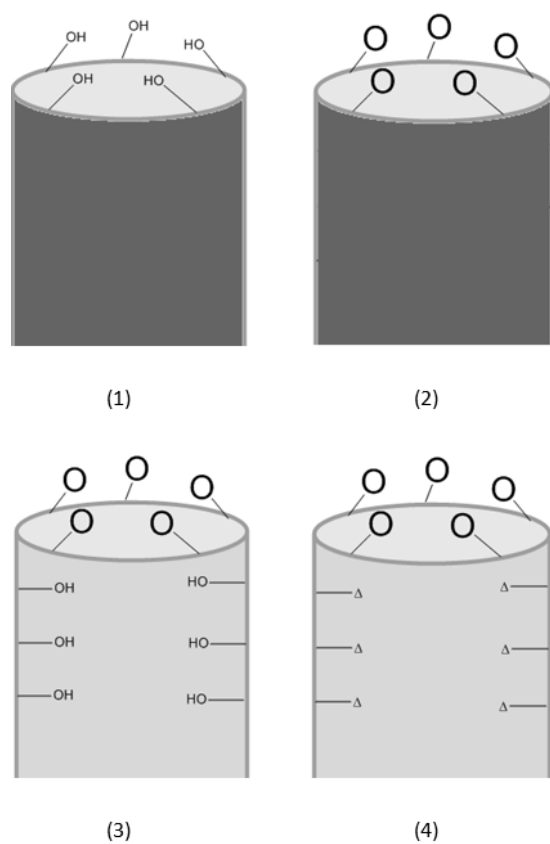


Figure 7.14: Schematic overview to graft the inner silanols by HMDS. The dark colored cylinder represents the MCM-41 with surfactant; the symbol $-O$, the grafted cyclic silane precursors; and Δ , the $-O-Si-(CH_3)_3$ functional groups.

To avoid this reaction with the inner silanol groups, the MCM-41 powder was grafted with the surfactant left inside. Next, the surfactant was thermally removed at 400°C under nitrogen and a HMDS treatment was performed. Because the outer silanols are already grafted, HMDS will only end-cap the silanols inside the pores and also make the pores hydrophobic. A schematic illustration is presented in figure 7.14.

The DRIFT spectrum gives evidence that the free silanol groups are end-capped with trimethyl silyl groups (figure 7.15). Before the HMDS treatment, the DRIFT spectrum shows CH vibrations peaks around 2950 cm^{-1} related to the grafted cyclic organosilane precursor and OH vibrations from the MCM-41 powder. After the HMDS treatment the silanol peak disappears and the peak at 2960 cm^{-1} increases due to the extra CH_3 groups. There are also no typical water absorption peaks present, confirming that the material is hydrophobic.

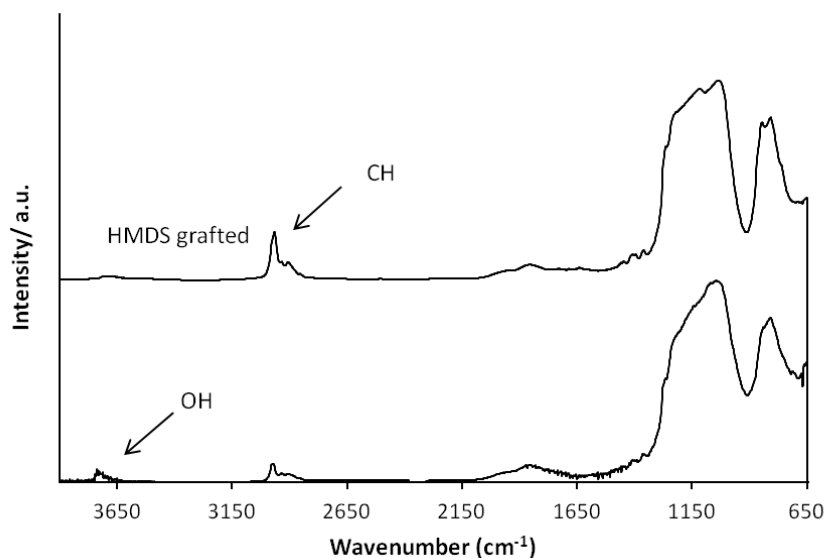


Figure 7.15: DRIFT spectrum of functionalized MCM-41 before and after HMDS treatment.

To attempt a complete pore sealing, a second grafting cycle was performed on the HMDS treated material. Now, reactions only take place outside the pores and on the pore entrances. The resulting isotherms are given in figure 7.16.

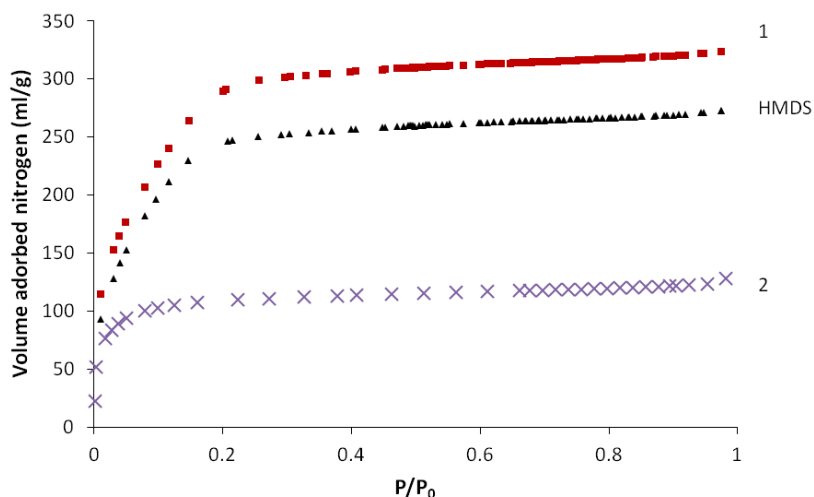


Figure 7.16: Nitrogen adsorption isotherms of MCM-41 after 1 grafting cycle, MCM-41 after 1 grafting cycle and HMDS treatment and after 2 graftings with a HMDS treatment in between.

After the HMDS treatment, there is a slight decrease in pore volume due to the substitution of OH groups by $\text{OSi}(\text{CH}_3)_3$ groups. Unfortunately, the pore volume after the second grafting was still 0.2 ml/g and thus no complete sealing is obtained. A possible explanation for this is that after the grafting not all the entrances are well blocked for the small nitrogen atoms and that the addition of high molecular weight molecules increases the weight to volume ratio and thus also decreases the pore volume per g.

Although the pore sealing is not complete, the grafting before template removal to only narrow the pore entrances, followed by hydrophobization of the pores has some interesting features to apply on low- k materials to improve their characteristics.

Therefore, this method with HMDS end-capping was applied on porous thin organosilica films. The resulting toluene adsorption isotherms before and after the grafting are presented in figure 7.17. It can be seen that after the grafting, the adsorption takes place at lower pressures indicating that the pores are indeed narrower. Further, the total porosity is slightly higher after the grafting. This can be explained by the fact that the material is hydrophobic after the grafting preventing water adsorption which is the case for the pristine film.

This is also confirmed by the higher water contact angle which is 80° after the grafting and 65° for the pristine film.

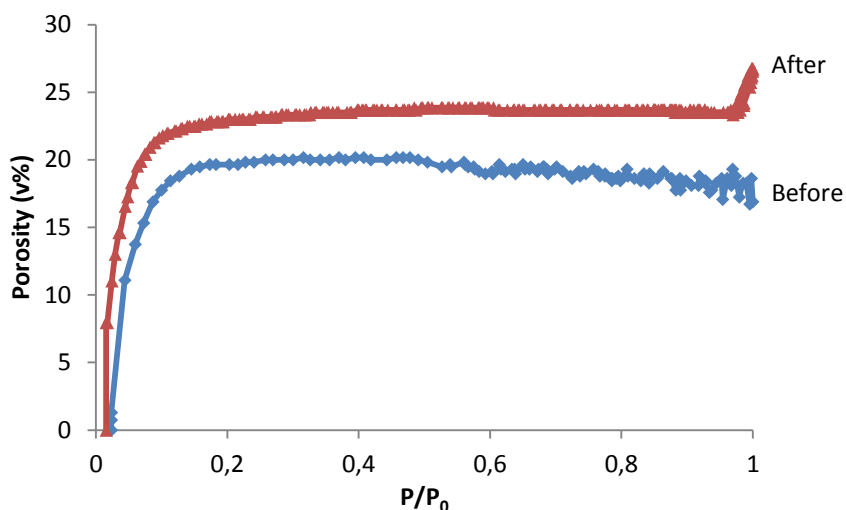


Figure 7.17: Toluene adsorption isotherms before and after grafting followed with HMDS treatment.

7.4 Conclusions for sealing through grafting

It is shown that it is possible to graft several cycles of cyclic bridged organosilane precursors on mesoporous silicas thereby narrowing the pore sizes. While keeping the surfactant inside the material during the grafting, only the silanols at the outer surface and pore entrances are end-capped. With this approach, pore narrowing can be obtained without decreasing the total porosity the material.

The silanols inside the pores can be grafted with HMDS, making them unreactive and hydrophobic. Unfortunately, by further grafting on the cyclic bridged organosilane molecules, it is not possible to completely seal the pores for nitrogen. However, the narrowing of the pores can already be considered as a huge improvement which was already reported in section 7.1.1.

Transferring this method to thin films showed that it is also possible to narrow the pore size without decreasing the total porosity. Furthermore, the film is more hydrophobic after the grafting with the cyclic carbon-bridged organosilane precursors.

7.5 Supporting information: NMR study of the substituted cyclic organosilane precursor

The substituted tri-silacyclohexane mixture is studied with 1D ^1H (figure 7.18) and ^{13}C NMR (figure 7.19) spectra complemented with 2D experiments such as homonuclear $^1\text{H}\{-^1\text{H}\}$ COSY and heteronuclear $^1\text{H}\{-^{13}\text{C}\}$ HSQC and HMBC experiments. In figure 7.18 the ^1H resonances at 1.20 ppm and at 3.8 ppm are clearly visible. Based upon their multiplicity, signal integrations and COSY correlations, these resonances can be attributed to the $-\text{CH}_2-$ and $-\text{CH}_3$ moieties of the ethoxy functionality. Using HSQC and HMBC experiments additional to the ^{13}C spectrum, the carbon atoms can be assigned.

Furthermore a set of broad resonances in the region of 0.3 to -0.01 is observed in the 1D ^1H spectrum. They are identified by using the 2D NMR techniques as the protons of the $-\text{CH}_2-$ moieties of the ring structure and of the additional substituent $-\text{CH}_2\text{Si}(\text{OEt})_3$. This is in good agreement with the chemical shift values described in literature.³⁶ Although rather sharp singlets are expected for these particular protons, a more complex spectrum is observed. This can be explained by a non-equivalent chemical environment of the protons due to a conformational inversion of the six-membered ring.

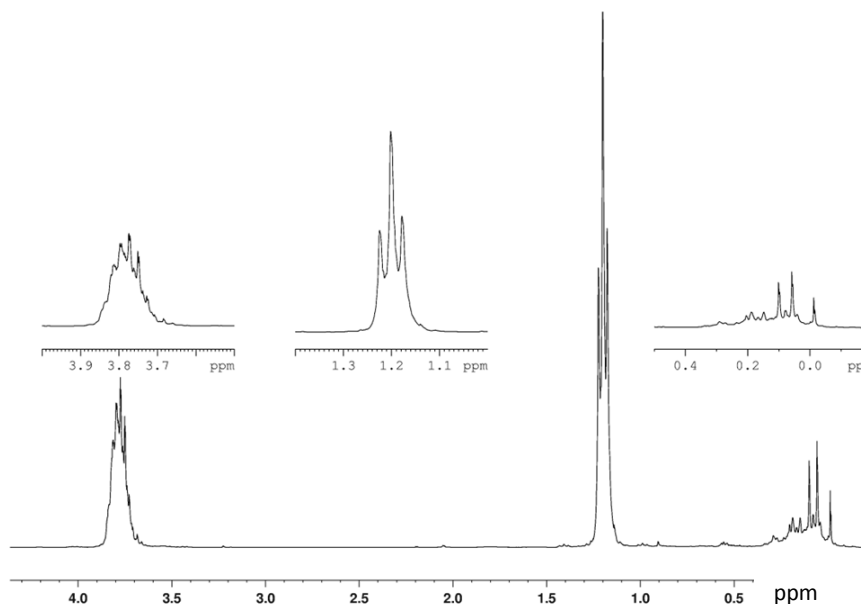


Figure 7.18: 1D ^1H NMR spectrum of the cyclic organosilane mixture.

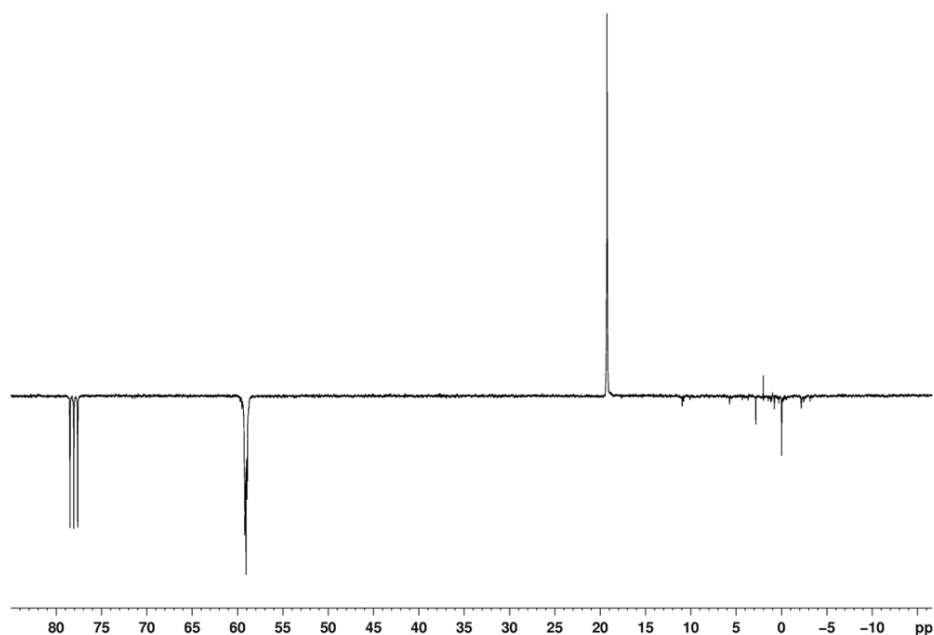


Figure 7.19: ^{13}C APT NMR spectrum.

The possibility exists that during synthesis, the substituted tri-silacyclohexane, **2**, of figure 7.4 reacts further with the formation of more branched products. Additional $-\text{CH}_2\text{-Si}(\text{OEt})_3$ are at first sight not observed in the ^1H and ^{13}C NMR spectra and furthermore the signal integrations of the protons do not sustain the presence of more branched compounds in the mixture. Nevertheless, these products can be present in a very small amount and therefore perhaps not detectable. Thus, although it was not possible to completely exclude the presence of more branched silanes, these NMR results definitely confirm that the organosilane oil consists almost completely of the substituted tri-silacyclohexane.

7.6 Experimental section for sealing with top layer deposition

7.6.1 Chemicals

Chloromethyltriethoxysilane, 1,2-bis(triethoxysilyl)ethane, tetraethyl orthosilicate (TEOS) and HMDS were purchased from ABCR, hydrochloric acid (HCl, 37 %), THF, pentane and absolute ethanol were obtained from Fiers, and Brij-76 was purchased from Aldrich. All materials were used as received.

7.6.2 Synthesis

Preparation of mesoporous silica film.

0.3 g Brij-76 was dissolved in 20 ml ethanol and 0.5 ml (0.1M) HCl. Then 1 ml of TEOS and 0.5 ml H₂O were added to the solution and this was aged for 1 day. The solution was then spin-coated on a Si-wafer at a rate of 5000 rpm. The porogen was removed by treating the film at 400°C for 5 hours.

Preparation of ethane PMO film.

1.2 g Brij-76 was dissolved in 20 ml ethanol and 1.5 ml (0.1M) HCl. Then 3 ml of 1,2-bis(triethoxysilyl)ethane and 1.5 ml H₂O were added to the solution and this was aged for 1 day. The solution was then spin coated on a Si-wafer at a rate of 5000 rpm. The porogen was removed by treating the film at 400°C for 5 hours.

Preparation of the cyclic carbon-bridged organosilanes³⁶

The synthesis recipe of cyclic carbon-bridged organosilane precursor is the same as the recipe used for grafting and can be found in section 7.2.2. However, in this case no extra distillation to separate the precursors was performed.

Preparation of the organosilica dense layer

0.5 ml of the cyclic carbon-bridged organosilane mixture was dissolved in 20 ml ethanol, 0.5 ml (0.1M) HCl and 0.5 ml H₂O and aged for a certain time. Solutions with different aging times were then spin-coated at 5000 rpm on top of the mesoporous silica film or ethane PMO film to form an organosilica top layer.

An additional baking step was performed at 400°C under nitrogen atmosphere to remove all the volatiles and to complete the condensation of the cyclic carbon-bridged precursor.

A reference thin film of the prepared oligomers was also deposited directly on a silicon wafer to determine the thickness of the carbon-bridged organosilica layer and was found to be 20 nm.

HMDS treatment

The obtained films were vacuum dried film and exposed to HMDS vapor for 2 hours at 130°C and rinsed with pentane, followed by drying at 300°C under nitrogen to remove unreacted HMDS.

7.6.3 Characterization

The refractive index and thickness of the layer is analyzed on a J. A. Woollam ellipsometer alpha-SE. The total porosity is calculated from the refractive index using the Lorentz-Lorentz formula already described in chapter 5.

The open and total porosity were determined with ellipsometric porosimetry using the same setup as described in chapter 6.

To check the water affinity of the films, water adsorption isotherms were measured with ellipsometric porosimetry also using the same equipment, but water was used as adsorbate instead of toluene.

Water contact angles values were obtained by using a Krüss-DSA 30 Drop Shape Analysis System using the tangent 1 model.

Diffuse reflectance Fourier transform infra-red (DRIFT) spectra were obtained on a Nicolet 6700 FT-IR from Thermo Scientific. A spectrum of a pristine silicon wafer was first measured to use as background.

The dielectric constant of the films was calculated from the capacitance of a parallel plate capacitor at 100 kHz using a HP 4192A LF impedance analyzer. Aluminum dots were used as top contacts and a heavily doped silicon wafer was used as bottom contact. The bottom of the silicon wafer was scratched to remove the native silicon dioxide and an eutectic indium/gallium alloy was attached to make a good ohmic contact with the impedance analyzer. With the same equipment also the leakage current and breakdown voltage were obtained by performing current/voltage (*I*/*V*) measurements.

The Young's modulus of the low-k dielectric films was measured by nano-indentation using a Nano Indenter XP system from MTS Corporation, with a dynamic contact module (DCM) and a continuous-stiffness measurement (CSM) option under constant strain rate condition (0.05 s^{-1}).

High resolution transmission electron microscopy (TEM) measurements were performed on a Jeol JEM 3010 apparatus.

7.7 Results and discussion for sealing with top layer deposition

7.7.1 Investigation of effective sealing

Because diffusion of the sealant into the porous material is a main issue, possible diffusion of the top layer was first investigated with ellipsometry. Therefore, the thickness and refractive index of the pristine porous silica film was determined using the Cauchy model.

Next the sealing layer was deposited on top of the porous silica and the total thickness (porous silica + top layer) was determined. By knowing the thickness of the porous film and the total thickness, the thickness of the top layer can be calculated. To know the refractive index (and thus the porosity) of the porous silica film after the dense layer deposition, a two layer Cauchy model was used. One layer model fits the porous film and the other the top film. Assuming that the thickness of the porous film does not significantly change after the top layer deposition, this parameter can be fixed and only the parameters that influence the refractive index are fitted. In the case that the refractive index of the porous film is similar before and after the top layer deposition, there is no significant diffusion of the top layer. A more detailed explanation about the ellipsometry measurements and calculations can be found in the characterization appendix.

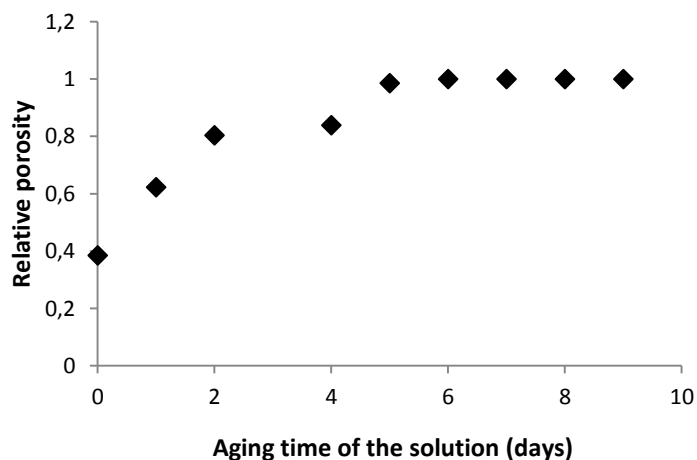


Figure 7.20: Relative porosity of mesoporous silica film after deposition of top layer.

To see if the aging time leads to large oligomers that can exceed the pore size, the sealant solution was spin-coated every 24 hour on porous silica samples with pore sizes around 3 nm. The results are shown in figure 7.20. Due to the fact that the porosity of

the different porous silica samples was not exactly the same, the relative porosity (ratio porosity after/before deposition) was plotted in function of the aging time.

It can be seen from the figure that before 5 days the porosity of the silica film after deposition is lower than the pristine film. This means that the sealant molecules are not large enough and will diffuse in the porous material, filling up the pores. After 5 days of aging the porosity of the porous films does not change, meaning that the sealant molecules are too large to enter the pores.

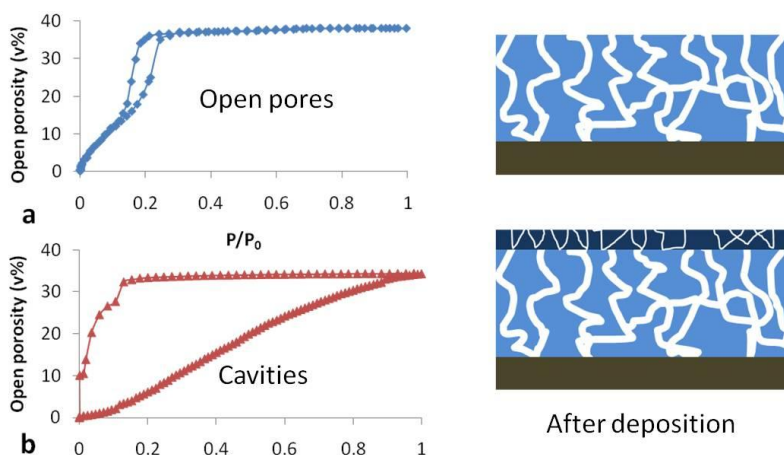


Figure 7.21: Toluene adsorption/desorption isotherms and schematic illustrations of a) the porous silica layer and b) the silica layer after organosilica layer deposition.

To verify if the pores are sealed, figure 7.21 shows the toluene sorption isotherms of the pristine porous silica film and the porous silica film with top layer deposition. The isotherm of the porous silica film (figure 7.21a) shows a steep capillary condensation step with a H1 hysteresis which is typical for mesoporous materials with a uniform pore size distribution.

In table 7.1 which shows the physical properties of the films, it can be seen that the open porosity is equal to the total porosity. The isotherm of the material after deposition of a organosilica layer on top (figure 7.21b), shows a gradual increase in toluene adsorption instead of a steep capillary condensation step, proving that toluene no longer easily diffuses into the pores. This is also confirmed by the delayed desorption of the toluene. These isotherms are typically observed when the porous material contains bottle necks³⁷ which is caused by the constitutive porosity of the self-assembled organosilica layer. This is presented by the schematic illustration in figure 7.21b. Although the open porosity is still equal to the total porosity as seen from table 7.1 (sample organosilica), the pore entrances are thus very narrow. This is already

considered to be a major achievement because this effect will prevent the metal penetration during barrier deposition processes.

Table 7.1: Physical properties of the pristine mesoporous silica film (pristine), after dense layer deposition (organosilica) and after HMDS treatment (HMDS).

Sample	Thickness ^[a] (nm)	P_{tot} ^[a] (v%)	P_{open} ^[b] (v%)	P_{closed} ^[c] (v%)	Contact angle ^[d] (°)
Pristine	80	38	38	0	57
Organosilica	100	34	34	0	70
HMDS	100	34	0	34	86

[a] determined with spectroscopic ellipsometry

[b] determined with toluene adsorption (ellipsometric porosimetry)

[c] $P_{closed} = P_{tot} - P_{open}$

[d] calculated water contact angle

Also, compared to the original silica film, the total porosity of the combined film (*i.e.* combination of the mesoporous silica layer and the organosilica top layer) is only decreased by 4% and the thickness is increased with 20 nm (see table 7.1) which is equal to the measured thickness of the native organosilica layer. Because of this additional increase in thickness and the very small decrease in porosity, we can also conclude that there is no significant diffusion of the sealant layer into the porous material and a high porosity can be maintained after deposition.

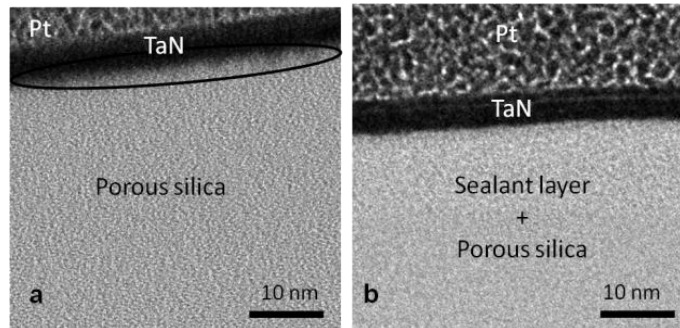


Figure 7.22: HRTEM images of a) cross section of a non-sealed porous silica film and b) cross section of a partial sealed silica film.

To prove that the partial sealing, realized after deposition of the organosilica layer without extra HMDS treatment, is already sufficient for the deposition of copper barrier layers in actual device applications, approximately 7 nm TaN was sputtered on partial sealed and non-sealed mesoporous silica films. Focused Ion Beam (FIB) cutting was applied to obtain cross sections of the films and these were examined with high

resolution transmission electron microscopy (HRTEM). The TEM images of the cross sections are shown in figure 7.22.

TaN on the porous film results in a diffuse interface which could be attributed to TaN diffusion in the porous materials. This is clearly visible in the circled area of image 7.22a. Although it is not possible to distinguish the sealant layer and the porous silica film on TEM image 7.22b due to their similar chemical composition, it can be clearly seen that a really sharp interface is present between the TaN layer and the cyclic carbon-bridged layer, proving its perfect sealing property.

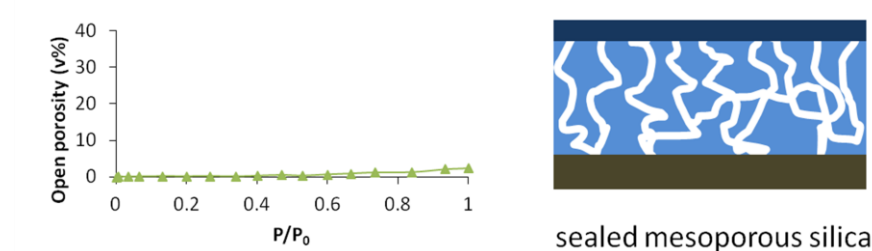


Figure 7.23: Toluene adsorption/desorption isotherms and schematic illustration of the porous silica film after top layer deposition and HMDS treatment.

To attempt a complete sealing the top layer was grafted with HMDS and the toluene isotherm is given in figure 7.23. The figure shows that the toluene isotherm of the HMDS treated film remains almost completely flat. This indicates that toluene does not diffuse into the pores. The small adsorption that is still observed can be attributed to condensation of the toluene at the surface of the film.

As seen in table 7.1, no changes in total porosity and thickness are observed after the grafting with HMDS, but the open porosity is decreased to 0% (sample HMDS). This means that the pores are now completely sealed and thus the closed porosity (P_{closed}) is equal to the total porosity. The last column of table 7.1 shows the water contact angles after each deposition step. An increase to a value of 86° was obtained after the HMDS treatment, meaning that a hydrophobic surface is produced and the sealed film will therefore no longer adsorb moisture.

Proof for this was also given by Diffuse Reflectance Fourier Transform (DRIFT) infra-red spectroscopy and water adsorption measurements. The DRIFT spectrum of the porous silica layer shows a broad band between 3200 and 3600 cm^{-1} , typical for physisorbed moisture. This band is less intense after the organosilica deposition and almost completely disappears after the grafting with HMDS (see figure 7.24a). The water adsorption measurements of the sealed sample after HMDS treatment revealed that no

moisture is adsorbed and the porous film is effectively sealed against water molecules (see figure 7.24b).

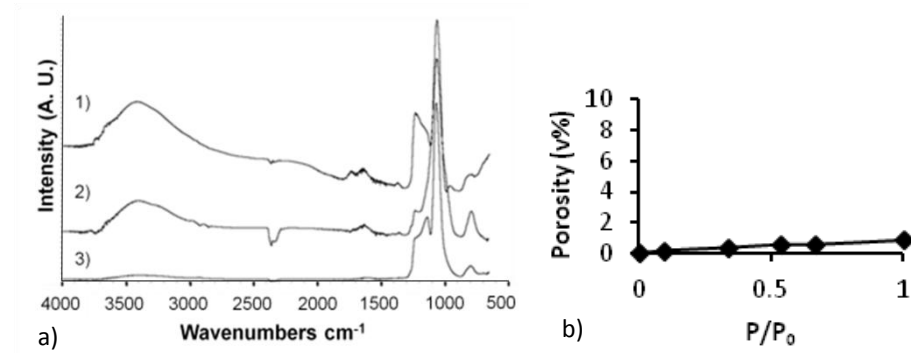


Figure 7.24: DRIFT spectrum of 1) porous silica layer, 2) porous silica layer with organosilica layer and 3) silica layer after organosilica layer deposition and HMDS treatment, and b) the water adsorption isotherm after HMDS treatment.

7.7.2 Impact on the electrical and mechanical properties

To investigate the influence of the sealing on the electrical and mechanical properties, the method was tested on low- k ethane PMO films. To compare the results, 4 samples with porosities around 40% and thicknesses around 250 nm were prepared. These samples are a pristine ethane PMO film (EPMO), a HMDS treated ethane PMO film (HEPMO), an ethane PMO film with organosilica top deposition (sealed; EPMOD) and an HMDS treated ethane PMO film with organosilica top deposition (sealed; HEPMOD). The porosities, contact angles and dielectric constants are given in table 7.2

Table 7.2: porosity, water contact angle and k -value of 2 sealed (EPMOD and HEPMOD) and 2 non-sealed (EPMO and HEPMO) ethane PMO films.

Sample	Porosity (%)	Contact angle (°)	k -value
EPMO	38	68	2.5
HEPMO	39.5	100	2.15
EPMOD	41.5	71	2.07
HEPMOD	38.3	75	2.22

It can be seen from the table that the lowest k -value is obtained for sample EPMOD while EPMO has the highest k -value. From chapter five, it is already explained that the high k -value of EPMOs can be attributed to adsorbed moisture which is also confirmed here by the lowest contact angle for the EPMO film. However, the contact angle of

sample EPMOD is also not very high although the k -value is in this case very low. This assumes that the top layer even without extra HMDS treatment is sufficient to block moisture. To confirm this, a water adsorption measurement was performed and the result is presented in figure 7.25. It can be seen that no significant amount of water is adsorbed.

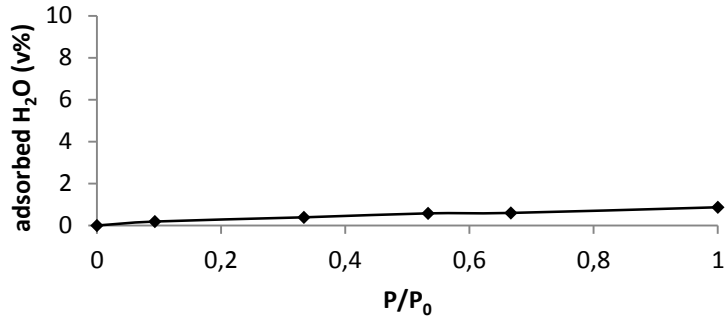


Figure 7.25: Water adsorption isotherm of EPMOD.

The k -values of the HMDS treated sealed and non-sealed ethane PMOs are slightly higher than sample EPMOD and this can be mainly attributed to the lower porosity of both samples.

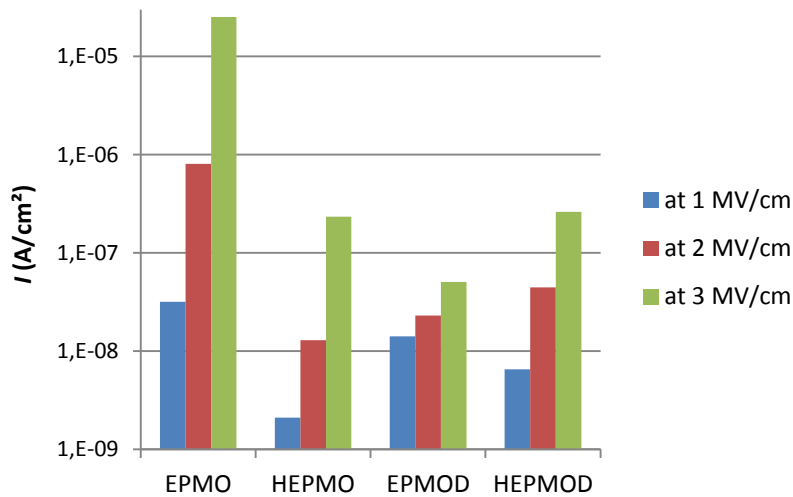


Figure 7.26: Leakage current measurements of sealed and non-sealed ethane PMO films at different applied voltages.

The leakage current at several voltages is given in figure 7.26. Similar as for the k -value the leakage current of the pristine EPMO film is the worst which is also due to the less hydrophobic character of the film. It increases quite rapidly when the voltage is raised.

The HMDS treated films (HEPMO and HEPMOD) have the lowest leakage current at 1 MV/cm but it steadily increases when the applied voltage gets higher.

The best result is again obtained for sample EPMOD. At low voltage they have a sufficient low leakage current and even at 3 MV/cm, the leakage current is in the same order as at 1 MV/cm. The electrical breakdown voltage is for all the 4 films higher than 3.5 MV/cm which satisfies the low-k application requirements. This means that the top sealing of the films is beneficial for the electrical properties of the low-k film and there is no need for an extra HMDS treatment.

The influence of the sealing on the mechanical properties of the ethane PMO films is shown in figure 7.27. The Young's moduli of the sealed PMO samples are similar and significantly higher than the non-sealed samples even with the fact that sample EPMOD has the highest porosity. Also the hardness of the sealed samples is slightly higher proving that the sealing is also beneficial for the mechanical properties of the low-k dielectric, making especially EPMOD very interesting for further integration experiments. In contrast to earlier reports,³⁸ the trimethyl silylation with HMDS has no positive effect on the mechanical stability.

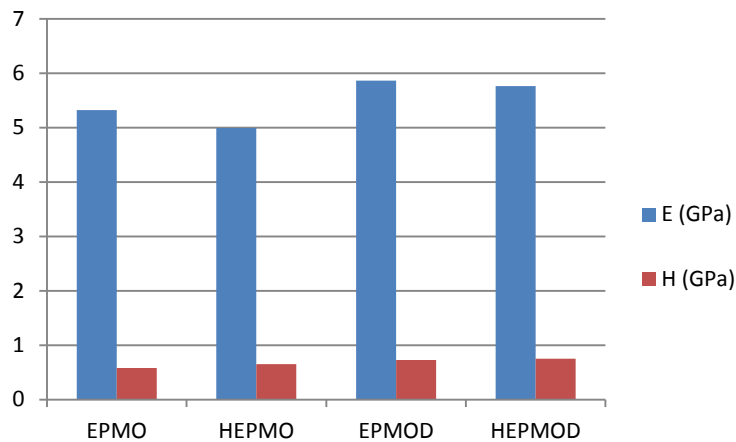


Figure 7.27: Young's modulus and hardness of sealed and non-sealed ethane PMO films.

7.8 Conclusions for sealing with top layer deposition

In summary, it was possible to seal mesoporous silica thin films with an average pore size diameter of 3 nm by a new method of spin-coating of a cyclic carbon-bridged organosilica layer followed by a grafting with HMDS. Careful control of the self-

assembling process of the sealant precursor allows the formation of intermediate fragments with molecular sizes exceeding the pore size, thus avoiding penetration of the sealant into the pores of the silica layer, resulting in a complete sealing combined with a preservation of the high porosity of the thin film.

Moreover, a complete hydrophobic material is obtained after HMDS treatment and thus the adsorption of moisture, which really damages the low-k properties, is also prevented. It is also shown that a partial sealing of the mesopores is already sufficient to prevent metal penetration into the porous material. Finally, this method can be transferred to more advanced low-k materials with improving the electrical and mechanical properties of the dielectric, thereby meeting the stringent standards for use of low-k mesoporous thin films in practical electronic applications of today.

7.9 References

1. C. M. Whelan, Q. T. Le, F. Cecchet, A. Satta, J. J. Pireaux, P. Rudolf and K. Maex, *Electrochemical and Solid State Letters*, 2004, **7**, F8-F10.
2. H. J. Lee, E. K. Lin, W. L. Wu, B. M. Fanconi, J. K. Lan, Y. L. Cheng, H. C. Liou, Y. L. Wang, M. S. Feng and C. G. Chao, *Journal of the Electrochemical Society*, 2001, **148**, F195-F199.
3. T. Furusawa, D. Ryuzaki, R. Yoneyama, Y. Homma and K. Hinode, *Electrochemical and Solid State Letters*, 2001, **4**, G31-G34.
4. K. Maex, M. R. Baklanov, D. Shamiryan, F. Iacopi, S. H. Brongersma and Z. S. Yanovitskaya, *Journal of Applied Physics*, 2003, **93**, 8793-8841.
5. H. G. Peng, D. Z. Chi, W. D. Wang, J. H. Li, K. Y. Zeng, R. S. Vallery, W. E. Frieze, M. A. Skalsey, D. W. Gidley and A. F. Yee, *Journal of the Electrochemical Society*, 2007, **154**, G85-G94.
6. H. Cui, R. J. Carter, D. L. Moore, H. G. Peng, D. W. Gidley and P. A. Burke, *Journal of Applied Physics*, 2005, **97**.
7. M. Aimadeddine, V. Arnal, A. Farcy, C. Guedj, T. Chevolleau, N. Posseme, T. David, M. Assous, O. Louveau, F. Volpi and J. Torres, *Microelectronic Engineering*, 2005, **82**, 341-347.
8. W. Puyrenier, V. Rouessac, L. Broussous, D. Rebiscoul and A. Ayril, *Microelectronic Engineering*, 2006, **83**, 2314-2318.
9. L. Broussous, W. Puyrenier, D. Rebiscoul, V. Rouessac and A. Ayril, *Microelectronic Engineering*, 2007, **84**, 2600-2605.
10. W. Puyrenier, V. Rouessac, L. Broussous, D. Rebiscoul and A. Ayril, *Microporous and Mesoporous Materials*, 2007, **106**, 40-48.
11. N. Posseme, T. Chevolleau, T. David, M. Darnon, J. P. Barnes, O. Louveau, C. Licitra, D. Jalabert, H. Feldis, M. Fayolle and O. Joubert, *Microelectronic Engineering*, 2008, **85**, 1842-1849.
12. Q. T. Le, C. M. Whelan, H. Struyf, H. Bender, T. Conard, S. H. Brongersma, W. Boullart, S. Vanhaelemeersch and K. Maex, *Electrochemical and Solid State Letters*, 2004, **7**, F49-F53.
13. J. Shoeb and M. J. Kushner, *Journal of Vacuum Science & Technology A*, 2011, **29**.
14. R. Hoofman, G. Verheijden, J. Michelon, F. Iacopi, Y. Travalay, M. R. Baklanov, Z. Tokei and G. P. Beyer, *Microelectronic Engineering*, 2005, **80**, 337-344.
15. F. Iacopi, Z. Tokei, Q. T. Le, D. Shamiryan, T. Conard, B. Brijs, U. Kreissig, M. Van Hove and K. Maex, *Journal of Applied Physics*, 2002, **92**, 1548-1554.
16. X. T. Chen, D. Gui, D. Z. Chi, W. D. Wang, N. Babu, N. Hwang, G. Q. Lo, R. Kumar, N. Balasubramanian and D. L. Kwong, *Ieee Electron Device Letters*, 2005, **26**, 616-618.
17. X. T. Chen, D. Gui, Z. Q. Mo, A. Y. Du, D. Z. Chi, W. D. Wang, Y. H. Wang, D. Lu, L. J. Tang, W. H. Li and L. Y. Wong, *Thin Solid Films*, 2006, **504**, 248-251.
18. K. Ito, K. Kohama, T. Tanaka, K. Mori, K. Maekawa, Y. Shirai and M. Murakami, *Journal of Electronic Materials*, 2010, **39**, 1326-1333.
19. K. Kohama, K. Ito, Y. Sonobayashi, T. Tanaka, K. Mori, K. Maekawa, Y. Shirai and M. Murakami, *Japanese Journal of Applied Physics*, 2010, **49**.

20. N. Jourdan, M. B. Krishtab, M. R. Baklanov, J. Meersschaut, C. J. Wilson, J. M. Ablett, E. Fonda, L. Zhao, S. Van Elshocht, Z. Tokei and E. Vancoille, *Electrochemical and Solid State Letters*, 2012, **15**, H176-H178.
21. Y. H. Wang, M. R. Moitreyee, R. Kumar, L. Shen, K. Y. Zeng, J. W. Chai and J. S. Pan, *Thin Solid Films*, 2004, **460**, 211-216.
22. L. Y. Yang, D. H. Zhang, C. Y. Li, R. Liu, P. W. Lu, P. D. Foo and A. T. S. Wee, *Thin Solid Films*, 2006, **504**, 265-268.
23. A. Mallikarjunan, A. D. Johnson, L. Matz, R. N. Vrtis, A. Derecskei-Kovacs, X. Z. Jiang and M. C. Xiao, *Microelectronic Engineering*, 2012, **92**, 83-85.
24. J. Bonitz, S. E. Schulz and T. Gessner, *Microelectronic Engineering*, 2004, **76**, 82-88.
25. V. Jousseume, M. Fayolle, C. Guedj, P. H. Haumesser, C. Huguet, F. Pierre, R. Pantel, H. Feldis and G. Passemard, *Journal of the Electrochemical Society*, 2005, **152**, F156-F161.
26. C. Jezewski, C. J. Wiegand, D. X. Ye, A. Mallikarjunan, D. L. Liu, C. M. Jin, W. A. Lanford, G. C. Wang, J. J. Senkevich and T. M. Lu, *Journal of the Electrochemical Society*, 2004, **151**, F157-F161.
27. J. S. Juneja, P. I. Wang, T. Karabacak and T. M. Lu, *Thin Solid Films*, 2006, **504**, 239-242.
28. J. Liu, W. Kim, J. Bao, H. Shi, W. Baek and P. S. Ho, *Journal of Vacuum Science & Technology B*, 2007, **25**, 906-912.
29. Y. Travaly, J. Schuhmacher, M. R. Baklanov, S. Giangrandi, O. Richard, B. Brijs, M. Van Hove, K. Maex, T. Abell, K. R. F. Somers, M. F. A. Hendrickx, L. G. Vanquickenborne, A. Ceulemans and A. M. Jonas, *Journal of Applied Physics*, 2005, **98**.
30. P. de Rouffignac, Z. W. Li and R. G. Gordon, *Electrochemical and Solid State Letters*, 2004, **7**, G306-G308.
31. Y. B. Jiang, N. G. Liu, H. Gerung, J. L. Cecchi and C. J. Brinker, *J Am Chem Soc*, 2006, **128**, 11018-11019.
32. T. Seo, T. Yoshino, N. Ohnuki, Y. Seino, Y. Cho, N. Hata and T. Kikkawa, *Journal of the Electrochemical Society*, 2009, **156**, H98-H105.
33. M. Kruk and C. M. Hui, *J Am Chem Soc*, 2008, **130**, 1528-+.
34. B. D. Hatton, K. Landskron, W. J. Hunks, M. R. Bennett, D. Shukaris, D. D. Perovic and G. A. Ozin, *Materials Today*, 2006, **9**, 22-31.
35. R. Mortera, B. Onida, S. Fiorilli, V. Cauda, C. V. Brovarone, F. Baino, E. Verne and E. Garrone, *Chem Eng J*, 2008, **137**, 54-61.
36. D. J. Brondani, R. J. P. Corriu, S. Elayoubi, J. J. E. Moreau and M. W. C. Man, *Tetrahedron Lett*, 1993, **34**, 2111-2114.
37. M. R. Baklanov, K. P. Mogilnikov and J. H. Yim, *Mater Res Soc Symp P*, 2004, **812**, 55-60.
38. J. Y. Chen, F. M. Pan, A. T. Cho, K. J. Chao, T. G. Tsai, B. W. Wu, C. M. Yang and L. Chang, *J. Electrochem. Soc.*, 2003, **150**, F123-F127.

Chapter Eight: General Conclusions and Outlook

In this chapter, the main findings of this PhD work are summarised, and suggestions for further investigations and improvements in this research field are provided. These suggestions are intended to give guidelines for further research on fundamental or applied issues related to the previous work.

8.1 General conclusions

In this thesis, ethane, ethene and ring PMO materials were synthesized using non-ionic surfactants as templates and they were evaluated for their ultra low- k applicability (k -value < 2). Therefore important parameters such as porosity, pore size, hydrophobicity, hydrothermal, mechanical and chemical stability, and dielectric constant were evaluated.

In the first part, the materials were synthesized as powders to allow a quick and easy characterization of their stability as bulk material. It was found that the stability of the ethene PMOs was much less than the other two and therefore only the ethane and ring PMOs were further investigated.

In the second part, ethane and ring PMOs were successfully prepared as thin films with high porosities. The films were obtained by spin-coating making use of the evaporation induced self-assembly. In the case of ethane PMOs, hydrophobic materials were obtained after end-capping of the silanol groups with HMDS. The resulted k -value and Young's modulus were 2.15 and 5 GPa respectively which is comparable with the values of the state of art low- k materials. On the other hand, hydrophobic ring PMO materials can be obtained without an extra HMDS treatment. The ring PMOs possess an ultra low k -value of 1.8 and a very good resistance against alkaline solutions. Unfortunately, the mechanical stability of these films is not sufficient and should be improved.

In the last part, two methods to seal or narrow the pores were developed. The first method is currently a proof of concept which shows that pore sizes can be narrowed without losing significant porosity by sequentially grafting with organosilane precursors on the silanols of a porous silica material. By grafting before the template removal, grafting only occurs at the outer surface. Afterwards, the template can be thermally removed and the inner silanols can be end-capped with HMDS. With this approach, hydrophobic silicas with narrow pore entrances are achieved.

The second developed method is sealing by top layer deposition of pre-assembled cyclic carbon-bridged organosilane molecules. This pre-assembling increases the molecular size of the sealants, avoiding diffusion into the pores. After the deposition, the pores were only partially sealed, but this was already sufficient to prevent metal penetration during barrier deposition. Furthermore, this partial sealing improved the electrical and mechanical properties of ethane PMO films, making this approach very promising for further investigation towards integration. Finally, by grafting the top layer with HMDS a completely sealed porous film can be obtained.

Finally, a comparison between our developed low- k materials and the state of the art low- k materials is presented in figure 8.1. This figure compares the most important low-

k properties (*i.e.* k -value and Young's modulus) of the best (in this thesis) synthesized low- k materials, which are the ring PMO (RPMO) and the partially sealed ethane PMO (EPMOD), with the state-of-the-art low- k materials.

The blue bar is the commonly reported minimum threshold value for the Young's modulus and the red bar the upper threshold value for the dielectric constant. The first 9 materials are prepared by PECVD. OP_A and OP_B are spin-coated organic materials, ZLK is a zeolite like low- k material and SBA 2.0, SBA 1.8, RPMO and EPMOD are hybrid spin-coated materials.

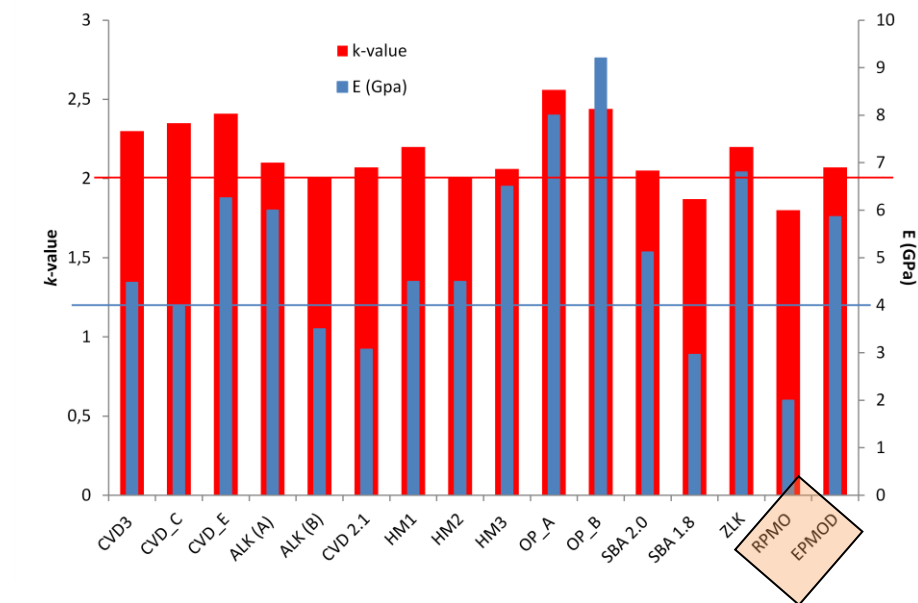


Figure 8.1: k -value and Young's modulus of the state of the art low- k materials. (Data were received from IMEC except ZLK. For ZLK, the values were taken from ref. 16 of chapter 2). Our developed materials are in the red rectangle.

It can be seen from the figure that RPMO has the lowest k -value and only SBA 1.8 also have a k -value below 2. However, the Young's modulus of both materials has to be improved (values are below the blue bar).

Other interesting materials for further investigation are the ones that have a high Young's modulus (significantly higher than the blue bar) and a k -value almost equal to 2 (just above the red bar). These materials are ALK (A), HM2, HM3, SBA 2.0, ZLK and EPMOD. Especially our developed EPMOD film is very promising, because the pores are already partially sealed. This means that, in contrast to non-sealed porous films, metal penetration during technological processing is prevented and the good insulating properties of the low- k material are maintained.

8.2 Outlook

8.2.1 Concerning PMO as low-k materials

The results obtained in this research show that although the k -value of the low-k materials can be sufficiently decreased, the mechanical stability should be improved to be applicable.

Therefore, further investigations to improve the stability of the PMOs are needed. From OSG films, it is known that ordering, matrix composition and UV-after treatment increase the mechanical stability.¹⁻³

Keeping this in mind, a first possible approach for improving the mechanical stability is the investigation of the impact of synthesis conditions, different morphologies and after treatments on the mechanical stability of PMO films.

Below an overview of the parameters that can be varied are presented, including some examples:

<u>Parameters</u>	<u>Examples</u>
- Precursors:	ethane, methane, ethene, benzene, cyclic-silane precursors, methyltriethoxysilane and mixtures thereof.
- Surfactants:	CTAC/CTAB, OTAC/OTAB, Brij-30, Brij-56, Brij-76, P123, F127, Tween
- Acids:	HCl/ HNO ₃
- Synthesis conditions:	aging time, temperature
- After treatments:	NH ₃ vapor treatment/ different thermal treatments/ UV/ HMDS/ TMCS

Also the concentrations and ratios of the utilized starting products can be varied.

As a first test, the influence of a UV-treatment on ring PMOs with different porosities has already been investigated. The porous materials were heated to 400°C under nitrogen atmosphere and exposed to a 256 nm UV-lamp for 1 hour. The Young's modulus was determined before and after the UV-treatment and the results are presented in figure 8.2.

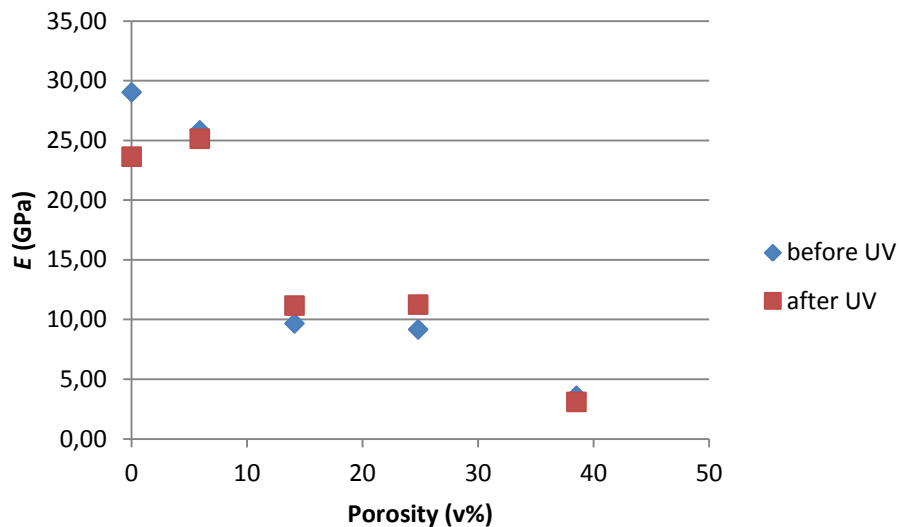


Figure 8.2: Influence of UV-treatment on the Young's modulus of ring PMO films with different porosities.

It can be seen from the figure that there is no significant difference after the UV-treatment. The reason for this can possibly be that the matrix can not be rearranged anymore due to the fixation step during the EISA method. Other possibilities could be that the synthesis conditions were not ideal (UV exposure time/ wavelength of UV lamp). Therefore, more experiments are needed to solve this unambiguously.

A second approach to improve the mechanical stability could be by preparing zeolite like films consisting of a silica matrix with carbon bridges, because zeolites have the best mechanical stability/porosity trade off.

Finally, it was shown in chapter 7 that the partial sealing by top layer deposition resulted in a better mechanical stability of the low-k film. So, by further optimizing this method, partially sealed ultra low-k materials with sufficient mechanical stability might be obtained.

8.2.2 Concerning pore sealing

Grafting

Further investigations concerning the grafting method could try to close completely the pores of PMO films by applying several grafting cycles in a controlled way, preferably by using a real ALD setup. The method should be also applied and evaluated on porous materials with higher porosities and larger pore sizes.

Another possibility to prevent grafting inside the pores could be starting from hydrophobic low- k films of which only the outer surface is hydrolyzed. This could be achieved by a short etching procedure or plasma treatment. Next, organosilane precursors could be grafted on the outer surface. By performing several grafting cycles, an efficiently sealed low- k film should be obtained without increasing the effective k -value.

When this approach is successful, it should also be possible with this method to close the sidewalls after trench creation.

Top layer deposition

Although the k -value of the top layer is relatively low, it is still higher than the k -value of the low- k material underneath. Therefore, the thickness of the top layer should be as thin as possible without losing the sealing property. Further, an aging time of five days before the sealing layer can be deposited is quite long. This means that a faster way to get oligomers is preferable.

Preliminary experiments to deal with these issues have already been performed. To speed up the condensation reaction, the prepared precursor solution was boiled to evaporate ethanol until a high viscous liquid was obtained, indicating that condensation reactions took place. Next, ethanol was added again to obtain the original solution volume (see section 7.2.2) and the solution was further exponentially diluted (10, 100, 1000, 10000 times) with ethanol to control the thickness of the layer and speed up oligomer formation.

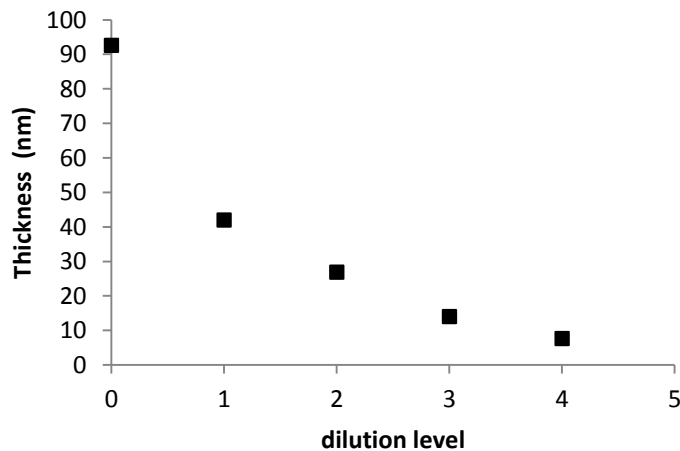


Figure 8.3: Thickness of sealant layer in function of precursor dilution level.

The influence of the ethanol concentration on the thickness is shown in figure 8.3. It can be seen that after every dilution step the thickness of the layer is more or less divided by two. Further confirmation of the oligomer formation is given by the fact that at dilution level 0, the thickness of the sealant layer is much higher than when the pristine starting solution is deposited (90 vs. 20-40 nm). Also, with this dilution approach very thin layers can be obtained (< 10 nm).

To investigate if the ageing time needed to avoid diffusion is decreased with this method, the level 1 diluted solution was deposited on a porous silica material and the remaining porosity of this layer was determined with ellipsometry. When the solution was deposited 90 minutes after dilution (day 0), there is only a slight diffusion of the precursors into the porous material, because almost 90% of the original porosity is remained (figure 8.4). After 1 day ageing, the remaining porosity is very close to 100% of the original value. This means that the ageing time can be drastically reduced.

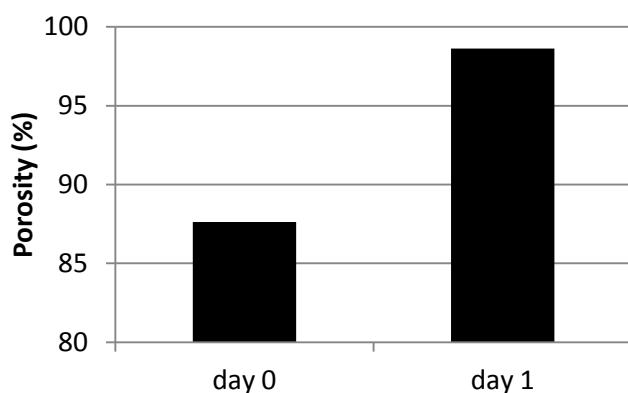


Figure 8.4: Remaining porosity of porous film after top layer deposition in function of the aging time.

A 5 nm thick sealant layer was then deposited on a porous silica material followed by a grafting with HMDS. The pore sealing efficiency was determined with ellipsometric porosimetry and the toluene sorption isotherm is presented in figure 8.5.

In contrast to the 20 nm thick sealant layer, no complete sealing is obtained after a 5 nm thick layer deposition. However, the shape of the isotherm indicates that cavity formation took place and thus metal diffusion during barrier deposition should be prevented.

By using other, more bulky grafting molecules such as the cyclic carbon-bridged organosilane precursors even a complete pore sealing might be obtained.

A second research topic is to investigate if this method can be used to seal the side walls which arise after the creation of trenches in the low-k film. Probably, this will be difficult with spin-coating, but dip-coating or ink-jet printing could be possible alternatives.

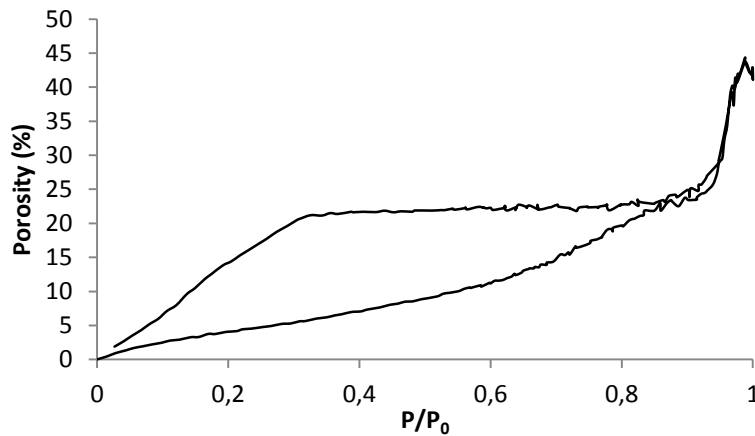


Figure 8.5: Toluene sorption isotherm of porous silica film after top layer deposition and HMDS treatment.

8.3 References

1. C. Y. Ting, H. S. Sheu, W. F. Wu and B. Z. Wan, *J Electrochem Soc*, 2007, **154**, G1-G5.
2. P. Verdonck, E. Van Besien, K. Vanstreels, C. Trompoukis, A. Urbanowicz, D. De Roest and M. R. Baklanov, *Jpn J Appl Phys*, 2011, **50**.
3. S. Takada, N. Hata, Y. Seino, N. Fujii and T. Kikkawa, *J Appl Phys*, 2006, **100**.

Appendix: Applied Characterization Methods for Thin Film Analysis

This appendix provides some more background and detailed measuring conditions of the applied thin film characterization techniques (ellipsometry, ellipsometric porosimetry, nano-indentation and C-V measurements). This is because these methods are no standard analysis tools for researchers with a chemical background. Ellipsometry measurements were performed at the department of solid state sciences (UGent) as well as some ellipsometric porosimetry measurements. Other ellipsometric porosimetry measurements, nano-indentation measurements and C-V measurements were performed at IMEC.

Details on the measuring conditions of the more common characterization techniques (N_2 adsorption, XRD, SEM, TEM, DRIFT, CHN elemental analysis, NMR, TGA, water contact angle measurements) are mostly sufficiently described in the chapters were they were used. In other cases, a standard measuring procedure was followed.

All these more common characterization methods are available at the department of inorganic and physical chemistry (Ghent University) except NMR (organic chemistry department), SEM (department of solid state sciences) and TEM (Technological Park, Zwijnaarde).

A.1 Ellipsometry¹⁻³

Ellipsometry is a non destructive characterization method to determine thickness and optical constants of thin layers. This is based on the change in polarity, amplitude change and phase change, expressed by Ψ (amplitude) and Δ (phase) when linear polarized light is reflected by the film. The primary tools for collecting ellipsometry data all include the following: light source, polarization generator, sample, polarization analyzer and detector. The light of the source will be first linear polarized before it hits the sample. The electric field wave of the incident light beam can be decomposed into two vector components. The two vector components are characterized as parallel to the plane of incidence (p-plane) and perpendicular to the plane of incidence (s-plane) shown in figure A.1.

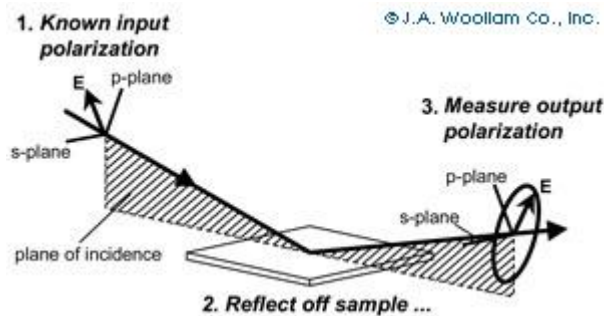


Figure A.1: Typical ellipsometry configuration, where linearly polarized light is reflected from the sample surface and the polarization change is measured to determine the sample response.¹

Similar to the incoming beam, the electric field of the reflected or transmitted beam is also decomposed into p-plane and s-plane components. The reflected beam is elliptically polarized and reaches the analyzer which passes the light with the right orientation. The detector converts the light into an electric signal.

The fundamental equation of ellipsometry is based on the changes of the polarization state from incoming and reflected light. Spectroscopic ellipsometry measures Ψ - and Δ -values as a function of wavelength and incident angle. These numbers are related to the complex Fresnel coefficient for p and s polarized light. The change in polarization can be written as:

$$\tan(\Psi) e^{i\Delta} = R_p/R_s$$

Where R_p and R_s are the complex Fresnel coefficients (which are derived from Maxwell's equations of electrodynamics) of the sample for p and s polarized light. These coefficients contain desired information related to material optical properties

and physical dimensions. Spectroscopic Ellipsometry (SE) measures this complex ratio as a function of wavelength.

To relate these data to the physical properties such as refractive index and thickness of the film, a model, which includes the optical and thickness properties, of the film has to be designed which makes it possible to recalculate the Ψ - and Δ -values in function of the wave lengths. The adjustable model parameters are varied until the best fit is found. The objective is to quickly determine the minimum difference or “best fit” between the measured and calculated Ψ - and Δ -values. The (Root) Mean Squared Error (MSE) quantifies this difference. A smaller MSE implies a better model fit to the data.

The film thickness is determined by interference between light reflecting from the surface and light that travels through the film. Depending on the relative phase of the rejoining light to the surface reflection, interference can be defined as constructive or destructive. The interference involves both amplitude and phase information. The phase information from Δ is very sensitive to films down to sub-monolayer thickness.

In the case for transparent low-k dielectric films the Cauchy model can be used. The Cauchy equation describes the dispersion of the refractive index of the film as a varying function of wavelength (λ):

$$N_{(\lambda)} = A + B/\lambda + C/\lambda^2$$

The parameters A, B, C and thickness of the film are used to calculate the Ψ - and Δ -values.

When the refractive index is known the total porosity can be calculated using the Lorenz-Lorenz formula:

$$\frac{n^2 - 1}{n^2 + 2} = V_p \frac{n_p^2 - 1}{n_p^2 + 2} + (1 - V_p) \frac{n_s^2 - 1}{n_s^2 + 2}$$

In this formula, n_p stands for the refractive index of the material inside the pores. The refractive index of the material containing the pores n_s . By measuring n by ellipsometry, we can now easily calculate the porosity V_p .

This Cauchy model was used to determine the thickness and porosity of all the films prepared in this thesis. The applied software is *CompleteEASE* version 4.29. As an example the way to determine the porosity of a porous film after top layer deposition (chapter 7) is now explained in detail. The graph in figure A.2 shows the measured Ψ

Appendix: Applied characterization methods for thin film analysis

and Δ -values in function of the wavelength as well as the fitted values for a pristine silica film. It can be seen that there is a good correlation.

The right box shows the fitted parameters. As model the Cauchy model named "Si with native oxide" was used because the utilized Si substrates had a native oxide layer on top with a thickness of 1 nm (represented by layer 1). Layer 2 provides thickness and the Cauchy parameters A, B and C of the film. The left box gives the calculated refractive index. The thickness of this pristine porous film is 61.88 nm and the porosity (derived from the refractive index using the Lorenz-Lorenz formula) is 37%.

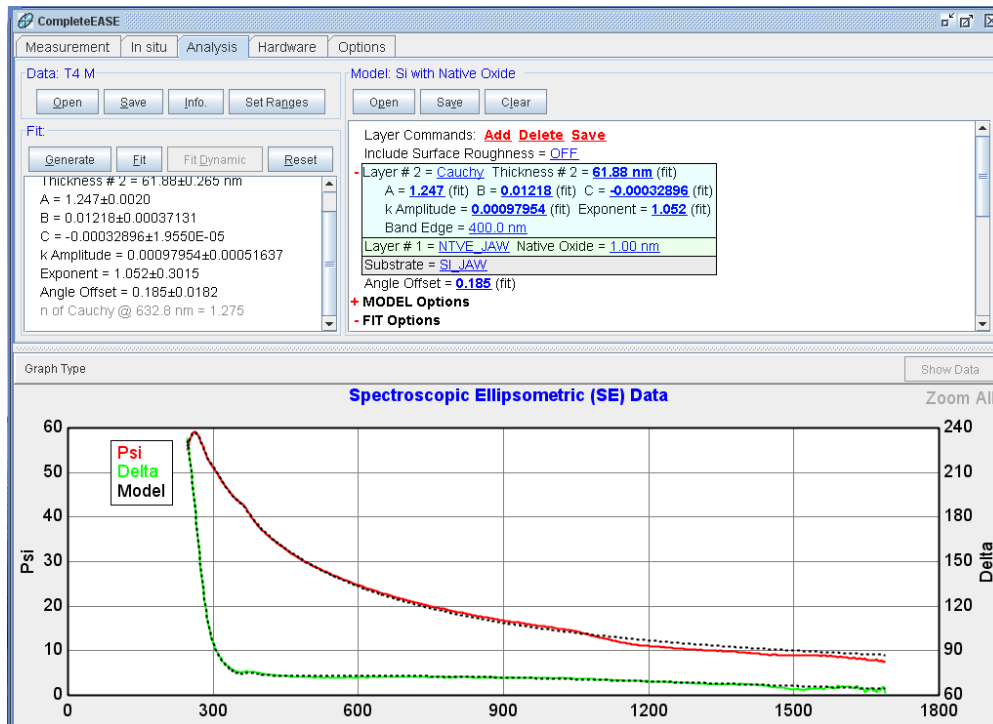


Figure A.2: ellipsometry measurement and determination of the thickness and refractive index of a porous silica film.

Next, a top organosilica layer after 9 days ageing was deposited and the resulting 2-layered film was thermally treated to remove the solvents. Then, again an ellipsometry measurement was performed. To know the total thickness (porous layer and top layer) a single layer fitting model was used and a thickness of 101.40 nm was determined (figure A.3). This shows that the top layer is effectively deposited on top of the porous silica film with a thickness of 39.52 nm, but it gives no indication if the precursor molecules also entered the pores. Therefore a two layer Cauchy model was applied, the bottom one for the fitting of the silica film, the top one for the top layer (figure A.4).

Appendix: Applied characterization methods for thin film analysis

The parameters of the porous silica film were fixed except the Cauchy parameters (A, B and C) from which the refractive index was calculated. In the case that diffusion took place, the refractive index should be higher than before the deposition. In this case, the refractive index was found to be 1.254 corresponding with a porosity of 41%. This porosity is even higher than before the deposition. The non decrease in porosity indicates that there was no diffusion of the top layer. The higher porosity can probably explained by the fact that after the deposition the film is more hydrophobic and water is not (or much less) adsorbed in the pores.

The determined refractive index of the top layer was found to be 1.44 which corresponds to a porosity of 7% meaning that the top layer is slightly porous which was already mentioned in chapter 7.

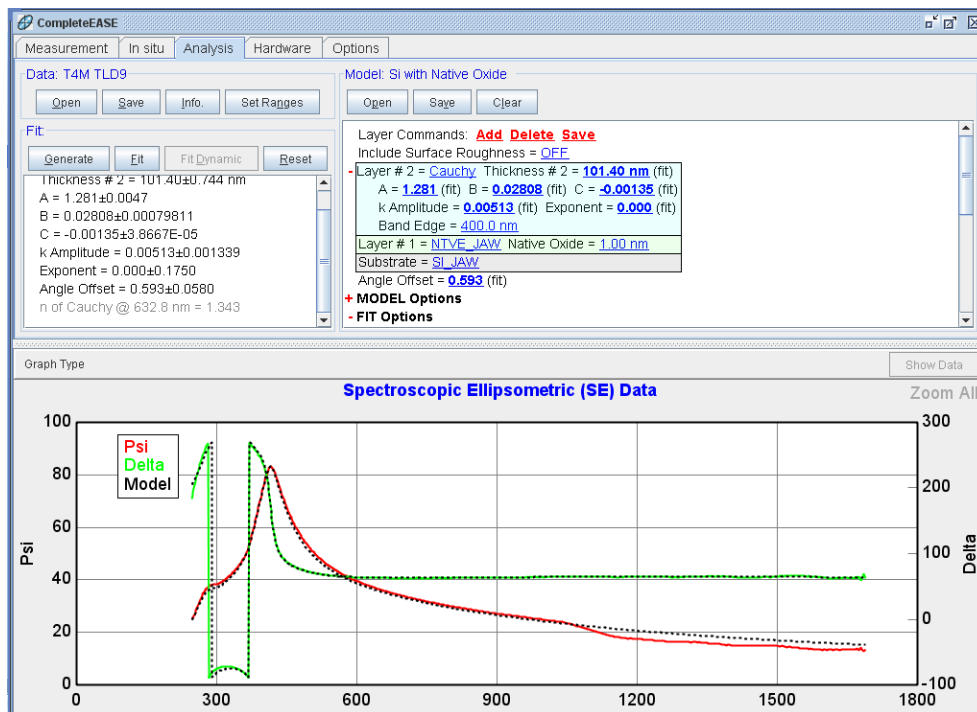


Figure A.3: Ellipsometry measurement and single layer Cauchy fitting model.

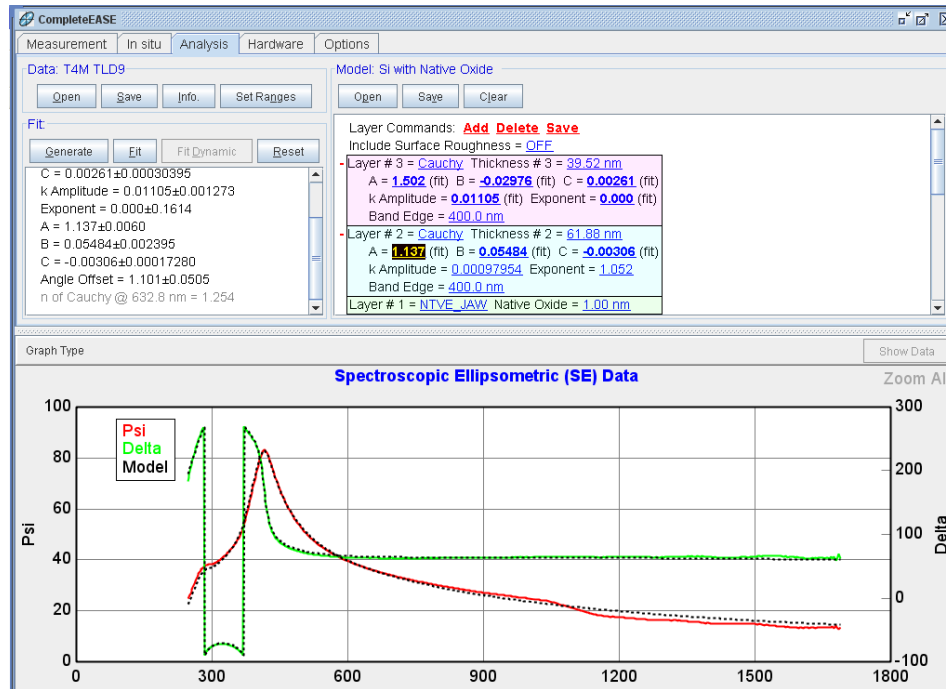


Figure A.4: Ellipsometry measurement and two layer Cauchy fitting model.

A.2 Ellipsometric porosimetry^{4, 5}

Ellipsometric porosimetry (EP) is based on the combination of spectroscopic ellipsometry (SE) and gas adsorption measurements. Similar to conventional gas adsorption techniques, an isotherm can be obtained by monitoring the adsorbed amount of gas in function of pressure. However, the amount of sample is too low to obtain accurate results when the amount of adsorbed vapour would be expressed as ml/g. Therefore, the change in refractive index during adsorption is monitored in situ by ellipsometry. When the vapour enters the pores the refractive index will increase and this allows plotting an isotherm (figure A.5). As adsorbent toluene is mostly used, because measurements can be performed at room temperature (when the pressure is low enough) and it does not chemically interact with the porous sample.

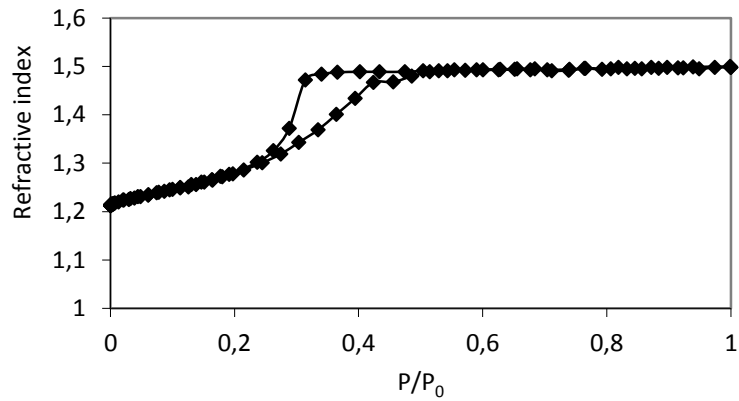


Figure A.5: Toluene sorption isotherm; refractive index in function of the relative toluene pressure.

An experimental setup is depicted in figure A.6. The porous film is placed in a vacuum chamber mounted with an ellipsometer. The chamber is evacuated and gradually filled with toluene to saturation pressure. After each addition step of toluene, an ellipsometric measurement is performed. This can then be repeated during desorption. The porosity and pore size distribution of the porous film are then calculated from the isotherm as already explained in chapter 6.

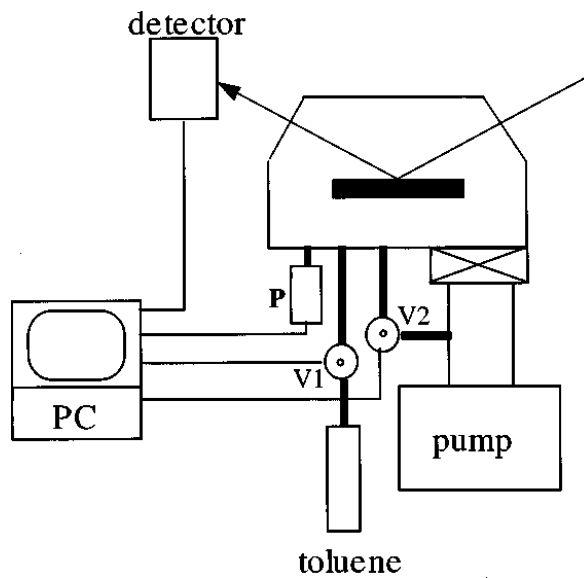


Figure A.6: Schematic view of an ellipsometric porosimeter.⁴

A.3 Nano-indentation⁶⁻⁸

Nano-indentation is used to investigate the mechanical properties of materials by indenting the test material with a diamond tip to the material surface producing an imprint. For the measurements performed in this thesis a Berkovich indenter was used. The force (load) and displacement are controlled and/or measured simultaneously and continuously throughout an indentation experiment.

In a nano-indentation test where a sharp indenter such as the Berkovich indenter is used, plastic deformations occur even at the very early stage of loading. The plastic zone in the indented specimen is enlarged with increasing loading.

Figure A.7 is a schematic illustration of the corresponding load–displacement curve for loading and unloading. In this figure, h_{max} is the maximum penetration depth associated with the applied maximum load (P_{max}), h_p is the plastic or residual penetration depth at full unloading while $h_e = h_{max} - h_p$ is the elastic penetration depth recovered at full unloading.

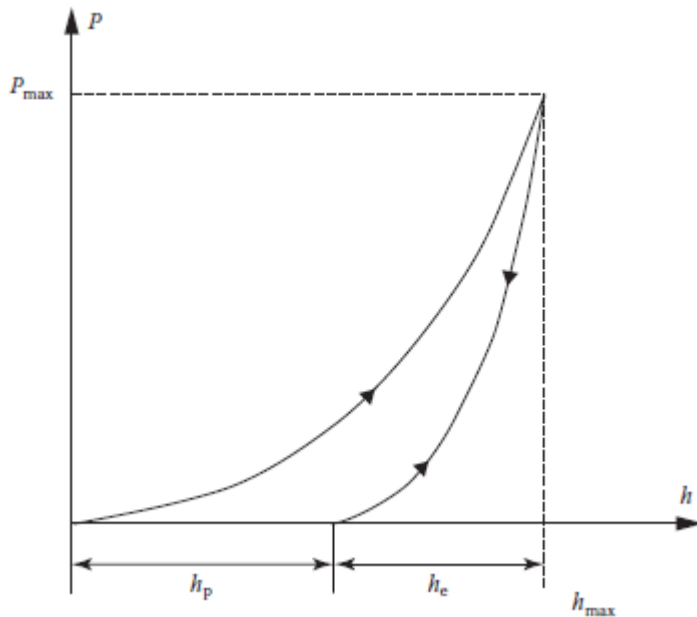


Figure A.7: Schematic of the load–displacement curve corresponding to the nano-indentation.⁶

The first part of the unloading curve is assumed to be purely elastic and the stiffness (S) can be estimated from the slope of the unloading curve.

The contact area of the indenter can only be indirectly measured because the size of residual impressions is too small to measure accurately.

Therefore, it is customary to determine the area of contact by measuring the depth of penetration of the indenter into the specimen surface. This, together with the known geometry of the indenter, provides an indirect measurement of contact area at full load. In nano-indentation testing, the depth of penetration beneath the specimen surface is measured as the load is applied to the indenter. The known geometry of the indenter then allows the size of the area of contact to be determined. For a Berkovich tip, the geometry yields the following area-to-contact depth (h_c) ratio:

$$A = 24.5 h_c^2$$

From the contact area and stiffness, the Young's modulus and hardness of the sample film can be determined:

$$S = \beta \frac{2}{\sqrt{\pi}} E_r \sqrt{A}$$

β is a correction coefficient ($\beta = 1.034$ for a Berkovich tip) and E_r is the effective Young's modulus defined by,

$$E_r = \left[\frac{1-\nu^2}{E} + \frac{1-\nu_i^2}{E_i} \right]^{-1}$$

With ν the Poisson ratio of the sample, ν_i the Poisson ratio of the Berkovich tip, E the Young's modulus of the sample and E_i the Young's modulus of the Berkovich tip.

The hardness is calculated from the load (P) and contact area,

$$H = P/A$$

However, when the films have thicknesses in the range 0-500 nm, the mechanical properties of the substrate could interfere, leading to wrong (mostly overestimated) mechanical properties of the film. To reduce this substrate effect as much as possible the continuous stiffness method was developed. This method combines a dynamic oscillation in the load with the quasi-static testing capabilities of the nano-indentation systems. The load is then expressed by:

$$P = P_{os} e^{(i\omega t)}$$

And the corresponding displacement oscillation by:

$$h(\omega) = h_0 e^{(i\omega t + \phi)}$$

Appendix: Applied characterization methods for thin film analysis

The dynamic model is normally treated as a simple harmonic oscillator under conditions of an applied harmonic force (see figure A.8).

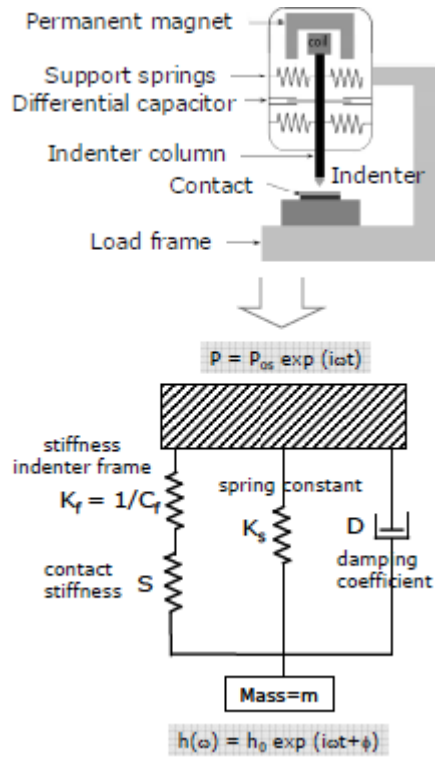


Figure A.8: Continuous stiffness method (taken from presentation of Kris Vanstreels, IMEC).

The contact stiffness can then be determined from

$$\left| \frac{P_{os}}{h_0} \right| = \sqrt{\left\{ (S^{-1} + C_f)^{-1} + K_s - m\omega^2 \right\}^2 + \omega^2 D^2}$$

This method allows the characterization of E and H in function of depth, making it possible to avoid substrate effects. An example is shown in figure A.9.

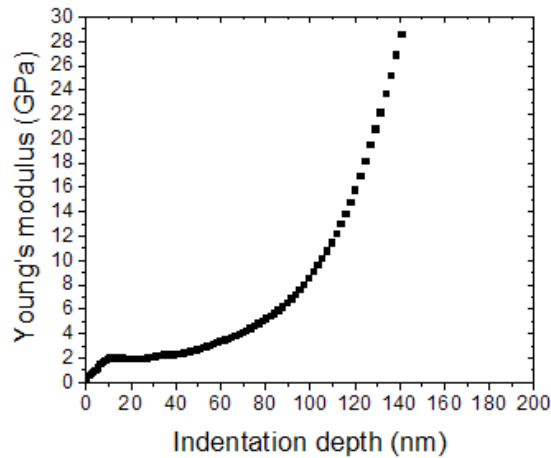


Figure A.9: The Young's modulus (E) depth profile of a PMO thin film.

The profile can be divided into 3 regions:

- Region I (below 10 nm): the values for E cannot be trusted because in this range the contact between tip and film is not well defined.
- Region II: The Young's modulus is more or less constant from about 10-40 nm and this is the E of the film.
- Region III: >40 nm mixed properties (film + substrate) are measured.

A.4 C-V measurements^{9,10}

As mentioned in chapter one, the dielectric constant of the low-k films can be calculated from the measured capacitance of a metal-insulator-semiconductor (MIS) capacitor. The metal is the aluminum top contact, the insulator is the low-k film and the semiconductor is the silicon wafer.

In practice, the procedure for performing C-V measurements involves the application of DC-bias voltages across the capacitor while the measurements are performed with an AC signal. AC frequencies are typically in the range 10kHz -1 MHz. Because the C-V measurements are performed at AC frequencies, the capacitance is obtained with following formula:

$$C = I/(2\pi fV)$$

Appendix: Applied characterization methods for thin film analysis

With I the magnitude of the AC current, f the frequency and V the magnitude and phase angle of the measured AC voltage.

This measurement takes into account series and parallel resistance associated with the capacitance as well as the dissipation factor (D , leakage). The dissipation factor should be as low as possible because as D increases, the accuracy of C is rapidly degraded.

For our measurements the series model was used, and the capacitance can then be derived from:

$$C = 1/(2\pi f Z \sin\theta)$$

With Z the impedance and θ the phase angle.

In the case that MIS capacitors are used to determine the dielectric constant, the capacitance should be extracted from the accumulation region of the capacitor (see figure A.10). Further a good ohmic back contact is necessary to avoid extra resistance between the MIS capacitor and the C-V analyzer. This can be achieved by scratching the backside of the silicon wafer and depositing for example a Ti/Au layer or applying Ga-In alloy paste on the scratched backside.

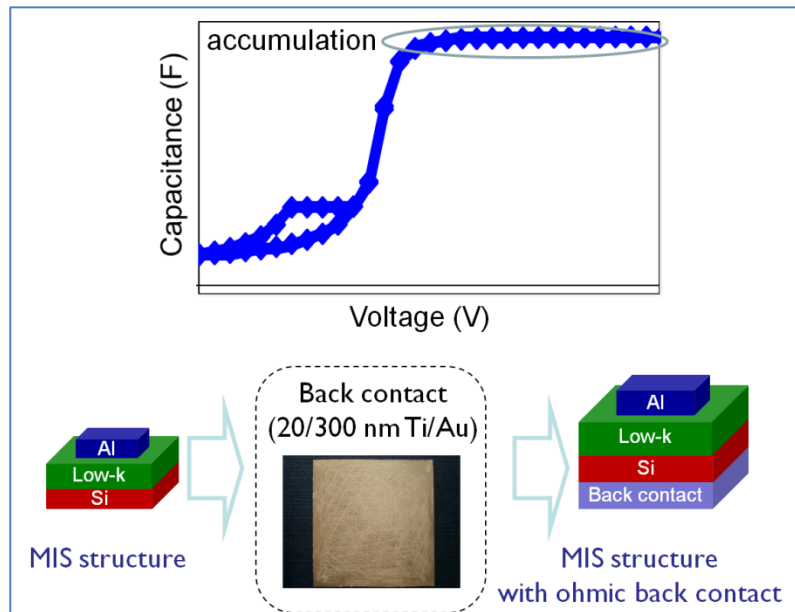


Figure A.10: C-V measurement showing the accumulation region and an example to provide a back contact on the MIS capacitor.

Appendix: Applied characterization methods for thin film analysis

The next section will describe in detail how the k -values were obtained because the accuracy of the k -value is extremely important to evaluate the low- k material.

A first important step is a good sample preparation. Therefore, PMO films were spin-coated on 4x4 cm n-type silicon substrates. The size of the substrate allows the deposition of a sufficient amount of top contacts. The top contacts (Al dots) were deposited on the low- k film by e-beam evaporation through a shadow mask which was magnetically attached to the low- k film (see figure A.11).

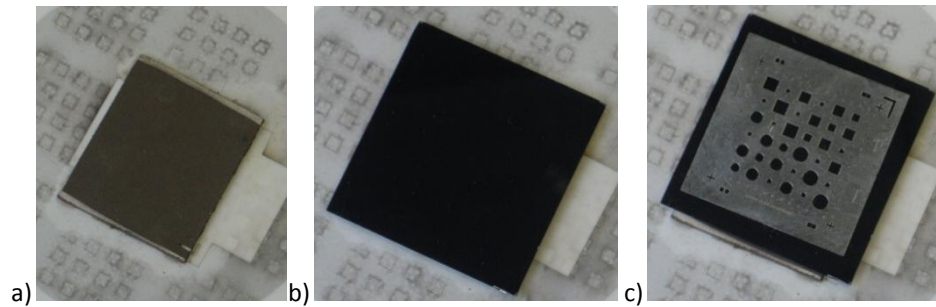


Figure A.11: Good attachment of shadow mask: a) magnet; b) sample on top of magnet; c) shadow mask on top of sample.

This is needed to prevent shadow effects which would make it impossible to calculate the surface area of the top electrode accurately (see figure A.12).

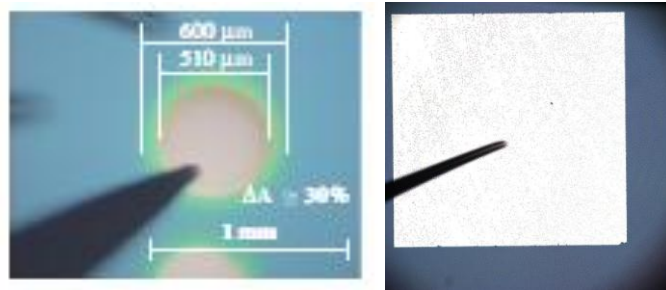


Figure A.12: Left shadow effect of top contact (taken from ref. 10), right no shadow effect.

The holes of the shadow mask have different shapes and sizes. This means that the top contacts also have different shapes and sizes reducing the systematic error on the surface area calculation of the top electrode. For our samples, aluminum dots with diameters of 1070, 1954, 2764 and 3385 μm were used as top contacts. Visual microscopy was used to magnify the size of the contact, allowing a more precise calculation of the surface area.

Appendix: Applied characterization methods for thin film analysis

The backside of the silicon substrate is scratched and provided with a back contact as described earlier. The sample is placed on a chuck and the chuck and top contact are then connected with the impedance analyzer as shown in figure A.13

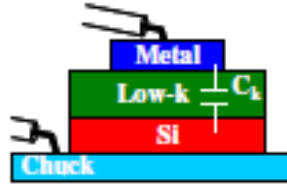


Figure A.13: Connection of top and bottom electrode to the analyzing tool.¹⁰

By performing a CV measurement, the voltage when the silicon substrate is in accumulation can be detected as shown in figure A.10. At this voltage, the frequency can be changed to evaluate the low-k material and to extract the k -value from the capacitance (while checking that $D < 0.1$) as described in chapter 5 and 6. Coifi *et al.* investigated in depth what happens when some of these steps are not well performed. It usually results in an underestimated (lower) k -value.¹⁰

A.5 References

1. www.jawoollam.com.
2. J. A. Woollam, J. N. Hilfiker, T. E. Tiwald, C. L. Bungay, R. A. Synowicki, D. E. Meyer, C. M. Herzinger, G. L. Pfeiffer, G. T. Cooney and S. E. Green, *P Soc Photo-Opt Ins*, 2000, **4099**, 197-205.
3. M. T. Othman, University of Missouri - Columbia, Missouri, 2007.
4. M. R. Baklanov, K. P. Mogilnikov, V. G. Polovinkin and F. N. Dultsev, *J Vac Sci Technol B*, 2000, **18**, 1385-1391.
5. M. R. Baklanov and K. P. Mogilnikov, *Opt Appl*, 2000, **30**, 491-496.
6. K. Sattler, ed., *Handbook of Nanophysics: Functional Materials*, Taylor & Francis, Boca Raton, 2010.
7. X. D. Li and B. Bhushan, *Mater Charact*, 2002, **48**, 11-36.
8. T. ADEOGBA, THE UNIVERSITY OF TEXAS AT ARLINGTON, 2009.
9. L. Stauffer, Keithley Instruments, Inc, 2009.
10. I. Ciofi, M. R. Baklanov, Z. Tokei and G. P. Beyer, *Microelectron Eng*, 2010, **87**, 2391-2406.

The front cover image was taken from:

<http://www03.ibm.com/press/us/en/photos.wss?topic=21>